



# **PHOTOMULTIPLIER TUBES**

---

**Basics and Applications**

**THIRD EDITION (Edition 3a)**

**PHOTON IS  
OUR BUSINESS**

**HAMAMATSU**



▲ Photomultiplier Tubes



▲ Photomultiplier Tube Modules

# Introduction

Light detection technology is a powerful tool that provides deeper understanding of more sophisticated phenomena. Measurement using light offers unique advantages: for example, nondestructive analysis of a substance, high-speed properties and extremely high detectability. Recently, in particular, such advanced fields as scientific measurement, medical diagnosis and treatment, high energy physics, spectroscopy and biotechnology require development of photodetectors that exhibit the ultimate in various performance parameters.

Photodetectors or light sensors can be broadly divided by their operating principle into three major categories: external photoelectric effect, internal photoelectric effect and thermal types. The external photoelectric effect is a phenomenon in which when light strikes a metal or semiconductor placed in a vacuum, electrons are emitted from its surface into the vacuum. Photomultiplier tubes (often abbreviated as PMT) make use of this external photoelectric effect and are superior in response speed and sensitivity (low-light-level detection). They are widely used in medical equipment, analytical instruments and industrial measurement systems.

Light sensors utilizing the internal photoelectric effect are further divided into photoconductive types and photovoltaic types. Photoconductive cells represent the former, and PIN photodiodes the latter. Both types feature high sensitivity and miniature size, making them well suited for use as sensors in camera exposure meters, optical disk pickups and in optical communications. The thermal types, though their sensitivity is low, have no wavelength-dependence and are therefore used as temperature sensors in fire alarms, intrusion alarms, etc.

This handbook has been structured as a technical handbook for photomultiplier tubes in order to provide the reader with comprehensive information on photomultiplier tubes.

This handbook will help the user gain maximum performance from photomultiplier tubes and show how to properly operate them with higher reliability and stability. In particular, we believe that the first-time user will find this handbook beneficial as a guide to photomultiplier tubes. We also hope this handbook will be useful for engineers already experienced in photomultiplier tubes for upgrading performance characteristics.

---

Information furnished by Hamamatsu Photonics is believed to be reliable. However, no responsibility is assumed for possible inaccuracies or omission. The contents of this manual are subject to change without notice. No patent rights are granted to any of the circuits described herein.

©2007 Hamamatsu Photonics K. K.

# CONTENTS

<b>CHAPTER 1 INTRODUCTION .....</b>	<b>1</b>
1.1 Overview of This Manual .....	2
1.2 Photometric Units .....	4
1.2.1 Spectral regions and units .....	4
1.2.2 Units of light intensity .....	5
1.3 History .....	10
1.3.1 History of photocathodes .....	10
1.3.2 History of photomultiplier tubes .....	10
References in Chapter 1 .....	12
<b>CHAPTER 2 BASIC PRINCIPLES OF PHOTOMULTIPLIER TUBES .....</b>	<b>13</b>
2.1 Photoelectron Emission .....	14
2.2 Electron Trajectory .....	16
2.3 Electron Multiplier (Dynode Section) .....	17
2.4 Anode .....	18
References in Chapter 2 .....	19
<b>CHAPTER 3 BASIC OPERATING METHODS OF PHOTOMULTIPLIER TUBES .....</b>	<b>21</b>
3.1 Using Photomultiplier Tubes .....	22
3.1.1 How to make the proper selection .....	22
3.1.2 Peripheral devices .....	23
High-voltage power supply .....	23
Voltage-divider circuit .....	24
Housing .....	26
Integral power supply module .....	27
3.1.3 Operating methods (connection circuits) .....	28

## CHAPTER 4 CHARACTERISTICS OF PHOTOMULTIPLIER TUBES ..... 29

4.1	Basic Characteristics of Photocathodes .....	30
4.1.1	Photocathode materials .....	30
	(1) Cs-I .....	30
	(2) Cs-Te .....	30
	(3) Sb-Cs .....	30
	(4) Bialkali (Sb-Rb-Cs, Sb-K-Cs) .....	30
	(5) High temperature, low noise bialkali (Sb-Na-K) .....	31
	(6) Multialkali (Sb-Na-K-Cs) .....	31
	(7) Ag-O-Cs .....	31
	(8) GaAsP (Cs) .....	31
	(9) GaAs (Cs) .....	31
	(10) InGaAs (Cs) .....	31
	(11) InP/InGaAsP(Cs), InP/InGaAs(Cs) .....	31
	Reflection mode photocathodes .....	34
	Transmission mode photocathodes .....	35
4.1.2	Window materials .....	36
	(1) MgF <sub>2</sub> crystal .....	36
	(2) Sapphire .....	36
	(3) Synthetic silica .....	36
	(4) UV glass (UV-transmitting glass) .....	36
	(5) Borosilicate glass .....	36
4.1.3	Spectral response characteristics .....	37
	(1) Radiant sensitivity .....	37
	(2) Quantum efficiency .....	37
	(3) Measurement and calculation of spectral response characteristics ....	38
	(4) Spectral response range (short and long wavelength limits) .....	38
4.1.4	Luminous sensitivity .....	38
	(1) Cathode luminous sensitivity .....	39
	(2) Anode luminous sensitivity .....	40
	(3) Blue sensitivity index and red-to-white ratio .....	41
4.1.5	Luminous sensitivity and spectral response .....	42
4.2	Basic Characteristics of Dynodes .....	43
4.2.1	Dynode types and features .....	43
	(1) Circular-cage type .....	44
	(2) Box-and-grid type .....	44
	(3) Linear-focused type .....	44
	(4) Venetian blind type .....	44
	(5) Mesh type .....	44
	(6) MCP (Microchannel plate) .....	44

	(7) Metal channel dynode .....	44
	(8) Electron bombardment type .....	44
4.2.2	Collection efficiency and gain (current amplification) .....	45
	(1) Collection efficiency .....	45
	(2) Gain (current amplification) .....	46
4.3	Characteristics of Photomultiplier Tubes .....	48
4.3.1	Time characteristics .....	48
	(1) Rise time, fall time and electron transit time .....	49
	(2) TTS (transit time spread) .....	50
	(3) CTTD (cathode transit time difference) .....	52
	(4) CRT (coincident resolving time) .....	53
4.3.2	Linearity .....	54
	(1) Cathode linearity .....	54
	(2) Anode linearity .....	54
	(3) Linearity measurement .....	56
4.3.3	Uniformity .....	59
	(1) Spatial uniformity .....	60
	(2) Angular response .....	62
4.3.4	Stability .....	63
	(1) Drift (time stability) and life characteristics .....	63
	(2) Aging and warm-up .....	64
4.3.5	Hysteresis .....	65
	(1) Light hysteresis .....	65
	(2) Voltage hysteresis .....	66
	(3) Reducing the hysteresis .....	67
4.3.6	Dark current .....	67
	(1) Causes of dark current .....	67
	(2) Expression of dark current .....	71
4.3.7	Signal-to-noise ratio of photomultiplier tubes .....	73
4.3.8	Afterpulsing .....	77
	Types of afterpulses .....	77
4.3.9	Polarized-light dependence .....	78
	References in Chapter 4 .....	81

## **CHAPTER 5 HOW TO USE PHOTOMULTIPLIER TUBES AND PERIPHERAL CIRCUITS ..... 83**

5.1	Voltage-Divider Circuits .....	84
5.1.1	Basic operation of voltage-divider circuits .....	84

5.1.2	Anode grounding and cathode grounding .....	85
5.1.3	Voltage-divider current and output linearity .....	86
	(1) DC-operation output linearity and its countermeasures .....	86
	(2) Pulse-operation output linearity and its countermeasures .....	88
5.1.4	Voltage distribution in voltage-divider circuits .....	90
	(1) Voltage distribution in the anode and latter stages .....	90
	(2) Voltage distribution for the cathode and earlier stages .....	92
5.1.5	Countermeasures for fast response circuits .....	93
5.1.6	Practical fast-response voltage-divider circuit .....	94
5.1.7	High output linearity voltage-divider circuit (1) .....	94
5.1.8	High output linearity voltage-divider circuit (2) .....	96
5.1.9	Gating circuit .....	97
5.1.10	Anode sensitivity adjustment circuits .....	98
5.1.11	Precautions when fabricating a voltage-divider circuit .....	100
	(1) Selecting the parts used for a voltage-divider circuit .....	100
	(2) Precautions for mounting components .....	101
5.2	Selecting a High-Voltage Power Supply .....	102
5.3	Connection to an External Circuit .....	102
5.3.1	Observing an output signal .....	102
5.3.2	Influence of a coupling capacitor .....	104
5.3.3	Current-to-voltage conversion for photomultiplier tube output ..	105
	(1) Current-to-voltage conversion using load resistance .....	105
	(2) Current-to-voltage conversion using an operational amplifier .....	107
	(3) Charge-sensitive amplifier using an operational amplifier .....	109
5.3.4	Output circuit for a fast response photomultiplier tube .....	111
5.4	Housing .....	113
5.4.1	Light shield .....	113
5.4.2	Electrostatic shield .....	113
5.4.3	Magnetic shield .....	113
	(1) Shielding factor of magnetic shield case and orientation of magnetic field...	114
	(2) Saturation characteristics .....	116
	(3) Frequency characteristics .....	118
	(4) Edge effect .....	119
	(5) Photomultiplier tube magnetic characteristics and shielding effect ....	119
	(6) Handling the magnetic shield case .....	120
5.5	Cooling .....	122
	References in Chapter 5 .....	123

**CHAPTER 6 PHOTON COUNTING ..... 125**

6.1 Analog and Digital (Photon Counting) Modes ..... 126

6.2 Principle of Photon Counting ..... 127

6.3 Operating Method and Characteristics of Photon Counting .. 129

    (1) Circuit configuration ..... 129

    (2) Basic characteristics of photon counting ..... 129

References in Chapter 6 ..... 134

**CHAPTER 7 SCINTILLATION COUNTING ..... 135**

7.1 Scintillators and Photomultiplier Tubes ..... 136

7.2 Characteristics ..... 139

    (1) Energy resolution ..... 139

    (2) Relative pulse height ..... 142

    (3) Linearity ..... 142

    (4) Uniformity ..... 144

    (5) Stability ..... 145

    (6) Noise ..... 146

    (7) Plateau characteristic ..... 148

References in Chapter 7 ..... 151

**CHAPTER 8 PHOTOMULTIPLIER TUBE MODULES..... 153**

8.1 What Are Photomultiplier Tube Modules? ..... 154

8.2 Characteristics of Power Supply Circuits ..... 154

    (1) Power supply circuits ..... 154

    (2) Ripple noise ..... 156

    (3) Settling time ..... 156

8.3 Current Output Type and Voltage Output Type ..... 157

    (1) Connection method ..... 157

    (2) Gain adjustment ..... 157

    (3) Current output type module ..... 158

    (4) Voltage output type module ..... 158

8.4 Photon Counting Head ..... 159

    (1) Output characteristics ..... 159

    (2) Counting sensitivity ..... 159

    (3) Count linearity ..... 160

    (4) Improving the count linearity ..... 160

    (5) Temperature characteristics ..... 161

    (6) Photon counting ASIC (Application Specific Integrated Circuit) ..... 162



8.5	Gate Function .....	163
	(1) Gate noise .....	163
	(2) Extinction ratio .....	164
8.6	Built-in CPU and IF Type .....	165
	(1) Photon counting type .....	165
	(2) Charge amplifier and AD converter type .....	166
	References in Chapter 8 .....	166

## **CHAPTER 9 POSITION SENSITIVE PHOTOMULTIPLIER TUBES ..... 167**

9.1	Multianode Photomultiplier Tubes .....	169
9.1.1	Metal channel dynode type multianode photomultiplier tubes ...	169
	(1) Structure .....	169
	(2) Characteristics .....	170
9.1.2	Multianode MCP-PMT .....	176
9.1.3	Flat panel type multianode photomultiplier tubes .....	176
	(1) Characteristics .....	176
9.2	Center-of-Gravity Position Sensitive Photomultiplier Tubes .....	178
9.2.1	Metal channel dynode type multianode photomultiplier tubes (cross-plate anodes) .....	178
	(1) Structure .....	178
	(2) Characteristics .....	179
9.2.2	Grid type dynode photomultiplier tubes (Cross-wire anodes) ..	182
	(1) Structure .....	182
	(2) Characteristics .....	182

## **CHAPTER 10 MCP-PMT ..... 187**

10.1	Structure .....	188
10.1.1	Structure of MCPs .....	188
10.1.2	Structure of MCP-PMTs .....	189
10.1.3	Voltage-divider circuit and housing structure .....	190
10.2	Basic Characteristics of MCP-PMTs .....	191
10.2.1	Gain characteristics .....	191
10.2.2	Time characteristics .....	192
	(1) Rise/fall times .....	192
	(2) Transit time .....	192

(3) TTS (transit time spread) .....	192
(4) Cathode transit time difference .....	194
(5) Time characteristics of various products .....	194
10.2.3 Temperature characteristics and cooling .....	195
10.2.4 Saturation characteristics .....	196
(1) Dead time .....	196
(2) Saturation in DC operation .....	197
(3) Pulse gain saturation characteristics (pulse linearity) .....	198
(4) Saturation gain characteristics in photon counting mode .....	200
(5) Count rate linearity in photon counting .....	200
10.2.5 Magnetic characteristics .....	201
10.3 Gated MCP-PMTs .....	203
10.4 Multianode MCP-PMTs .....	205
References in Chapter 10 .....	208

## **CHAPTER 11 HPD (Hybrid Photo-Detector) ..... 209**

11.1 Operating Principle of HPDs .....	210
11.2 Comparison with Photomultiplier Tubes .....	212
11.3 Various Characteristics of HPDs .....	213
11.3.1 Multi-photoelectron resolution .....	213
11.3.2 Gain characteristics and electron bombardment gain uniformity ...	213
11.3.3 Time response characteristics .....	215
11.3.4 Uniformity .....	216
11.3.5 Light hysteresis characteristics .....	216
11.3.6 Drift characteristics (short-term stability) .....	217
11.3.7 Magnetic characteristics .....	218
11.3.8 Temperature characteristics .....	218
11.4 Connection Examples (R7110U Series) .....	219
11.4.1 When handling DC signal (including connection to transimpedance amp) .....	219
11.4.2 When handling pulse signal (including connection to charge amp) ..	220
References in Chapter 11 .....	220

**CHAPTER 12 ELECTRON MULTIPLIER TUBES  
AND ION DETECTORS ..... 221**

12.1 Structure ..... 222

12.2 Characteristics ..... 223

    12.2.1 Sensitivity to soft X-rays, VUV, electrons and ions ..... 223

    12.2.2 Gain ..... 227

    12.2.3 Dark current and noise ..... 227

    12.2.4 Linearity ..... 230

    12.2.5 Life characteristics ..... 231

References in Chapter 12 ..... 231

**CHAPTER 13 ENVIRONMENTAL RESISTANCE  
AND RELIABILITY ..... 233**

13.1 Effects of Ambient Temperature ..... 234

    13.1.1 Temperature characteristics ..... 234

        (1) Sensitivity ..... 234

        (2) Dark current ..... 235

    13.1.2 High temperature photomultiplier tubes ..... 236

    13.1.3 Storage temperature and cooling precautions ..... 239

13.2 Effects of Humidity ..... 239

    13.2.1 Operating humidity ..... 239

    13.2.2 Storage humidity ..... 239

13.3 Effects of External Magnetic Fields ..... 240

    13.3.1 Magnetic characteristics ..... 240

    13.3.2 Photomultiplier tubes for use in highly magnetic fields ..... 241

    13.3.3 Magnetization ..... 242

    13.3.4 Photomultiplier tubes made of nonmagnetic materials ..... 242

13.4 Vibration and Shock ..... 243

    13.4.1 Resistance to vibration and shock during non-operation ... 243

    13.4.2 Resistance to vibration and shock during operation (resonance) .. 243

    13.4.3 Testing methods and conditions ..... 245

    13.4.4 Ruggedized photomultiplier tubes ..... 247

13.5 Effects of Helium Gas ..... 248

13.6	Effects of Radiation .....	249
13.6.1	Deterioration of window transmittance .....	249
13.6.2	Glass scintillation .....	253
13.7	Effects of Atmosphere .....	254
13.8	Effects of External Electric Potential .....	255
13.8.1	Experiment .....	255
13.8.2	Taking corrective action .....	257
13.9	Reliability .....	258
13.9.1	Stability over time (life characteristic) .....	258
13.9.2	Current stress and stability .....	259
13.9.3	Reliability .....	261
(1)	Failure mode .....	261
(2)	Failure rate .....	261
(3)	Mean life .....	261
(4)	Reliability .....	262
13.9.4	Reliability tests and criteria used by Hamamatsu Photonics ...	263
	References in Chapter 13 .....	264

## **CHAPTER 14 APPLICATIONS ..... 265**

14.1	Spectrophotometry .....	266
14.1.1	Overview .....	266
14.1.2	Specific applications .....	267
(1)	UV, visible and infrared spectrophotometers .....	267
(2)	Atomic absorption spectrophotometers .....	268
(3)	Atomic emission spectrophotometers .....	268
(4)	Fluorospectrophotometers .....	269
14.2	Medical Equipment .....	270
14.2.1	PET (Positron Emission Tomography) .....	270
14.2.2	Gamma cameras .....	273
14.2.3	Planar imaging device .....	274
14.2.4	X-ray image diagnostic equipment .....	275
(1)	X-ray phototimer .....	275
(2)	Computed radiography (CR) .....	276
14.2.5	In-vitro assay .....	277
(1)	RIA (Radioimmunoassay) method .....	279
(2)	Luminescent / fluorescent immunoassay .....	280

	(3) Chemiluminescent immunoassay .....	281
14.3	Biotechnology .....	282
	14.3.1 Overview .....	282
	14.3.2 Application examples .....	282
	(1) Flow cytometers .....	282
	(2) Confocal laser microscopes .....	283
	(3) DNA microarray scanners .....	283
	(4) DNA sequencers .....	284
14.4	High-Energy Physics Experiments .....	285
	14.4.1 Overview .....	285
	14.4.2 Collision experiments .....	285
	(1) Hodoscopes .....	286
	(2) TOF counters .....	286
	(3) Calorimeters .....	287
	(4) Cherenkov counters .....	287
	14.4.3 Proton decay, neutrino observation experiments .....	288
14.5	Oil Well Logging .....	290
14.6	Environmental Measurement .....	291
	14.6.1 Overview .....	291
	14.6.2 Application examples .....	291
	(1) Dust counters .....	291
	(2) Laser radar (LIDAR) .....	291
	(3) NO <sub>x</sub> analyzers .....	292
	(4) SO <sub>x</sub> analyzers .....	293
14.7	Radiation Monitors .....	294
	14.7.1 Overview .....	294
	14.7.2 Application examples .....	294
	(1) Handheld radiation monitor (pager) .....	294
	(2) Door monitors .....	295
14.8	Industrial Measurement .....	296
	14.8.1 Overview .....	296
	14.8.2 Application examples .....	296
	(1) Thickness gauges .....	296
	(2) Laser scanners .....	297
14.9	Aerospace Applications .....	298
	14.9.1 Overview .....	298
	14.9.2 Application examples .....	298

	(1) X-ray astronomy .....	298
	(2) Ozone measurement (solar backscatter radiometer) .....	300
14.10	Mass Spectrometry / Solid Surface Analysis .....	301
14.10.1	Mass spectrometers .....	301
14.10.2	Solid surface analyzers .....	302
	References in Chapter 14 .....	304
<b>Index</b>	.....	<b>305</b>

**CHAPTER 1**  
**INTRODUCTION**

## 1.1 Overview of This Manual

The following provides a brief description of each chapter in this technical manual.

### Chapter 1 Introduction

Before starting to describe the main subjects, this chapter explains basic photometric units used to measure or express properties of light such as wavelength and intensity. This chapter also describes the history of the development of photocathodes and photomultiplier tubes.

### Chapter 2 Basic Principles of Photomultiplier Tubes

This chapter describes the basic operating principles and elements of photomultiplier tubes, including photoelectron emission, electron trajectories, electron multiplication by use of electron multipliers (dynodes), and anodes.

### Chapter 3 Basic Operating Methods of Photomultiplier Tubes

This chapter is aimed at first-time photomultiplier tube users. It describes how to select and operate photomultiplier tubes and how to process their signals.

### Chapter 4 Characteristics of Photomultiplier Tubes

Chapter 4 explains in detail the basic performance and various characteristics of photomultiplier tubes.

### Chapter 5 How to Use Photomultiplier Tubes and Peripheral Circuits

This chapter describes how to use the basic circuits and accessories needed for correct operation of photomultiplier tubes.

### Chapter 6 Photon Counting

Chapter 6 describes the principle, method of use, characteristics and advantages of photon counting used for optical measurement at very low light levels where the absolute amount of light is extremely small.

### Chapter 7 Scintillation Counting

Chapter 7 explains scintillation counting with photomultiplier tubes for radiation measurement. It includes descriptions of characteristics, measurement methods, and typical examples of data.

### Chapter 8 Photomultiplier Tube Modules

This chapter describes photomultiplier tube modules (PMT modules) developed to make photomultiplier tubes easier to use and also to expand their applications.



## **Chapter 9 Position Sensitive Photomultiplier Tubes**

Chapter 9 describes multianode position-sensitive photomultiplier tubes and center-of-gravity detection type photomultiplier tubes, showing their structure, characteristics and application examples.

## **Chapter 10 MCP-PMT**

This chapter explains MCP-PMTs (photomultiplier tubes incorporating microchannel plates) that are high-sensitivity and ultra-fast photodetectors.

## **Chapter 11 HPD (Hybrid Photo-Detectors)**

This chapter describes new hybrid photo-detectors (HPD) that incorporate a semiconductor detector in an electron tube.

## **Chapter 12 Electron Multiplier Tubes and Ion Detectors**

Chapter 12 describes electron multiplier tubes (sometimes called EMT) and ion detectors ideal for mass spectroscopy, showing the basic structure and various characteristics.

## **Chapter 13 Environmental Resistance and Reliability**

In this chapter, photomultiplier tube performance and usage are discussed in terms of environmental durability and operating reliability. In particular, this chapter describes ambient temperature, humidity, magnetic field effects, mechanical strength, etc. and the countermeasures against these factors.

## **Chapter 14 Applications**

Chapter 14 introduces major applications of photomultiplier tubes, and explains how photomultiplier tubes are used in a variety of fields and applications.

## 1.2 Photometric Units

Before starting to describe photomultiplier tubes and their characteristics, this section briefly discusses photometric units commonly used to measure the quantity of light. This section also explains the wavelength regions of light (spectral range) and the units to denote them, as well as the unit systems used to express light intensity. Since information included here is just an overview of major photometric units, please refer to specialty books for more details.<sup>1)2)</sup>

### 1.2.1 Spectral regions and units

Electromagnetic waves cover a very wide range from gamma rays up to millimeter waves. So-called "light" is a very narrow range of these electromagnetic waves.

Table 1-1 shows how spectral regions are designated when light is classified by wavelength, along with the conversion diagram for light units. In general, what we usually refer to as light covers a range from  $10^2$  to  $10^6$  nanometers (nm) in wavelength. The spectral region between 350 and 750nm shown in the table is usually known as the visible region. The region with wavelengths shorter than the visible region is divided into near UV (shorter than 350nm), vacuum UV (shorter than 200nm) where air is absorbed, and extreme UV (shorter than 100nm). Even shorter wavelengths span into the region called soft X-rays (shorter than 10nm) and X-rays. In contrast, longer wavelengths beyond the visible region extend from near IR (750nm or up) to the infrared (several micrometers or up) and far IR (several tens of micrometers or up) regions.

Wavelength	Spectral Range	Frequency	Energy
nm		(Hz)	(eV)
10	X-ray Soft X-ray		
10 <sup>2</sup>	Extreme UV region	10 <sup>16</sup>	10 <sup>2</sup>
200	Vacuum UV region		10
350	Ultraviolet region	10 <sup>15</sup>	
750	Visible region		
10 <sup>3</sup>	Near infrared region		1
10 <sup>4</sup>	Infrared region	10 <sup>14</sup>	
10 <sup>5</sup>		10 <sup>13</sup>	10 <sup>-1</sup>
10 <sup>6</sup>	Far infrared region	10 <sup>12</sup>	10 <sup>-2</sup>
			10 <sup>-3</sup>

Table 1-1: Spectral regions and unit conversions

Light energy E (J) is given by the following equation (Eq. 1-1).

$$E = h\nu = h \cdot \frac{c}{\lambda} \dots\dots\dots \text{(Eq. 1-1)}$$

- h : Planck's constant 6.626×10<sup>-34</sup>(J·s)
- ν: Frequency of light (Hz)
- c : Velocity of light 3×10<sup>8</sup>m/s
- λ: Wavelength (nm)

Eq. 1-1 can be rewritten as Eq. 1-2, by substituting E in eV, wavelength in nanometers (nm) and constants h and c in Eq. 1-1. Here, 1 eV equals 1.6×10<sup>-19</sup> J.

$$E(\text{eV}) = \frac{1240}{\lambda} \dots\dots\dots \text{(Eq. 1-2)}$$

From Eq. 1-2, it can be seen that light energy increases in proportion to the reciprocal of wavelength.

### 1.2.2 Units of light intensity

This section explains the units used to represent light intensity and their definitions.

The radiant quantity of light or radiant flux is a pure physical quantity expressed in units of watts (J/s). In contrast, the photometric quantity of light or luminous flux is represented in lumens which correlate to the visual sensation of light.

If the number of photons per second is n and the wavelength is λ, then Eq. 1-1 can be rewritten as Eq. 1-3 from the relation of W=J/S.

$$W = NE = \frac{Nhc}{\lambda} \dots\dots\dots \text{(Eq. 1-3)}$$

Here, the following equation can be obtained by substituting specific values for the above equation.

$$W = \frac{N \times 2 \times 10^{-16}}{\lambda}$$

The above equation shows the relation between the radiant power (W) of light and the number of photons (N), and will be helpful if you remember it.

Table 1-2 shows comparisons of radiant units with photometric units (in brackets [ ]). Each unit is described in subsequent sections.

Quantity	Unit Name	Symbol
Radiant flux [Luminous flux]	watts [lumens]	W [lm]
Radiant energy [Quantity of light]	joules [lumen· sec.]	J [lm·s]
Irradiance [Illuminance]	watts per square meter [lux]	W/m <sup>2</sup> [lx]
Radiant emittance [Luminous emittance]	watts per square meter [lumens per square meter]	W/m <sup>2</sup> [lm/m <sup>2</sup> ]
Radiant intensity [Luminous intensity]	watts per steradian [candelas]	W/sr [cd]
Radiance [Luminance]	watts per steradian· square meter [candelas per square meter]	W/sr/m <sup>2</sup> [cd/m <sup>2</sup> ]

Table 1-2: Comparisons of radiant units with photometric units (shown in brackets [ ] )

## 1. Radiant flux [Luminous flux]

Radiant flux is a unit to express radiant quantity, while luminous flux shown in brackets [ ] in Table 1-2 and the subhead just above is a unit to represent luminous quantity. (Units are shown this way in the rest of this chapter.) Radiant flux ( $\Phi_e$ ) is the flow of radiant energy ( $Q_e$ ) past a given point in a unit time period, and is defined as follows:

$$\Phi_e = dQ_e/dt \text{ (J/s)} \dots\dots\dots \text{(Eq. 1-4)}$$

On the other hand, luminous flux ( $\Phi$ ) is measured in lumens and defined as follows:

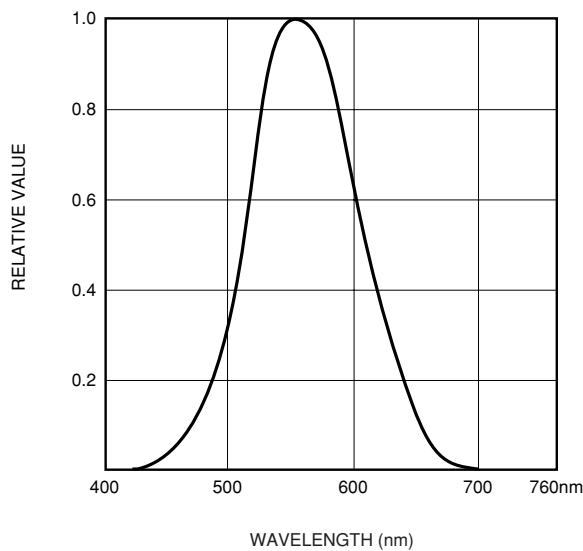
$$\Phi = k_m \int \Phi_e(\lambda)v(\lambda)d\lambda \dots\dots\dots \text{(Eq. 1-5)}$$

where  $\Phi_e(\lambda)$  : Spectral radiant density of a radiant flux, or spectral radiant flux

$k_m$  : Maximum sensitivity of the human eye (638 lm/W)

$v(\lambda)$  : Typical sensitivity of the human eye

The maximum sensitivity of the eye ( $k_m$ ) is a conversion coefficient used to link the radiant quantity and luminous quantity. Here,  $v(\lambda)$  indicates the typical spectral response of the human eye, internationally established as spectral luminous efficiency. A typical plot of spectral luminous efficiency versus wavelength (also called the luminosity curve) and relative spectral luminous efficiency at each wavelength are shown in Figure 1-1 and Table 1-3, respectively.



THBV3\_0101EA

Figure 1-1: Spectral luminous efficiency distribution

Wavelength (nm)	Luminous Efficiency	Wavelength (nm)	Luminous Efficiency
400	0.0004	600	0.631
10	0.0012	10	0.503
20	0.0040	20	0.381
30	0.0116	30	0.265
40	0.023	40	0.175
450	0.038	650	0.107
60	0.060	60	0.061
70	0.091	70	0.032
80	0.139	80	0.017
90	0.208	90	0.0082
500	0.323	700	0.0041
10	0.503	10	0.0021
20	0.710	20	0.00105
30	0.862	30	0.00052
40	0.954	40	0.00025
550	0.995	750	0.00012
555	1.0	60	0.00006
60	0.995		
70	0.952		
80	0.870		
90	0.757		

Table 1-3: Relative spectral luminous efficiency at each wavelength

**2. Radiant energy [Quantity of light]**

Radiant energy (Qe) is the integral of radiant flux over a duration of time. Similarly, the quantity of light (Q) is defined as the integral of luminous flux over a duration of time. Each term is respectively given by Eq. 1-6 and Eq. 1-7.

$$Q_e = \int \Phi_e dt \text{ (W}\cdot\text{s)} \dots\dots\dots \text{(Eq. 1-6)}$$

$$Q = \int \Phi dt \text{ (lm}\cdot\text{s)} \dots\dots\dots \text{(Eq. 1-7)}$$

**3. Irradiance [Illuminance]**

Irradiance (Ee) is the radiant flux incident per unit area of a surface, and is also called radiant flux density. (See Figure 1-2.) Likewise, illuminance (E) is the luminous flux incident per unit area of a surface. Each term is respectively given by Eq. 1-8 and Eq. 1-9.

$$\text{Irradiance } E_e = d\Phi_e/ds \text{ (W/m}^2\text{)} \dots\dots\dots \text{(Eq. 1-8)}$$

$$\text{Illuminance } E = d\Phi/ds \text{ (lx)} \dots\dots\dots \text{(Eq. 1-9)}$$

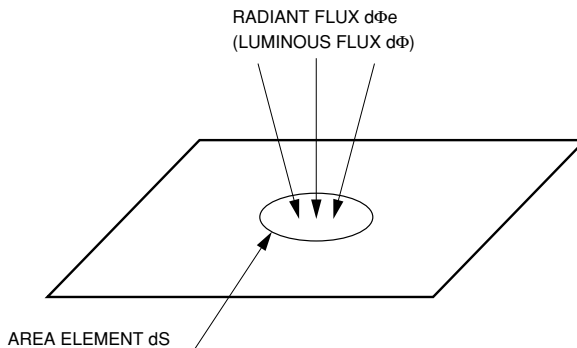


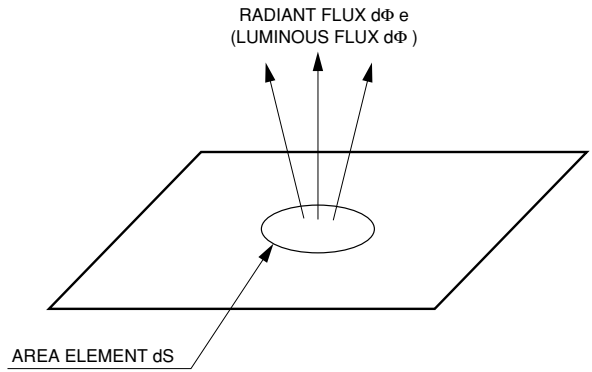
Figure 1-2: Irradiance (Illuminance)

#### 4. Radiant emittance [Luminous emittance]

Radiant emittance ( $M_e$ ) is the radiant flux emitted per unit area of a surface. (See Figure 1-3.) Likewise, luminous emittance ( $M$ ) is the luminous flux emitted per unit area of a surface. Each term is respectively expressed by Eq. 1-10 and Eq. 1-11.

Radiant emittance  $M_e = d\Phi_e/ds$  ( $W/m^2$ ) ..... (Eq. 1-10)

Luminous emittance  $M = d\Phi/ds$  ( $lm/m^2$ ) ..... (Eq. 1-11)



THBV3\_0103EA

Figure 1-3: Radiant emittance (Luminous emittance)

#### 5. Radiant intensity [Luminous intensity]

Radiant intensity ( $I_e$ ) is the radiant flux emerging from a point source, divided by the unit solid angle. (See Figure 1-4.) Likewise, luminous intensity ( $I$ ) is the luminous flux emerging from a point source, divided by the unit solid angle. These terms are respectively expressed by Eq. 1-12 and Eq. 1-13.

Radiant intensity  $I_e = d\Phi_e/dw$  ( $W/sr$ ) ..... (Eq. 1-12)

Where

$\Phi_e$ : radiant flux (W)

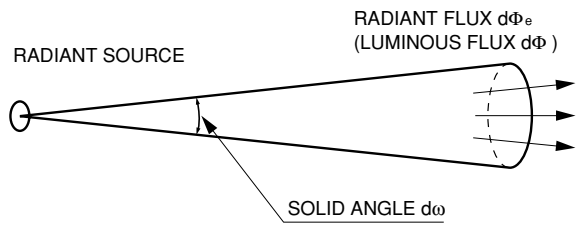
$w$  : solid angle (sr)

Luminous intensity  $I = d\Phi/dw$  (cd) ..... (Eq. 1-13)

Where

$\Phi$  : luminous flux (lm)

$w$  : solid angle (sr)



THBV3\_0104EA

Figure 1-4: Radiant intensity (Luminous intensity)

### 6. Radiance [Luminance]

Radiance ( $L_e$ ) is the radiant intensity emitted in a certain direction from a radiant source, divided by unit area of an orthographically projected surface. (See Figure 1-5.) Likewise, luminance ( $L$ ) is the luminous flux emitted from a light source, divided by the unit area of an orthographically projected surface. Each term is respectively given by Eq. 1-14 and Eq. 1-15.

$$\text{Radiance } L_e = dI_e/ds \cdot \cos\theta \text{ (W/sr/m}^2\text{)} \dots\dots\dots \text{(Eq. 1-14)}$$

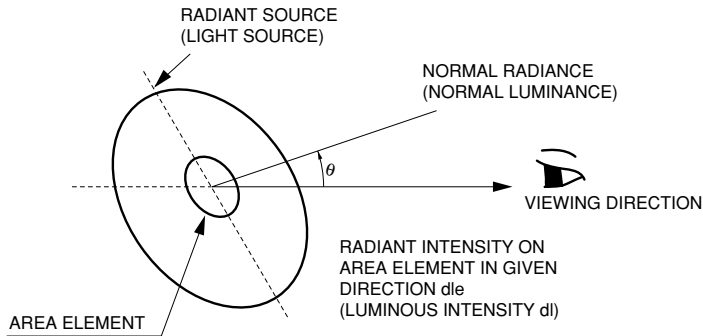
Where

- le: radiant intensity
- s : area
- $\theta$  : angle between viewing direction and small area surface

$$\text{Luminance } L = dI/ds \cdot \cos\theta \text{ (cd/m}^2\text{)} \dots\dots\dots \text{(Eq. 1-15)}$$

Where

- I: luminous intensity (cd)



THBV3\_0105EA

**Figure 1-5: Radiant intensity (Luminous intensity)**

In the above sections, we discussed basic photometric units which are internationally specified as SI units for quantitative measurements of light. However in some cases, units other than SI units are used.

Tables 1-4 and 1-5 show conversion tables for SI units and non-SI units, with respect to luminance and illuminance. Refer to these conversion tables as necessary.

	Unit Name	Symbol	Conversion Formula
SI Unit	nit stilb apostilb lambert	nt sb asb L	1nt = 1cd/m <sup>2</sup> 1sb = 1cd/cm <sup>2</sup> = 10 <sup>4</sup> cd/m <sup>2</sup> 1asb = 1/π cd/m <sup>2</sup> 1L = 1/π cd/cm <sup>2</sup> = 10 <sup>4</sup> /π cd/m <sup>2</sup>
Non SI Unit	foot lambert	fL	1fL = 1/π cd/ft <sup>2</sup> = 3.426 cd/m <sup>2</sup>

**Table 1-4: Luminance units**

	Unit Name	Symbol	Conversion Formula
SI Unit	photo	ph	1ph = 1 lm/cm <sup>2</sup> = 10 <sup>4</sup> lx
Non SI Unit	food candle	fc	1fc = 1 lm/ft <sup>2</sup> = 10.764 lx

**Table 1-5: Illuminance units**

## 1.3 History

### 1.3.1 History of photocathodes<sup>3)</sup>

The photoelectric effect was discovered in 1887 by Hertz<sup>4)</sup> through experiments exposing a negative electrode to ultraviolet radiation. In the next year 1888, the photoelectric effect was conclusively confirmed by Hallwachs.<sup>5)</sup> In 1889, Elster and Geitel<sup>6)</sup> reported the photoelectric effect which was induced by visible light striking an alkali metal (sodium-potassium). Since then, a variety of experiments and discussions on photoemission have been made by many scientists. As a result, the concept proposed by Einstein (in the quantum theory in 1905),<sup>7)</sup> "On a Heuristic Viewpoint Concerning the production and Transformation of Light", has been proven and accepted.

During this historic period of achievement, Elster and Geitel produced a photoelectric tube in 1913. Then, a compound photocathode made of Ag-O-Cs (silver oxygen cesium, also called S-1) was discovered in 1929 by Koller<sup>8)</sup> and Campbell.<sup>9)</sup> This photocathode showed photoelectric sensitivity about two orders of magnitude higher than previously used photocathode materials, achieving high sensitivity in the visible to near infrared region. In 1930, they succeeded in producing a phototube using this S-1 photocathode. In the same year, a Japanese scientist, Asao reported a method for enhancing the sensitivity of silver in the S-1 photocathode. Since then, various photocathodes have been developed one after another, including alkali photocathodes for the visible region, multialkali photocathodes with high sensitivity extending to the infrared region and alkali halide photocathodes intended for ultraviolet detection.<sup>10)-13)</sup>

In addition, photocathodes using III-V compound semiconductors such as GaAs<sup>14)-19)</sup> and InGaAs<sup>20) 21)</sup> have been developed and put into practical use. These semiconductor photocathodes have an NEA (negative electron affinity) structure and offer high sensitivity from the ultraviolet through near infrared region. Currently, a wide variety of photomultiplier tubes utilizing the above photocathodes are available. They are selected and used according to the application required.

### 1.3.2 History of photomultiplier tubes

Photomultiplier tubes have been making rapid progress since the development of photocathodes and secondary emission multipliers (dynodes).

The first report on a secondary emissive surface was made by Austin et al.<sup>22)</sup> in 1902. Since that time, research into secondary emissive surfaces (secondary electron emission) has been carried out to achieve higher electron multiplication. In 1935, Iams et al.<sup>23)</sup> succeeded in producing a triode photomultiplier tube with a photocathode combined with a single-stage dynode (secondary emissive surface), which was used for movie sound pickup. In the next year 1936, Zworykin et al.<sup>24)</sup> developed a photomultiplier tube having multiple dynode stages. This tube enabled electrons to travel in the tube by using an electric field and a magnetic field. Then, in 1939, Zworykin and Rajchman<sup>25)</sup> developed an electrostatic-focusing type photomultiplier tube (this is the basic structure of photomultiplier tubes currently used). In this photomultiplier tube, an Ag-O-Cs photocathode was first used and later an Sb-Cs photocathode was employed.

An improved photomultiplier tube structure was developed and announced by Morton in 1949<sup>26)</sup> and in 1956.<sup>27)</sup> Since then the dynode structure has been intensively studied, leading to the development of a variety of dynode structures including circular-cage, linear-focused and box-and-grid types. In addition, photomultiplier tubes using magnetic-focusing type multipliers,<sup>28)</sup> transmission-mode secondary-emissive surfaces<sup>29)-31)</sup> and channel type multipliers<sup>32)</sup> have been developed.

At Hamamatsu Photonics, the manufacture of various phototubes such as types with an Sb-Cs photocathode was established in 1953. (The company was then called Hamamatsu TV Co., Ltd. until 1983.) In 1959, Hamamatsu Photonics marketed side-on photomultiplier tubes (931A, 1P21 and R106 having an Sb-Cs pho-



---

tocathode) which have been widely used in spectroscopy. Hamamatsu Photonics also developed and marketed side-on photomultiplier tubes (R132 and R136) having an Ag-Bi-O-Cs photocathode in 1962. This photocathode had higher sensitivity in the red region of spectrum than that of the Sb-Cs photocathode, making them best suited for spectroscopy in those days. In addition, Hamamatsu Photonics put head-on photomultiplier tubes (6199 with an Sb-Cs photocathode) on the market in 1965.

In 1967, Hamamatsu Photonics introduced a 1/2-inch diameter side-on photomultiplier tube (R300 with an Sb-Cs photocathode) which was the smallest tube at that time. In 1969, Hamamatsu Photonics developed and marketed photomultiplier tubes having a multialkali (Na-K-Cs-Sb) photocathode, R446 (side-on) and R375 (head-on). Then, in 1974 a new side-on photomultiplier tube (R928) was developed by Hamamatsu Photonics, which achieved much higher sensitivity in the red to near infrared region. This was an epoch-making event in terms of enhancing photomultiplier tube sensitivity. Since that time, Hamamatsu Photonics has continued to develop and produce a wide variety of state-of-the-art photomultiplier tubes. The current product line ranges in size from the world's smallest 3/8-inch tubes (R1635) to the world's largest 20-inch hemispherical tubes (R1449 and R3600). Hamamatsu Photonics also offers ultra-fast photomultiplier tubes using a microchannel plate for the dynodes (R3809 with a time resolution of 30 picoseconds) and mesh-dynode type photomultiplier tubes (R5924) that maintain an adequate gain of  $10^5$  even in high magnetic fields of up to one Tesla. More recently, Hamamatsu Photonics has developed TO-8 metal package type photomultiplier tubes (R7400) using metal channel dynodes, various types of position-sensitive photomultiplier tubes capable of position detection, and flat panel photomultiplier tubes. Hamamatsu Photonics is constantly engaged in research and development for manufacturing a wide variety of photomultiplier tubes to meet a wide range of application needs.

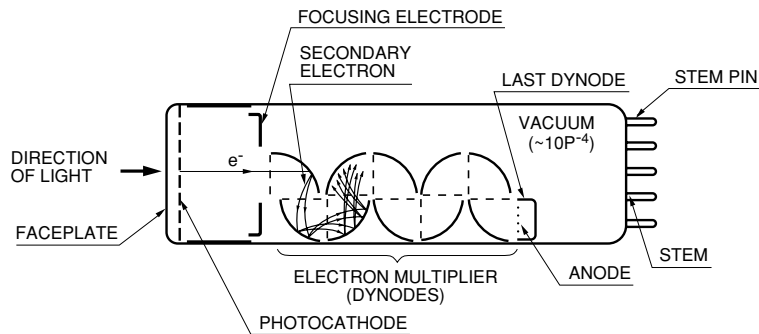
## References in Chapter 1

- 1) Society of Illumination: Lighting Handbook, Ohm-Sha (1987).
- 2) John W. T. WALSH: Photometry, DOVER Publications, Inc. New York
- 3) T. Hiruma: SAMPE Journal, 24, 35 (1988).  
A. H. Sommer: Photoemissive Materials, Robert E. Krieger Publishing Company (1980).
- 4) H. Hertz: Ann. Physik, 31, 983 (1887).
- 5) W. Hallwachs: Ann. Physik, 33, 301 (1888).
- 6) J. Elster and H. Geitel: Ann. Physik, 38, 497 (1889).
- 7) A. Einstein: Ann. Physik, 17, 132 (1905).
- 8) L. Koller: Phys. Rev., 36, 1639 (1930).
- 9) N.R. Campbell: Phil. Mag., 12, 173 (1931).
- 10) P. Gorlich: Z. Physik, 101, 335 (1936).
- 11) A.H. Sommer: U. S. Patent 2,285, 062, Brit. Patent 532,259.
- 12) A.H. Sommer: Rev. Sci. Instr., 26, 725 (1955).
- 13) A.H. Sommer: Appl. Phys. Letters, 3, 62 (1963).
- 14) A.N. Arsenova-Geil and A. A. Kask: Soviet Phys.- Solid State, 7, 952 (1965).
- 15) A.N. Arsenova-Geil and Wang Pao-Kun: Soviet Phys.- Solid State, 3, 2632 (1962).
- 16) D.J. Haneman: Phys. Chem. Solids, 11, 205 (1959).
- 17) G.W. Gobeli and F.G. Allen: Phys. Rev., 137, 245A (1965).
- 18) D.G. Fisher, R.E. Enstrom, J.S. Escher, H.F. Gossenberger: IEEE Trans. Elect. Devices, Vol ED-21, No.10, 641(1974).
- 19) C.A. Sanford and N.C. Macdonald: J. Vac. Sci. Technol. B8(6), Nov/Dec 1853(1990).
- 20) D.G. Fisher and G.H. Olsen: J. Appl. Phys. 50(4), 2930 (1979).
- 21) J.L. Bradshaw, W.J. Choyke and R.P. Devaty: J. Appl. Phys. 67(3), 1, 1483 (1990).
- 22) H. Bruining: Physics and applications of secondary electron emission, McGraw-Hill Book Co., Inc. (1954).
- 23) H.E. Iams and B. Salzberg: Proc. IRE, 23, 55(1935).
- 24) V.K. Zworykin, G.A. Morton, and L. Malter: Proc. IRE, 24, 351 (1936).
- 25) V.K. Zworykin and J. A. Rajchman: Proc. IRE, 27, 558 (1939).
- 26) G.A. Morton: RCA Rev., 10, 529 (1949).
- 27) G.A. Morton: IRE Trans. Nucl. Sci., 3, 122 (1956).
- 28) Heroux, L. and H.E. Hinteregger: Rev. Sci. Instr., 31, 280 (1960).
- 29) E.J. Sternglass: Rev. Sci. Instr., 26, 1202 (1955).
- 30) J.R. Young: J. Appl. Phys., 28, 512 (1957).
- 31) H. Dormont and P. Saget: J. Phys. Radium (Physique Appliquee), 20, 23A (1959).
- 32) G.W. Goodrich and W.C. Wiley: Rev. Sci. Instr., 33, 761 (1962).

## CHAPTER 2

# BASIC PRINCIPLES OF PHOTOMULTIPLIER TUBES 1)-5)

A photomultiplier tube is a vacuum tube consisting of an input window, a photocathode, focusing electrodes, an electron multiplier and an anode usually sealed into an evacuated glass tube. Figure 2-1 shows the schematic construction of a photomultiplier tube.



THBV3\_0201EA

**Figure 2-1: Construction of a photomultiplier tube**

Light which enters a photomultiplier tube is detected and produces an output signal through the following processes.

- (1) Light passes through the input window.
- (2) Light excites the electrons in the photocathode so that photoelectrons are emitted into the vacuum (external photoelectric effect).
- (3) Photoelectrons are accelerated and focused by the focusing electrode onto the first dynode where they are multiplied by means of secondary electron emission. This secondary emission is repeated at each of the successive dynodes.
- (4) The multiplied secondary electrons emitted from the last dynode are finally collected by the anode.

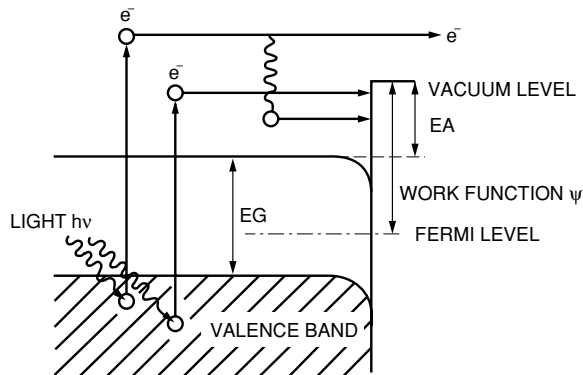
This chapter describes the principles of photoelectron emission, electron trajectory, and the design and function of electron multipliers. The electron multipliers used for photomultiplier tubes are classified into two types: normal discrete dynodes consisting of multiple stages and continuous dynodes such as microchannel plates. Since both types of dynodes differ considerably in operating principle, photomultiplier tubes using microchannel plates (MCP-PMTs) are separately described in Chapter 10. Furthermore, electron multipliers for various particle beams and ion detectors are discussed in Chapter 12.

## 2.1 Photoelectron Emission<sup>6) 7)</sup>

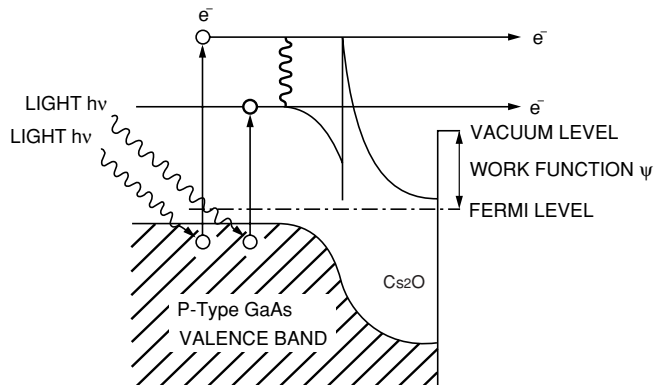
Photoelectric conversion is broadly classified into external photoelectric effects by which photoelectrons are emitted into the vacuum from a material and internal photoelectric effects by which photoelectrons are excited into the conduction band of a material. The photocathode has the former effect and the latter are represented by the photoconductive or photovoltaic effect.

Since a photocathode is a semiconductor, it can be described using band models as shown in Figure 2-2: (1) alkali photocathode and (2) III-V compound semiconductor photocathode.

(1) ALKALI PHOTOCATHODE



(2) III-V SEMICONDUCTOR PHOTOCATHODE



THBV3\_0202EA

Figure 2-2: Photocathode band models

In a semiconductor band model, there exist a forbidden-band gap or energy gap (EG) that cannot be occupied by electrons, electron affinity (EA) which is an interval between the conduction band and the vacuum level barrier (vacuum level), and work function ( $\psi$ ) which is an energy difference between the Fermi level and the vacuum level. When photons strike a photocathode, electrons in the valence band absorb photon energy ( $h\nu$ ) and become excited, diffusing toward the photocathode surface. If the diffused electrons have enough energy to overcome the vacuum level barrier, they are emitted into the vacuum as photoelectrons. This can be expressed in a probability process, and the quantum efficiency  $\eta(\nu)$ , i.e., the ratio of output electrons to incident photons is given by

$$\eta(\nu) = (1-R) \frac{P_v}{k} \cdot \left( \frac{1}{1+1/kL} \right) \cdot P_s$$

where

R : reflection coefficient

k : full absorption coefficient of photons

$P_v$  : probability that light absorption may excite electrons to a level greater than the vacuum level

L : mean escape length of excited electrons

$P_s$  : probability that electrons reaching the photocathode surface may be released into the vacuum

$\nu$  : frequency of light

In the above equation, if we have chosen an appropriate material which determines parameters R, k and  $P_v$ , the factors that dominate the quantum efficiency will be L (mean escape length of excited electrons) and  $P_s$  (probability that electrons may be emitted into the vacuum). L becomes longer by use of a better crystal and  $P_s$  greatly depends on electron affinity (EA).

Figure 2-2 (2) shows the band model of a photocathode using III-V compound semiconductors.<sup>8)-10)</sup> If a surface layer of electropositive material such as  $\text{Cs}_2\text{O}$  is applied to this photocathode, a depletion layer is formed, causing the band structure to be bent downward. This bending can make the electron affinity negative. This state is called NEA (negative electron affinity). The NEA effect increases the probability ( $P_s$ ) that the electrons reaching the photocathode surface may be emitted into the vacuum. In particular, it enhances the quantum efficiency at long wavelengths with lower excitation energy. In addition, it lengthens the mean escape distance (L) of excited electrons due to the depletion layer.

Photocathodes can be classified by photoelectron emission process into a reflection mode and a transmission mode. The reflection mode photocathode is usually formed on a metal plate, and photoelectrons are emitted in the opposite direction of the incident light. The transmission mode photocathode is usually deposited as a thin film on a glass plate which is optically transparent. Photoelectrons are emitted in the same direction as that of the incident light. (Refer to Figures 2-3, 2-4 and 2-5. ) The reflection mode photocathode is mainly used for the side-on photomultiplier tubes which receive light through the side of the glass bulb, while the transmission mode photocathode is used for the head-on photomultiplier tubes which detect the input light through the end of a cylindrical bulb.

The wavelength of maximum response and long-wavelength cutoff are determined by the combination of alkali metals used for the photocathode and its fabrication process. As an international designation, photocathode sensitivity<sup>11)</sup> as a function of wavelength is registered as an "S" number by the JEDEC (Joint Electron Devices Engineering Council). This "S" number indicates the combination of a photocathode and window material and at present, numbers from S-1 through S-25 have been registered. However, other than S-1, S-11, S-20 and S-25 these numbers are scarcely used. Refer to Chapter 4 for the spectral response characteristics of various photocathodes and window materials.

## 2.2 Electron Trajectory

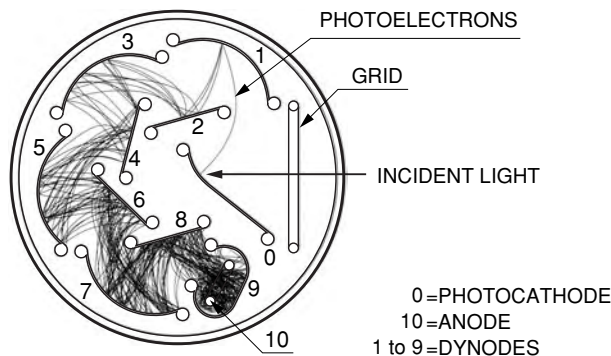
In order to collect photoelectrons and secondary electrons efficiently on a dynode and also to minimize the electron transit time spread, electrode design must be optimized through an analysis of the electron trajectory.<sup>12)-16)</sup>

Electron movement in a photomultiplier tube is influenced by the electric field which is dominated by the electrode configuration, arrangement, and also the voltage applied to the electrode. Numerical analysis of the electron trajectory using high-speed, large-capacity computers have come into use. This method divides the area to be analyzed into a grid-like pattern to give boundary conditions, and obtains an approximation by repeating computations until the error converges to a certain level. By solving the equation for motion based on the potential distribution obtained using this method, the electron trajectory can be predicted.

When designing a photomultiplier tube, the electron trajectory from the photocathode to the first dynode must be carefully designed in consideration of the photocathode shape (planar or spherical window), the shape and arrangement of the focusing electrode and the supply voltage, so that the photoelectrons emitted from the photocathode are efficiently focused onto the first dynode. The collection efficiency of the first dynode is the ratio of the number of electrons landing on the effective area of the first dynode to the number of emitted photoelectrons. This is usually better than 60 to 90 percent. In some applications where the electron transit time needs to be minimized, the electrode should be designed not only for optimum configuration but also for higher electric fields than usual.

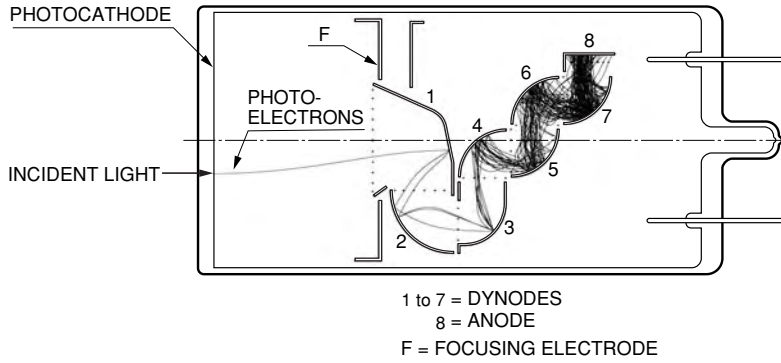
The dynode section is usually constructed from several to more than ten stages of secondary-emissive electrodes (dynodes) having a curved surface. To enhance the collection efficiency of each dynode and minimize the electron transit time spread, the optimum configuration and arrangement should be determined from an analysis of the electron trajectory. The arrangement of the dynodes must be designed in order to prevent ion or light feedback from the latter stages.

In addition, various characteristics of a photomultiplier tube can also be calculated by computer simulation. For example, the collection efficiency, uniformity, and electron transit time can be calculated using a Monte Carlo simulation by setting the initial conditions of photoelectrons and secondary electrons. This allows collective evaluation of photomultiplier tubes. Figures 2-3, 2-4 and 2-5 are cross sections of photomultiplier tubes having a circular-cage, box-and-grid, and linear-focused dynode structures, respectively, showing their typical electron trajectories.



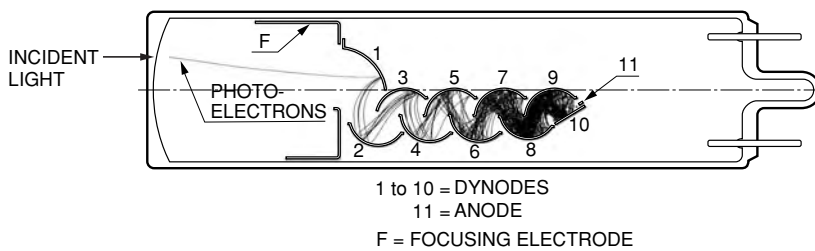
THBV3\_0203EA

Figure 2-3: Circular-cage type



THBV3\_0204EA

Figure 2-4: Box-and-grid type



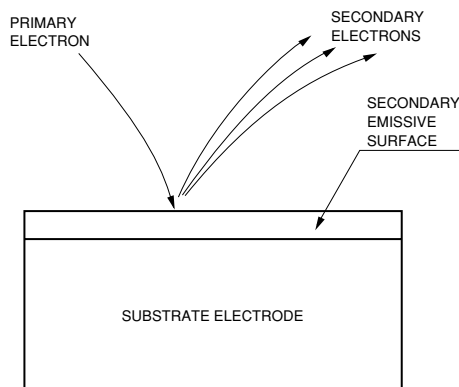
THBV3\_0205EA

Figure 2-5: Linear-focused type

## 2.3 Electron Multiplier (Dynode Section)

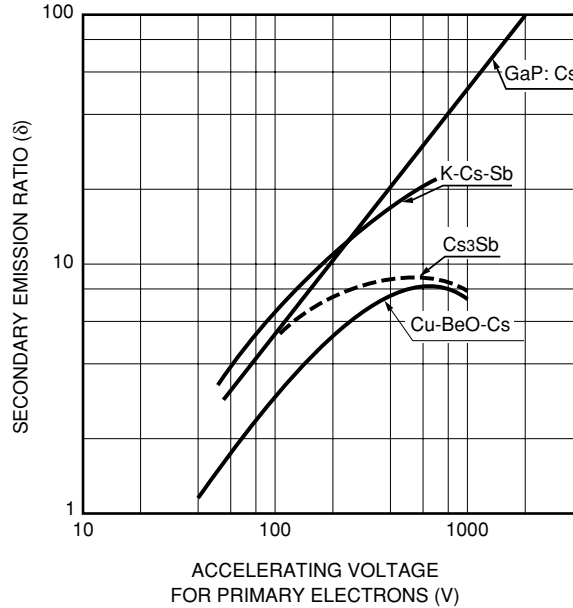
As stated above, the potential distribution and electrode structure of a photomultiplier tube is designed to provide optimum performance. Photoelectrons emitted from the photocathode are multiplied by the first dynode through the last dynode (up to 19 dynodes), with current amplification ranging from 10 to as much as 108 times, and are finally sent to the anode.

Major secondary emissive materials<sup>(17)-21)</sup> used for dynodes are alkali antimonide, beryllium oxide (BeO), magnesium oxide (MgO), gallium phosphide (GaP) and gallium phosphide (GaAsP). These materials are coated onto a substrate electrode made of nickel, stainless steel, or copper-beryllium alloy. Figure 2-6 shows a model of the secondary emission multiplication of a dynode.



THBV3\_0206EA

Figure 2-6: Secondary emission of dynode



THBV3\_0207EA

Figure 2-7: Secondary emission ratio

When a primary electron with initial energy  $E_p$  strikes the surface of a dynode,  $\delta$  secondary electrons are emitted. This  $\delta$ , the number of secondary electrons per primary electron, is called the secondary emission ratio. Figure 2-7 shows the secondary emission ratio  $\delta$  for various dynode materials as a function of the accelerating voltage for the primary electrons.

Ideally, the current amplification or gain of a photomultiplier tube having the number of dynode stages  $n$  and the average secondary emission ratio  $\delta$  per stage will be  $\delta^n$ . Refer to section 4.2.2 in Chapter 4 for more details on the gain.

Because a variety of dynode structures are available and their gain, time response and linearity differ depending on the number of dynode stages and other factors, the optimum dynode type must be selected according to your application. These characteristics are described in Chapter 4, section 4.2.1.

## 2.4 Anode

The anode of a photomultiplier tube is an electrode that collects secondary electrons multiplied in the cascade process through multi-stage dynodes and outputs the electron current to an external circuit.

Anodes are carefully designed to have a structure optimized for the electron trajectories discussed previously. Generally, an anode is fabricated in the form of a rod, plate or mesh electrode. One of the most important factors in designing an anode is that an adequate potential difference can be established between the last dynode and the anode in order to prevent space charge effects and obtain a large output current.



## References in Chapter 2

- 1) Hamamatsu Photonics: "Photomultiplier Tubes and Related Products" (revised Feb. 2006)
- 2) Hamamatsu Photonics: "Characteristics and Uses of Photomultiplier Tubes" No.79-57-03 (1982).
- 3) S.K. Poultney: *Advances in Electronics and Electron Physics* 31, 39 (1972).
- 4) D.H. Seib and L.W. Ankerman: *Advances in Electronics and Electron Physics*, 34, 95 (1973).
- 5) J.P. Boutot, et al.: *Advances in Electronics and Electron Physics* 60, 223 (1983).
- 6) T. Hiruma: *SAMPE Journal*, 24, 6, 35-40 (1988).
- 7) T. Hayashi: *Bunkou Kenkyuu*, 22, 233 (1973).
- 8) H. Sonnenberg: *Appl. Phys. Lett.*, 16, 245 (1970).
- 9) W.E. Spicer, et al.: *Pub. Astrom. Soc. Pacific*, 84, 110 (1972).
- 10) M. Hagino, et al.: *Television Journal*, 32, 670 (1978).
- 11) A. Honma: *Bunseki*, 1, 52 (1982).
- 12) K.J. Van Oostrum: *Philips Technical Review*, 42, 3 (1985).
- 13) K. Oba and Ito: *Advances in Electronics and Electron Physics*, 64B, 343.
- 14) A.M. Yakobson: *Radiotekh & Electron*, 11, 1813 (1966).
- 15) H. Bruining: *Physics and Applications of Secondary Electron Emission*, (1954).
- 16) J. Rodney and M. Vaughan: *IEEE Transaction on Electron Devices*, 36, 9 (1989).
- 17) B. Gross and R. Hessel: *IEEE Transaction on Electrical Insulation*, 26, 1 (1991).
- 18) H.R. Krall, et al.: *IEEE Trans. Nucl. Sci. NS-17*, 71 (1970).
- 19) J.S. Allen: *Rev. Sci. Instr.*, 18 (1947).
- 20) A.M. Tyutikov: *Radio Engineering And Electronic Physics*, 84, 725 (1963).
- 21) A.H. Sommer: *J. Appl. Phys.*, 29, 598 (1958).

# MEMO

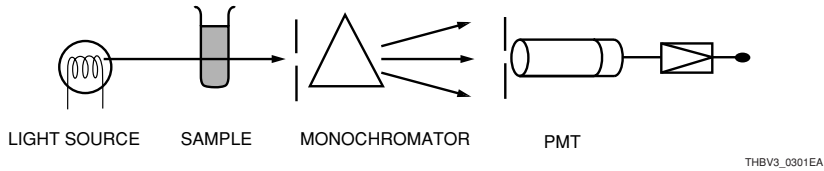
# **CHAPTER 3**

## **BASIC OPERATING METHODS OF PHOTOMULTIPLIER TUBES**

*This section provides the first-time photomultiplier tube users with general information on how to choose the ideal photomultiplier tube (often abbreviated as PMT), how to operate them correctly and how to process the output signals. This section should be referred to as a quick guide. For more details, refer to the following chapters.*

## 3.1 Using Photomultiplier Tubes

### 3.1.1 How to make the proper selection



**Figure 3-1: Atomic absorption application**

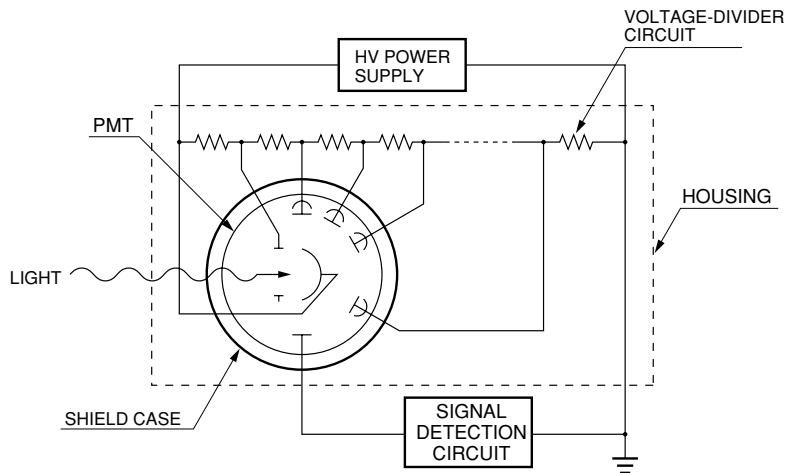
Figure 3-1 shows an application example in which a photomultiplier tube is used in absorption spectroscopy. The following parameters should be taken into account when making a selection.

Incident light conditions	Selection reference	
	<Photomultiplier tubes>	<Circuit Conditions>
Light wavelength	Window material Photocathode spectral response	
Light intensity	Number of dynodes Dynode type Voltage applied to dynodes	Signal processing method (analog or digital method)
Light beam size	Effective diameter (size) Viewing configuration (side-on or head-on)	
Speed of optical phenomenon	Time response	Bandwidth of associated circuit

It is important to know beforehand the conditions of the incident light to be measured. Then, choose a photomultiplier tube that is best suited to detect the incident light and also select the optimum circuit conditions that match the application. Referring to the table above, select the optimum photomultiplier tubes, operating conditions and circuit configurations according to the incident light wavelength, intensity, beam size and the speed of optical phenomenon. More specific information on these parameters and conditions are detailed in Chapter 2 and later chapters.

### 3.1.2 Peripheral devices

As shown in Figure 3-2, operating a photomultiplier tube requires a stable source of high voltage (normally 1 to 2 kilovolts), voltage-divider circuit for distributing an optimum voltage to each dynode, a housing for external light shielding, and sometimes a shield case for protecting the photomultiplier tube from magnetic or electric fields.



THBV3\_0302EA

Figure 3-2: Basic operating method

### High-voltage power supply

A negative or positive high-voltage power supply of one to two kilovolts is usually required to operate a photomultiplier tube. There are two types of power supplies available: modular power supplies like that shown in Figure 3-3 and bench-top power supplies like that shown in Figure 3-4.



C4900  
High voltage output: -1250 V  
Current output: 600  $\mu$ A



C9525  
High voltage output: -2000 V  
Current output: 2 mA

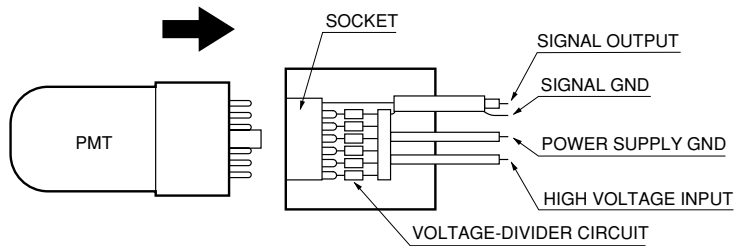
Figure 3-3: Modular high-voltage power supply      Figure 3-4: Bench-top high-voltage power supply

Since the gain of photomultiplier tubes is extremely high, they are very susceptible to variations in the high-voltage power supply. If the output stability of a photomultiplier tube should be maintained within one percent, the power supply stability must be held within 0.1 percent.

### Voltage-divider circuit

Supply voltage must be distributed to each dynode. For this purpose, a voltage-divider circuit is usually used to divide the high voltage and provide a proper voltage gradient between each dynode. To allow easy operation of photomultiplier tubes, Hamamatsu provides socket assemblies that incorporate a photomultiplier tube socket and a matched divider circuit as shown in Figures 3-5 to 3-8.

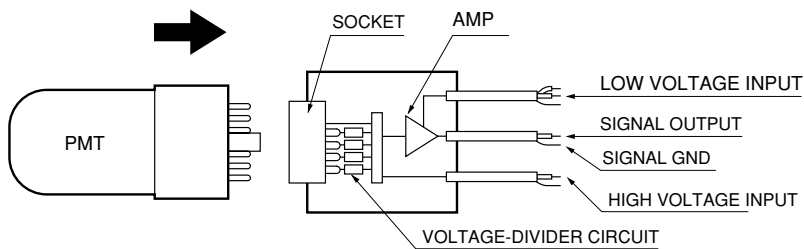
- (1) D-type socket assembly with built-in divider circuit



THBV3\_0305EA

Figure 3-5: D-type socket assembly

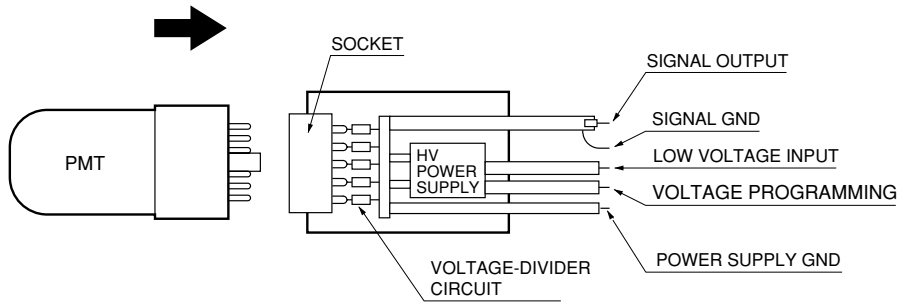
- (2) DA-type socket assembly with built-in divider circuit and amplifier



THBV3\_0306EA

Figure 3-6: DA-type socket assembly

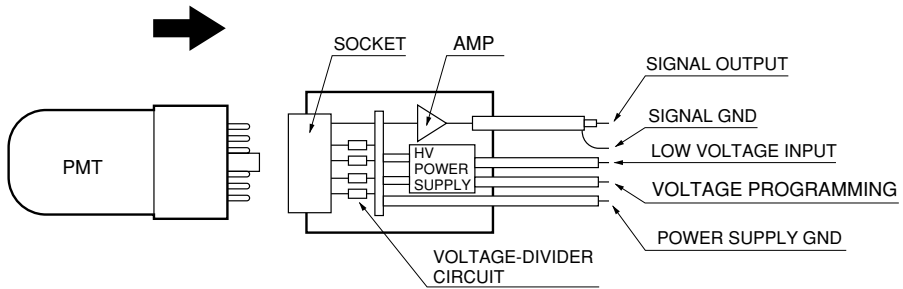
(3) DP-type socket assembly with built-in voltage divider and power supply



THBV3\_0307EA

Figure 3-7: DP-type socket assembly

(4) DAP-type socket assembly with built-in voltage divider, amplifier and power supply



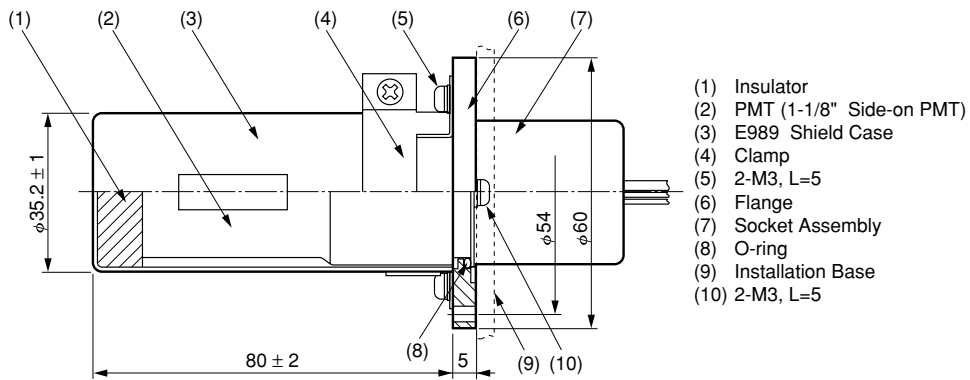
THBV3\_0308EA

Figure 3-8: DAP-type socket assembly

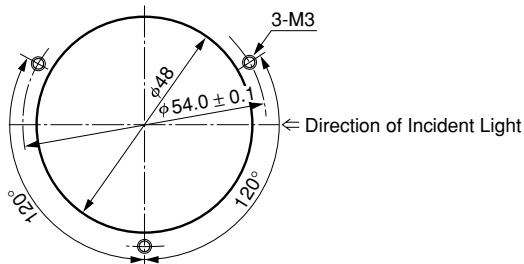
## Housing

Since photomultiplier tubes have very high sensitivity, they may detect extraneous light other than the light to be measured. This decreases the signal-to-noise ratio, so a housing is required for external light shielding.

Photomultiplier tube characteristics may vary with external electromagnetic fields, ambient temperature, humidity, or mechanical stress applied to the photomultiplier tube. For this reason, a magnetic or electric shield is also required to protect the photomultiplier tube from such adverse environmental factors. Moreover, a cooled housing is sometimes used to maintain the photomultiplier tube at a constant temperature or at a low temperature for more stable operation.



[Flange Fastening Positions to Installation Base]



THBV3\_0309EA

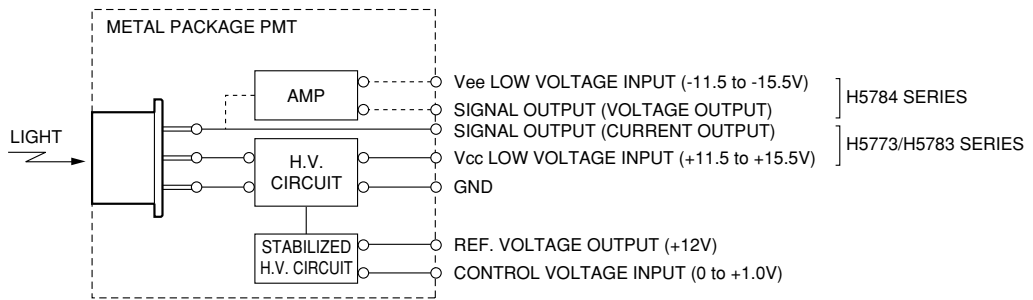
Figure 3-9: Housing example (with built-in magnetic shield case)



## Integral power supply module

To make the use of photomultiplier tubes as easy as possible, Hamamatsu Photonics provides PMT modules which incorporate a photomultiplier tube in a compact case, along with all the necessary components such as a high-voltage power supply and operating circuit. (Figure 3-10)

PMT modules are easy to handle since they operate by supplying only low voltage, making the equipment compact and simple to use.



THBV3\_0310EA



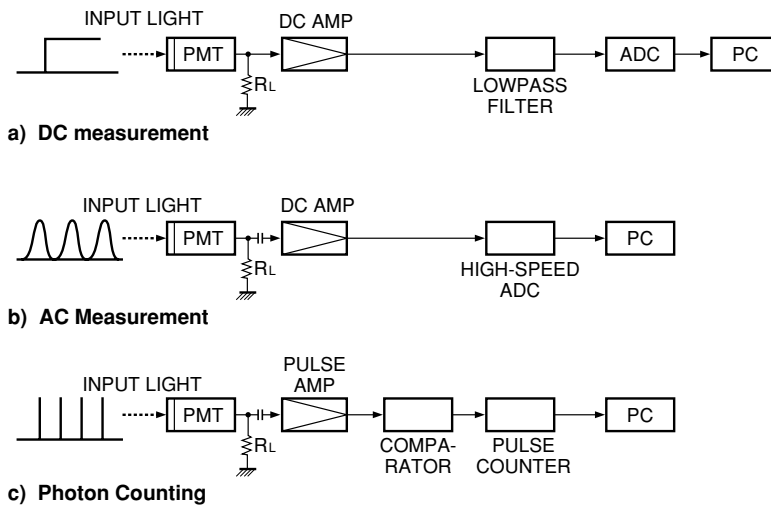
Figure 3-10: Structure of an integral power supply module

Various types of PMT modules are available, including those that have internal gate circuits, photon counting circuits or modulation circuits. Refer to Chapter 8 for detailed information.

### 3.1.3 Operating methods (connection circuits)

The output from a photomultiplier tube can be processed electrically as a constant current source. It is best, however, to connect it to an optimum circuit depending on the incident light and frequency characteristics required. Figure 3-11 shows typical light measurement circuits which are commonly used. The DC method and AC method (analog method) are mainly used in rather high light levels to moderate light levels. At very low light levels, the photon counting method is most effective. In this method, light is measured by counting individual photons which are the smallest unit of light.

The DC method shown in Figure 3-11 (a) detects DC components in the photomultiplier tube output by means of an amplifier and a lowpass filter. This method is suited for detection of relatively high light levels and has been widely used. The AC method shown in (b) extracts only AC components from the photomultiplier tube output via a capacitor and converts them into digital signals by using an AD converter. This method is used in regions where modulated light or light intensity is low and the AC components are predominant in the output signal over the DC components. In the photon counting method shown in (c), the output pulses from the photomultiplier tube are amplified and only the pulses with an amplitude higher than the preset discrimination pulse height are counted as photon signals. This method allows observation of discrete output pulses from the photomultiplier tube, and is the most effective technique in detecting very low light levels. Other measurement methods include a lock-in detection technique using an optical chopper, which features low noise and is used for detecting low-light-level signals.



THBV3\_0311EA

Figure 3-11: Light measurement methods using PMT

These light measurement methods using a photomultiplier tube and the connection circuit must be optimized according to the intensity of incident light and the speed of the event to be detected. In particular, when the incident light is very low and the resultant signal is small, consideration must be given to minimize the influence of noise in the succeeding circuits. As stated, the lock-in detection technique and photon counting method are more effective than the DC method in detecting low level light. When the incident light to be detected changes in a very short period, the connected circuit should be designed for a wider frequency bandwidth as well as using a fast response photomultiplier tube. Additionally, impedance matching at high frequencies must also be taken into account. Refer to Chapters 5 and 6 for more details on these precautions.

# **CHAPTER 4**

## **CHARACTERISTICS OF PHOTOMULTIPLIER TUBES**

*This chapter details various characteristics of photomultiplier tubes, including basic and performance. For example, section 4.1 shows spectral response characteristics of typical photocathodes and also gives the definition of photocathode sensitivity and its measurement procedure. Section 4.2 explains dynode types, structures and typical characteristics. Section 4.3 describes various performance characteristics such as time response, operating stability, sensitivity, uniformity, and signal-to-noise ratio as well as their definitions, measurement procedures and specific product examples. It also provides precautions and suggestions for use.*

## 4.1 Basic Characteristics of Photocathodes

This section introduces photocathodes and window materials which have been used in practical applications from the past to the present and also explains the terms used to define photocathodes such as quantum efficiency, radiant sensitivity, and luminous sensitivity.

### 4.1.1 Photocathode materials

Most photocathodes<sup>1)-15)</sup> are made of compound semiconductors which consist of alkali metals with a low work function. There are approximately ten kinds of photocathodes currently employed in practical applications. Each photocathode is available as a transmission (semitransparent) type or a reflection (opaque) type, with different device characteristics. In the early 1940's, the JEDEC (Joint Electron Devices Engineering Council) introduced the "S number" to designate photocathode spectral response which is classified by the combination of the photocathode and window material. Presently, since many photocathode and window materials are available, the "S number" is no longer frequently used except for S-1, S-20, etc. The photocathode spectral response is instead expressed in terms of material type. The photocathode materials commonly used in photomultiplier tubes are as follows.

#### (1) Cs-I

Cs-I is not sensitive to solar radiation and therefore often called "solar blind". Its sensitivity sharply falls off at wavelengths longer than 200 nanometers and it is exclusively used for vacuum ultraviolet detection. As a window material, MgF<sub>2</sub> crystals or synthetic silica are used because of high ultraviolet transmittance. Although Cs-I itself has high sensitivity to wavelengths shorter than 115 nanometers, the MgF<sub>2</sub> crystal used for the input window does not transmit wavelengths shorter than 115 nanometers.

To measure light with wavelengths shorter than 115 nanometers, an electron multiplier having a first dynode on which Cs-I is deposited is often used with the input window removed (in a vacuum).

#### (2) Cs-Te

Cs-Te is not sensitive to wavelengths longer than 300 nanometers and is also called "solar blind" just as with Cs-I. With Cs-Te, the transmission type and reflection type show the same spectral response range, but the reflection type exhibits higher sensitivity than the transmission type. Synthetic silica or MgF<sub>2</sub> is usually used for the input window.

#### (3) Sb-Cs

This photocathode has sensitivity in the ultraviolet to visible range, and is widely used in many applications. Because the resistance of the Sb-Cs photocathode is lower than that of the bialkali photocathode described later on, it is suited for applications where light intensity to be measured is relatively high so that a large current can flow in the cathode. Sb-Cs is also suitable for applications where the photocathode is cooled so its resistance becomes larger and causes problems with the dynamic range. Sb-Cs is chiefly used for reflection type photocathode.

#### (4) Bialkali (Sb-Rb-Cs, Sb-K-Cs)

Since two kinds of alkali metals are employed, these photocathodes are called "bialkali". The transmission type of these photocathodes has a spectral response range similar to the Sb-Cs photocathode, but has higher sensitivity and lower dark current. It also provides sensitivity that matches the emission of a NaI(Tl) scintillator, thus being widely used for scintillation counting in radiation measurements. On the other hand, the reflection-type bialkali photocathodes are fabricated by using the same materials, but different processing. As a result, they offer enhanced sensitivity on the long wavelength side, achieving a spectral response from the ultraviolet region to around 700 nanometers.

**(5) High temperature, low noise bialkali (Sb-Na-K)**

As with bialkali photocathodes, two kinds of alkali metals are used in this photocathode type. The spectral response range is almost identical to that of bialkali photocathodes, but the sensitivity is somewhat lower. This photocathode can withstand operating temperatures up to 175°C while other normal photocathodes are guaranteed to no higher than 50°C. For this reason, it is ideally suited for use in oil well logging where photomultiplier tubes are often subjected to high temperatures. In addition, when used at room temperatures, this photocathode exhibits very low dark current, which makes it very useful in low-level light measurement such as photon counting applications where low noise is a prerequisite.

**(6) Multialkali (Sb-Na-K-Cs)**

This photocathode uses three or more kinds of alkali metals. Due to high sensitivity over a wide spectral response range from the ultraviolet through near infrared region around 850 nanometers, this photocathode is widely used in broad-band spectrophotometers. Hamamatsu also provides a multialkali photocathode with long wavelength response extending out to 900 nanometers, which is especially useful in the detection of gas phase chemiluminescence in NO<sub>x</sub>, etc.

**(7) Ag-O-Cs**

Transmission type photocathodes using this material are sensitive from the visible through near infrared region, from 400 to 1200 nanometers, while the reflection type exhibits a slightly narrower spectral response region from 300 to 1100 nanometers. Compared to other photocathodes, this photocathode has lower sensitivity in the visible region, but it also provides sensitivity at longer wavelengths in the near infrared region. So both transmission and reflection type Ag-O-Cs photocathodes are chiefly used for near infrared detection.

**(8) GaAsP (Cs)**

A GaAsP crystal activated with cesium is used as a transmission type photocathode. This photocathode does not have sensitivity in the ultraviolet region but has a very high quantum efficiency in the visible region. Note that if exposed to incident light with high intensity, sensitivity degradation is more likely to occur when compared with other photocathodes composed of alkali metals.

**(9) GaAs (Cs)**

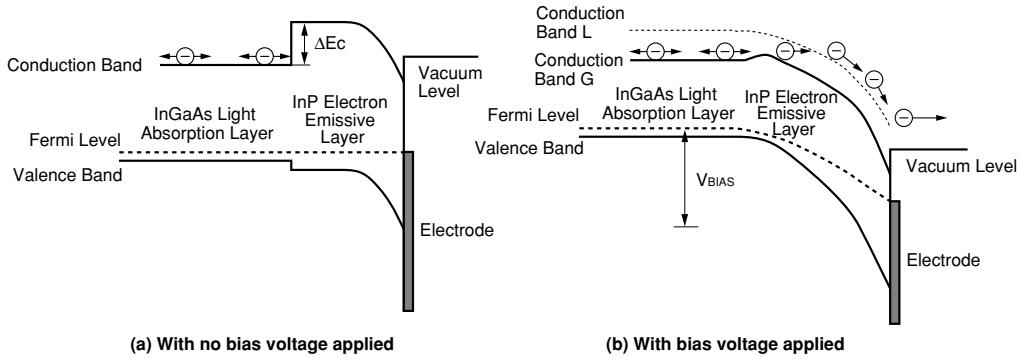
A GaAs crystal activated with cesium is used for both reflection type and transmission type photocathodes. The reflection type GaAs(Cs) photocathode has sensitivity across a wide range from the ultraviolet through near infrared region around 900 nanometers. It demonstrates a nearly flat, high-sensitivity spectral response curve from 300 and 850 nanometers. The transmission type has a narrower spectral response range because shorter wavelengths are absorbed. It should be noted that if exposed to incident light with high intensity, these photocathodes tend to suffer sensitivity degradation when compared with other photocathodes primarily composed of alkali metals.

**(10) InGaAs (Cs)**

This photocathode provides a spectral response extending further into the infrared region than the GaAs photocathode. Additionally, it offers a superior signal-to-noise ratio in the neighborhood of 900 to 1000 nanometers in comparison with the Ag-O-Cs photocathode.

**(11) InP/InGaAsP(Cs), InP/InGaAs(Cs)**

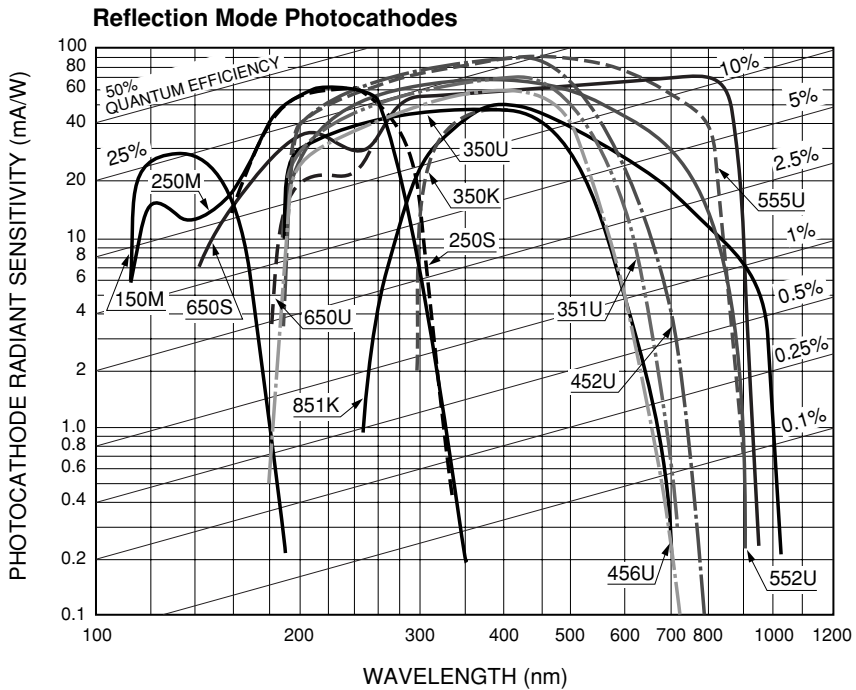
These are field-assisted photocathodes utilizing a PN junction formed by growing InP/InGaAsP or InP/InGaAs on an InP substrate. These photocathodes were developed by our own in-house semiconductor microprocess technology.<sup>16) 17)</sup> Applying a bias voltage to this photocathode lowers the conduction band barrier, and allows for higher sensitivity at long wavelengths extending to 1.4 μm or even 1.7 μm which have up till now been impossible to detect with a photomultiplier tube. Since these photocathodes produce large amounts of dark current when used at room temperatures, they must be cooled to between -60°C to -80°C during operation. The band model of these photocathodes is shown in Figure 4-1.



THBV3\_0401EA

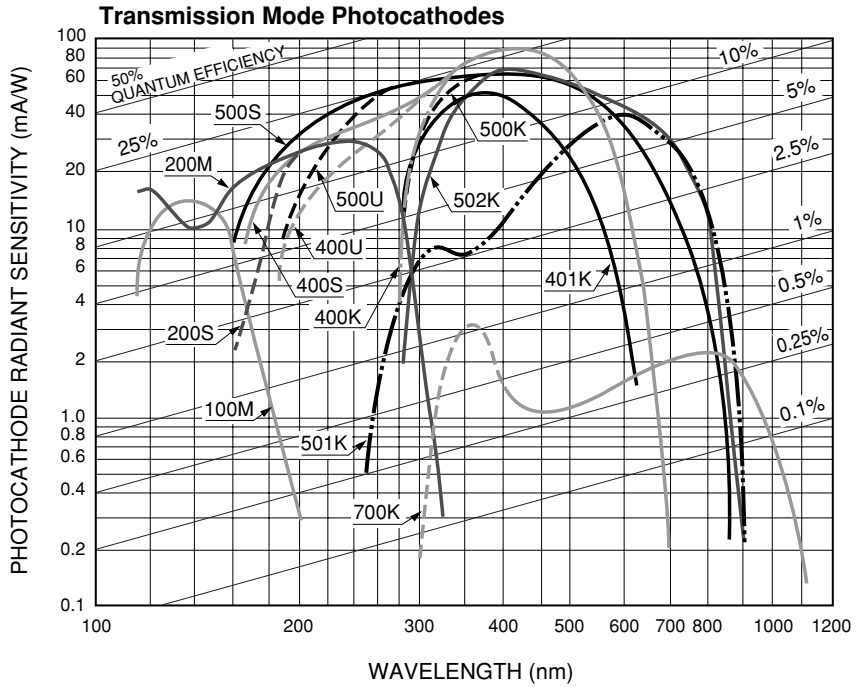
Figure 4-1: Band model

Typical spectral response characteristics of major photocathodes are illustrated in Figures 4-2 and 4-3 and Table 4-1. The JEDEC "S numbers" frequently used are also listed in Table 4-1. The definition of photocathode radiant sensitivity expressed in the ordinate of the figures is explained in section 4.1.3, "Spectral response characteristics". Note that Figures 4-2 and 4-3 and Table 4-1 only show typical characteristics and actual data may differ from tube to tube.



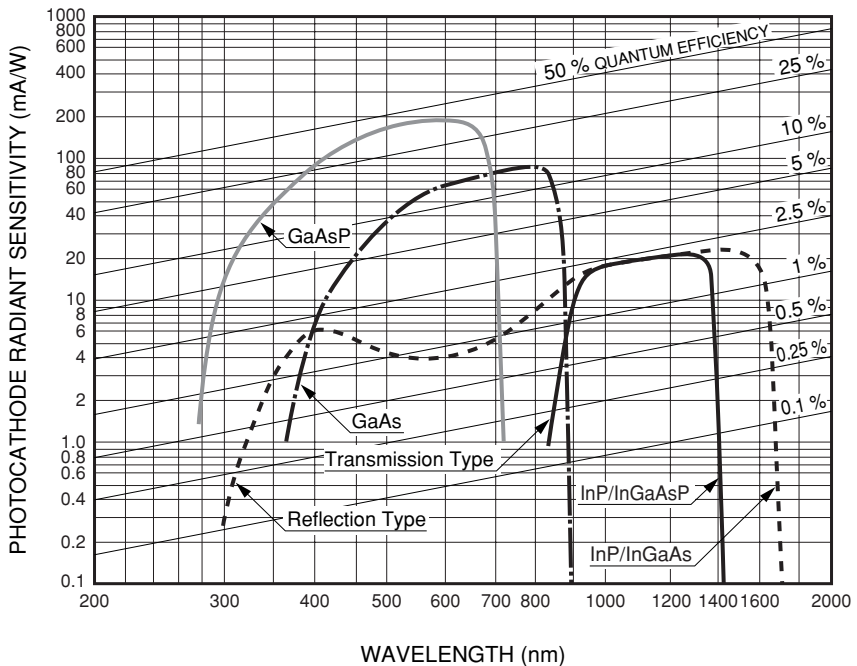
THBV3\_0402EAa

Figure 4-2 (a): Typical spectral response characteristics of reflection mode photocathodes



THBV3\_0402Eb

Figure 4-2 (b): Typical spectral response characteristics of transmission mode photocathodes



THBV3\_0403EA

Figure 4-3: Typical spectral response characteristics of semiconductor crystal photocathodes

**Reflection mode photocathodes**

Curve Code (S number)	Photocathode Material	Window Material	Luminous Sensitivity (Typ.) ( $\mu\text{A/lm}$ )	Spectral Response				
				Spectral Range (nm)	Peak Wavelength			
					Radiant Sensitivity		Quantum Efficiency	
					(mA/W)	(nm)	(%)	(nm)
150M	Cs-I	MgF <sub>2</sub>	—	115 to 200	25.5	135	26	125
250S	Cs-Te	Quartz	—	160 to 320	62	240	37	210
250M	Cs-Te	MgF <sub>2</sub>	—	115 to 320	63	220	35	220
350K (S-4)	Sb-Cs	Borosilicate	40	300 to 650	48	400	15	350
350U (S-5)	Sb-Cs	UV	40	185 to 650	48	340	20	280
351U (Extd S-5)	Sb-Cs	UV	70	185 to 750	70	410	25	280
452U	Bialkali	UV	120	185 to 750	90	420	30	260
456U	Low dark bialkali	UV	60	185 to 680	60	400	19	300
552U	Multialkali	UV	200	185 to 900	68	400	26	260
555U	Multialkali	UV	525	185 to 900	90	450	30	260
650U	GaAs(Cs)	UV	550	185 to 930	62	300 to 800	23	300
650S	GaAs(Cs)	Quartz	550	160 to 930	62	300 to 800	23	300
851K	InGaAs(Cs)	Borosilicate	150	300 to 1040	50	400	16	370
—	InP/InGaAsP(Cs)	Borosilicate	—	300 to 1400	10	1250	1.0	1000 to 1200
—	InP/InGaAs(Cs)	Borosilicate	—	300 to 1700	10	1550	1.0	1000 to 1200

**Table 4-1: Quick reference for typical spectral response characteristics (1)**



**Transmission mode photocathodes**

Curve Code (S number)	Photocathode Material	Window Material	Luminous Sensitivity (Typ.) ( $\mu\text{A/lm}$ )	Spectral Response				
				Spectral Range (nm)	Peak Wavelength			
					Radiant Sensitivity		Quantum Efficiency	
					(mA/W)	(nm)	(%)	(nm)
100M	Cs-I	MgF <sub>2</sub>	—	115 to 200	14	140	13	130
200S	Cs-Te	Quartz	—	160 to 320	29	240	14	210
200M	Cs-Te	MgF <sub>2</sub>	—	115 to 320	29	240	14	200
400K	Bialkali	Borosilicate	95	300 to 650	88	420	27	390
400U	Bialkali	UV	95	185 to 650	88	420	27	390
400S	Bialkali	Quartz	95	160 to 650	88	420	27	390
401K	High temp. bialkali	Borosilicate	40	300 to 650	51	375	17	375
500K (S-20)	Multialkali	Borosilicate	150	300 to 850	64	420	20	375
500U	Multialkali	UV	150	185 to 850	64	420	25	280
500S	Multialkali	Quartz	150	160 to 850	64	420	25	280
501K (S-25)	Multialkali	Borosilicate	200	300 to 900	40	600	8	580
502K	Multialkali	Borosilicate (prism)	230	300 to 900	69	420	20	390
700K (S-1)	Ag-O-Cs	Borosilicate	20	400 to 1200	2.2	800	0.36	740
—	GaAsP(Cs)	—	—	300 to 720	180	580	40	540
—	GaAs(Cs)	—	—	380 to 890	85	800	14	760
—	InP/InGaAsP(Cs)	—	—	950 to 1400	21	1300	2.0	1000 to 1300
—	InP/InGaAs(Cs)	—	—	950 to 1700	24	1500	2.0	1000 to 1550

**Table 4-1: Quick reference for typical spectral response characteristics (2)**

### 4.1.2 Window materials

As stated in the previous section, most photocathodes have high sensitivity down to the ultraviolet region. However, because ultraviolet radiation tends to be absorbed by the window material, the short wavelength limit is determined by the ultraviolet transmittance of the window material.<sup>18)-22)</sup> The window materials commonly used in photomultiplier tubes are as follows:

#### (1) $\text{MgF}_2$ crystal

The crystals of alkali halide are superior in transmitting ultraviolet radiation, but have the disadvantage of deliquescence. A magnesium fluoride ( $\text{MgF}_2$ ) crystal is used as a practical window material because it offers very low deliquescence and allows transmission of vacuum ultraviolet radiation down to 115 nanometers.

#### (2) Sapphire

Sapphire is made of  $\text{Al}_2\text{O}_3$  crystal and shows an intermediate transmittance between the UV-transmitting glass and synthetic silica in the ultraviolet region. Sapphire glass has a short wavelength cutoff in the neighborhood of 150 nanometers, which is slightly shorter than that of synthetic silica.

#### (3) Synthetic silica

Synthetic silica transmits ultraviolet radiation down to 160 nanometers and in comparison to fused silica, offers lower levels of absorption in the ultraviolet region. Since silica has a thermal expansion coefficient greatly different from that of the Kovar alloy used for the stem pins (leads) of photomultiplier tubes, it is not suited for use as the bulb stem. As a result, a borosilicate glass is used for the bulb stem and then a graded seal, using glasses with gradually changing thermal expansion coefficient, is connected to the synthetic silica bulb, as shown in Figure 4-4. Because of this structure, the graded seal is very fragile and proper care should be taken when handling the tube. In addition, helium gas may permeate through the silica bulb and cause an increase in noise. Avoid operating or storing such tubes in environments where helium is present.

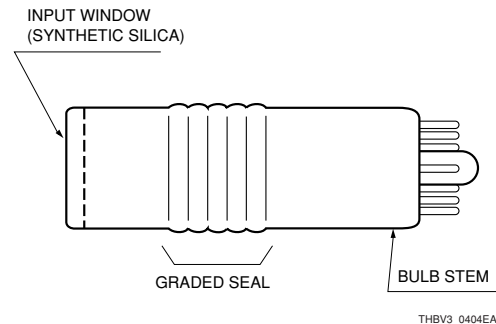


Figure 4-4: Grated seal

#### (4) UV glass (UV-transmitting glass)

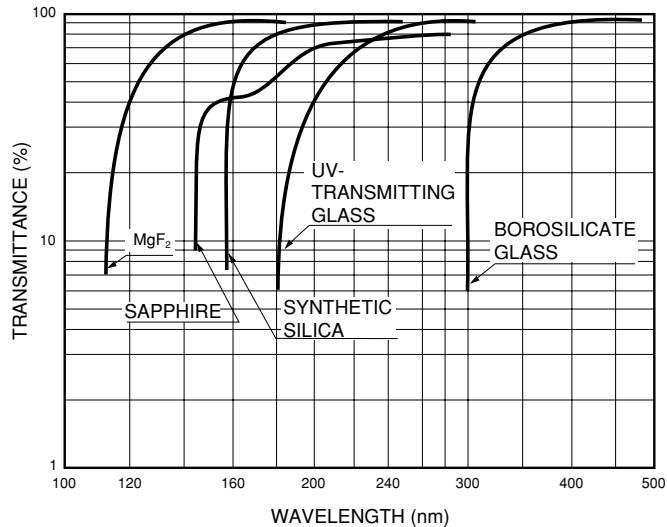
As the name implies, this transmits ultraviolet radiation well. The short wavelength cutoff of the UV glass extends to 185 nanometers.

#### (5) Borosilicate glass

This is the most commonly used window material. Because the borosilicate glass has a thermal expansion coefficient very close to that of the Kovar alloy which is used for the leads of photomultiplier tubes, it is often called "Kovar glass". The borosilicate glass does not transmit ultraviolet radiation shorter than 300 nanometers. It is not suited for ultraviolet detection shorter than this wavelength. Moreover, some types of head-on photomultiplier tubes using a bialkali photocathode employ a special borosilicate glass (so-called "K-free glass") containing a very small amount of potassium ( $\text{K}^{40}$ ) which may cause unwanted background counts. The K-free glass is mainly used for photomultiplier tubes designed for scintillation counting where

low background counts are desirable. For more details on background noise caused by  $K^{40}$ , refer to section 4.3.6, "Dark current".

Spectral transmittance characteristics of various window materials are shown in Figure 4-5.



THBV3\_0405EA

Figure 4-5: Spectral transmittance of window materials

### 4.1.3 Spectral response characteristics

The photocathode of a photomultiplier converts the energy of incident photons into photoelectrons. The conversion efficiency (photocathode sensitivity) varies with the incident light wavelength. This relationship between the photocathode and the incident light wavelength is referred to as the spectral response characteristics. In general, the spectral response characteristics are expressed in terms of radiant sensitivity and quantum efficiency.

#### (1) Radiant sensitivity

Radiant sensitivity is defined as the photoelectric current generated by the photocathode divided by the incident radiant flux at a given wavelength, expressed in units of amperes per watts (A/W). Furthermore, relative spectral response characteristics in which the maximum radiant sensitivity is normalized to 100% are also conveniently used.

#### (2) Quantum efficiency

Quantum efficiency is the number of photoelectrons emitted from the photocathode divided by the number of incident photons. Quantum efficiency is symbolized by  $\eta$  and is generally expressed as a percent. Incident photons transfer energy to electrons in the valence band of a photocathode, however not all of these electrons are emitted as photoelectrons. This photoemission takes place according to a certain probability process. Photons at shorter wavelengths carry higher energy compared to those at longer wavelengths and contribute to an increase in the photoemission probability. As a result, the maximum quantum efficiency occurs at a wavelength slightly shorter the wavelength of peak radiant sensitivity.

### (3) Measurement and calculation of spectral response characteristics

To measure radiant sensitivity and quantum efficiency, a standard phototube or semiconductor detector which is precisely calibrated is used as a secondary standard. At first, the incident radiant flux  $L_p$  at the wavelength of interest is measured with the standard phototube or semiconductor detector. Next, the photomultiplier tube to be measured is set in place and the photocurrent  $I_k$  is measured. Then the radiant sensitivity  $S_k$  (A/W) of the photomultiplier tube can be calculated from the following equation:

$$S_k = \frac{I_k}{L_p} \text{ (A/W)} \dots\dots\dots \text{ (Eq. 4-1)}$$

The quantum efficiency  $\eta$  can be obtained from  $S_k$  using the following equation:

$$\eta(\%) = \frac{h \cdot c}{\lambda \cdot e} \cdot S_k = \frac{1240}{\lambda} \cdot S_k \cdot 100\% \dots\dots\dots \text{ (Eq. 4-2)}$$

$$h : 6.63 \times 10^{-34} \text{ J}\cdot\text{s}$$

$$c : 3.00 \times 10^8 \text{ m}\cdot\text{s}^{-1}$$

$$e : 1.6 \times 10^{-19} \text{ C}$$

where  $h$  is Planck's constant,  $\lambda$  is the wavelength of incident light (nanometers),  $c$  is the velocity of light in vacuum and  $e$  is the electron charge. The quantum efficiency  $\eta$  is expressed in percent.

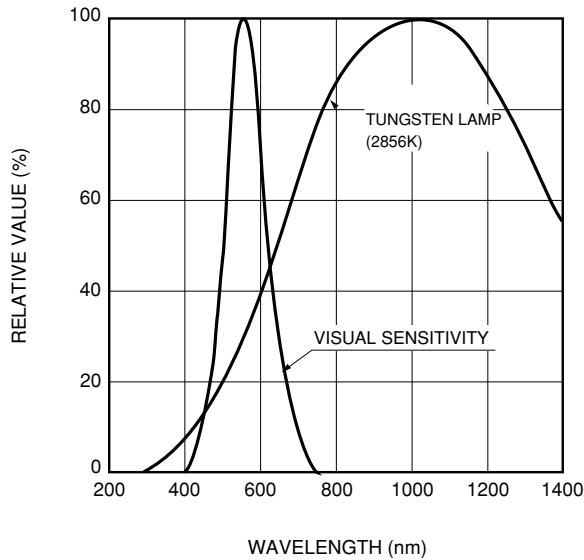
### (4) Spectral response range (short and long wavelength limits)

The wavelength at which the spectral response drops on the short wavelength side is called the short wavelength limit or cutoff while the wavelength at which the spectral response drops on the long wavelength side is called the long wavelength limit or cutoff. The short wavelength limit is determined by the window material, while the long wavelength limit depends on the photocathode material. The range between the short wavelength limit and the long wavelength limit is called the spectral response range.

In this handbook, the short wavelength limit is defined as the wavelength at which the incident light is abruptly absorbed by the window material. The long wavelength limit is defined as the wavelength at which the photocathode sensitivity falls to 1 percent of the maximum sensitivity for alkali and Ag-O-Cs photocathodes and 0.1 percent of the maximum sensitivity for multialkali photocathodes. However, these wavelength limits will depend on the actual operating conditions such as the amount of incident light, photocathode sensitivity, dark current and signal-to-noise ratio of the measurement system.

#### 4.1.4 Luminous sensitivity

The spectral response measurement of a photomultiplier tube requires an expensive, sophisticated system and also takes much time. It is therefore more practical to evaluate the sensitivity of common photomultiplier tubes in terms of luminous sensitivity. The illuminance on a surface one meter away from a point light source of one candela (cd) is one lux. One lumen equals the luminous flux of one lux passing an area of one square meter. Luminous sensitivity is the output current obtained from the cathode or anode divided by the incident luminous flux (lumen) from a tungsten lamp at a distribution temperature of 2856K. In some cases, a visual-compensation filter is interposed between the photomultiplier tube and the light source, but in most cases it is omitted. Figure 4-6 shows the visual sensitivity and relative spectral distribution of a 2856K tungsten lamp.



THBV3\_0406EA

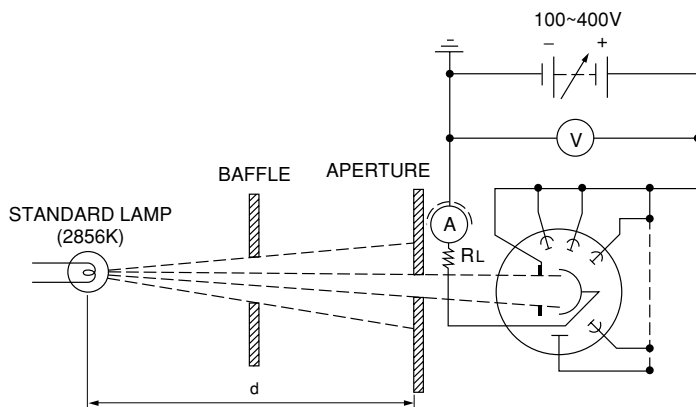
**Figure 4-6: Response of eye and spectral distribution of 2856 K tungsten lamp**

Luminous sensitivity is a convenient parameter when comparing the sensitivity of photomultiplier tubes of the same type. However, it should be noted that "lumen" is the unit of luminous flux with respect to the standard visual sensitivity and there is no physical significance for photomultiplier tubes which have a spectral response range beyond the visible region (350 to 750 nanometers). To evaluate photomultiplier tubes using Cs-Te or Cs-I photocathodes which are insensitive to the spectral distribution of a tungsten lamp, radiant sensitivity at a specific wavelength is measured.

Luminous sensitivity is divided into two parameters: cathode luminous sensitivity which defines the photocathode performance and anode luminous sensitivity which defines the performance characteristics after multiplication.

### (1) Cathode luminous sensitivity

Cathode luminous sensitivity<sup>23)25)</sup> is defined as the photoelectron current generated by the photocathode (cathode current) per luminous flux from a tungsten lamp operated at a distribution temperature of 2856K. In this measurement, each dynode is shorted to the same potential as shown in Figure 4-7, so that the photomultiplier tube is operated as a bipolar tube.



THBV3\_0407EA

**Figure 4-7: Cathode luminous sensitivity measuring diagram**

The incident luminous flux used for measurement is in the range of  $10^{-5}$  to  $10^{-2}$  lumens. If the luminous flux is too large, measurement errors may occur due to the surface resistance of the photocathode. Consequently, the optimum luminous flux must be selected according to the photocathode size and material.

A picoammeter is usually used to measure the photocurrent which changes from several nanoamperes to several microamperes. Appropriate countermeasures against leakage current and other possible noise source must be taken. In addition, be careful to avoid contamination on the socket or bulb stem and to keep ambient humidity levels low so that an adequate electrical safeguard is provided.

The photomultiplier tube should be operated at a supply voltage at which the cathode current fully saturates. A voltage of 90 to 400 volts is usually applied for this purpose. Cathode saturation characteristics are discussed in section 4.3.2, "Linearity". The ammeter is connected to the cathode via a serial load resistance ( $R_L$ ) of 100 k $\Omega$  to 1 M $\Omega$  for circuitry protection.

## (2) Anode luminous sensitivity

Anode luminous sensitivity<sup>(23) (25)</sup> is defined as the anode output current per luminous flux incident on the photocathode. In this measurement, a proper voltage distribution is given to each electrode as illustrated in Figure 4-8. Although the same tungsten lamp that was used to measure the cathode luminous sensitivity is used again, the light flux is reduced to  $10^{-10}$  to  $10^{-5}$  lumens using a neutral density filter. The ammeter is connected to the anode via the series resistance. The voltage-divider resistors used in this measurement must have minimum tolerance and good temperature characteristics.

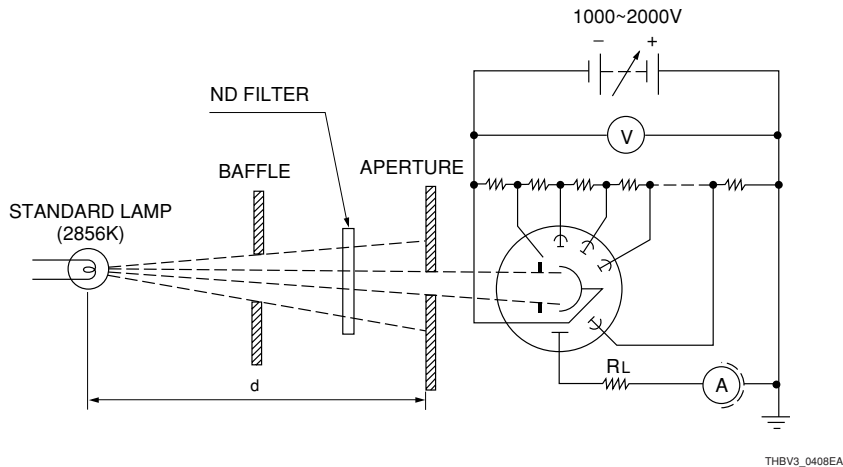


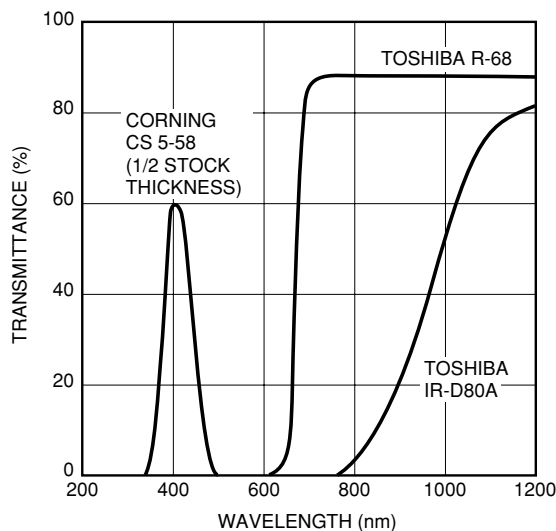
Figure 4-8: Anode luminous sensitivity measuring diagram

### (3) Blue sensitivity index and red-to-white ratio

Blue sensitivity index and red-to-white ratio are often used for simple comparison of the spectral response of photomultiplier tubes.

Blue sensitivity is the cathode current obtained when a blue filter is placed in front of the photomultiplier tube under the same conditions for the luminous sensitivity measurement. The blue filter used is a Corning CS 5-58 polished to half stock thickness. Since the light flux entering the photomultiplier tube has been transmitted through the blue filter once, it cannot be directly represented in lumens. Therefore at Hamamatsu Photonics, it is expressed as a blue sensitivity index without using units. The spectral transmittance of this blue filter matches well the emission spectrum of a NaI(Tl) scintillator (peak wavelength 420 nanometers) which is widely used for scintillation counting. Photomultiplier tube sensitivity to the scintillation flash correlates well with the anode sensitivity using this blue filter. The blue sensitivity index is an important factor that affects energy resolution in scintillation measurement. For detailed information, refer to Chapter 7, "Scintillation counting".

The red-to-white ratio is used to evaluate photomultiplier tubes with a spectral response extending to the near infrared region. This parameter is defined as the quotient of the cathode sensitivity measured with a red or near infrared filter interposed under the same conditions for cathode luminous sensitivity divided by the cathode luminous sensitivity without a filter. The filter used is a Toshiba IR-D80A for Ag-O-Cs photocathodes or a Toshiba R-68 for other photocathodes. If other types of filters are used, the red-to-white ratio will vary. Figure 4-9 shows the spectral transmittance of these filters.

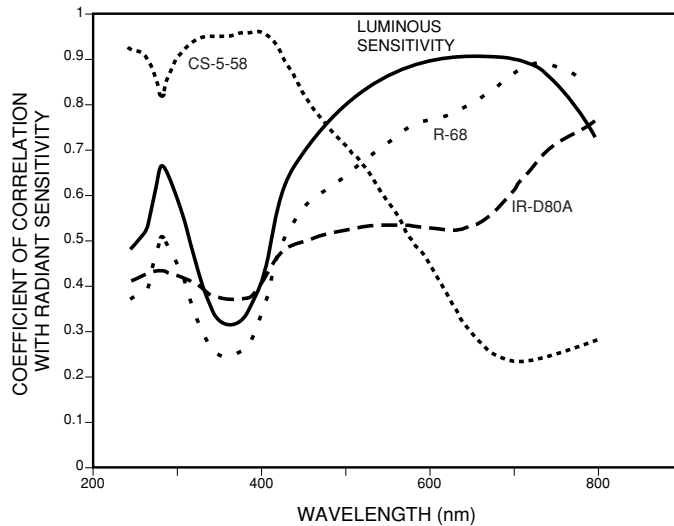


THBV3\_0409EA

Figure 4-9: Typical spectral transmittance of optical filters.

### 4.1.5 Luminous sensitivity and spectral response

To some extent, there is a correlation between luminous sensitivity and spectral response at a specific wavelength. Figure 4-10 describes the correlation between luminous sensitivity, blue sensitivity index (CS 5-58) and red-to-white ratio (R-68, IR-D80A) as a function of wavelength.



THEV3\_0410EA

**Figure 4-10: Correlation between luminous sensitivities and radiant sensitivity**

It can be seen from the figure that the radiant sensitivity of a photomultiplier tube correlates well with the blue sensitivity index at wavelengths shorter than 450 nanometers, with the luminous sensitivity at 700 to 800 nanometers, with the red-to-white ratio using the Toshiba R-68 filter at 700 to 800 nanometers, and with the red-to-white ratio using the Toshiba IR-D80A filter at 800 nanometers or longer. From these correlation values, a photomultiplier tube with optimum sensitivity at a certain wavelength can be selected by simply measuring the sensitivity using a filter which has the best correlation value at that wavelength rather than measuring the spectral response.

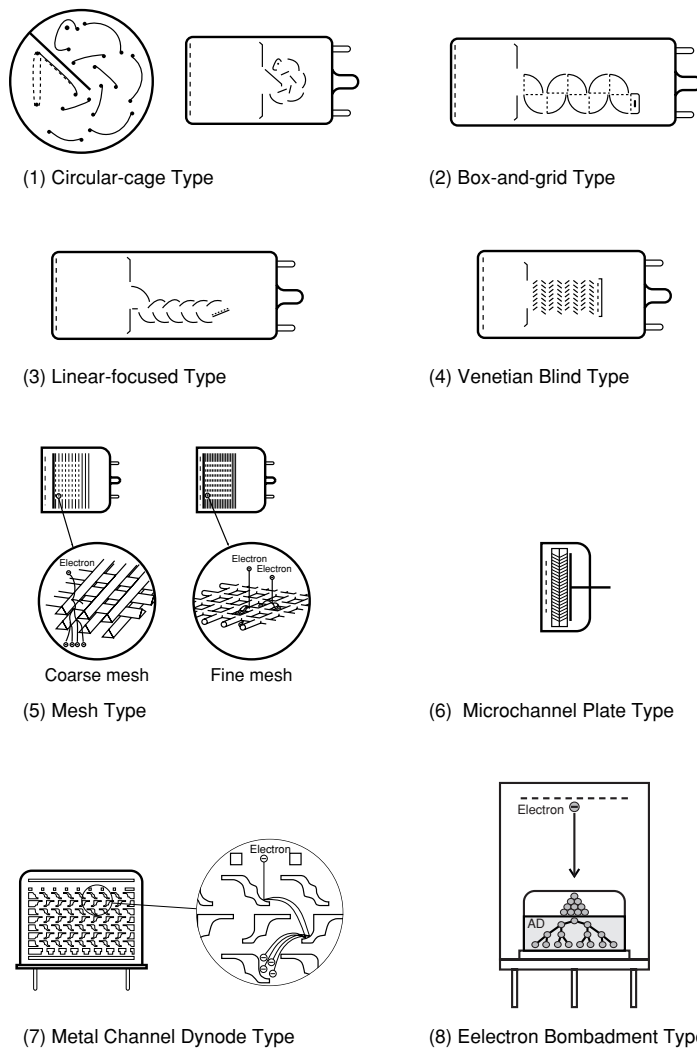


## 4.2 Basic Characteristics of Dynodes

This section introduces typical dynode types currently in use and describes their basic characteristics: collection efficiency and gain (current amplification).

### 4.2.1 Dynode types and features

There are a variety of dynode types available and each type exhibits different gain, time response, uniformity and secondary-electron collection efficiency depending upon the structure and the number of stages. The optimum dynode type must be selected according to application. Figure 4-11 illustrates the cross sectional views of typical dynodes and their features are briefly discussed in the following sections. MCP-PMT's incorporating a microchannel plate for the dynode and photomultiplier tubes using a mesh dynode are respectively described in detail in Chapter 9 and Chapter 10. The electron bombardment type is explained in detail in Chapter 11.



THBV3\_0411EA

Figure 4-11: Types of electron multipliers

**(1) Circular-cage type**

The circular-cage type has an advantage of compactness and is used in all side-on photomultiplier tubes and in some head-on photomultiplier tubes. The circular-cage type also features fast time response.

**(2) Box-and-grid type**

This type, widely used in head-on photomultiplier tubes, is superior in photoelectron collection efficiency. Accordingly, photomultiplier tubes using this dynode offer high detection efficiency and good uniformity.

**(3) Linear-focused type**

As with the box-and-grid type, the linear-focused type is widely used in head-on photomultiplier tubes. Its prime features include fast time response, good time resolution and excellent pulse linearity.

**(4) Venetian blind type**

The venetian blind type creates an electric field that easily collects electrons, and is mainly used for head-on photomultiplier tubes with a large photocathode diameter.

**(5) Mesh type**

This type of dynode uses mesh electrodes stacked in close proximity to each other. There are two types: coarse mesh type and fine mesh type. Both are excellent in output linearity and have high immunity to magnetic fields. When used with a cross wire anode or multianode, the position of incident light can be detected. Fine mesh types are developed primarily for photomultiplier tubes which are used in high magnetic fields. (Refer to Chapter 9 for detailed information.)

**(6) MCP (Microchannel plate)**

A microchannel plate (MCP) with 1 millimeter thickness is used as the base for this dynode structure. This structure exhibits dramatically improved time resolution as compared to other discrete dynode structure. It also assures stable gain in high magnetic fields and provides position-sensitive capabilities when combined with a special anode. (Refer to Chapter 10 for detailed information.)

**(7) Metal channel dynode**

This dynode structure consists of extremely thin electrodes fabricated by our advanced micromachining technology and precisely stacked according to computer simulation of electron trajectories. Since each dynode is in close proximity to one another, the electron path length is very short ensuring excellent time characteristics and stable gain even in magnetic fields. (Refer to Chapter 9 for detailed information.)

**(8) Electron bombardment type**

In this type, photoelectrons are accelerated by a high voltage and strike a semiconductor so that the photoelectron energy is transferred to the semiconductor, producing a gain. This simple structure features a small noise figure, excellent uniformity and high linearity.

The electrical characteristics of a photomultiplier tube depend not only on the dynode type but also on the photocathode size and focusing system. As a general guide, Table 4-2 summarizes typical performance characteristics of head-on photomultiplier tubes (up to 2-inch diameter) classified by the dynode type. Magnetic characteristics listed are measured in a magnetic field in the direction of the most sensitive tube axis.

Dynode Type	Rise Time (ns)	Pulse Linearity at 2% (mA)	Magnetic Immunity (mT)	Uniformity	Collection Efficiency	Features
Circular-cage	0.9 to 3.0	1 to 10	0.1	Poor	Good	Compact, high speed
Box-and-grid	6 to 20			Good	Very good	High collection efficiency
Linear-focused	0.7 to 3	10 to 250		Poor	Good	High speed, high linearity
Venetian blind	6 to 18	10 to 40		Good	Poor	Suited for large diameter
Fine mesh	1.5 to 5.5	300 to 1000	500 to 1500*	Good	Poor	High magnetic immunity, high linearity
MCP	0.1 to 0.3	700	1500*	Good	Poor	high speed
Metal channel	0.65 to 1.5	30	5**	Good	Good	Compact, high speed
Electron bombardment type	Depends on internal semiconductor		—	Very good	Very good	High electron resolution

\* In magnetic field parallel to tube axis

\*\* Metal package PMT

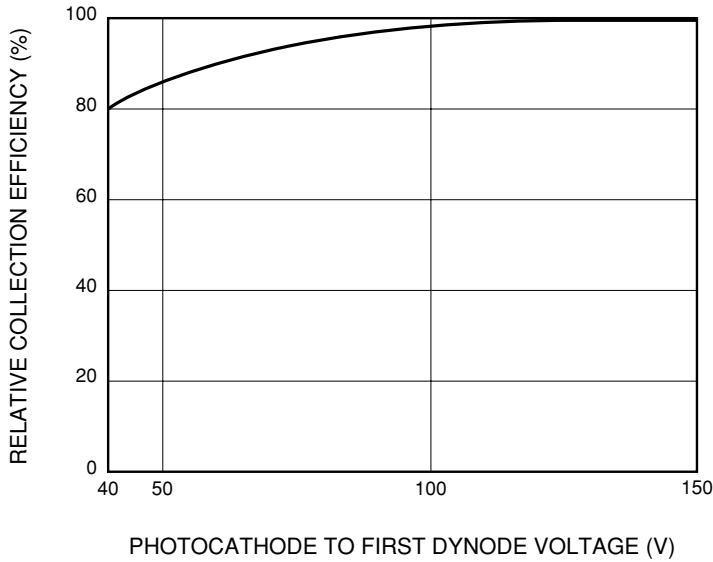
Table 4-2: Typical characteristics for dynode types

## 4.2.2 Collection efficiency and gain (current amplification)

### (1) Collection efficiency

The electron multiplier mechanism of a photomultiplier tube is designed with consideration to the electron trajectories so that electrons are efficiently multiplied at each dynode stage. However, some electrons may deviate from their favorable trajectories, not contributing to multiplication.

In general, the probability that photoelectrons will land on the effective area of the first dynode is termed the collection efficiency ( $\alpha$ ). This effective area is the area of the first dynode where photoelectrons can be multiplied effectively at the successive dynode stages without deviating from their favorable trajectories. Although there exist secondary electrons which do not contribute to multiplication at the second dynode or latter dynodes, they will tend to have less of an effect on the total collection efficiency as the number of secondary electrons emitted increases greatly. So the photoelectron collection efficiency at the first dynode is important. Figure 4-12 shows typical collection efficiency of a 28-mm diameter head-on photomultiplier tube (R6095) as a function of cathode-to-first dynode voltage. If the cathode-to-first dynode voltage is low, the number of photoelectrons that enter the effective area of the first dynode becomes low, resulting in a slight decrease in the collection efficiency.



THBV3\_0412EA

**Figure 4-12: Collection efficiency vs. photocathode-to-first dynode voltage**

Figure 4-12 shows that about 100 volts should be applied between the cathode and the first dynode. The collection efficiency influences energy resolution, detection efficiency and signal-to-noise ratio in scintillation counting. The detection efficiency is the ratio of the detected signal to the input signal of a photomultiplier tube. In photon counting this is expressed as the product of the photocathode quantum efficiency and the collection efficiency.

**(2) Gain (current amplification)**

Secondary emission ratio  $\delta$  is a function of the interstage voltage of dynodes  $E$ , and is given by the following equation:

$$\delta = a \cdot E^k \dots\dots\dots \text{(Eq. 4-3)}$$

Where  $a$  is a constant and  $k$  is determined by the structure and material of the dynode and has a value from 0.7 to 0.8.

The photoelectron current  $I_k$  emitted from the photocathode strikes the first dynode where secondary electrons  $I_{d1}$  are released. At this point, the secondary emission ratio  $\delta_1$  at the first dynode is given by

$$\delta_1 = \frac{I_{d1}}{I_k} \dots\dots\dots \text{(Eq. 4-4)}$$

These electrons are multiplied in a cascade process from the first dynode  $\rightarrow$  second dynode  $\rightarrow$  .... the  $n$ -th dynode. The secondary emission ratio  $\delta_n$  of  $n$ -th stage is given by

$$\delta_n = \frac{I_{dn}}{I_{d(n-1)}} \dots\dots\dots \text{(Eq. 4-5)}$$

The anode current  $I_p$  is given by the following equation:

$$I_p = I_k \cdot \alpha \cdot \delta_1 \cdot \delta_2 \cdots \delta_n \dots\dots\dots \text{(Eq. 4-6)}$$

Then

$$\frac{I_p}{I_k} = \alpha \cdot \delta_1 \cdot \delta_2 \cdots \delta_n \dots\dots\dots \text{(Eq. 4-7)}$$

where  $\alpha$  is the collection efficiency.

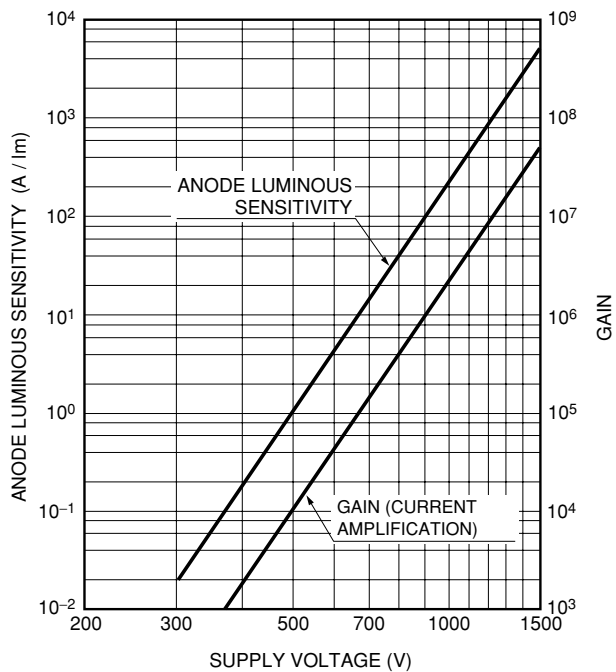
The product of  $\alpha, \delta_1, \delta_2, \dots, \delta_n$  is called the gain  $\mu$  (current amplification), and is given by the following equation:

$$\mu = \alpha \cdot \delta_1 \cdot \delta_2 \cdots \delta_n \quad \text{..... (Eq. 4-8)}$$

Accordingly, in the case of a photomultiplier tube with  $a=1$  and the number of dynode stages =  $n$ , which is operated using an equally-distributed divider, the gain  $m$  changes in relation to the supply voltage  $V$ , as follows:

$$\mu = (a \cdot E^k)^n = a^n \left( \frac{V}{n+1} \right)^{kn} = A \cdot V^{kn} \quad \text{..... (Eq. 4-9)}$$

where  $A$  should be equal to  $a^n / (n+1)^{kn}$ . From this equation, it is clear that the gain  $\mu$  is proportional to the  $kn$  exponential power of the supply voltage. Figure 4-13 shows typical gain vs. supply voltage. Since Figure 4-13 is expressed in logarithmic scale for both the abscissa and ordinate, the slope of the straight line becomes  $kn$  and the current multiplication increases with the increasing supply voltage. This means that the gain of a photomultiplier tube is susceptible to variations in the high-voltage power supply, such as drift, ripple, temperature stability, input regulation, and load regulation.



THBV3\_0413EA

Figure 4-13: Gain vs. supply voltage

## 4.3 Characteristics of Photomultiplier Tubes

This section describes important characteristics for photomultiplier tube operation and their evaluation methods, and photomultiplier tube usage.

### 4.3.1 Time characteristics

The photomultiplier tube is a photodetector that has an exceptionally fast time response.<sup>1)23)-27)</sup> The time response is determined primarily by the transit time required for the photoelectrons emitted from the photocathode to reach the anode after being multiplied as well as the transit time difference between each photoelectron. Accordingly, fast response photomultiplier tubes are designed to have a spherical inner window and carefully engineered electrodes so that the transit time difference can be minimized.

Table 4-3 lists the timing characteristics of 2-inch diameter head-on photomultiplier tubes categorized by their dynode type. As can be seen from the table, the linear-focused type and metal channel type exhibit the best time characteristics, while the box-and-grid and venetian blind types display rather poor properties.

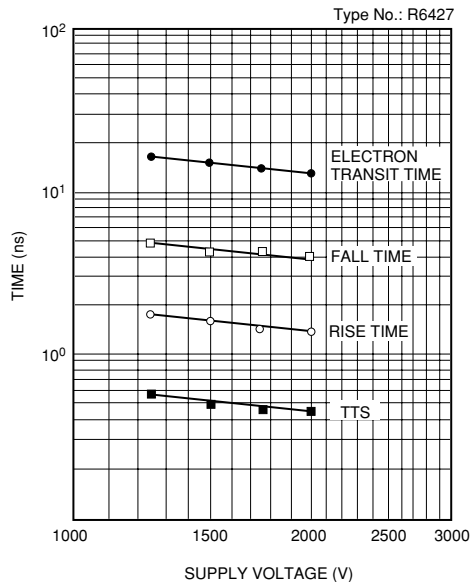
Unit : ns

Dynode Type	Rise Time	Fall Time	Pulse Width (FWHM)	Electron Transit Time	TTS
Linear-focused	0.7 to 3	1 to 10	1.3 to 5	16 to 50	0.37 to 1.1
Circular-cage	3.4	10	7	31	3.6
Box-and-grid	to 7	25	13 to 20	57 to 70	Less than 10
Venetian blind	to 7	25	25	60	Less than 10
Fine mesh	2.5 to 2.7	4 to 6	5	15	Less than 0.45
Metal channel	0.65 to 1.5	1 to 3	1.5 to 3	4.7 to 8.8	0.4

Table 4-3: Typical time characteristics (2-inch dia. photomultiplier tubes)

The time response is mainly determined by the dynode type, but also depends on the supply voltage. Increasing the electric field intensity or supply voltage improves the electron transit speed and thus shortens the transit time. In general, the time response improves in inverse proportion to the square root of the supply voltage. Figure 4-14 shows typical time characteristics vs. supply voltage.

The following section explains and defines photomultiplier tube time characteristics and their measurement methods.

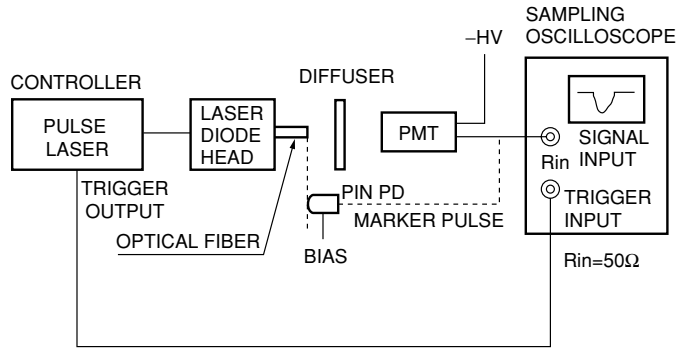


THBV3\_0414EA

Figure 4-14: Time characteristics vs. supply voltage

### (1) Rise time, fall time and electron transit time

Figure 4-15 shows a schematic diagram for time response measurements and Figure 4-16 illustrates the definitions of the rise time, fall time and electron transit time of a photomultiplier tube output.

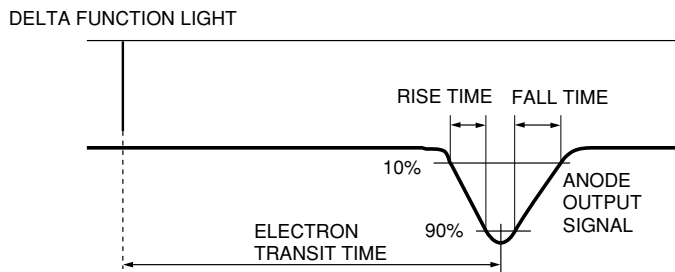


THBV3\_0415EA

**Figure 4-15: Measurement block diagram for rise/fall times and electron transit time**

A pulsed laser diode is used as the light source. Its pulse width is sufficiently short compared to the light pulse width that can be detected by a photomultiplier tube. Thus it can be regarded as a delta-function light source. A sampling oscilloscope is used to sample the photomultiplier tube output many times so that a complete output waveform is created. The output signal generated by the photomultiplier tube is composed of waveforms which are produced by electrons emitted from every position of the photocathode. Therefore, the rise and fall times are mainly determined by the electron transit time difference and also by the electric field distribution and intensity (supply voltage) between the electrodes.

As indicated in Figure 4-16, the rise time is defined as the time for the output pulse to increase from 10 to 90 percent of the peak pulse height. Conversely, the fall time is defined as the time required to decrease from 90 to 10 percent of the peak output pulse height. In time response measurements where the rise and fall times are critical, the output pulse tends to suffer waveform distortion, causing an erroneous signal. To prevent this problem, proper impedance matching must be provided including the use of a voltage-divider circuit with damping resistors. (See Chapter 5.)

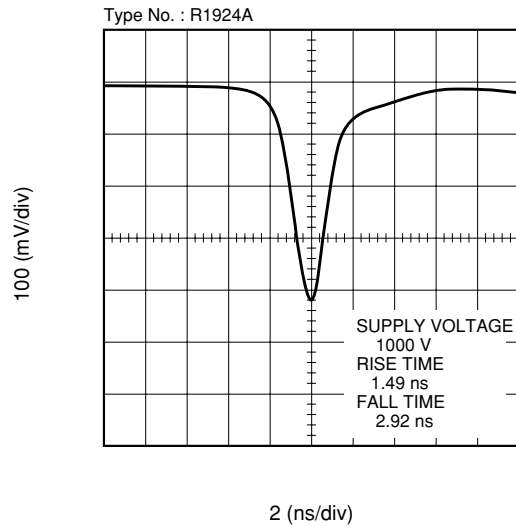


THBV3\_0416EA

**Figure 4-16: Definitions of rise/fall times and electron transit time**

Figure 4-17 shows an actual output waveform obtained from a photomultiplier tube. In general, the fall time is two or three times longer than the rise time. This means that when measuring repetitive pulses, care must be taken so that each output pulse does not overlap. The FWHM (full width at half maximum) of the output pulse will usually be about 2.5 times the rise time.

The transit time is the time interval between the arrival of a light pulse at the photocathode and the appearance of the output pulse. To measure the transit time, a PIN photodiode is placed as reference (zero second) at the same position as the photomultiplier tube photocathode. The time interval between the instant the PIN photodiode detects a light pulse and the instant the output pulse of the photomultiplier tube reaches its peak amplitude is measured. This transit time is a useful parameter in determining the delay time of a measurement system in such applications as fluorescence lifetime measurement using repetitive light pulses.

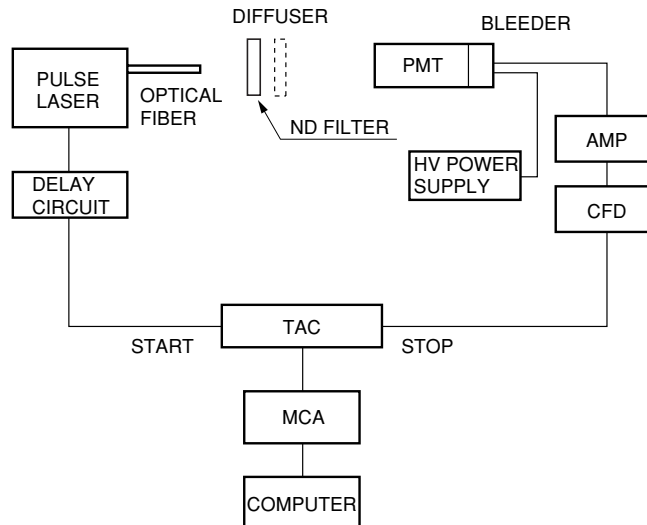


THBV3\_0417EA

Figure 4-17: Output waveform

## (2) TTS (transit time spread)

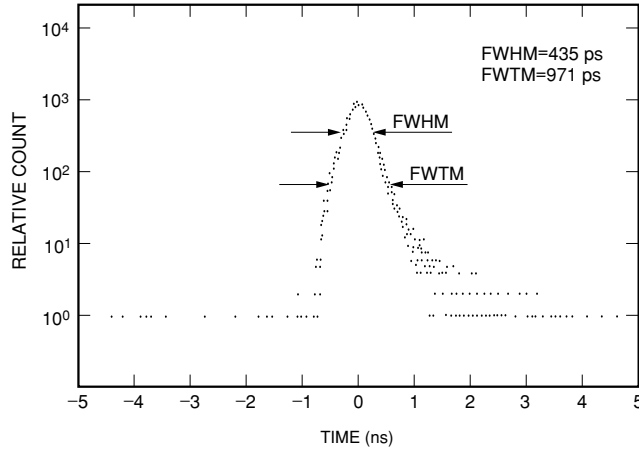
When a photocathode is fully illuminated with single photons, the transit time of each photoelectron pulse has a fluctuation. This fluctuation is called TTS (transit time spread). A block diagram for TTS measurement is shown in Figure 4-18 and typical measured data is shown in Figure 4-19.



THBV3\_0418EA

Figure 4-18: Block diagram for TTS measurement



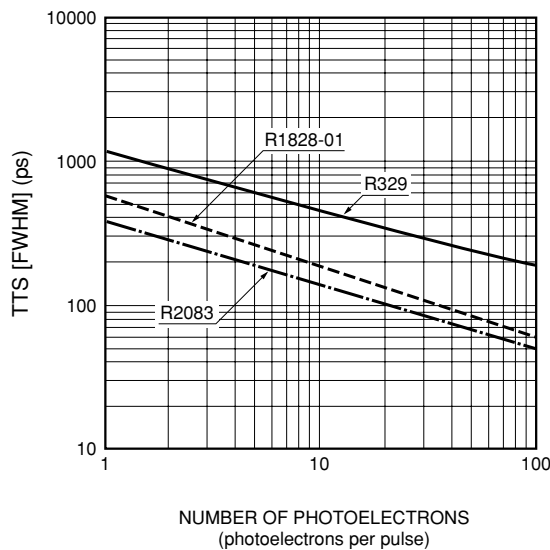


THBV3\_0419EA

Figure 4-19: TTS (transit time spread)

In this measurement, a trigger signal from the pulsed laser is passed through the delay circuit and then fed as the start to the TAC (time-to-amplitude converter) which converts the time difference into pulse height. Meanwhile, the output from the photomultiplier tube is fed as the stop signal to the TAC via the CFD (constant fraction discriminator) which reduces the time jitter resulting from fluctuation of the pulse height. The TAC generates a pulse height proportional to the time interval between the "start" and "stop" signals. This pulse is fed to the MCA (multichannel analyzer) for pulse height analysis. Since the time interval between the "start" and "stop" signals corresponds to the electron transit time, a histogram displayed on the MCA, by integrating individual pulse height values many times in the memory, indicates the statistical spread of the electron transit time.

At Hamamatsu Photonics, the TTS is usually expressed in the FWHM of this histogram, but it may also be expressed in standard deviation. When the histogram shows a Gaussian distribution, the FWHM is equal to a value which is 2.35 times the standard deviation. The TTS improves as the number of photoelectrons per pulse increases, in inverse proportion to the square root of the number of photoelectrons. This relation is shown in Figure 4-20.

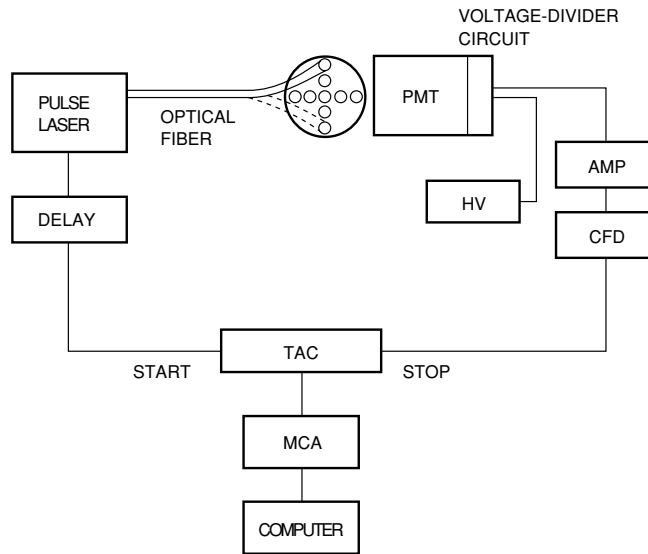


THBV3\_0420EA

Figure 4-20: TTS vs. number of photoelectrons

### (3) CTTD (cathode transit time difference)

The CTTD (cathode transit time difference) is the difference in transit time when the incident light position on the photocathode is shifted. In most time response measurements the entire photocathode is illuminated. However, as illustrated in Figure 4-21, the CTTD measurement employs an aperture plate to shift the position of a light spot entering the photocathode, and the transit time difference between each incident position is measured.



THBV3\_0421EA

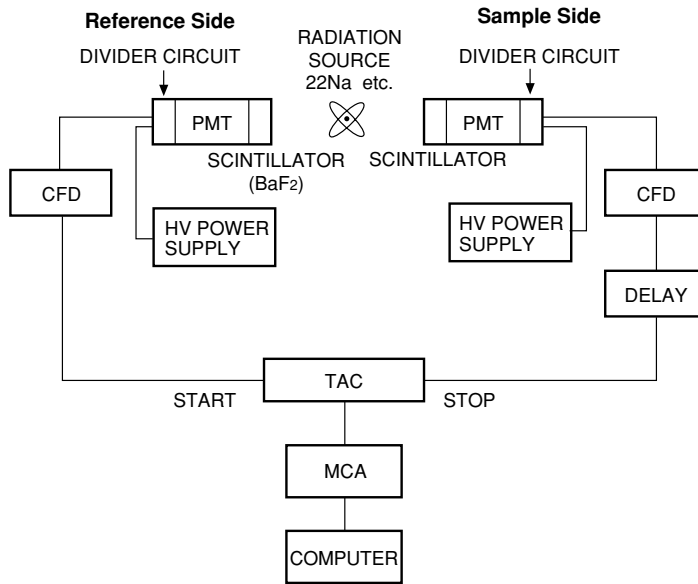
**Figure 4-21: Block diagram for CTTD measurement**

Basically, the same measurement system as for TTS measurement is employed, and the TTS histogram for each of the different incident light positions is obtained. Then the change in the peak pulse height of each histogram, which corresponds to the CTTD, is measured. The CTTD data of each position is represented as the transit time difference with respect to the transit time measured when the light spot enters the center of the photocathode.

In actual applications, the CTTD data is not usually needed but rather primarily used for evaluation in the photomultiplier tube manufacturing process. However, the CTTD is an important factor that affects the rise time, fall time and TTS described previously and also CRT (coincident resolving time) discussed in the next section.

**(4) CRT (coincident resolving time)**

As with the TTS, this is a measure of fluctuations in the transit time. The CRT measurement system resembles that used for positron CT or TOF (time of flight) measurement. Therefore, the CRT is a very practical parameter for evaluating the performance of photomultiplier tubes used in the above fields or similar applications. Figure 4-22 shows a block diagram of the CRT measurement.



THBV3\_0422EA

**Figure 4-22: Block diagram for CRT measurement**

As a radiation source <sup>22</sup>Na or <sup>68</sup>Ge-Ga is commonly used. As a scintillator, a BaF<sub>2</sub> is used on the reference side, while a BGO, BaF<sub>2</sub>, CsF or plastic scintillator is used on the sample side. A proper combination of radiation source and scintillator should be selected according to the application. The radiation source is placed in the middle of a pair of photomultiplier tubes and emits gamma-rays in opposing directions at the same time. A coincident flash occurs from each of the two scintillators coupled to the photomultiplier tube. The signal detected by one photomultiplier tube is fed as the start signal to the TAC, while the signal from the other photomultiplier tube is fed as the stop signal to the TAC via the delay circuit used to obtain proper trigger timing. Then, as in the case of the TTS measurement, this event is repeatedly measured many times and the pulse height (time distribution) is analyzed by the MCA to create a CRT spectrum. This spectrum statistically displays the time fluctuation of the signals that enter the TAC. This fluctuation mainly results from the TTS of the two photomultiplier tubes. As can be seen from Figures 4-14 and 4-20, the TTS is inversely proportional to the square root of the number of photoelectrons per pulse and also to the square root of the supply voltage. In general, therefore, the higher the radiation energy and the supply voltage, the better the CRT will be. If the TTS of each photomultiplier tube is  $\tau_1$  and  $\tau_2$ , the CRT is given by

$$\text{C.R.T.} = (\tau_1^2 + \tau_2^2)^{1/2} \dots\dots\dots (\text{Eq. 4- 10})$$

The CRT characteristic is an important parameter for TOF measurements because it affects the position resolution.

### 4.3.2 Linearity

The photomultiplier tube exhibits good linearity<sup>1) 24) 27) 28)</sup> in anode output current over a wide range of incident light levels as well as the photon counting region. In other words, it offers a wide dynamic range. However, if the incident light amount is too large, the output begins to deviate from the ideal linearity. This is primarily caused by anode linearity characteristics, but it may also be affected by cathode linearity characteristics when a photomultiplier tube with a transmission mode photocathode is operated at a low supply voltage and large current. Both cathode and anode linearity characteristics are dependent only on the current value if the supply voltage is constant, while being independent of the incident light wavelength.

#### (1) Cathode linearity

Photocathode Materials	Spectral Response [Peak Wavelength] (nm)	Upper Limit of Linearity (Average Current)
Ag-O-Cs	300 to 1200 [800]	1 $\mu$ A
Sb-Cs	up to 650 [440]	1 $\mu$ A
Sb-Rb-Cs	up to 650 [420]	0.1 $\mu$ A
Sb-K-Cs	up to 650 [420]	0.01 $\mu$ A
Sb-Na-K	up to 650 [375]	10 $\mu$ A
Sb-Na-K-Cs	up to 850 [420], up to 900 [600] extended red	10 $\mu$ A
Ga-As(Cs)	up to 930 [300~700]	(*) 0.1 $\mu$ A
Cs-Te	up to 320 [210]	0.1 $\mu$ A
Cs-I	up to 200 [140]	0.1 $\mu$ A

(\*) Linearity considerably degrades if this current is exceeded.

**Table 4-4: Photocathode materials and cathode linearity limits**

The photocathode is a semiconductor and its electrical resistance depends on the photocathode materials. Therefore, the cathode linearity also differs depending on the photocathode materials as listed in Table 4-4. It should be noted that Table 4-4 shows characteristics only for transmission mode photocathodes. In the case of reflection mode photocathodes which are formed on a metal plate and thus have a sufficiently low resistivity, the linearity will not be a significant problem. To reduce the effects of photocathode resistivity on the device linearity without degrading the collection efficiency, it is recommended to apply a voltage of 50 to 300 volts between the photocathode and the first dynode, depending on the structure. For semiconductors, the photocathode surface resistivity increases as the temperature decreases. Thus, consideration must be given to the temperature characteristics of the photocathode resistivity when cooling the photomultiplier tube.

#### (2) Anode linearity

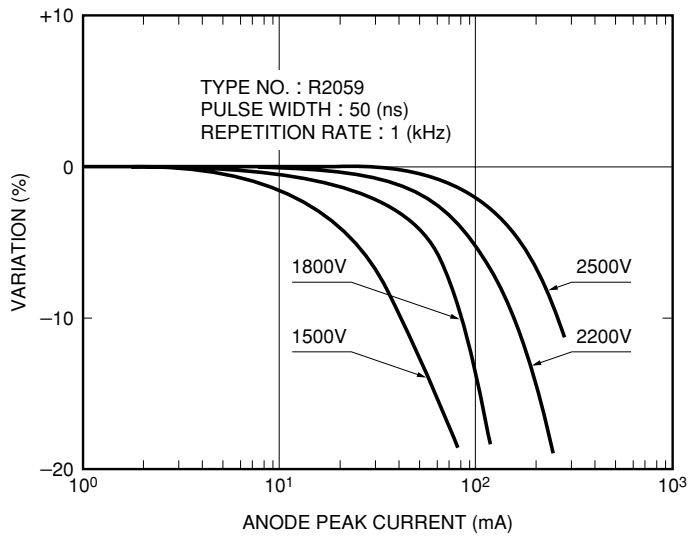
The anode linearity is limited by two factors: the voltage-divider circuit and space charge effects due to a large current flowing in the dynodes.

As shown below, the linearity in DC mode operation is mainly limited by the voltage-divider circuit, while the pulse mode operation is limited by space charge effects.

Linearity —  $\left\{ \begin{array}{l} \text{Pulse mode : Limited by the space charge effects.} \\ \text{DC mode : Limited by a change in the voltage-divider voltage} \\ \text{due to the magnitude of signal current.} \end{array} \right.$

The linearity limit defined by the voltage-divider circuit is described in Chapter 5. The pulse linearity in pulse mode is chiefly dependent on the peak signal current. When an intense light pulse enters a photomultiplier tube a large current flows in the latter dynode stages, increasing the space charge density, and causing current saturation. The extent of these effects depends on the dynode structure, as indicated in Table 4-2. The space charge effects also depend on the electric field distribution and intensity between each dynode. The mesh type dynodes offer superior linearity because they have a structure resistant to the space charge effects. Each dynode is arranged in close proximity providing a higher electric field strength and the dynode area is large so that the signal density per unit area is lower. In general, any dynode type provides better pulse linearity when the supply voltage is increased, or in other words, when the electric field strength between each dynode is enhanced.

Figure 4-23 shows the relationship between the pulse linearity and the supply voltage of a Hamamatsu photomultiplier tube R2059. The linearity can be improved by use of a special voltage-divider (called "a tapered voltage-divider") designed to increase the interstage voltages at the latter dynode stages. This is described in Chapter 5. Because such a tapered voltage-divider must have an optimum electric field distribution and intensity that match each dynode, determining the proper voltage distribution ratio is a rather complicated operation.



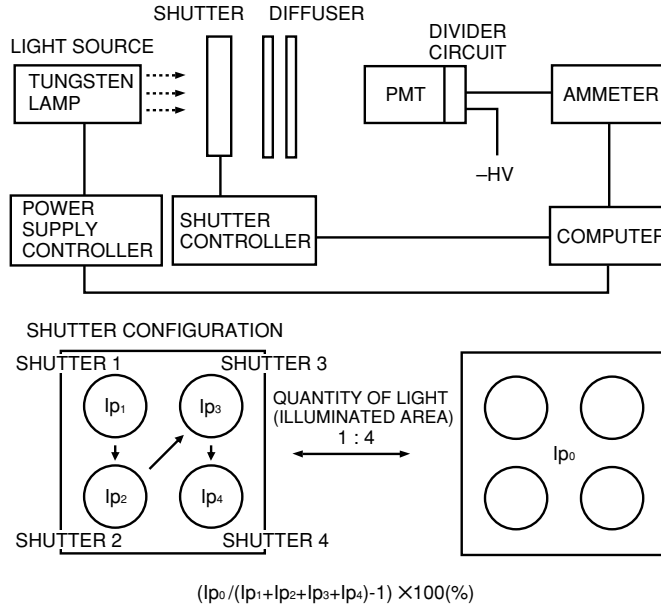
THBV3\_0423EA

Figure 4-23: Voltage dependence of linearity

**(3) Linearity measurement**

The linearity measurement methods include the DC mode and the pulse mode. Each mode is described below.

**(a) DC mode**



THEV3\_0424EA

**Figure 4-24: Block diagram for DC mode linearity measurement**

This section introduces the DC linearity measurement method used by Hamamatsu Photonics. As Figure 4-24 shows, a 4-aperture plate equipped with shutters is installed between the light source and the photomultiplier tube. Each aperture is opened in the order of 1, 2, 3 and 4, finally all four apertures are opened, and the photomultiplier tube outputs are measured (as  $I_{p1}$ ,  $I_{p2}$ ,  $I_{p3}$ ,  $I_{p4}$  and  $I_{p0}$ , respectively). Then the ratio of  $I_{p0}$  to  $(I_{p1}+I_{p2}+I_{p3}+I_{p4})$  is calculated as follows:

$$(I_{p0} / (I_{p1} + I_{p2} + I_{p3} + I_{p4}) - 1) \times 100(\%) \dots\dots\dots (Eq. 4-11)$$

This value represents a deviation from linearity and if the output is within the linearity range,  $I_{p0}$  becomes

$$I_{p0} = I_{p1} + I_{p2} + I_{p3} + I_{p4} \dots\dots\dots (Eq. 4-12)$$

Repeating this measurement by changing the intensity of the light source (i.e. changing the photomultiplier tube output current) gives a plot as shown in Figure 4-25. This indicates an output deviation from linearity. This linearity measurement greatly depends on the magnitude of the current flowing through the voltage-divider circuit and its structure.

As a simple method, linearity can also be measured using neutral density filters which are calibrated in advance for changes in the incident light level.

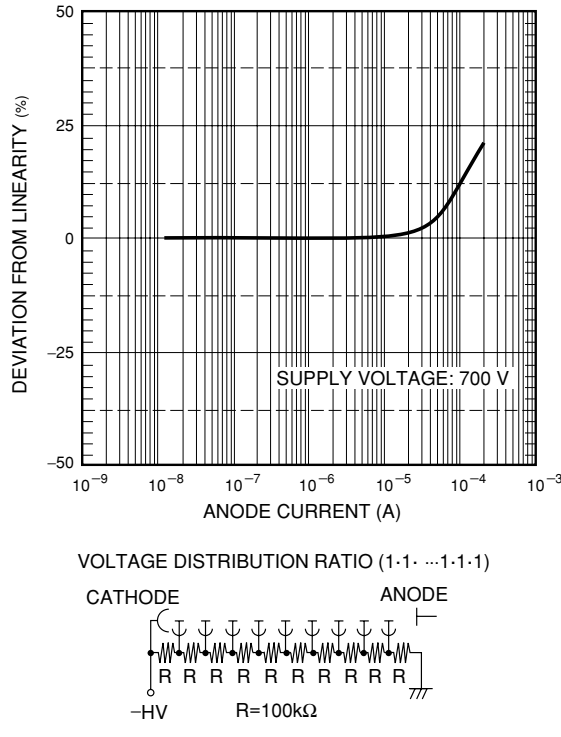


Figure 4-25: DC linearity (side-on type)

**(b) Pulse mode**

A simplified block diagram for the pulse mode linearity measurement is shown in Figure 4-26. In this measurement, an LED operated in a double-pulsed mode is used to provide higher and lower pulse amplitudes alternately. The higher and lower pulse amplitudes are fixed at a ratio of approximately 4:1. If the photomultiplier tube outputs in response to the higher and lower pulsed light at sufficiently low light levels, the peak currents are  $I_{p01}$  and  $I_{p02}$  respectively, then the ratio of  $I_{p02}/I_{p01}$  is proportional to the pulse amplitude; thus

$$I_{p02}/I_{p01} = 4 \dots\dots\dots \text{(Eq. 4-13)}$$

When the LED light sources are brought close to the photomultiplier tube (See Figure 4-26.) and the subsequent output current increases, the photomultiplier tube output begins to deviate from linearity. If the output for the lower pulsed light ( $A_1$ ) is  $I_{p1}$  and the output for the higher pulsed light ( $A_2$ ) is  $I_{p2}$ , the ratio between the two output pulses has the following relation:

$$I_{p2}/I_{p1} \neq I_{p02}/I_{p01} \dots\dots\dots \text{(Eq. 4-14)}$$

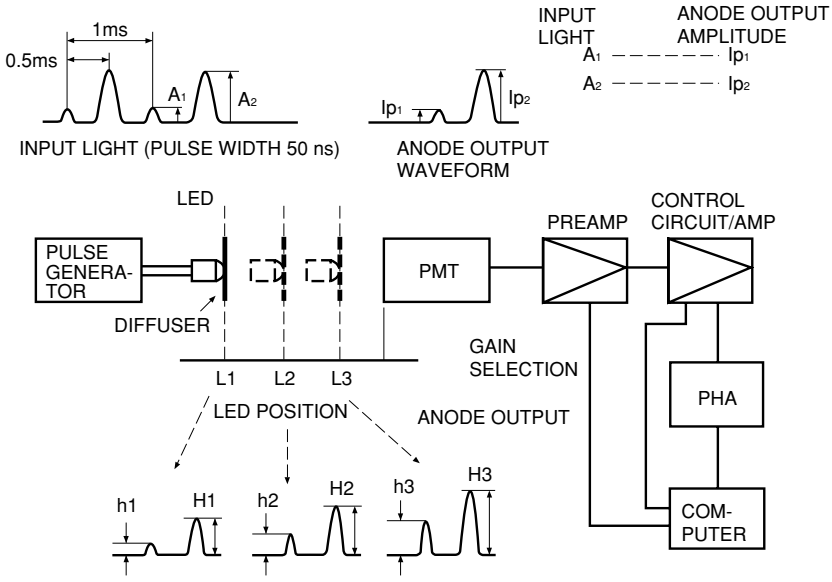
Linearity can be measured by measuring the ratio between the two outputs of the photomultiplier tube, produced by the two different intensities of pulsed light,  $I_{p2}/I_{p1}$ . Linearity is then calculated as follows:

$$\frac{(I_{p2}/I_{p1}) - (I_{p02}/I_{p01})}{(I_{p02}/I_{p01})} \times 100 (\%) \dots\dots\dots \text{(Eq. 4-15)}$$

This indicates the extent of deviation from linearity at the anode output  $I_{p2}$ . If the anode output is in the linearity range, the following relation is always established:

$$(I_{p2}/I_{p1}) = (I_{p02}/I_{p01}) \dots\dots\dots \text{(Eq. 4-16)}$$

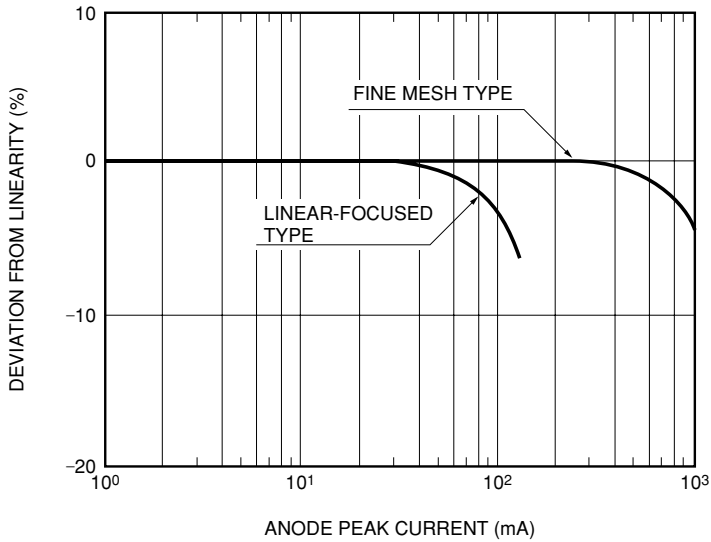
Under these conditions, Eq. 4-15 becomes zero.



THBV3\_0426EA

Figure 4-26: Block diagram for pulse mode linearity measurement

By repeating this measurement while varying the distance between the LED light source and the photomultiplier tube so as to change the output current of the photomultiplier tube, linearity curves like those shown in Figure 4-27 can be obtained.



THBV3\_0427EA

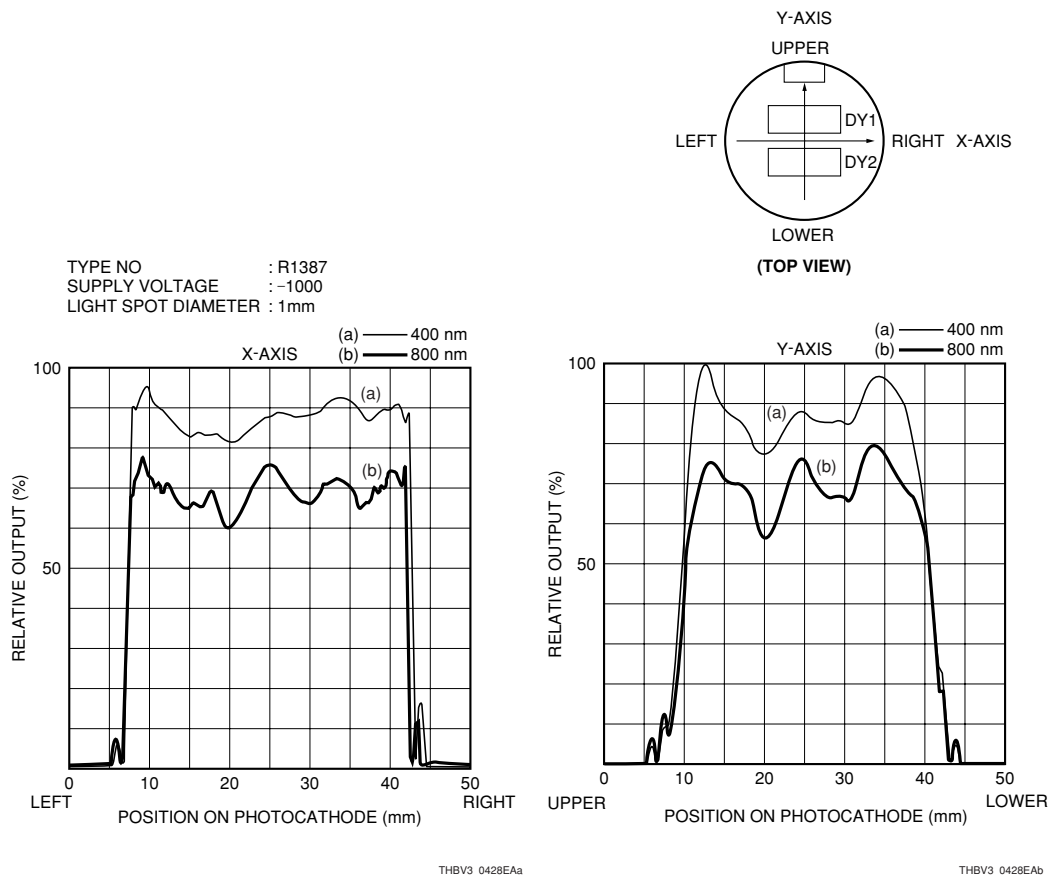
Figure 4-27: Pulse linearity



### 4.3.3 Uniformity

Uniformity is the variation of the output signal with respect to the photocathode position. Anode output uniformity is thought to be the product of the photocathode uniformity and the electron multiplier (dynode section) uniformity.

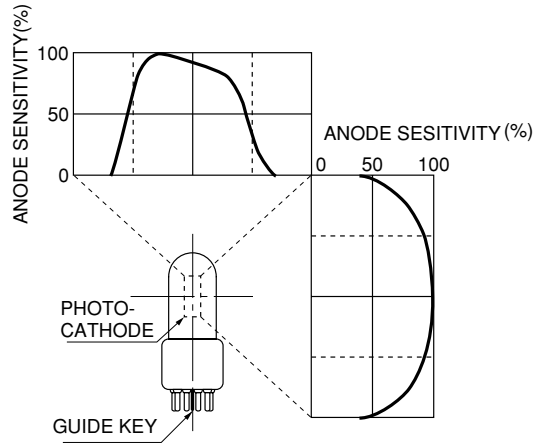
Figure 4-28 shows anode uniformity data measured at wavelengths of 400 nanometers and 800 nanometers. This data is obtained with a light spot of 1 mm diameter scanned over the photocathode surface.



**Figure 4-28: Difference in uniformity with wavelength**

In general, both photocathode uniformity and anode uniformity deteriorate as the incident light shifts to a longer wavelength, and especially as it approaches the long-wavelength limit. This is because the cathode sensitivity near the long-wavelength limit greatly depends on the surface conditions of the photocathode and thus fluctuations increase. Moreover, if the supply voltage is too low, the electron collection efficiency between dynodes may degrade and adversely affect uniformity.

Head-on photomultiplier tubes provide better uniformity in comparison with side-on types. In such applications as gamma cameras used for medical diagnosis where good position detecting ability is demanded, uniformity is an important parameter in determining equipment performance. Therefore, the photomultiplier tubes used in this field are specially designed and selected for better uniformity. Figure 4-29 shows typical uniformity data for a side-on tube. The same measurement procedure as for head-on tubes is used. Uniformity is also affected by the dynode structure. As can be seen from Table 4-2, the box-and-grid type, venetian blind type and mesh type offer better uniformity.



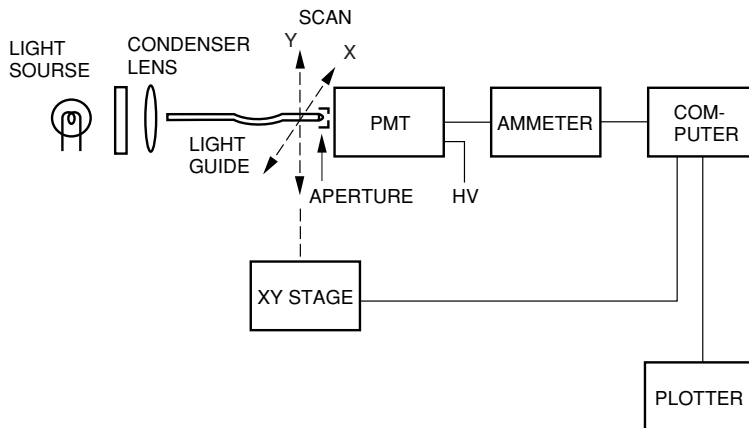
THBV3\_0429EA

**Figure 4-29: Uniformity of a side-on photomultiplier tube**

Considering actual photomultiplier tube usage, uniformity is evaluated by two methods: one measured with respect to the position of incidence (spatial uniformity) and one with respect to the angle of incidence (angular response). The following sections explain their measurement procedures and typical characteristics.

### (1) Spatial uniformity

To measure spatial uniformity, a light spot is scanned in two-dimensions over the photocathode of a photomultiplier tube and the variation in output current is graphically displayed. Figure 4-30 shows a schematic diagram for the spatial uniformity measurement.

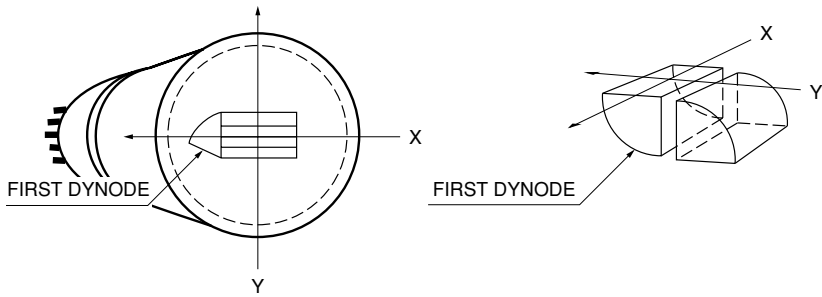


THBV3\_0430EA

**Figure 4-30: Schematic diagram for spatial uniformity measurement**

For convenience, the photocathode is scanned along the X-axis and Y-axis. The direction of the X-axis or Y-axis is determined with respect to the orientation of the first dynode as shown in Figure 4-31.

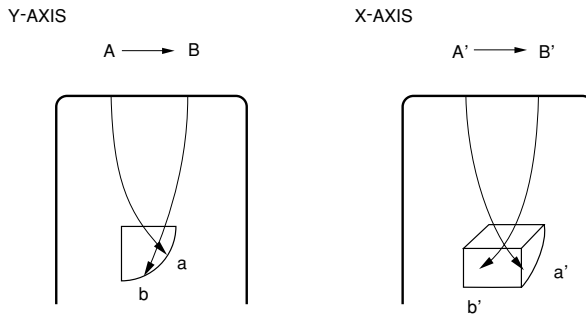
Figure 4-31 also shows the position relation between the XY axes and the first dynode. The degree of loss of electrons in the dynode section significantly depends on the position of the first dynode on which the photoelectrons strike. Refer to Figure 4-28 for specific uniformity data.



THBV3\_0431EA

**Figure 4-31: Spatial uniformity measurement for head-on types**

While the photocathode is scanned by the light spot, the emitted photoelectrons travel along the X-axis or Y-axis of the first dynode as shown in Figure 4-32.



THBV3\_0432EA

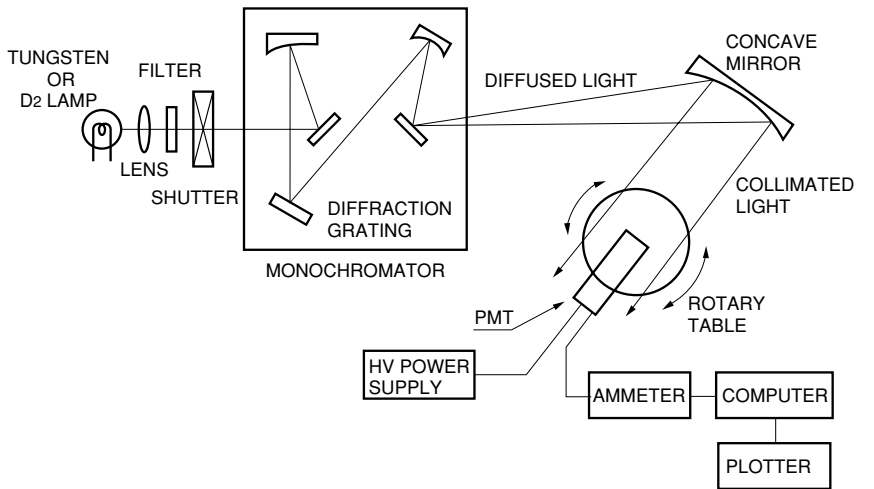
**Figure 4-32: Position of photoemission and the related position on the first dynode**

This method for measuring spatial uniformity is most widely used because the collective characteristics can be evaluated in a short time. In some cases, spatial uniformity is measured by dividing the photocathode into a grid pattern, so that sensitivity distribution is displayed in two or three dimensions.

The spatial uniformity of anode output ranges from 20 to 40 percent for head-on tubes, and may exceed those values for side-on tubes. The adverse effects of the spatial uniformity can be minimized by placing a diffuser in front of the input window of a photomultiplier tube or by using a photomultiplier tube with a frosted glass window.

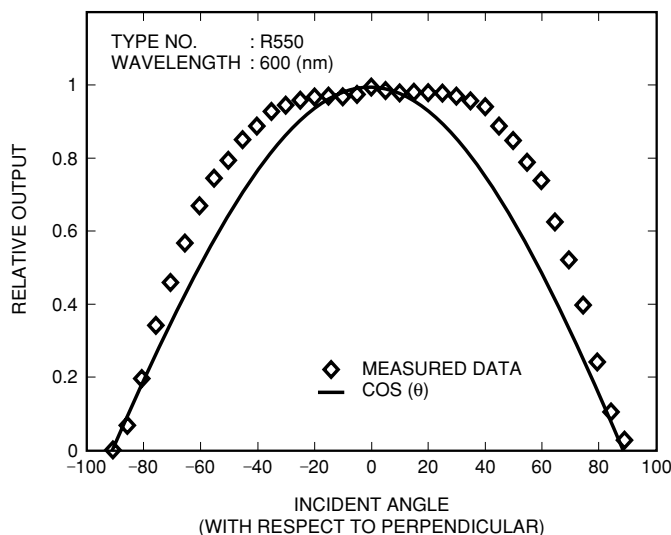
## (2) Angular response

Photomultiplier tube sensitivity somewhat depends on the angle of incident light on the photocathode. This dependence on the incident angle is called the angular response.<sup>28)-30)</sup> To measure the angular response, the entire photocathode is illuminated with collimated light, and the output current is measured while rotating the photomultiplier tube. A schematic diagram for the angular response measurement is shown in Figure 4-33 and specific data is plotted in Figure 4-34. As the rotary table is rotated, the projected area of the photocathode is reduced. This means that the output current of a photomultiplier tube is plotted as a cosine curve of the incident angle even if the output has no dependence on the incident angle. Commonly, the photocathode sensitivity improves at larger angles of incidence and thus the output current is plotted along a curve showing higher sensitivity than the cosine ( $\cos \theta$ ) curve. This is because the incident light transmits across a longer distance at large angles of incidence. In addition, this increase in sensitivity usually becomes larger at longer wavelengths.



THBV3\_0433EA

Figure 4-33: Schematic diagram for angular response measurement



THBV3\_0434EA

Figure 4-34: Typical angular response

### 4.3.4 Stability

The output variation of a photomultiplier tube with operating time is commonly termed as "drift" or "life" characteristics. On the other hand, the performance deterioration resulting from the stress imposed by the supply voltage, current, and ambient temperature is called "fatigue".

#### (1) Drift (time stability) and life characteristics

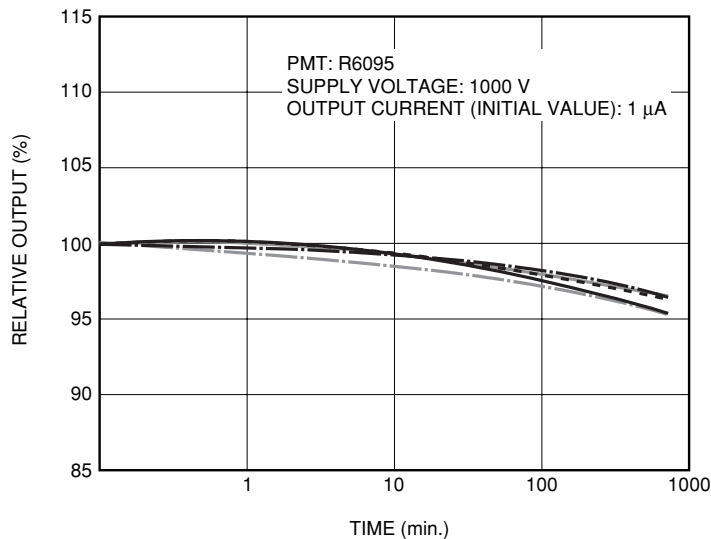
Variations (instability) over short time periods are mainly referred to as drift<sup>1)31)</sup>, while variations (instability) over spans of time longer than  $10^3$  to  $10^4$  hours are referred to as the life characteristics. Since the cathode sensitivity of a photomultiplier tube exhibits good stability even after long periods of operating time, the drift and life characteristics primarily depend on variations in the secondary emission ratio. In other words, these characteristics indicate the extent of gain variation with operating time.

Drift per unit time generally improves with longer operating time and this tendency continues even if the photomultiplier tube is left unused for a short time after operation. Aging or applying the power supply voltage to the photomultiplier tube prior to use ensures more stable operation.

Since drift and life characteristics greatly depend on the magnitude of signal output current, keeping the average output current within a few microamperes is usually recommended.

At Hamamatsu Photonics, drift is usually measured in the DC mode by illuminating a photomultiplier tube with a continuous light and recording the output current with the operating time. Figure 4-35 shows specific drift data for typical Hamamatsu photomultiplier tubes. In most cases, the drift of a photomultiplier tube tends to vary largely during initial operation and stabilizes as operating time elapses. In pulsed or intermittent operation (cyclic on/off operation), the drift shows a variation pattern similar to those obtained with continuous light if the average output current is of the same level as the output current in the DC mode.

In addition, there are other methods for evaluating the drift and life characteristics, which are chiefly used for photomultiplier tubes designed for scintillation counting. For more details refer to Chapter 7, "Scintillation counting".



THBV3\_0435EA

Figure 4-35: Examples of drift data

## (2) Aging and warm-up

In applications where output stability within a few percent is required, aging or warm-up is recommended as explained below.

### (a) Aging

Aging is a technique in which a photomultiplier tube is continuously operated for a period ranging from several hours to several tens of hours, with the anode output current not exceeding the maximum rating. Through this aging, drift can be effectively stabilized. In addition, if the photomultiplier tube is warmed up just before actual use, the drift will be further stabilized.

### (b) Warm-up

For stable operation of a photomultiplier tube, warm-up of the photomultiplier tube for about 30 to 60 minutes is recommended. The warm-up period should be longer at the initial phase of photomultiplier tube operation, particularly in intermittent operation. After a long period of operation warm-up can be shortened. At a higher anode current the warm-up period can be shortened and at a lower anode current the warm-up should be longer. In most cases, a warm-up is performed for several ten minutes at a supply voltage near the actual operating voltage and an anode current of several microamperes. However, in low current operation (average output current from less than one hundred up to several hundred nanoamperes), a warm-up is done by just applying a voltage to the photomultiplier tube for about one hour in the dark state.

### 4.3.5 Hysteresis

When the incident light or the supply voltage is changed in a step function, a photomultiplier tube may not produce an output comparable with the same step function. This phenomenon is known as "hysteresis".<sup>1) 32)</sup> Hysteresis is observed as two behaviors: "overshoot" in which the output current first increases greatly and then settles and "undershoot" in which the output current first decreases and then returns to a steady level. Hysteresis is further classified into "light hysteresis" and "voltage hysteresis" depending on the measurement conditions. Some photomultiplier tubes have been designed to suppress hysteresis by coating the insulator surface of the electrode supports with a conductive material so as to minimize the electrostatic charge on the electrode supports without impairing their insulating properties.

#### (1) Light hysteresis

When a photomultiplier tube is operated at a constant voltage, it may exhibit a temporary variation in the anode output after the incident light is changed in a step function. This variation is called light hysteresis. Figure 4-36 shows the Hamamatsu test method for light hysteresis and typical hysteresis waveforms.

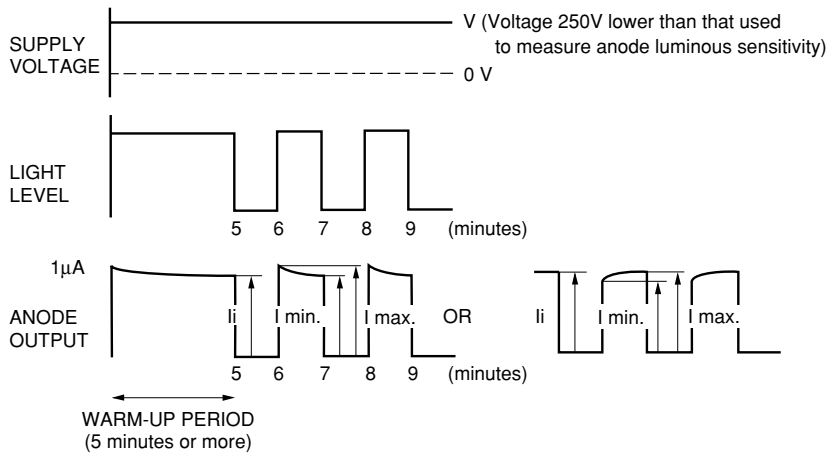


Figure 4-36: Light hysteresis

As shown in Figure 4-36, a photomultiplier tube is operated at a voltage V, which is 250 volts lower than the voltage used to measure the anode luminous sensitivity. The photomultiplier tube is warmed up for five minutes or more at a light level producing an anode current of approximately 1 microampere. Then the incident light is shut off for one minute and then input again for one minute. This procedure is repeated twice to confirm the reproducibility. By measuring the variations of the anode outputs, the extent of light hysteresis can be expressed in percent, as follows:

$$\text{Light hysteresis } H_L = ((I_{MAX} - I_{MIN}) / I_i) \times 100(\%) \dots\dots\dots (\text{Eq. 4-17})$$

where  $I_{MAX}$  is the maximum output value,  $I_{MIN}$  is the minimum output value and  $I_i$  is the initial output value.

Table 4-5 shows typical hysteresis data for major Hamamatsu photomultiplier tubes. Since most photomultiplier tubes have been designed to minimize hysteresis, they usually only display a slight hysteresis within  $\pm 1$  percent. It should be noted that light hysteresis behaves in different patterns or values, depending on the magnitude of the output current.

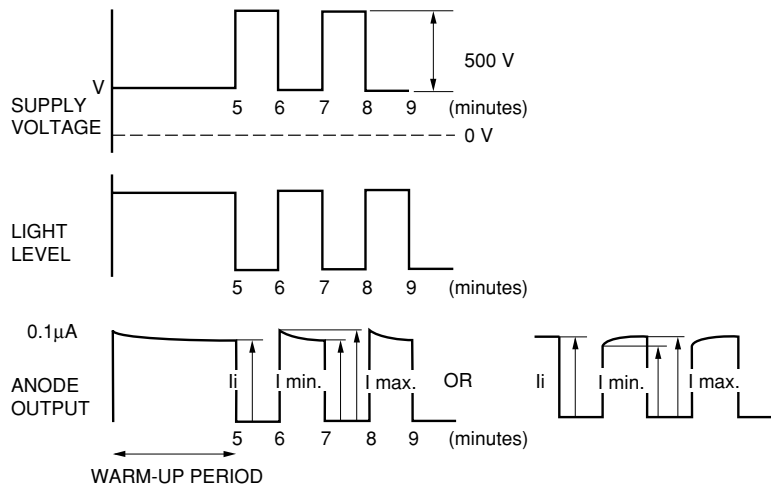
**(2) Voltage hysteresis**

When the incident light level cycles in a step function, the photomultiplier tube is sometimes operated with a feedback circuit that changes the supply voltage in a complimentary step function so that the photomultiplier tube output is kept constant. In this case, the photomultiplier tube output may overshoot or undershoot immediately after the supply voltage is changed. This phenomenon is called voltage hysteresis and should be suppressed to the minimum possible value. Generally, this voltage hysteresis is larger than light hysteresis and even tubes with small light hysteresis may possibly exhibit large voltage hysteresis. Refer to Table 4-5 below for typical hysteresis data.

PMT	Light Hysteresis H <sub>L</sub> (%)	Voltage Hysteresis H <sub>V</sub> (%)	Tube Diameter (mm)
R6350	0.3	0.5	13mm side-on
R212	0.2	1.0	28mm side-on
R928	0.1	1.0	28mm side-on
R647	0.9	2.5	13mm head-on
R6095	0.4	2.0	28mm head-on
R1306	0.07	0.06	52mm head-on

**Table 4-5: Typical hysteresis data for major Hamamatsu photomultiplier tubes**

Figure 4-37 shows a procedure for measuring voltage hysteresis. A photomultiplier tube is operated at a voltage V, which is 700 volts lower than the voltage used to measure the anode luminous sensitivity. The tube is warmed up for five minutes or more at a light level producing an anode current of approximately 0.1 microamperes.



THEV3\_0437EA

**Figure 4-37: Voltage hysteresis**

Then the incident light is shut off for one minute while the supply voltage is increased in 500 volt step. Then the light level and supply voltage are returned to the original conditions. This procedure is repeated to confirm the reproducibility. By measuring the variations in the anode outputs, the extent of voltage hysteresis is expressed in percent, as shown in Eq. 4-8 below. In general, the higher the change in the supply voltage, the larger the voltage hysteresis will be. Other characteristics are the same as those for light hysteresis.

$$\text{Voltage hysteresis } H_V = ((I_{MAX} - I_{MIN}) / I_i) \times 100(\%) \dots\dots\dots (\text{Eq. 4-18})$$

where I<sub>MAX</sub> is the maximum output value, I<sub>MIN</sub> is the minimum output value and I<sub>i</sub> is the initial output value.



### (3) Reducing the hysteresis

When a signal light is blocked for a long period of time, applying a dummy light to the photomultiplier tube to minimize the change in the anode output current is effective in reducing the possible light hysteresis. Voltage hysteresis may be improved by use of HA coating. (Refer to section 8.2 in Chapter 13.)

## 4.3.6 Dark current

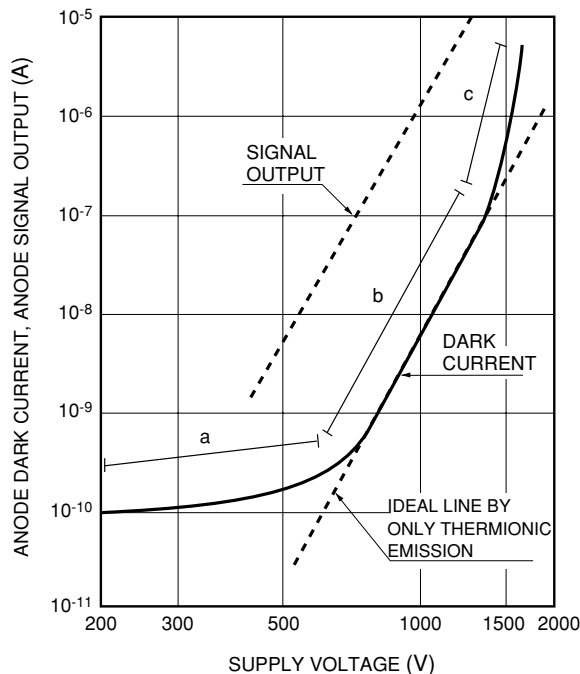
A small amount of current flows in a photomultiplier tube even when operated in a completely dark state. This output current is called the dark current<sup>1) 23) 25) 33)</sup> and ideally it should be kept as small as possible because photomultiplier tubes are used for detecting minute amounts of light and current.

### (1) Causes of dark current

Dark current may be categorized by cause as follows:

- (a) Thermionic emission current from the photocathode and dynodes
- (b) Leakage current (ohmic leakage) between the anode and other electrodes inside the tube and/or between the anode pin and other pins on the bulb stem
- (c) Photocurrent produced by scintillation from glass envelope or electrode supports
- (d) Field emission current
- (e) Ionization current from residual gases (ion feedback)
- (f) Noise current caused by cosmic rays, radiation from radioisotopes contained in the glass envelopes and environmental gamma rays

Dark current increases with an increasing supply voltage, but the rate of increase is not constant. Figure 4-38 shows a typical dark current vs. supply voltage characteristic.



THBV3\_0438EA

Figure 4-38: Typical dark current vs. supply voltage characteristic

This characteristic is related to three regions of the supply voltage: a low voltage region (a in Figure 4-38), a medium voltage region (b in Figure 4-38), and a high voltage region (c in Figure 4-38). Region a is dominated by the leakage current, region b by the thermionic emission, and region c by the field emission and glass or electrode support scintillation. In general, region b provides the best signal-to-noise ratio, so operating the photomultiplier tube in this region would prove ideal.

Ion feedback<sup>34)</sup> and noise<sup>34) 35) 36)</sup> originating from cosmic rays and radioisotopes will sometimes be a problem in pulse operation.

When a photocathode is exposed to room illumination, the dark current will return to the original level by storing the photomultiplier tube in a dark state for one to two hours. However, if exposed to sunlight or extremely intense light (10,000 lux or higher), this may cause unrecoverable damage and must therefore be avoided. It is recommended to store the photomultiplier tube in a dark state before use.

The dark current data furnished with Hamamatsu photomultiplier tubes is measured after the tube has been stored in a dark state for 30 minutes. This "30-minute storage in a dark state" condition allows most photomultiplier tubes to approach the average dark current level attained after being stored for a long period in a dark state. This is also selected in consideration of the work efficiency associated with measuring the dark current. If the tube is stored for a greater length of time in a dark state, the dark current will decrease further. The following sections explain each of the six causes of dark current listed above.

#### a) Thermionic emission

Since the photocathode and dynode surfaces are composed of materials with a very low work function, they emit thermionic electrons even at room temperatures. This effect has been studied by W. Richardson, and is stated by the following equation.<sup>37)</sup>

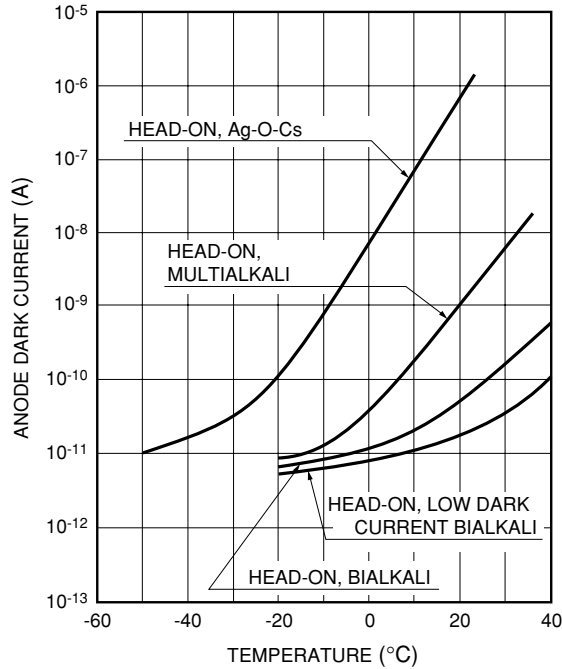
$$i_s = AT^{5/4} e^{(-e\psi/KT)} \dots\dots\dots \text{(Eq. 4-19)}$$

where,

$\psi$ : work function	T : absolute temperature
e : electron charge	A : constant
K : Boltzmann constant	

It can be seen from this equation that thermionic emission is a function of the photocathode work function and absolute temperature. Thus the magnitude of the work function as well as the photocathode material govern the amount of thermionic emission. When the photocathode work function is low, the spectral response extends to the light with lower energy or longer wavelengths, but with an increase in the thermionic emission. Among generally used photocathodes composed of alkali metals, the Ag-O-Cs photocathode with a spectral response in the longest wavelength range (see Figure 4-2) exhibits the highest dark current. In contrast, the photocathodes for the ultraviolet range (Cs-Te, Cs-I) exhibit the shortest wavelength upper limit and provide the lowest dark current.

Eq. 4-19 also implies that the dark current decreases with decreasing temperature. Therefore, as shown in Figure 4-39, cooling a photomultiplier tube is an effective technique for reducing the dark current.

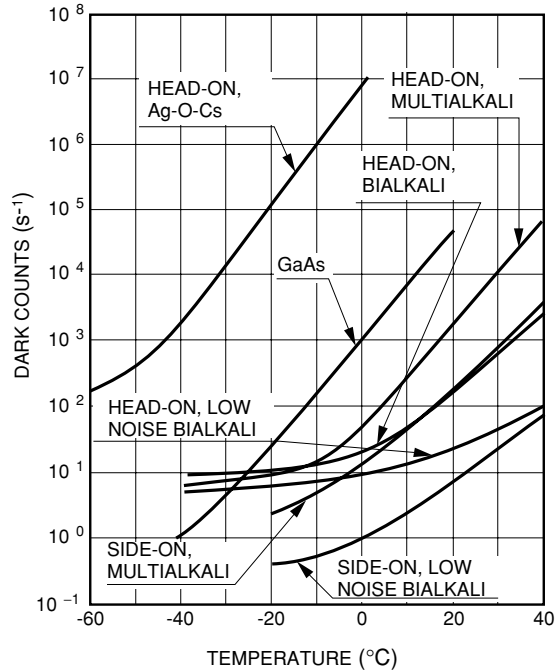


THBV3\_0439EA

**Figure 4-39: Temperature characteristics of anode dark current**

However, when the dark current reduces down to a level where the leakage current predominates, this effect becomes limited. Although thermionic emission occurs both from the photocathode and the dynodes, the thermionic emission from the photocathode has a much larger effect on the dark current. This is because the photocathode is larger than each dynode in size and also because the dynodes, especially at the latter stages, contribute less to the output current. Consequently, the dark current caused by the thermionic emission vs. the supply voltage characteristic will be nearly identical with the slope of gain vs. supply voltage.

Figure 4-40 describes temperature characteristics for dark pulses measured in the photon counting method. In this case as well, the number of dark pulses is decreased by cooling the photocathode.



THBV3\_0440EA

Figure 4-40: Temperature characteristics for dark current pulse

### b) Leakage current (ohmic leakage)

Photomultiplier tubes are operated at high voltages from 500 up to 3000 volts, but they handle very low currents from several nanoamperes to less than 100 microamperes. Therefore, the quality of the insulating materials used in the tubes is very important. For instance, if the insulation resistance is around  $10^{12}$  ohms, the leakage current may reach the nanoampere level. The relationship between the leakage current from the insulating materials and the supply voltage is determined by Ohm's law, i.e., current value ( $I$ ) = supply voltage ( $V$ )/insulation resistance ( $R$ ), regardless of the gain of the photomultiplier tube as seen in Figure 4-38. On the other hand, the dark current resulting from thermionic emission varies exponentially with the supply voltage. Thus, as mentioned in the previous section, the leakage current has relatively more effect on the dark current as the supply voltage is lowered.

A leakage current may be generated between the anode and the last dynode inside a tube. It may also be caused by imperfect insulation of the glass stem and base, and between the socket anode pin and other pins. Since contamination from dirt and moisture on the surface of the glass stem, base, or socket increases the leakage current, care should be taken to keep these parts clean and at low humidity. If contaminated, they can be cleaned with alcohol in most cases. This is effective in reducing the leakage current.

### c) Scintillation from the glass envelope or electrode support materials

Some electrons emitted from the photocathode or dynodes may deviate from their normal trajectories and do not contribute to the output signal. If these stray electrons impinge on the glass envelope, scintillations may occur and result in dark pulses. In general, a photomultiplier tube is operated with a negative high voltage applied to the photocathode and is housed in a metal case at ground potential. This arrangement tends to cause stray electrons to impinge on the glass envelope. However, this problem can be minimized by using a technique called "HA coating". Refer to section 8.2 in Chapter 13 for detailed information on HA coating.

**d) Field emission**

If a photomultiplier tube is operated at an excessive voltage, electrons may be emitted from the dynodes by the strong electric field. Subsequently the dark current increases abruptly. This phenomenon occurs in region c in Figure 4-38 and shortens the life of the photomultiplier tube considerably. Therefore, the maximum supply voltage is specified for each tube type and must be observed. As long as a photomultiplier tube is operated within this maximum rating there will be no problem. But for safety, operating the photomultiplier tube at a voltage 20 to 30 percent lower than the maximum rating is recommended.

**e) Ionization current of residual gases (ion feedback)**

The interior of a photomultiplier tube is kept at a vacuum as high as  $10^{-6}$  to  $10^{-5}$  Pa. Even so, there exist residual gases that cannot be ignored. The molecules of these residual gases may be ionized by collisions with electrons. The positive ions that strike the front stage dynodes or the photocathode produce many secondary electrons, resulting in a large noise pulse. During high current operation, this noise pulse is usually identified as an output pulse appearing slightly after the main photocurrent. This noise pulse is therefore called an afterpulse<sup>38) 39) 40)</sup> and may cause a measurement error during pulsed operation.

**f) Noise current caused by cosmic rays, radiation from radioisotopes contained in the glass envelopes and environmental gamma rays**

Many types of cosmic rays are always falling on the earth. Among them, muons ( $\mu$ ) can be a major source of photomultiplier tube noise. When muons pass through the glass envelope, Cherenkov radiation may occur, releasing a large number of photons. In addition, most glasses contain potassium oxide ( $K_2O$ ) which also contains a minute amount of the radioactive element  $^{40}K$ .  $^{40}K$  emits beta and gamma rays which may cause noise. Furthermore, environmental gamma rays emitted from radioisotopes contained in buildings may be another noise source. However, because these dark noises occur much less frequently, they are negligible except for applications such as liquid scintillation counting where the number of signal counts is exceptionally small.

**(2) Expression of dark current**

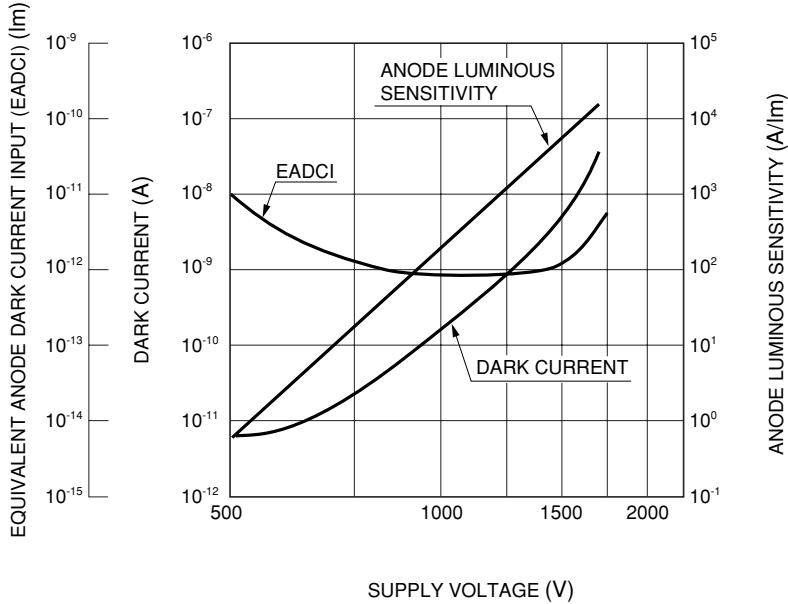
Dark current is a critical factor that governs the lower detection limit in low light level measurements. There are various methods and terms used to express dark current. The following introduces some of them.

**a) DC expression**

In general, most Hamamatsu photomultiplier tubes are supplied with dark current data measured at a constant voltage. The dark current may be measured at a voltage at which a particular value of anode sensitivity is obtained. In this case, the dark current is expressed in terms of equivalent dark current or EADCI (equivalent anode dark current input). The equivalent dark current is simply the dark current measured at the voltage producing a specific anode luminous sensitivity, and is a convenient parameter when the tube is operated with the anode sensitivity maintained at a constant value. The EADCI is the value of the incident light flux required to produce an anode current equal to the dark current and is represented in units of lumens or watts as follows:

$$\text{EADCI (lm)} = \text{Dark current (A)} / \text{Anode luminous sensitivity (A/lm)} \dots\dots (\text{Eq. 4-20})$$

When representing the EADCI in watts (W), a specified wavelength is selected and the dark current is divided by the anode radiant sensitivity (A/W) at that wavelength. Figure 4-41 illustrates an example of EADCI data along with the anode dark current and anode luminous sensitivity. A better signal-to-noise ratio can be obtained when the tube is operated in the supply voltage region with a small EADCI. It is obvious from this figure that the supply voltage region in the vicinity of 1000 volts displays a small, flat EADCI curve, yet offers an adequate anode sensitivity of three orders of magnitude.



THBV3\_0441EA

Figure 4-41: Example of EADCI

**b) AC expression**

In low-level-light measurements, the DC components of dark current can be subtracted. The lower limit of light detection is determined rather by the fluctuating components or noise. In this case, the noise is commonly expressed in terms of ENI (equivalent noise input). The ENI is the value of incident light flux required to produce an output current equal to the noise current, i.e., the incident light level that provides a signal-to-noise ratio of unity. When the ENI is expressed in units of watts (W) at the peak wavelength or at a specific wavelength, it is also referred to as the NEP (noise equivalent power).

Because the noise is proportional to the square root of the circuit bandwidth, the ENI<sup>23)</sup> is defined as follows:

$$ENI = (2e \cdot I_d \cdot \mu \cdot B)^{1/2} / S \text{ (W)} \dots\dots\dots \text{(Eq. 4-21)}$$

where

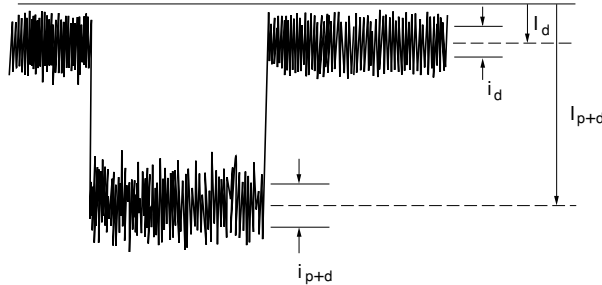
- e: electron charge ( $1.6 \times 10^{-19}$  C)
- $I_d$ : anode dark current (A)
- $\mu$ : current amplification
- B: circuit bandwidth (Hz)
- S: anode radiant sensitivity (A/W)

Commonly,  $\Delta f = 1\text{Hz}$  is used and the ENI value ranges from  $10^{-15}$  to  $10^{-16}$  (W) at the peak wavelength.

### 4.3.7 Signal-to-noise ratio of photomultiplier tubes

When observing the output waveform of a photomultiplier tube, two types of noise components can be seen: one is present even without light input, and the other is generated by the input of signal light. Normally, these noise components are governed by the dark current generated by the photocathode thermionic emission and the shot noise resulting from the signal current. Both of these noise sources are discussed here.

The signal-to-noise ratio referred to in the following description is expressed in r.m.s. (root mean square). When signal and noise waveforms like those shown in Figure 4-42 are observed, they can be analyzed as follows:



THBV3\_0442EA

Figure 4-42: Example of signal-to-noise ratio

- Mean value of noise component :  $I_d$
- AC component of noise :  $i_d$  (r.m.s.)
- Mean value of signal (noise component included) :  $I_{p+d}$
- AC component of signal (noise component included) :  $i_{p+d}$  (r.m.s.)

Using these factors, the signal-to-noise ratio<sup>25) 41) 42)</sup> is given by

$$\text{SN ratio} = I_p/i_{p+d} \dots\dots\dots \text{(Eq. 4-22)}$$

where  $I_p$  is the mean value of the signal component only, which is obtained by subtracting  $I_d$  from  $I_{p+d}$ .

If the dark current  $I_d$  is low enough to be ignored ( $I_p \gg I_d$ ), the signal-to-noise ratio will be

$$\text{SN ratio} \approx I_p/i_p \dots\dots\dots \text{(Eq. 4-23)}$$

where  $I_p$  is the mean value of the signal component and  $i_p$  is the AC component (r.m.s.) of the signal.  $i_p$  consists of a component associated with the statistical fluctuation of photons and the photoemission process and a component created in the multiplication process. The noise component produced in the multiplication process is commonly expressed in terms of the NF (noise figure)<sup>42)</sup>. The NF indicates how much the signal-to-noise ratio will degrade between the input and output, and is defined as follows:

$$F = (S/N)_{in}^2/(S/N)_{out}^2 \dots\dots\dots \text{(Eq. 4-24)}$$

where  $(S/N)_{in}$  is the signal-to-noise ratio on the photomultiplier tube input side and  $(S/N)_{out}$  is the signal-to-noise ratio on the photomultiplier tube output side. With a photomultiplier tube having  $n$  dynode stages, the NF from the cascade multiplication process is given by the following equation:

$$F = 1 + 1/\delta_1 + 1/\delta_1\delta_2 + \dots + 1/\delta_1\delta_2 \dots \delta_n \dots\dots\dots \text{(Eq. 4-25)}$$

where  $\delta_1, \delta_2 \dots \delta_n$  are the secondary emission ratios at each stage.

With  $\delta_1, \delta_2, \delta, \dots, \delta_n = \delta$ , Eq. 4-25 is simplified as follows:

$$F \approx \delta / (\delta - 1) \dots\dots\dots \text{(Eq. 4-26)}$$

Thus by adding the NF to the AC component  $i_p$ ,  $i_p$  is expressed by the following equation:

$$i_p = \mu \{ 2 \cdot e \cdot I_k \cdot \alpha \cdot B \cdot F \}^{1/2} \dots\dots\dots \text{(Eq. 4-27)}$$

where  $\alpha$  is the collection efficiency,  $\mu$  is the gain,  $e$  is the electron charge,  $I_k$  is the cathode current and  $B$  is the bandwidth of the measurement system. From this equation and Eq. 4-25,  $i_p$  becomes

$$i_p = \mu \{ 2 \cdot e \cdot I_k \cdot \alpha \cdot B (1 + 1/\delta_1 + 1/\delta_1\delta_2 + \dots + 1/\delta_1\delta_2 \dots \delta_n) \}^{1/2} \dots\dots\dots \text{(Eq. 4-28)}$$

On the other hand, the average anode current  $I_p$  is expressed in the following equation:

$$I_p = I_k \cdot \alpha \cdot \mu \dots\dots\dots \text{(Eq. 4-29)}$$

From Eqs. 4-28 and 4-29, the signal-to-noise ratio becomes

$$\begin{aligned} \text{SN ratio} &= I_p / i_p \\ &= \left( \frac{I_k \alpha}{2eB} \cdot \frac{1}{1 + 1/\delta_1 + 1/\delta_1\delta_2 + \dots + 1/\delta_1\delta_2 \dots \delta_n} \right)^{1/2} \end{aligned}$$

With  $\alpha = 1$  the above equation can be simplified using Eq. 4-26, as follows:

$$\text{SN ratio} \approx \left( \frac{I_k}{2eB} \cdot \frac{1}{\delta / (\delta - 1)} \right)^{1/2} \dots\dots\dots \text{(Eq. 4-30)}$$

From this relationship, it is clear that the signal-to-noise ratio is proportional to the square root of the cathode current  $I_k$  and is inversely proportional to the square root of the bandwidth  $B$ .

To obtain a better signal-to-noise ratio, the shot noise should be minimized and the following points observed:

- (1) Use a photomultiplier tube that has as high a quantum efficiency as possible in the wavelength range to be measured.
- (2) Design the optical system for better light collection efficiency so that the incident light is guided to the photomultiplier tube with minimum loss.
- (3) Use a photomultiplier tube that has an optimum configuration for light collection.
- (4) Narrow the bandwidth as much as possible, as long as no problems occur in the measurement system.

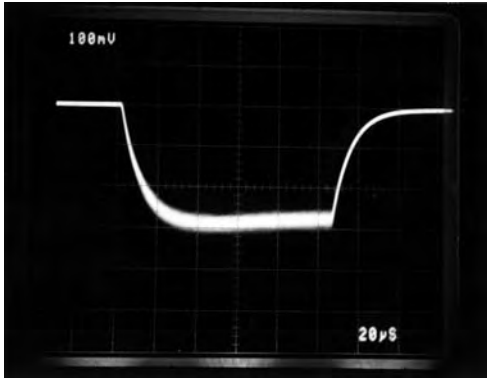
By substituting  $\delta = 6$  into Eq. 4-30, which is the typical secondary emission ratio of a normal photomultiplier tube, the value  $\delta / (\delta - 1)$  will be 1.2, a value very close to 1. Consequently, if the noise in the multiplication process is disregarded, the signal-to-noise ratio can be rearranged as follows:

$$\text{SN ratio} = (I_k / 2eB)^{1/2} \approx 1.75 \times 10^3 \sqrt{\frac{I_k (\mu\text{A})}{B (\text{MHz})}} \dots\dots\dots \text{(Eq. 4-31)}$$

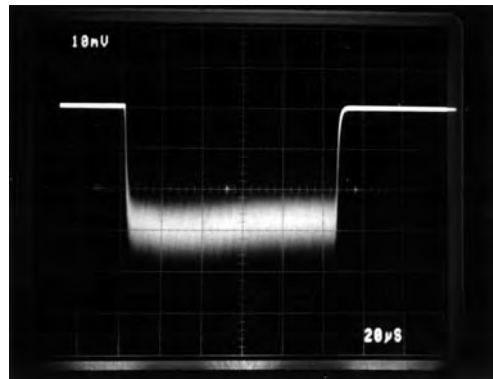
Figure 4-43 shows the output voltage waveforms obtained while the light level and load resistance are changed under certain conditions. These prove that the relation in Eq. 4-31 is correct.



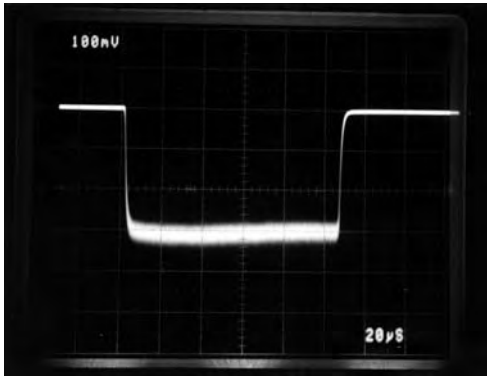
(a)  $R_L=20k\Omega$



(b)  $R_L=2k\Omega$  (Bandwidth is 10 times wider than (a))



(c) Light level is 10 times higher than (b)



THBV3\_0443EA

**Figure 4-43: Change in signal-to-noise ratio for R329 when light level and load resistance are changed**

The above description ignores the dark current. Taking into account the contribution of the cathode equivalent dark current ( $I_d$ ) and the noise current ( $N_A$ ) of the amplifier circuit, Eq. 4-30 can be rewritten as follows:

$$SN \text{ ratio} = \frac{I_k}{(2eB \cdot \delta / (\delta - 1) \cdot (I_k + 2I_d) + N_A^2)^{1/2}} \dots\dots\dots \text{(Eq. 4-32)}$$

In cases in which the noise of the amplifier circuit is negligible ( $N_A=0$ ), the signal-to-noise ratio becomes

$$SN \text{ ratio} = \frac{I_k}{(2eB \cdot \delta / (\delta - 1) \cdot (I_k + 2I_d))^{1/2}} \dots\dots\dots \text{(Eq. 4-33)}$$

where  $I_k = \eta \cdot e \cdot P \cdot \lambda \dots / hc$ , and each symbol stands for the following:

- |   |  |
|---|--|
| $I_k$ : cathode current (A)                 | $e$ : electron charge (C)              |
| $\lambda$ : wavelength (m)                  | $h$ : Planck's constant (J·s)          |
| $c$ : velocity of light (m/s)               | $\eta$ : quantum efficiency            |
| $P$ : power (W)                             | $B$ : bandwidth (Hz)                   |
| $\delta$ : secondary emission ratio         | $N_A$ : noise of amplifier circuit (A) |
| $I_d$ : cathode equivalent dark current (A) |  |

If  $F=(\delta/(\delta-1))$  is inserted in Eq. 4-33, then

$$\begin{aligned} \text{SN ratio} &= \frac{I_k}{(2 \cdot e \cdot (I_k + 2I_{da})FB)^{1/2}} = \frac{I_k \cdot \mu}{(2e(I_{ph} + 2I_{da})FB \cdot \mu^2)^{1/2}} \\ &= \frac{I_p}{\sqrt{2e(I_p + 2I_{da})\mu FB}} = \frac{S_p P_i}{\sqrt{2e(S_p P_i + 2I_{da})\mu FB}} \end{aligned}$$

where  $I_p$  is the anode signal current and  $I_{da}$  is the anode dark current.

$I_p$  is given by:  $I_p = I_h \cdot \mu = S_p \cdot P_i$

where  $S_p$  is the anode radiant sensitivity and  $P_i$  is the incident light power.

If the signal-to-noise ratio is 1, then

$$S_p P_i = \sqrt{2e(S_p P_i + 2I_{da})\mu FB}$$

This relation is expressed as follows to find the variable  $P_i$  that gives

$$(S_p P_i)^2 - 2e(S_p P_i + 2I_{da})\mu FB = 0$$

$$S_p P_i = \frac{-(-2eS_p \mu FB) \pm \sqrt{(-2eS_p \mu FB)^2 - 4S_p^2(-4eI_{da}\mu FB)}}{2S_p^2}$$

Therefore,  $P_i$  becomes

$$P_i = \frac{e\mu FB}{S_p} + \frac{\sqrt{(e\mu FB)^2 + 4eI_{da}\mu FB}}{S_p}$$

This is the detection limit.

Detection limits at different bandwidths are plotted in Figure 4-44. When compared to ENI (obtained from Eq. 4-21) that takes into account only the dark current, the difference is especially significant at higher bandwidths. The detection limit can be approximated as ENI when the frequency bandwidth  $B$  of the circuit is low (up to about a few kilohertz), but it is dominated by the shot noise component originating from signal light at higher bandwidths.

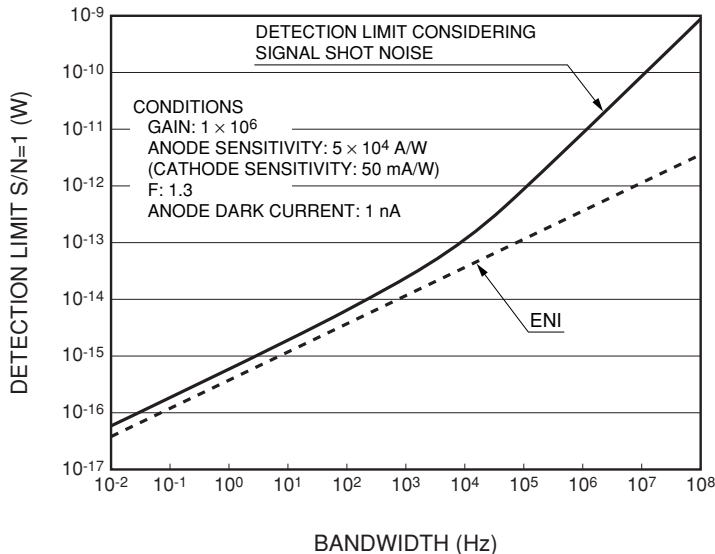


Figure 4-44: Detection limit considering signal shot noise component

Note that ENI is practical when the frequency bandwidth  $B$  of the circuit is low (up to about a few kilohertz), but is meaningless at higher bandwidths since the detection limit is dominated by the shot noise resulting from signal light. (Refer to Chapter 6, "Photon Counting".)

### 4.3.8 Afterpulsing

When a photomultiplier tube is operated in a pulse detection mode as in scintillation counting or in laser pulse detection, spurious pulses with small amplitudes may be observed. Since these pulses appear after the signal output pulse, they are called afterpulses. Afterpulses often disturb accurate measurement of low level signals following a large amplitude pulse, degrade energy resolution in scintillation counting (See Chapter 7.), and causes errors in pulse counting applications.

#### Types of afterpulses

There are two types of afterpulses: one is output with a very short delay (several nanoseconds to several tens of nanoseconds) after the signal pulse and the other appears with a longer delay ranging up to several microseconds, each being generated by different mechanisms. In general, the latter pulses appearing with a long delay are commonly referred to as afterpulses.

Most afterpulses with a short delay are caused by elastic scattering electrons on the first dynode. The probability that these electrons are produced can be reduced to about one-tenth in some types of photomultiplier tubes by placing a special electrode near the first dynode. Usually, the time delay of this type of afterpulse is small and hidden by the time constant of the subsequent signal processing circuit, so that it does not create significant problems in most cases. However, this should be eliminated in time-correlated photon counting for measuring very short fluorescence lifetime, laser radar (LIDAR), and fluorescence or particle measurement using an auto correlation technique.

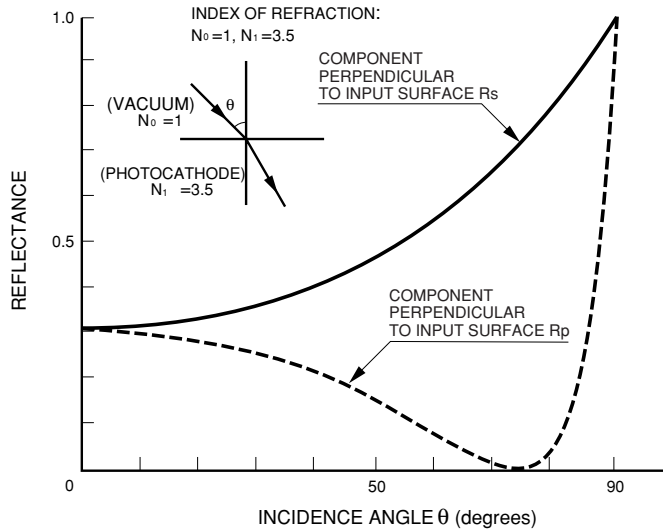
In contrast, afterpulses with a longer delay are caused by the positive ions which are generated by the ionization of residual gases in the photomultiplier tube. These positive ions return to the photocathode (ion feedback) and produce many photoelectrons which result in afterpulses. The amplitude of this type of afterpulse depends on the type of ions and the position where they are generated. The time delay with respect to the signal output pulse ranges from several hundred nanoseconds to over a few microseconds, and depends on the supply voltage for the photomultiplier tube. Helium gas is known to produce afterpulses because it easily penetrates through a silica bulb, so use caution with operating environments. Afterpulses can be reduced temporarily by aging (See 4.3.4, "Stability".), but this is not a permanent measure.

In actual measurements, the frequency of afterpulses and the amount of charge may sometimes be a problem. The amount of output charge tends to increase when the photomultiplier tube is operated at a higher supply voltage, to obtain a high gain, even though the number of generated ions is the same. In pulse counting applications such as photon counting, the frequency of afterpulses with an amplitude higher than a certain threshold level will be a problem.

As explained, afterpulses appear just after the signal pulse. Depending on the electrode structure, another spurious pulse (prepulse) may be observed just before the signal pulse output. But, this pulse is very close to the signal pulse and has a low amplitude, causing no problems.

### 4.3.9 Polarized-light dependence

Photomultiplier tube sensitivity may be affected by polarized light.<sup>43) 44)</sup> Tube characteristics must be taken into account when measuring polarized light. Also it should be noted that light may be polarized at such optical devices as monochromators. When polarized light enters the photocathode of a photomultiplier tube, the photocathode reflectance varies with the angle of incidence. This effect is also greatly dependent on the polarization component as shown in Figure 4-45. In this figure,  $R_p$  is the polarization component parallel to the photocathode surface (P component) and  $R_s$  is the polarization component perpendicular to the photocathode surface (S component). It is clear that the photocathode reflectance varies with the angle of incidence. Because this figure shows the calculated examples with the assumption that the absorption coefficient at the photocathode is zero, the actual data will be slightly more complicated.



THBV3\_0445EA

Figure 4-45: Angle dependence of reflectance

If the polarization plane of the incident light has an angle  $\theta$  with respect to the perpendicular of the photocathode surface, the photocurrent  $I_\theta$  is given by the following expression:

$$I_\theta = I_s \cos^2 \theta + I_p \sin^2 \theta = \frac{1}{2} (I_p + I_s) \left( 1 - \frac{I_p - I_s}{I_p + I_s} \cos^2 \theta \right) \dots\dots\dots (Eq. 4-34)$$

where

$I_s$ : Photocurrent produced by polarized component perpendicular to the photocathode

$I_p$ : Photocurrent produced by polarized component parallel to the photocathode

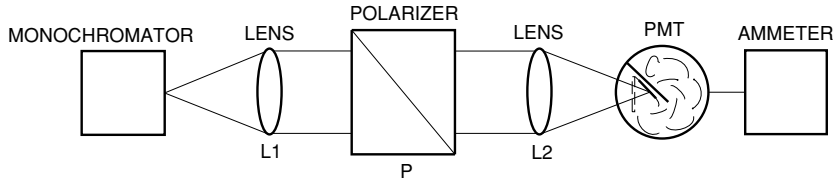
while

$$I_\theta = \frac{I_p + I_s}{2}, P = \frac{I_p - I_s}{I_p + I_s} \dots\dots\dots (Eq. 4-35)$$

then substituting Eq. 4-35 into Eq. 4-34 gives the following relationship

$$I_\theta = I_\theta (1 - P \cos^2 \theta) \dots\dots\dots (Eq. 4-36)$$

$P$  is called the polarization factor and indicates the polarized-light dependence of a photomultiplier tube, and is measured using the optical system like that shown in Figure 4-46.



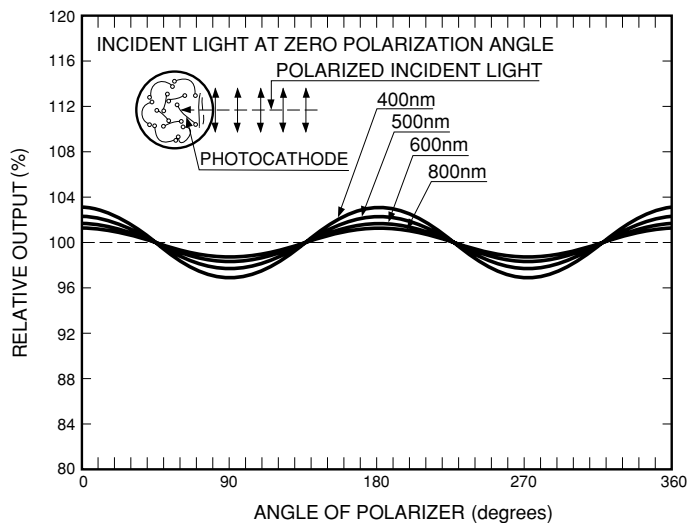
THBV3\_0446EA

**Figure 4-46: Optical system used for measuring polarized-light dependence**

In the above measurement, monochromatic light from the monochromator is collimated by  $L_1$  (collimator lens) and is linearly polarized by the polarizer (P). The polarized light is then focused onto the photomultiplier tube through  $L_2$  (condenser lens). The dependence on the polarized light is measured by recording the photomultiplier tube output in accordance with the rotating angle of the polarizer.

In this case, the polarization component of the light source must be removed. This is done by interposing a diffuser plate such as frosted glass or by compensating for the photomultiplier tube output values measured when the tube is at 0 degree and is then rotated to 90 degrees with respect to the light axis.

Figure 4-47 illustrates the polarized-light dependence of a side-on photomultiplier tube with a reflection type photocathode. In principle, this dependence exists when the light enters slantways with respect to the photocathode surface. In actual operation, the polarization factor P is almost zero when the light enters perpendicular to the transmission type photocathode surface.



THBV3\_0447EA

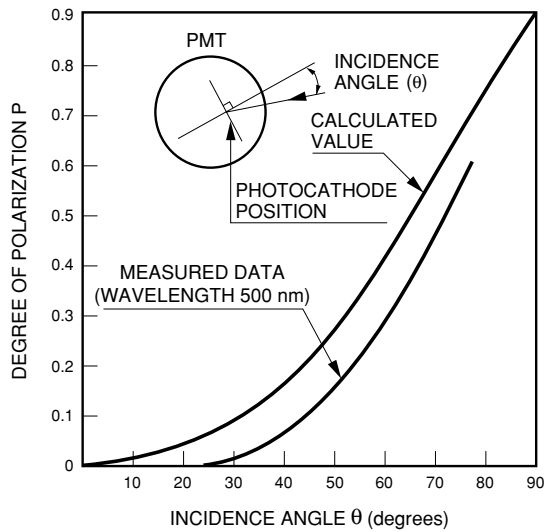
**Figure 4-47: Typical polarization-light dependence of a side-on photomultiplier tube**

In the case of reflection-type photocathode photomultiplier tubes, because the photocathode is arranged at a certain angle with respect to the input window, the sensitivity is affected by polarized light. Figure 4-48 indicates the relative output of a reflection-type photocathode photomultiplier tube as a function of the angle of incident light. It can be seen that the polarization factor P becomes smaller as the direction of the incident light nears the perpendicular of the photocathode surface.

The reflection-type photocathode photomultiplier tubes usually exhibit a polarization factor of about 10 percent or less, but tubes specially designed to minimize the polarization-light dependence offer three percent or less. A single crystal photocathode such as gallium arsenide (GaAs) has high reflectance and show a polarization factor of around 20 percent, which is higher than that of alkali antimonide photocathodes.

The polarization that provides the maximum sensitivity is the component perpendicular to the tube axis (P component). In contrast, the polarization that gives the minimum sensitivity is the component parallel to the tube axis (S component), independent of the type of tube and wavelength of incident light. As can be seen from Figure 4-45, this is probably due to a change in the photocathode transmittance. The S component increases in reflectance as the angle of incidence becomes larger, whereas the P component decreases. Moreover, as the wavelength shifts to the longer side, the reflectance generally decreases and the polarization factor P becomes smaller accordingly, as shown in Figure 4-47.

In applications where the polarized-light dependence of a photomultiplier tube cannot be ignored, it will prove effective to place a diffuser such as frosted glass or tracing paper in front of the input window of the photomultiplier tube or to use a photomultiplier tube with a frosted window.



THBV3\_0448EA

Figure 4-48: Relative output vs. incident angle of polarized light

## References in Chapter 4

- 1) Hamamatsu Photonics Catalog: Photomultiplier Tubes.
- 2) T. Hiruma, SAMPE Journal. 24, 35 (1988).
- 3) A. H. Sommer: Photoemissive Materials, Robert E. Krieger Publishing Company (1980).
- 4) T. Hirohata and Y. Mizushima: Japanese Journal of Applied Physics. 29, 8, 1527 (1990).
- 5) T. Hirohata, T. Ihara, M. Miyazaki, T. Suzuki and Y. Mizushima: Japanese Journal of Applied Physics. 28, 11, 2272 (1989).
- 6) W.A. Parkhurst, S. Dallek and B.F. Larrick: J. Electrochem. Soc, 131, 1739 (1984).
- 7) S. Dallek, W.A. Parkhurst and B.F. Larrick: J. Electrochem. Soc, 133, 2451 (1986).
- 8) R.J. Cook: Phys. Rev. A25, 2164; 26,2754 (1982).
- 9) H.J. Kimble and L. Mandel: Phys. Rev. A30, 844 (1984).
- 10) M. Miyao, T. Wada, T. Nitta and M. Hagino: Appl. Surf. Sci. 33/34, 364 (1988).
- 11) Tailing Guo: J. Vac. Sci. Technol. A7, 1563 (1989).
- 12) Huairong Gao: J. Vac. Sci. Technol. A5, 1295 (1987).
- 13) C.A. Sanford and N.C. MacDonald: J. Vac. Sci. Technol. B 6. 2005 (1988).
- 14) C.A. Sanford and N.C. MacDonald: J. Vac. Sci. Technol. B 7. 1903 (1989).
- 15) M. Domke, T. Mandle, C. Laubschat, M. Prietsch and G.Kaindl: Surf. Sci. 189/190, 268 (1987).
- 16) M. Niigaki, T. Hirohata, T. Suzuki, H. Kan and T. Hiruma: Appl. Phys. Lett. 71 (17) 27, Oct. 1997
- 17) K. Nakamura, H. Kyushima: Japanese Journal of Applied Physics, 67, 5, (1998)
- 18) D. Rodway: Surf. Sci. 147, 103 (1984).
- 19) "Handbook of Optics": McGraw-Hill (1978).
- 20) James A. R. Samson: "Techniques of Vacuum Ultraviolet Spectroscopy" John Wiley & Sons, Inc (1967).
- 21) C.R. Bamford: Phys. Chem. Glasses, 3, 189 (1962).
- 22) Corning Glass Works Catalog.
- 23) IEEE ET-61A 1969.5.8.
- 24) IEEE STD 398-1972.
- 25) IEC PUBLICATION 306-4, 1971.
- 26) H. Kume, K. Koyama, K. Nakatsugawa, S. Suzuki and D. Fatlowitz: Appl. Opt, 27, 1170 (1988).
- 27) T. Hayashi: "PHOTOMULTIPLIER TUBES FOR USE IN HIGH ENERGY PHYSICS".  
Hamamatsu Photonics Technical Publication (APPLICATION RES-0791-02).
- 28) Hamamatsu Photonics Technical Publication "USE OF PHOTOMULTIPLIER TUBES IN SCINTILLATION APPLICATIONS" (RES-0790)
- 29) T.H. Chiba and L. Mmandel: J. Opt. Soc. Am. B,5, 1305 (1988).
- 30) D.P. Jones: Appl. Opt. 15,14 (1976).
- 31) D.E. Persyk: IEEE Trans. Nucl. Sci. 38, 128 (1991).
- 32) Mikio Yamashita: Rev. Sci. Instrum., 49, 9 (1978).
- 33) "Time-Related Single-Photon Counting": Academic Press, Inc (1985).
- 34) G.F.Knoll: "RADIATION DETECTION and MEASUREMENT", John Wiley & Sons, Inc. (1979).
- 35) C.E. Miller, et al.: IEEE Trans. Nucl. Sci. NS-3, 91 (1956).
- 36) A.T. Young: Appl. Opt., 8, 12, (1969).
- 37) R.L. Bell: "Negative Electron Affinity Devices", Clarendon Press. Oxford (1973).
- 38) G.A. Morton et al.: IEEE Trans. Nucl. Sci. NS-14 No.1, 443 (1967).
- 39) R. Staubert et al.: Nucl. Instrum. & Methods 84, 297 (1970).
- 40) S.J. Hall et al.: Nucl. Instrum. & Methods 112, 545 (1973).
- 41) Illes P. Csorba "Image Tubes" Howard W, Sams & Co (1985).
- 42) F. Robber: Appl. Opt., 10, 4 (1971).
- 43) S.A. Hoenig and A. Cutler: Appl. Opt. 5,6, 1091 (1966).
- 44) H. Hora: Phys. Stat. Soli Vol (a), 159 (1971).

# MEMO



# **CHAPTER 5**

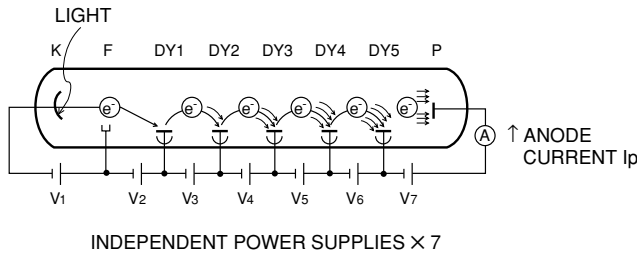
## **HOW TO USE PHOTOMULTIPLIER TUBES AND PERIPHERAL CIRCUITS**

*This chapter explains how to use the basic circuits and accessories necessary to operate a photomultiplier tube properly.<sup>1)</sup>*

## 5.1 Voltage-Divider Circuits

### 5.1.1 Basic operation of voltage-divider circuits

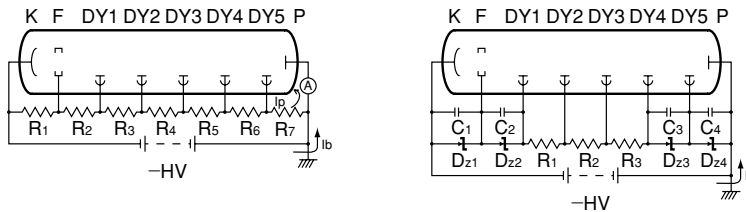
For photomultiplier tube operation, a high voltage from 500 to 3000 volts is usually applied across the cathode (K) and anode (P), with a proper voltage gradient set up between the photoelectron focusing electrode (F), dynodes and, depending on tube type, an accelerating electrode (accelerator). This voltage gradient can be set up using independent multiple power supplies as shown in Figure 5-1, but this method is not practical.



THBV3\_0501EA

Figure 5-1: Schematic diagram of photomultiplier tube operation

In practice, as shown in Figure 5-2 (1), the interstage voltage for each electrode is supplied by using voltage-dividing resistors (100 kΩ to 1 MΩ) connected between the anode and cathode. Sometimes Zener diodes are used with voltage-dividing resistors as shown in Figure 5-2 (2). These circuits are known as voltage-divider circuits.



(1) Circuit using resistors only

(2) Circuit using resistors and Zener diodes

THBV3\_0502EA

Figure 5-2: Voltage-divider circuits

The current I<sub>b</sub> flowing through the voltage-divider circuits shown in Figures 5-2 (1) and (2) is called divider current, and is closely related to the output linearity described later. The divider current I<sub>b</sub> is approximately the applied voltage V divided by the sum of resistor values as follows:

$$I_b = \frac{V}{(R_1 + R_2 + \dots + R_6 + R_7)} \dots\dots\dots \text{(Eq. 5-1)}$$

The Zener diodes (D<sub>z</sub>) shown in Figure 5-2 (2) are used to maintain the interstage voltages at constant values for stabilizing the photomultiplier tube operation regardless of the magnitude of the cathode-to-anode supply voltage. In this case, I<sub>b</sub> is obtained by using Eq. 5-1.

$$I_b = \frac{V - (\text{Sum of voltages generated at Dz1 to Dz4})}{R_1 + R_2 + R_3} \dots\dots\dots \text{(Eq. 5-2)}$$

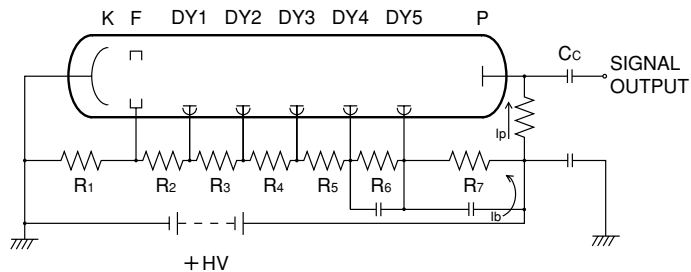
The capacitors C<sub>1</sub>, C<sub>2</sub>, C<sub>3</sub> and C<sub>4</sub> connected in parallel with the Zener diodes serve to minimize noise generated by the Zener diodes. This noise becomes significant when the current flowing through the Zener diodes is insufficient. Thus care is required at this point, as this noise can affect the signal-to-noise ratio of the photomultiplier tube output.

### 5.1.2 Anode grounding and cathode grounding

As shown in Figure 5-2, the general technique used for voltage-divider circuits is to ground the anode and apply a large negative voltage to the cathode. This scheme eliminates the potential voltage difference between the external circuit and the anode, facilitating the connection of circuits such as ammeters and current-to-voltage conversion operational amplifiers to the photomultiplier tube. In this anode grounding scheme, however, bringing a grounded metal holder, housing or magnetic shield case near the bulb of the photomultiplier tube, or allowing it to make contact with the bulb can cause electrons in the photomultiplier tube to strike the inner bulb wall. This may possibly produce glass scintillation, resulting in a significant increase in noise.

Also, for head-on photomultiplier tubes, if the faceplate or bulb near the photocathode is grounded, the slight conductivity of the glass material causes a small current to flow between the photocathode and ground. This may cause electric damage to the photocathode, possibly leading to considerable deterioration. For this reason, extreme care must be taken when designing the housing for a photomultiplier tube and when using an electromagnetic shield case. In addition, when wrapping the bulb of a photomultiplier tube with foam rubber or similar shock-absorbing materials before mounting the tube within its electromagnetic shield case at ground potential, it is very important to ensure that the materials have sufficiently good insulation properties.

The above problems concerning the anode grounding scheme can be solved by coating the bulb surface with black conductive paint and connecting it to the cathode potential. This technique is called "HA coating", and the conductive bulb surface is protected by a insulating cover for safety. In scintillation counting, however, because the grounded scintillator is usually coupled directly to the faceplate of a photomultiplier tube, the cathode is grounded with a high positive voltage applied to the anode, as shown in Figure 5-3. With this grounded cathode scheme, a coupling capacitor ( $C_c$ ) must be used to separate the positive high voltage (+HV) applied to the anode from the signal, making it impossible to extract a DC signal. In actual scintillation counting using this voltage-divider circuit, a problem concerning base-line shift may occur if the counting efficiency increases too much, or noise may be generated if a leakage current is present in the coupling capacitor. Thus care should be taken regarding these points.

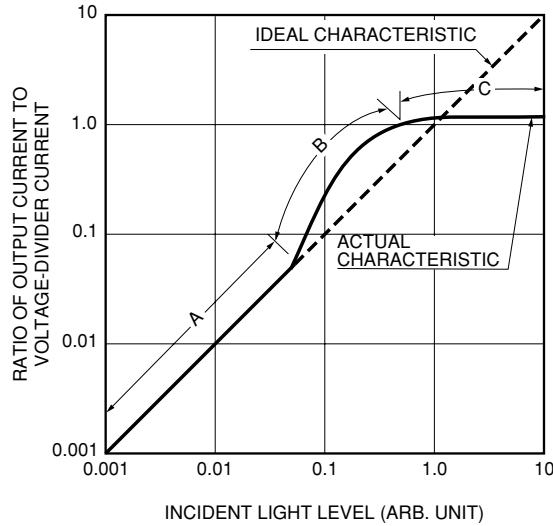


THBV3\_0503EA

Figure 5-3: Grounded-cathode voltage-divider circuit

### 5.1.3 Voltage-divider current and output linearity

In both the anode grounding and cathode grounding schemes and in both DC and pulse operation, when the light level incident on the photocathode is increased to raise the output current as shown in Figure 5-4, the relationship between the incident light level and the anode current begins to deviate from the ideal linearity at a certain current level (region B) and eventually, the photomultiplier tube output goes into saturation (region C).

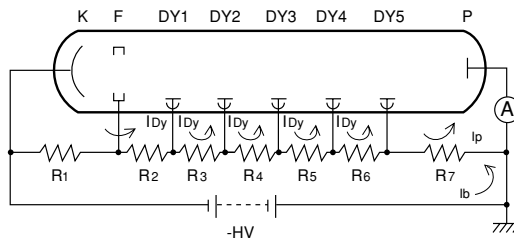


THBV3\_0504EA

Figure 5-4: Output linearity of a photomultiplier tube

#### (1) DC-operation output linearity and its countermeasures

In deriving a DC output from a photomultiplier tube using the basic operating circuit shown in Figure 5-5, the current which actually flows through a voltage-divider resistor, for example the current flowing across resistor  $R_7$ , equals the difference between the divider current  $I_b$  and the anode current  $I_p$  which flows in the opposite direction through the circuit loop of P-DY<sub>5</sub>-R<sub>7</sub>-P. Likewise, for other voltage-divider resistors, the actual current is the difference between the divider current  $I_b$  and the dynode current  $I_{Dy}$  flowing in the opposite direction through the voltage-divider resistor. The anode current and dynode current flow act to reduce the divider current and the accompanying loss of the interstage voltage becomes more significant in the latter dynode stages which handle larger dynode currents.

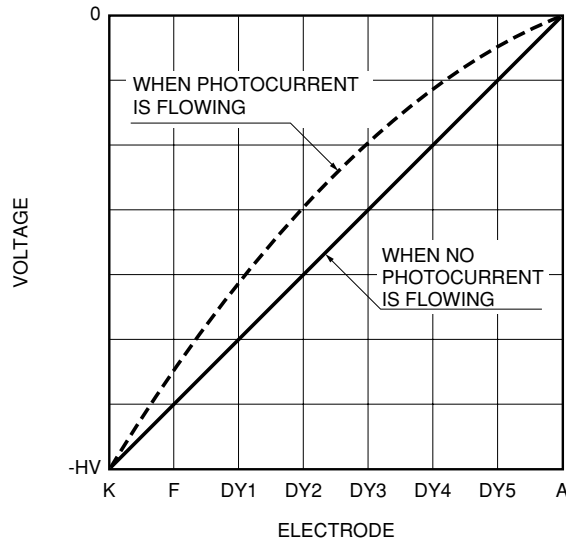


THBV3\_0505EA

Figure 5-5: Basic operating circuit for a photomultiplier tube

The reduction of the divider current can be ignored if the anode output current is small. However, when the incident light level is increased and the resultant anode and dynode currents are increased, the voltage distribution for each dynode varies considerably as shown in Figure 5-6. Because the overall cathode-to-

anode voltage is kept constant by the high-voltage power supply, the loss of the interstage voltage at the latter stages is redistributed to the previous stages so that there will be an increase in the interstage voltage.



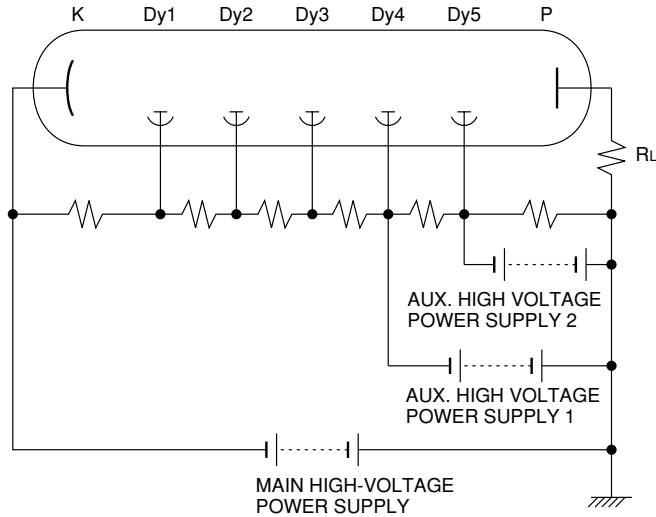
THBV3\_0506EA

**Figure 5-6: Influence of photocurrent on voltage applied to each electrode**

The loss of the interstage voltage by means of the multiplied electron current appears most significantly between the last dynode (DY<sub>5</sub> in Figure 5-5) and the anode, but the voltage applied to this area does not contribute to the secondary emission ratio of the last dynode. Therefore, the shift in the voltage distribution to the earlier stages results in a collective increase in current amplification, as shown at region B in Figure 5-4. If the incident light level is increased further so that the anode current becomes quite large, the secondary-electron collection efficiency of the anode degrades as the voltage between the last dynode and the anode decreases. This leads to the saturation phenomenon like that shown at region C in Figure 5-4.

While there are differences depending on the type of photomultiplier tube and divider circuit being used, the maximum practical anode current in a DC output is usually 1/20th to 1/50th of the divider current. If linearity better than  $\pm 1$  percent is required, the maximum output must be held to less than 1/100th of the divider current.

To increase the maximum linear output, there are two techniques: one is to use a Zener diode between the last dynode and the anode as shown in Figure 5-2 (2) and, if necessary, between the next to last or second to last stage as well, and the other is to lower the voltage-divider resistor values to increase the divider current. However, with the former technique, if the divider current is insufficient, noise will be generated from the Zener diode, possibly resulting in detrimental effects of the output. Because of this, it is essential to increase the divider current to an adequate level and connect a ceramic capacitor having good frequency response in parallel with the Zener diode for absorbing the possible noise. It is also necessary to narrow the subsequent circuit bandwidth as much as possible, insofar as the response speed will permit. With the latter technique, if the voltage-divider resistors are located very close to the photomultiplier tube, the heat emanating from their resistance may raise the photomultiplier tube temperature, leading to an increase in the dark current and possible fluctuation in the output. Furthermore, since this technique requires a high-voltage power supply with a large capacity, it is advisable to increase the divider current more than necessary. To solve the above problems in applications where a high linear output is required, individual power supply boosters may be used in place of the voltage-divider resistors at the last few stages.



THBV3\_0507

Figure 5-7: Booster circuit

## (2) Pulse-operation output linearity and its countermeasures

When a photomultiplier tube is pulse-operated using the voltage-divider circuit shown in Figure 5-2 (1) or Figure 5-3, the maximum linear output is limited to a fraction of the divider current just as in the case of DC operation. To prevent this problem, decoupling capacitors can be connected to the last few stages, as shown in Figures 5-8 (1) and (2). These capacitors supply the photomultiplier tube with an electric charge during the forming of signal pulse and restrain the voltage drop between the last dynode and the anode, resulting in a significant improvement in pulse linearity. If the pulse width is sufficiently short so that the duty cycle is small, this method makes it possible to derive an output current up to the saturation level which is caused by the space charge effects in the photomultiplier tube dynodes discussed in Chapter 4. Consequently, a high peak output current, more than several thousand times as large as the divider current can be attained.

There are two methods of using the decoupling capacitors: a serial connection method and a parallel connection method as illustrated in Figure 5-8 below. The serial connection is more commonly used because the parallel connection requires capacitors which can withstand a high voltage.

The following explains the procedure for calculating the capacitor values, using the circuit shown in Figure 5-8 (1) as an example.

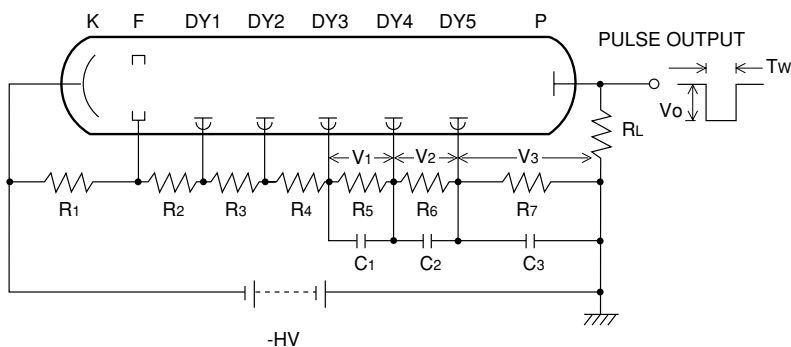
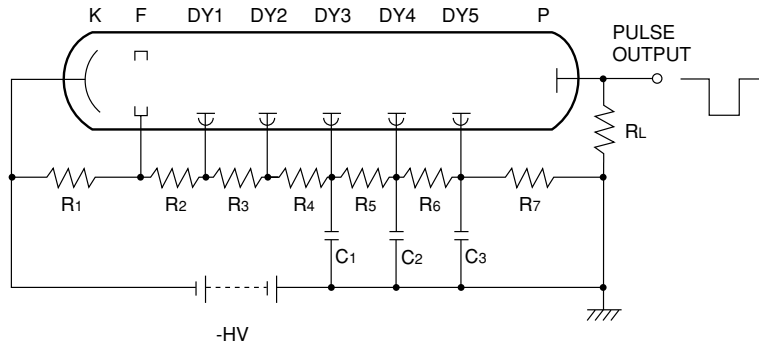


Figure 5-8 (1): Divider circuit with serial-connected decoupling capacitors



THBV3\_0508EA

**Figure 5-8 (2): Voltage-divider circuit with parallel-connected decoupling capacitors**

First of all, if we let the output-pulse peak voltage be  $V_0$ , and the pulse width be  $T_w$  and the load resistance be  $R_L$ , the output pulse charge  $Q_0$  per pulse is expressed by Eq. 5-3), as follows:

$$Q_0 = T_w \frac{V_0}{R_L} \dots\dots\dots \text{(Eq. 5-3)}$$

Next, let us find the capacitance values of the decoupling capacitors  $C_1$  to  $C_3$ , using  $Q_0$ . If we let the charge stored in capacitor  $C_3$  be  $Q_3$ , then to achieve good output linearity of better than  $\pm 3$  percent, the following relation should generally be established:

$$Q_3 \geq 100 Q_0 \dots\dots\dots \text{(Eq. 5-4)}$$

From the common relation of  $Q=CV$ ,  $C_3$  is given by Eq. 5-5.

$$C_3 \geq 100 \frac{Q_0}{V_3} \dots\dots\dots \text{(Eq. 5-5)}$$

Normally, the secondary emission ratio  $\delta$  per stage of a photomultiplier tube is 3 to 5 at the interstage voltage of 100 volts. However, considering occasions in which the interstage voltage drops to about 70 or 80 volts, the charges  $Q_2$  and  $Q_1$  stored in  $C_2$  and  $C_1$  respectively are calculated by assuming that  $\delta$  between each dynode is 2, as follows:

$$Q_2 = \frac{Q_3}{2} \quad Q_1 = \frac{Q_2}{2} = \frac{Q_3}{4}$$

Then, the capacitance values of  $C_2$  and  $C_1$  can be obtained in the same way as in  $C_3$ .

$$C_2 \geq 50 \frac{Q_0}{V_2}$$

$$C_1 \geq 25 \frac{Q_0}{V_1}$$

In cases where decoupling capacitors need to be placed in the dynode stages earlier than  $Dy_3$  in order to derive an even larger current output, the same calculation can also be used.

Here, as an example, with the output pulse peak voltage  $V_0=50$  mV, pulse width  $T_W=1$   $\mu$ s, load resistance  $R_L=50$   $\Omega$ , interstage voltages  $V_3=V_2=V_1=100$  V, each capacitor value can be calculated in the following steps:

First, the amount of charge per output pulse is obtained as follows:

$$Q_0 \geq \frac{50\text{mV}}{50\Omega} \times 1\mu\text{s} = 1\text{nC}$$

The capacitance values required of the decoupling capacitors  $C_3$ ,  $C_2$  and  $C_1$  are calculated respectively as follows:

$$C_3 \geq 100 \frac{1\text{nC}}{100\text{V}} = 1\text{nF}$$

$$C_2 \geq 50 \frac{1\text{nC}}{100\text{V}} = 0.5\text{nF}$$

$$C_1 \geq 25 \frac{1\text{nC}}{100\text{V}} = 0.25\text{nF}$$

The above capacitance values are minimum values required for proper operation. It is therefore suggested that the voltage-divider circuit be designed with a safety margin in the capacitance value, of about 10 times larger than the calculated values. If the output current increases further, additional decoupling capacitors should be connected as necessary to the earlier stages, as well as increasing the capacitance values of  $C_1$  to  $C_3$ . As with the DC operation, it should be noted that in pulse operation, even with the above countermeasures provided, the output deviates from the linearity range when the average output current exceeds 1/20th to 1/50th of the divider current. Particular care is required when operating at high counting rates even if the output peak current is low.

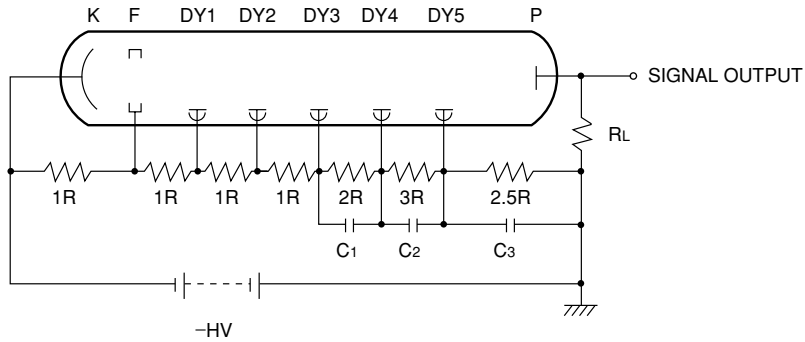
## 5.1.4 Voltage distribution in voltage-divider circuits

### (1) Voltage distribution in the anode and latter stages

Even under conditions where adequate countermeasures for pulse output linearity have been taken by use of decoupling capacitors, output saturation will occur at a certain level as the incident light is increased while the interstage voltage is kept fixed. This is caused by an increase in the electron density between the electrodes, causing space charge effects which disturb the electron current. This saturated current level varies, depending on the electrode structures of the anode and last few stages of the photomultiplier tube and also on the voltage applied between each electrode. As a corrective action to overcome space charge effects, the voltage applied to the last few stages, where the electron density becomes high, should be set at a higher value than the standard voltage distribution so that the voltage gradient between those electrodes is enhanced. For this purpose, a so-called tapered voltage-divider circuit is often employed, in which the interstage voltage is increased in the latter stages. But, sufficient care must be taken with regard to the interelectrode voltage tolerance capacity.

As an example, Figure 5-9 shows a tapered voltage-divider circuit used for a 5-stage photomultiplier tube. In this voltage-divider circuit, the  $Dy_5$ -to-anode voltage is set at a value lower than the  $Dy_4$ -to- $Dy_5$  voltage. This is because the electrode distance between the last dynode and the anode is usually short so that an adequate voltage gradient can be obtained with a relatively low voltage.

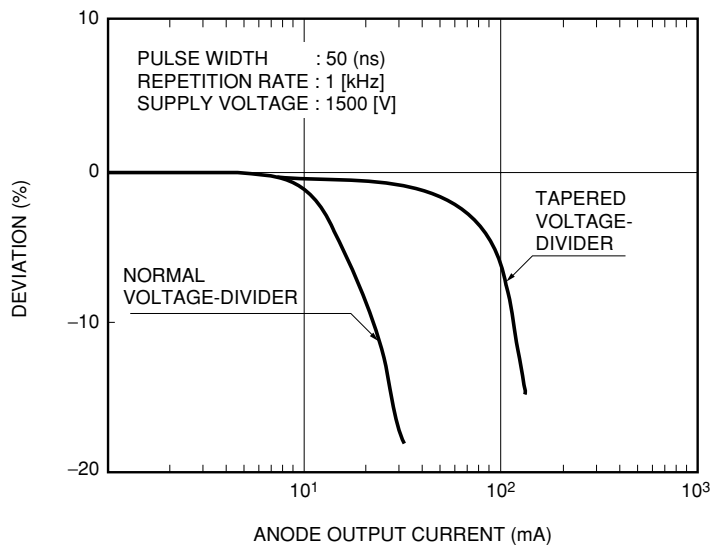




THBV3\_0509EA

**Figure 5-9: Pulse output linearity countermeasures using decoupling capacitors and tapered voltage-divider circuit**

The voltage distribution ratio for a voltage-divider circuit that provides optimum pulse linearity depends on the type of photomultiplier tube. In high energy physics applications, a higher pulse output is usually required. Our catalog "Photomultiplier Tubes and Assemblies for Scintillation Counting and High Energy Physics" lists the recommended voltage distribution ratios of individual voltage-divider circuits intended for high pulse linearity (tapered voltage-dividers) and their maximum output current values. Use of these recommended voltage-divider circuits improves pulse linearity 5 to 10 times more than that obtained with normal voltage-divider circuits (equally divided circuits). Figure 5-10 shows a comparison of pulse linearity characteristics measured with a tapered voltage-divider circuit versus that of a normal voltage-divider circuit. It is obvious that pulse linearity is improved about 10 times by using the tapered voltage-divider circuit. Note that when this type of tapered voltage-divider circuit is used, the anode output lowers to about 1/3rd to 1/5th in comparison with the normal voltage-divider anode output. Therefore, adjustment is required to increase the supply voltage for the photomultiplier tube.



THBV3\_0510EA

**Figure 5-10: Linearity characteristic using a tapered and a normal voltage-divider circuit**

The methods discussed for improving pulse output linearity by use of decoupling capacitors and tapered voltage-divider circuits are also applicable for the voltage-divider circuits with the cathode at ground potential and the anode at a high positive voltage.

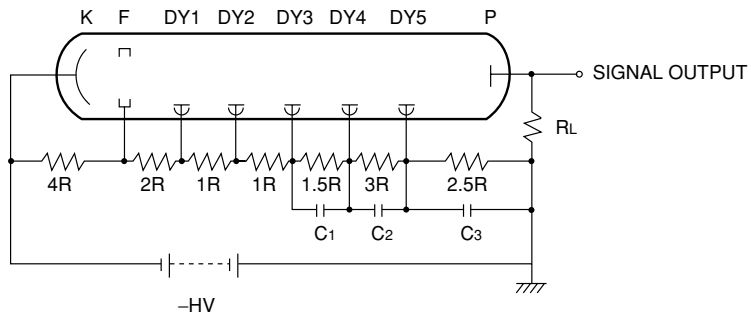
## (2) Voltage distribution for the cathode and earlier stages

As mentioned in the previous section, the voltage distribution ratio for the latter stages near the anode is an important factor that determines the output linearity of a photomultiplier tube. In contrast, the voltage distribution between the cathode, focusing electrode and first dynode has an influence on the photoelectron collection efficiency and the secondary emission ratio of the first dynode. These parameters are major factors in determining the output signal-to-noise ratio, pulse height dispersion in the single and multiple photon regions, and also electron transit time spread (TTS).

Furthermore, the voltage distribution at the earlier stages affects the cathode linearity, energy resolution in scintillation counting and magnetic characteristics of a photomultiplier tube, and therefore its setting requires care just as in the case of the latter stages. In general, the voltage distribution ratios for the earlier stages listed in our catalog are determined in consideration of the electron collection efficiency, time properties and signal-to-noise ratio. Note that since they are selected based on the recommended supply voltage, proper corrective actions may be required in cases where the supply voltage becomes less than one-half that of the recommended voltage. For example, increasing the voltage distribution ratio at the earlier stages or using Zener diodes to hold the dynode voltage constant are necessary. For more information on the photoelectron collection efficiency, output signal-to-noise ratio and other characteristics, refer to Chapter 4.

Figure 5-11 shows a variant of the voltage-divider circuit shown in Figure 5-9, which provides the above measures for the cathode to the first dynode.

In applications such as very low-light-level measurement and single photon counting where shot noise may create a problem, and TOF (time-of-flight) trigger counters and hodoscopes requiring fast time response, it is very important to apply the correct voltage to the cathode, focusing electrode and the precisely designed electron lens system near the first dynode.



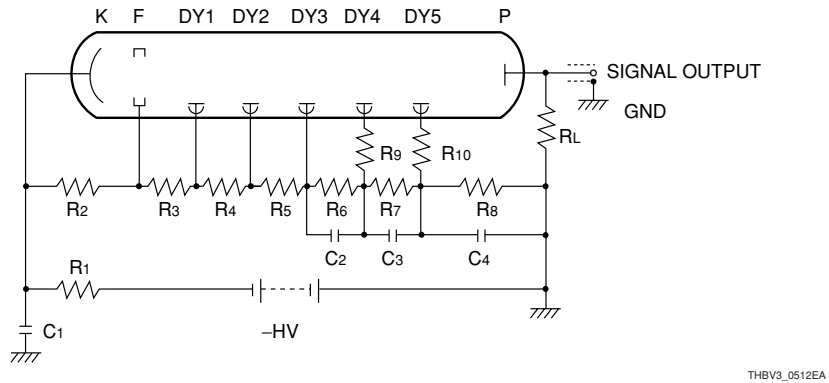
THBV3\_0511EA

**Figure 5-11: Voltage-divider circuit with tapered configurations at both the earlier and latter stages**

The recommended voltage distribution ratios listed in our catalog are selected for general-purpose applications, with consideration primarily given to the gain. Accordingly, when the photomultiplier tube must be operated at a lower supply voltage or must provide a higher output current, selecting a proper voltage distribution ratio that matches the application is necessary. As to the resistance values actually used for the voltage-divider circuit, they should basically be selected in view of the photomultiplier tube supply voltage, output current level and required linearity. It should be noted that if the resistance values are unnecessarily small, the resulting heat generation may cause various problems, such as an increase in the dark current, temperature drift in the output and lack of capacity in the power supply. Therefore, avoid allowing excessive divider current to flow.

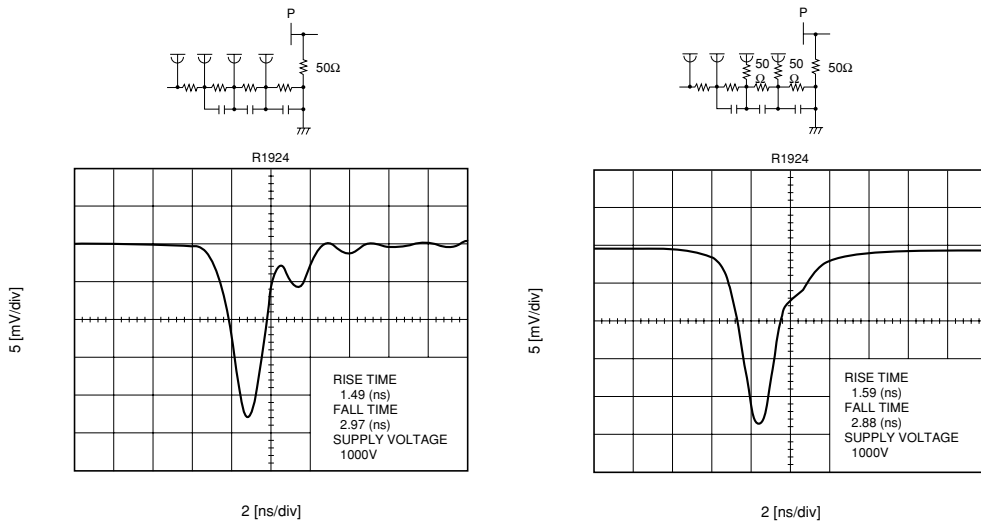
### 5.1.5 Countermeasures for fast response circuits

As shown in Figure 5-12, inserting a lowpass filter comprised of  $R_1$  and  $C_1$  into the high-voltage supply line is also effective in reducing noise pickup from the high-voltage line. The resistor  $R_1$  is usually several tens of kilohms, and a ceramic capacitor of 0.001 to 0.05 microfarads which withstands high voltage is frequently used as  $C_1$ .



**Figure 5-12: Voltage-divider circuit with countermeasure against pulse output linearity, ringing and high-voltage power supply noise**

In applications handling a fast pulsed output with a rise time of less than 10 nanoseconds, inserting damping resistors  $R_{10}$  into the last dynode as shown in Figure 5-11 and if necessary,  $R_9$  into the next to last dynode can reduce ringing in the output waveform. As damping resistors, noninduction type resistors of about 10 to 200 ohms are used. If these values are too large, the time response will deteriorate. Minimum possible values should be selected in the necessary range while observing the actual output waveforms. Figure 5-13 shows typical waveforms as observed in a normal voltage-divider circuit with or without damping resistors. It is clear that use of the damping resistors effectively reduces ringing.



**Figure 5-13: Effect of damping resistors on ringing**

### 5.1.6 Practical fast-response voltage-divider circuit

The circuit diagrams of the Hamamatsu H2431-50 photomultiplier tube assembly is shown in Figure 5-14 below as practical examples of fast-response voltage-divider circuits which have been designed based on the description in the preceding section.

H2431-50 circuit diagram

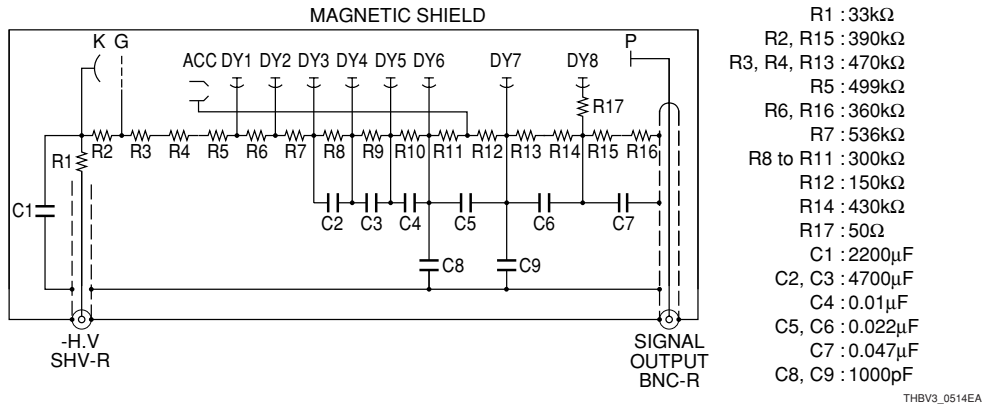


Figure 5-13: Fast-response voltage-divider circuits

### 5.1.7 High output linearity voltage-divider circuit (1)

In pulse applications such as scintillation counting, when a photomultiplier tube is operated at a high count rate, the output sometimes encounters linearity problems. In this case, use of transistors in place of the voltage-divider resistors at the latter stages can improve the output linearity degradation resulting from the divider current limitation.

As an example, Figure 5-14 shows a voltage-divider circuit for the Hamamatsu R329 photomultiplier tube, devised by FNAL (Fermi National Accelerator Laboratories)<sup>3)</sup>.

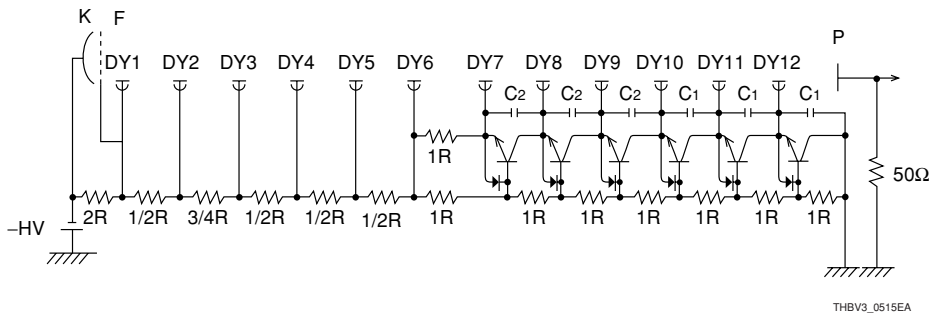


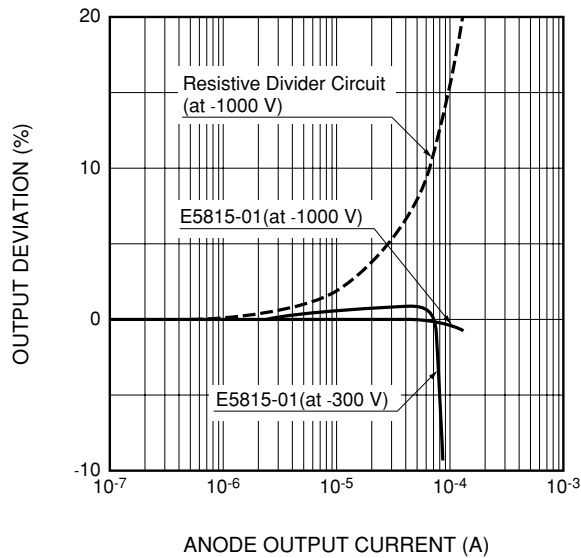
Figure 5-15: Voltage-divider circuit using transistors

In the circuit shown in Figure 5-15, a photoelectron current first flows into the first dynode, then secondary electrons flow through the successive dynodes and into the collector of each transistor. As a result, the emitter potential of each transistor increases while the collector current decreases along with a decrease in the base current. At this point, the decrease in the collector current is nearly equal to the current flowing through the photomultiplier tube and accordingly, the transistors supply the current for the photomultiplier tube.

When using these transistors, the following points must be taken into consideration.

1. Choose transistors having a large  $h_{fe}$  so that sufficient current can flow into the collector.
2. Choose transistors having good frequency characteristics.
3. Use capacitors having good frequency characteristics.
4. The number of stages to which transistors are added should be determined in view of the operating conditions of the photomultiplier tube to be used.

Figure 5-16 shows output linearity of a voltage-divider circuit (E5815-01) using transistors

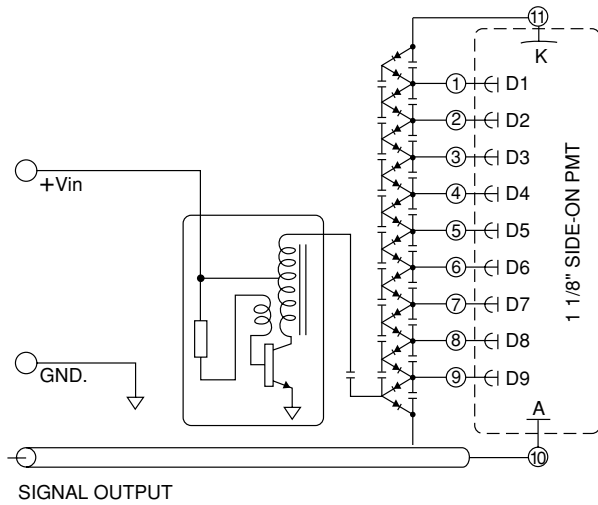


THBV3\_0516EA

Figure 5-16: Output linearity of a voltage-divider circuit (E5815-01) using transistors

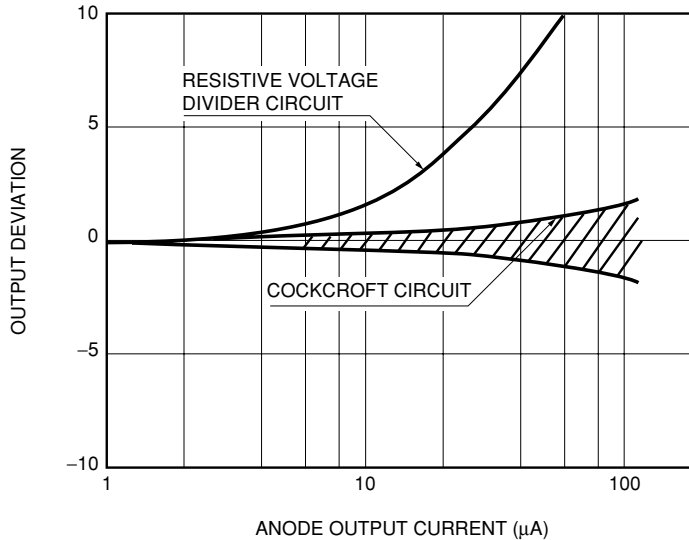
### 5.1.8 High output linearity voltage-divider circuit (2)

As shown in Figure 5-17, this circuit utilizes a Cockcroft-Walton voltage multiplier circuit in which an array of diodes is connected in series. Along each side of the alternate connection points, capacitors are connected in series. If the reference voltage  $V$  is placed at the input, this circuit provides voltage potentials of  $2V$ ,  $3V$  and so on at each connection point. Therefore, this power supply circuit functions just like a conventional resistive voltage-divider circuit. In addition, this circuit achieves good linearity for both DC and pulsed currents yet with low power consumption, making it suitable for use in compact circuits. As Figure 5-18 shows, the Cockcroft-Walton circuit assures higher DC linearity than that obtained with a resistive voltage-divider circuit.



THBV3\_0517EA

Figure 5-17: Cockcroft-Walton circuit



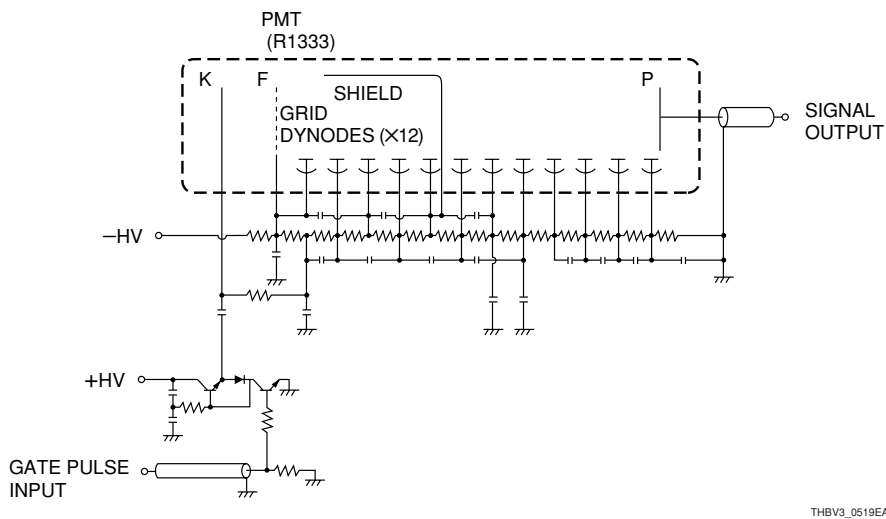
THBV3\_0518EA

Figure 5-18: Output linearity

### 5.1.9 Gating circuit

Next, let us introduce gating circuits as a variant of voltage-divider circuits.

In general, in applications such as; fluorescence measurement, plasma electron temperature measurement utilizing Thomson scattering, Raman spectroscopy and detection of defects in optical transmission paths, the signal light to be measured is extremely weak in comparison with primary light levels such as the excitation light. For this reason, the detector system is set up to have extremely high sensitivity. If even part of the primary light enters the detector system as stray light, it may cause saturation in the photomultiplier tube output and in the subsequent circuits, degrading their performance. This problem could be solved if only the excessive light was blocked by use of an ultra-fast shutter such as a liquid crystal. But this is not yet practical. A practical technique commonly used is "gating" by which a photomultiplier tube is electronically switched to eliminate the output during unnecessary periods when excess light may be present.



**Figure 5-19: Circuit diagram of the C1392 socket assembly with a gating circuit**

Figure 5-19 shows the circuit diagram of the Hamamatsu C1392 socket assembly with a gating circuit. The C1392 is a "normally OFF" type which normally sets the photomultiplier tube output to OFF, and when a gate signal is inputted, sets the photomultiplier output to ON. Also available are variant models with reverse operation, i.e., a "normally ON" type which sets the output to OFF by input of a gate signal.

The following explains the basic operation of the C1392 socket assembly when used in conjunction with a photomultiplier tube.

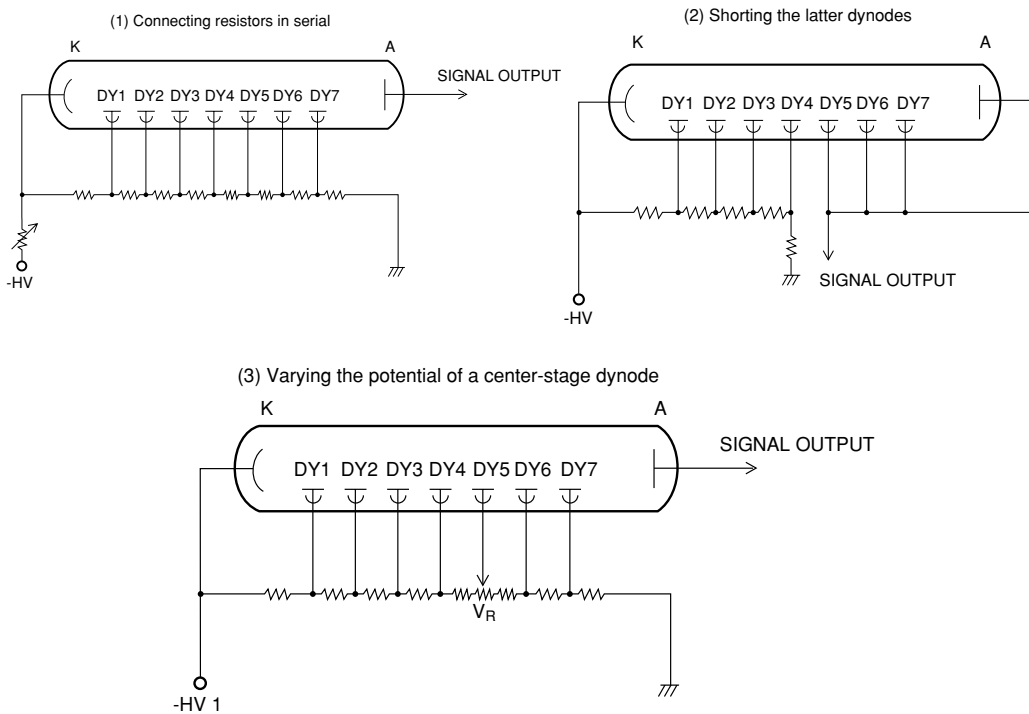
If the photomultiplier tube output is OFF at a gate input of 0V, a reverse bias of about 10 volts with respect to the focusing electrode and first dynode is supplied to the cathode. This prevents photoelectrons, if emitted by the cathode, from reaching the dynode section. Here, if a pulse signal of +3 to +4 volts is applied to the gate input terminal, the driver circuit gives a forward bias to the cathode via capacitance coupling, and sets the photomultiplier tube output to ON during the period determined by the gate pulse width and the time constant of the capacitance-coupled circuit. This gating circuit provides a switching ratio (or extinction ratio) of  $10^4$  or more. The capacitors are connected from the first through the center dynode to absorb the switching noises often encountered with this type of gating circuit.

### 5.1.10 Anode sensitivity adjustment circuits

The photomultiplier tube anode sensitivity is usually adjusted by changing the supply voltage. In some applications, however, a single power supply is used to operate two or more photomultiplier tubes or a sensitivity adjustment circuit is added to the voltage-divider circuit if the variable range of the high-voltage power supply and amplifier is narrow. The following explains how to provide a sensitivity adjustment circuit, using the circuits shown in Figure 5-20 as examples.

With the circuits shown in Figure 5-20, there are three techniques for adjusting the voltage applied to the photomultiplier tube. The first is, as shown in (1) in the figure, to use a variable resistor connected between the cathode and the negative high-voltage power supply so that the voltage applied to the photomultiplier tube can be varied. With this technique, depending on the conditions, the photomultiplier tube gain can be varied within a considerably wide range (up to 10 times). However, it should be noted that the higher the voltage-divider resistance value, the higher the variable resistance value should be and, in some cases, variable resistors with such a high wattage resistor may not be available. On the other hand, if the voltage-divider resistor value is too small, a variable resistor with high rated capacity is required, and problems with contact failure in the variable resistor tend to occur.

Moreover, when a negative high voltage is applied to the cathode as shown in the figure, a high voltage is also impressed on the variable resistor. Thus the housing that contains the photomultiplier tube and associated circuits must also be designed to have sufficiently high dielectric resistance.

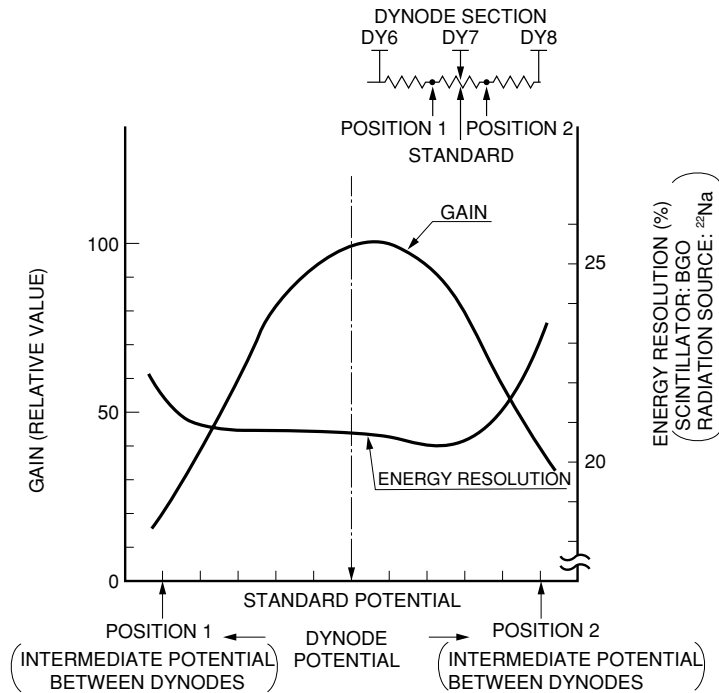


THBV3\_0520EA

Figure 5-20: Anode sensitivity adjustment circuits



The second technique, as shown in Figure 5-20 (2), is to short the latter dynode stages with the anode so that the signal is derived from a middle dynode. This is effective in cases where the photomultiplier tube gain is so high that the supply voltage may drop considerably and the resultant decrease in the interstage voltage degrades the collection efficiency and secondary electron emission ratio. Shorting the latter dynode stages as shown in (1) reduces the number of dynode stages and assures a higher interstage voltage which results in an improvement in the signal-to-noise ratio. However, this is accompanied by a sacrifice in linearity characteristics because the output is fetched from an earlier dynode. Furthermore, since the number of stages being used is changed, the sensitivity versus supply voltage characteristic also varies accordingly. The degree of this variation is different from tube to tube.



**Figure 5-19: Gain variation and energy resolution as a function of dynode potential**

The third technique is performed by varying the potential of a mid-stage dynode, as shown in Figure 5-20 (3). This makes use of the fact that with a varying dynode potential, the number of secondary electrons released from the dynode decreases while the collection efficiency between dynodes drops. To adjust the dynode potential, a variable resistor is added between the front and rear adjacent dynodes. Although this method is relatively easy to implement, there is a disadvantage that the signal-to-noise ratio may deteriorate if the dynode potential is varied too much. Figure 5-21 dictates the sensitivity variation and energy resolution of a photomultiplier tube when the dynode potential is varied continuously. It can be seen that the energy resolution begins to deteriorate near the points at which the sensitivity drops by more than 50 percent. This behavior is not constant but differs depending on individual photomultiplier tubes. In addition, the variable sensitivity range is not so wide. In most cases, the technique (1) or a combination of (1) and (3) is used.

### 5.1.11 Precautions when fabricating a voltage-divider circuit

This section describes the precautions to take when fabricating a voltage-divider circuit.

#### (1) Selecting the parts used for a voltage-divider circuit

Since the voltage-divider circuit has a direct influence on the photomultiplier tube operation, careful selection of parts is necessary.

##### Resistors

Because photomultiplier tubes are very susceptible to changes in the supply voltage and interstage voltage, metal-film resistors with a minimum temperature coefficient should be used. Preferably, use the same type of resistor for all stages, but if not available, select resistors with temperature coefficients which are close to each other. These resistors should also have good temperature characteristics, but their accuracy is not so critical. If non-uniformity between each resistor is held within  $\pm 5\%$ , it will work sufficiently. This is because the photomultiplier tube gain varies to some degree from tube to tube and also because a voltage difference of several volts will not affect the electron trajectories very much. If possible, we recommend using resistors with a sufficient power rating and dielectric resistance, for example, respectively at least 1.7 times and 1.5 times higher than necessary. As a rough guide, the resistance value per stage typically changes from 100 k $\Omega$  to 1 M $\Omega$ . For damping resistance and load resistance, use noninduction type resistors designed for operation at high frequency.

##### Decoupling capacitors

In pulsed light applications where a fast response photomultiplier tube handles the output with a rise time of less than 10 nanoseconds, decoupling capacitors are connected between dynodes. For these decoupling capacitors, use ceramic capacitors with sufficiently high impedance at a high frequency range and adequate dielectric resistance at least 1.5 times higher than the maximum voltage applied between dynodes.

For the bypass capacitor used to eliminate noise from the power supply connected to the high-voltage input terminal of a photomultiplier tube, use a ceramic capacitor having high impedance at high frequencies and adequate dielectric resistance.

##### Coupling capacitors

For the coupling capacitor which separates the signal from a positive high voltage applied to the anode in a grounded-cathode voltage-divider circuit, use a ceramic capacitor having minimum leakage current (which may also be a source of noise) as well as having superior frequency response and sufficient dielectric resistance.

##### PC boards for voltage-divider circuits

When a voltage-divider circuit is assembled on a PC board and not on a photomultiplier tube socket, use a high-quality PC board made of glass epoxy or similar materials which exhibit low leakage current even at a high voltage. If both sides of the PC board are used for assembly, select a board with adequate thickness.

On a glass epoxy board, the wiring space between patterns necessary to hold a potential difference of 1 kilovolt is typically 1 millimeter or more.

## Leads

For high voltage circuits, use teflon or silicone leads which can withstand a high voltage, or use coaxial cable such as the RG-59B/U. In either case, take sufficient care with regard to the dielectric resistance of leads or conductor wires.

For signal output lines, use of a coaxial cable such as RG-174/U and 3D-2V is recommended. For high-speed circuits, in particular, a 50-ohm coaxial cable is commonly used to provide the good impedance match with the measurement equipment. However, if the signal current to be derived is not very low (several microamperes or more) and the lead length is no longer than 20 centimeters, using normal leads does not create any problem in practice, as long as a noise source is not located near the photomultiplier tube.

Normal lead wires can be used for grounding. However, if there is a possibility that the ground wire may make contact with a high voltage component or socket pins, use a lead wire that withstands high voltage.

## (2) Precautions for mounting components

This section describes precautions to be observed when mounting components on a voltage-divider circuit. Refer to Figure 5-12 while reading the following precautions.

### Voltage-divider resistors

Considering heat dispersion, provide adequate space between voltage-divider resistors so as not to allow them to make contact with each other. When a low resistance is used or in low-light-level measurement where an increase in the dark current resulting from temperature rise may create a significant problem, avoid direct connections of voltage-divider resistors to the lead pins of the photomultiplier tube or to the socket so that Joule heat generated from the voltage-divider circuit is not directly conducted to the photomultiplier tube. Be sure to allow a distance between the photomultiplier tube and the voltage-divider circuit.

### Decoupling capacitors

The lead length of decoupling capacitors used for fast pulse operation affects the photomultiplier tube time properties and also causes ringing due to the lead inductance. Therefore lead length should be kept as short as possible. Even when mounting voltage-divider resistors remote from a photomultiplier tube, the decoupling capacitors must be mounted directly to the lead pins of the photomultiplier tube or to the socket.

### Signal output line

The wiring length of a signal output line including load resistance should be as short as possible. It must be wired away from the high voltage lines and the components to which a high voltage is applied. In particular, when handling fast pulse signals, grounding of the signal circuitry and power supply circuitry, as shown in Figure 5-12, is essential. If extra-low output currents are to be derived from a photomultiplier tube, attention must also be paid to shielding the signal line and to preventing ohmic leakage.

## 5.2 Selecting a High-Voltage Power Supply

Photomultiplier tube operation stability depends on the total stability of the power supply characteristics including drift, ripple, temperature dependence, input regulation and load regulation. The power supply must provide high stability which is at least 10 times as stable as the output stability required of the photomultiplier tube.

Series-regulator type high-voltage power supplies have been widely used with photomultiplier tubes. Recently, a variety of switching-regulator types have been put on the market and are becoming widely used. Most of the switching-regulator type power supplies offer compactness and light weight, yet provide high voltage and high current. However, with some models, the switching noise is superimposed on the AC input and high voltage output or the noise is radiated. Thus, sufficient care is required when selecting this type of power supply, especially in low-light-level detection, measurement involving fast signal processing, and photon counting applications.

The high-voltage power supply should have sufficient capacity to supply a maximum output current which is at least 1.5 times the current actually flowing through the voltage-divider circuit used with the photomultiplier tube.

The following table shows the guide for selecting the correct high-voltage power supply.

High voltage power supply characteristics

(1) Line regulation	$\pm 0.1\%$ or less
(2) Load regulation	$\pm 0.2\%$ or less
(3) Ripple noise	0.05 % or less
(4) Temperature coefficient	$\pm 0.05\%/^{\circ}\text{C}$ or less

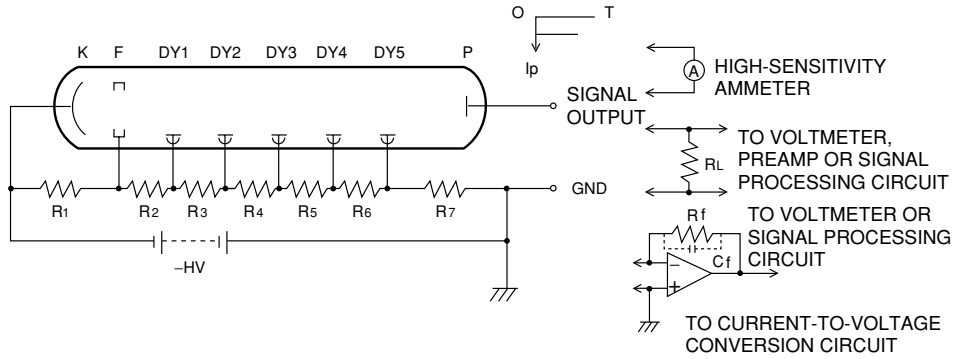
- (1) This is the percentage (%) change in the output voltage caused by varying, for example,  $\pm 10\%$  the input voltage when the power supply is operated to provide the maximum voltage.
- (2) This is the difference between the output voltage at the maximum output (with full load connected) and the output voltage with no load, expressed as a percentage (%) of the output voltage.
- (3) Ripple is fluctuations (peak values) in the output caused by the oscillation frequency of the high voltage generating circuit.
- (4) This is the rate of output change ( $\%/^{\circ}\text{C}$ ) measured over the operating temperature range at the maximum output.

## 5.3 Connection to an External Circuit

### 5.3.1 Observing an output signal

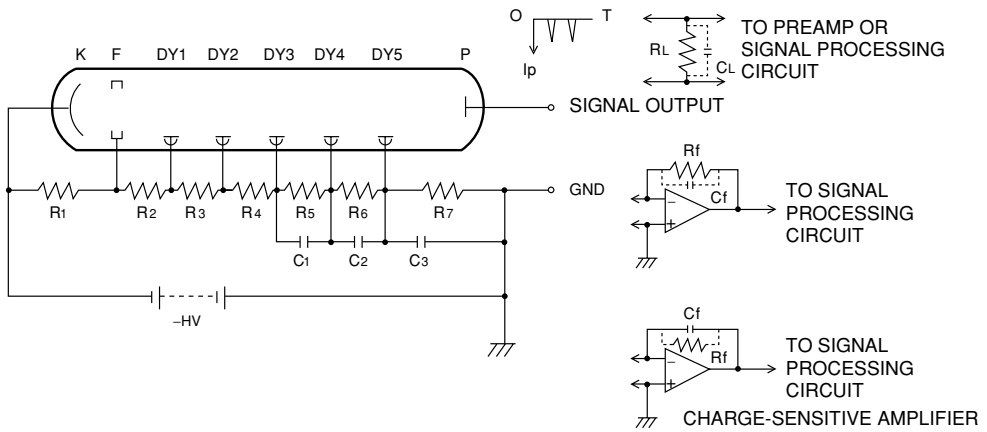
To observe the output signal of a photomultiplier tube, various methods are used depending on the operating conditions as illustrated in Figures 5-22, 5-23 and 5-24.

As described in section 5.1.2 in this chapter, there are two schemes for voltage-divider circuit operation: the anode grounding and the cathode grounding schemes. The anode grounding scheme permits both DC and pulse operation as shown in Figures 5-22 and 5-23. On the other hand, the cathode grounding scheme uses a coupling capacitor to separate the high voltage applied to the anode as shown in Figure 5-24, so that only pulse operation is feasible. But this scheme eliminates DC components produced by such factors as background light, making it suitable for pulse operation.



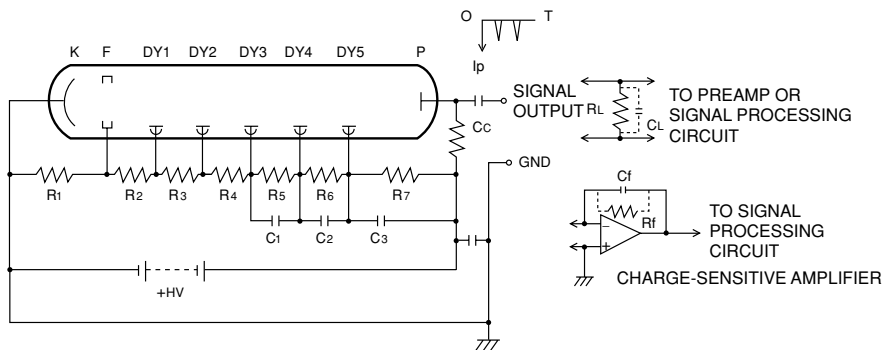
THBV3\_0522EA

Figure 5-22: Anode grounding scheme in DC operation



THBV3\_0523EA

Figure 5-23: Anode grounding scheme in pulse operation



THBV3\_0524EA

Figure 5-24: Cathode grounding scheme in pulse operation

It should be noted that when wiring the photomultiplier tube output to an amplifier circuit, the amplifier circuit must be wired before turning on the high-voltage power supply. When a high voltage is applied to the voltage-divider circuit even in a dark state, the possible dark current creates a charge on the anode. If the voltage-divider circuit is wired to the amplifier circuit under this condition, the charge will instantaneously flow into the amplifier, probably leading to damage of the amplifier circuit. Extreme care should be taken when using high speed circuits, as they are more susceptible to damage.

### 5.3.2 Influence of a coupling capacitor

A coupling capacitor, required by the cathode grounding scheme, can also be used in the anode grounding scheme in order to eliminate the DC components. This section describes precautions for using a voltage-divider circuit to which a coupling capacitor is connected.

#### Output waveform

When a photomultiplier tube is operated with the circuit shown in Figure 5-25, if the anode output pulse width  $P_w$  is sufficiently shorter than the time constant  $CR$  ( $R$  is parallel resistance of  $R_a$  and  $R_L$ ), the impedance of the coupling capacitor can be ignored so the signal pulse current is divided to flow into  $R_L$  and  $R_a$ . In this case, the input waveform is transmitted to the output waveform without distortion, regardless of the capacitance value of the coupling capacitor. However, if  $P_w$  is close to or longer than  $CR$ , the output will have a differential waveform. Because the coupling capacitor is merely used as a coupling element between the voltage-divider circuit and the amplifier circuit,  $P_w$  must be at least several tens of times shorter than  $C_R$  so that the output waveform has good fidelity to the input waveform. When a 50-ohm resistor is used for  $R_a$  to optimize fast response operation, the time constant  $C_R$  becomes small, so care should be taken of this point.

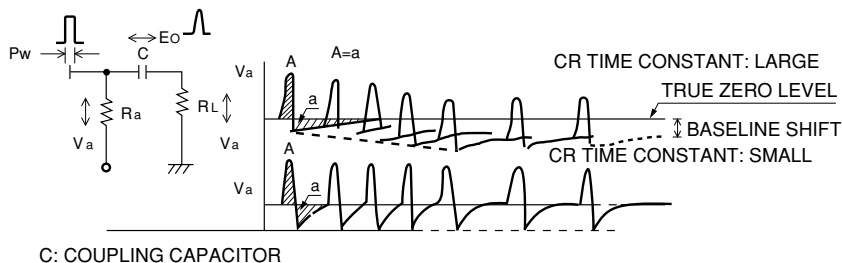
In the case of low frequency applications, the impedance of the coupling capacitor cannot be ignored. Since its impedance  $Z_c = \frac{1}{2\pi f C}$ , the output signal decays by 3 dB (approximately to 7/10th of the pulse height) at a frequency  $f = 1/2\pi CR_L$ .

#### Base-line shift

As stated above, the amount of the signal passing through the coupling capacitor is stored as a corresponding charge on the capacitor. This stored charge  $Q$  generates a voltage of  $E_0 = Q/C$  across both sides of the capacitor in the reverse direction of the signal. This voltage  $E_0$  attenuates by a factor of  $V = E_0 e^{-t/RC}$  related to the time constant  $C_R$  which is determined by the capacitance value  $C$  and the serial resistance value  $R$  of  $R_a$  and  $R_L$ . The voltage induced in the capacitor is divided by  $R_a$  and  $R_L$ , and the output voltage  $V_a$  is given by the following equation:

$$V_a = E_0 e^{-t/RC} \times \frac{R_a}{R_a + R_L} \dots\dots\dots (Eq. 5-6)$$

Here, if the signal pulse repetition rate increases, the base line does not return to the true zero level as Figure 5-25 shows. This is known as base-line shift, and can be minimized by reducing the time constant  $CR$ . Since the output from a photomultiplier tube is viewed as a current source, reducing the capacitor value increases the initial voltage  $E_0$ , but shortens the discharge time. Decreasing the resistor value also shortens the discharge time, but this is accompanied by a decrease in the signal voltage, causing a problem with the signal-to-noise ratio. In contrast, increasing the resistor value produces a larger output and results in an improvement in the signal-to-noise ratio, but a base-line shift tends to occur due to the long time constant. If  $R_a$  is large, it lowers the anode potential, so care is required when excessive current including DC current flows.



THBV3\_0525EA

Figure 5-25: Base-line shift

Eventually, when the amount of charge stored on the capacitor (portion A in Figure 5-25) is discharged in a certain time period (portion a in Figure 5-25), the area of portion A is equal to the area of portion a, regardless of the discharge time constant. In general, the circuit time constant is longer than the signal pulse width, so this discharge time will have less effect on the pulse height. However, when the signal pulse repetition rate is extremely high or accurate information on the output pulse height is needed, the discharge time cannot be neglected. If a base-line shift occurs, the signal is observed at an apparently lower level. Therefore, when designing the circuit it, the optimum resistor and capacitor values must be selected so that the output pulse height exhibits no fluctuations even if the signal repetition rate is increased.

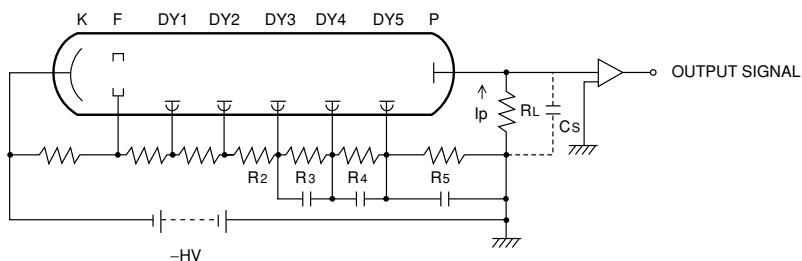
Furthermore, when multiple pulses enter the measurement system including an amplifier, these pulses are added to create a large pulse, and a so-called "pile-up" problem occurs. Because of this, some applications utilize a pulse height discriminator to discern the height of individual pulses and in this case the time resolution of the measurement device must be taken into account.

### 5.3.3 Current-to-voltage conversion for photomultiplier tube output

The output of a photomultiplier tube is a current (charge), while the external signal processing circuit is usually designed to handle a voltage signal. Therefore, the current output must be converted into a voltage signal by some means, except when the output is measured with a high-sensitivity ammeter. The following describes how to perform the current-to-voltage conversion and major precautions to be observed.

#### (1) Current-to-voltage conversion using load resistance

One method for converting the current output of a photomultiplier tube into a voltage output is to use a load resistance. Since the photomultiplier tube may be thought of as an ideal constant-current source at low output current levels, a load resistance with a considerably large value can theoretically be used and an output voltage of  $I_p \times R_L$  can be obtained. In practice, however, the load resistance value is limited by such factors as the required frequency response and output linearity as discussed below.



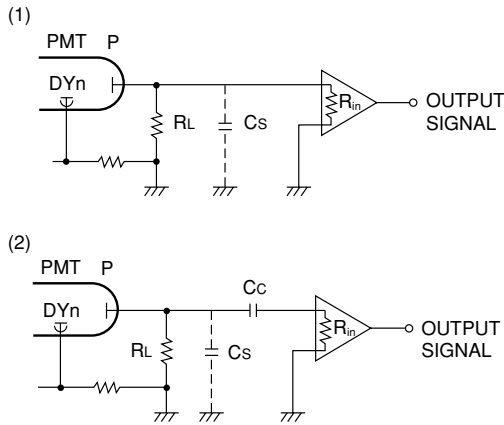
THBV3\_0526EA

Figure 5-26: Photomultiplier tube and output circuit

If, in the circuit of Figure 5-26, we let the load resistance be  $R_L$  and the total electrostatic capacitance of the photomultiplier tube anode to all other electrodes including stray capacitance such as wiring capacitance be  $C_s$ , then the high-range cutoff frequency  $f_c$  is given by the following equation:

$$f_c = \frac{1}{2\pi C_s R_L} \text{ (Hz)} \dots\dots\dots \text{ (Eq. 5-7)}$$

From this relation, it can be seen that, even if the photomultiplier tube and amplifier have fast response, the response is limited to the cutoff frequency  $f_c$  determined by the subsequent output circuits. If the load resistance is made unnecessarily large, the voltage drop by  $I_p \cdot R_L$  at the anode potential is increased accordingly, causing the last-dynode-to-anode voltage to decrease. This will increase the space charge effect and result in degradation of output linearity. In most cases, therefore, use a load resistance that provides an output voltage of about 1 volt.



THBV3\_0527EA

**Figure 5-27: Amplifier internal input resistance**

When selecting the optimum load resistance, it is also necessary to take account of the internal input resistance of the amplifier connected to the photomultiplier tube. Figure 5-27 shows equivalent circuits of the photomultiplier tube output when connected to an amplifier. In this figure, if the load resistance is  $R_L$  and the input resistance is  $R_{in}$ , the resultant parallel output resistance  $R_0$  is calculated from the following relation:

$$R_0 = \frac{R_{in} \cdot R_L}{R_{in} + R_L} \dots\dots\dots \text{ (Eq. 5-8)}$$

This value of  $R_0$ , less than the  $R_L$  value, is then the effective load resistance of the photomultiplier tube. The relation between the output voltage  $V_0$  at  $R_{in} = \infty \Omega$  and the output voltage  $V_0'$  when the output was affected by  $R_{in}$  is expressed as follows:

$$V_0' = V_0 \times \frac{R_{in}}{R_{in} + R_L} \dots\dots\dots \text{ (Eq. 5-9)}$$

With  $R_{in} = R_L$ ,  $V_0'$  is one-half the value of  $V_0$ . This means that the upper limit of the load resistance is actually the input resistance  $R_{in}$  of the amplifier and that making the load resistance greater than this value does not have a significant effect. Particularly, when a coupling capacitor  $C_c$  is placed between the photomultiplier tube and the amplifier, as shown in Figure 5-27 (2), an unnecessarily large load resistance may create a problem with the output level.

While the above description assumed the load resistance and internal input resistance of the amplifier to be purely resistive, in practice, stray capacitance and stray inductance are added. Therefore, these circuit elements must be considered as compound impedances, especially in high frequency operation.

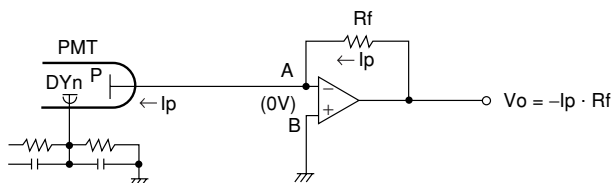
Summarizing the above discussions, the following guides should be used in determining the load resistance:



1. When frequency and amplitude characteristics are important, make the load resistance value as small as possible (50 ohms). Also, minimize the stray capacitance such as cable capacitance which may be present in parallel with the load resistance.
2. When the linearity of output amplitude is important, select a load resistance value such that the output voltage developed across the load resistance is several percent of the last-dynode-to-anode voltage.
3. Use a load resistance value equal to or less than the input impedance of the amplifier connected to the photomultiplier tube.

## (2) Current-to-voltage conversion using an operational amplifier

The combination of a current-to-voltage conversion circuit using an operational amplifier and an analog or digital voltmeter enables accurate measurement of the output current from a photomultiplier tube, without having to use an expensive, high-sensitivity ammeter. A basic current-to-voltage conversion circuit using an operational amplifier is shown in Figure 5-28.



THBV3\_0528EA

**Figure 5-28: Current-to-voltage conversion circuit using an operational amplifier**

With this circuit, the output voltage  $V_0$  is given by

$$V_0 = -I_p \cdot R_f \text{ ..... (Eq. 5-10)}$$

This relation can be understood as follows:

Since the input impedance of the operational amplifier is extremely high, the output current of the photomultiplier tube is blocked from flowing into the inverting input terminal (-) of the operational amplifier at point A in Figure 5-28. Therefore, most of the output current flows through the feedback resistance  $R_f$  and a voltage of  $I_p \cdot R_f$  is developed across  $R_f$ . On the other hand, the operational amplifier gain (open loop gain) is as high as  $10^5$ , and it always acts so as to maintain the potential of the inverting input terminal (point A) at a potential equal to that (ground potential) of the non-inverting input terminal (point B). (This effect is known as an imaginary short or virtual ground.) Because of this, the operational amplifier outputs voltage  $V_0$  which is equal to that developed across  $R_f$ . Theoretically, use of a preamplifier performs the current-to-voltage conversion with an accuracy as high as the reciprocal of the open loop gain.

When a preamplifier is used, factors that determine the minimum measurable current are the preamplifier offset current ( $I_{OS}$ ), the quality of  $R_f$  and insulating materials used, and wiring methods.

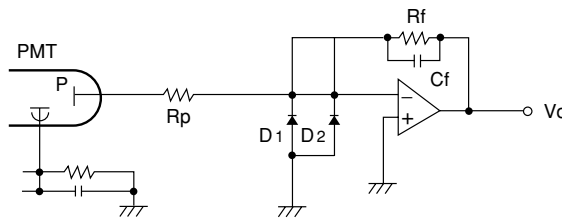
To accurately measure a very low current on the order of picoamperes ( $10^{-12}$ A), the following points should be noted in addition to the above factors:

1. Use a low-noise type coaxial cable with sufficiently high insulating properties for the signal output cable.
2. Select a connector with adequate insulating properties, for example, a teflon connector.
3. For connection of the photomultiplier tube anode to the input signal pin of the preamplifier, do not use a trace on the printed circuit board but use a teflon standoff instead.
4. For the actual output  $V_0 = -(I_p + I_{OS})R_f + V_{OS}$ , if the  $R_f$  value is large,  $I_{OS}$  may cause a problem. Therefore, select a FET input preamplifier which has a small  $I_{OS}$  of less than 0.1 picoamperes and also exhibits minimum input conversion noise and temperature drift.

5. Provide adequate output-offset adjustment and phase compensation for the preamplifier.
6. Use a metal-film resistor with a minimum temperature coefficient and tolerance for the feedback resistance  $R_f$ . Use clean tweezers to handle the resistor so that no dirt or foreign material gets on its surface. In addition, when the resistance value must be  $10^9$  ohms or more, use a glass-sealed resistor that assures low leakage current.
7. Carbon-film resistors are not suitable as a load resistance because of insufficient accuracy and temperature characteristics and, depending on the type, noise problems. When several feedback resistors are used to switch the current range, place a ceramic rotary switch with minimum leakage current or a high-quality reed relay between the feedback resistance and the preamplifier output. Also connect a low-leakage capacitor with good temperature characteristics, for example a styrene capacitor, in parallel with the feedback resistors so that the frequency range can be limited to a frequency permitted by the application.
8. Use a glass-epoxy PC board or other boards with better insulating properties.

On the other hand, since the maximum output voltage of a preamplifier is typically 1 to 2 volts lower than the supply voltage, multiple feedback resistors are usually used for switching to extend the measurement current range. In this method, grounding the non-inverting input terminal of the preamplifier for each range, via a resistor with a resistance equal to the feedback resistance while observing the above precautions can balance the input bias current, so that the offset current  $I_{OS}$  between the input terminals can be reduced.

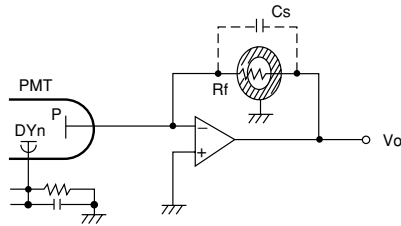
A high voltage is applied during photomultiplier tube operation. If for some reason this high voltage is accidentally output from the photomultiplier tube, a protective circuit consisting of a resistor  $R_p$  and diodes  $D_1$  and  $D_2$  as shown in Figure 5-29 is effective in protecting the preamplifier from being damaged. In this case, these diodes should have minimum leakage current and junction capacitance. The B-E junction of a low-signal-amplification transistor or FET is commonly used. If  $R_p$  in Figure 5-29 is too small, it will not effectively protect the circuit, but if too large, an error may occur when measuring a large current. It is suggested that  $R_p$  be selected in a range from several kilohms to several tens of kilohms.



THBV3\_0529EA

**Figure 5-29: Protective circuit for preamplifier**

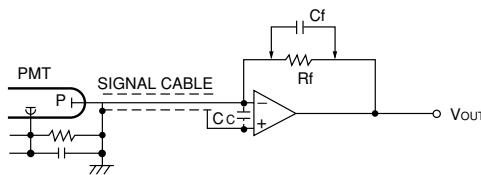
When a feedback resistance,  $R_f$ , and of as high as  $10^{12}$  ohms is used, if a stray capacitance,  $C_s$ , exists in parallel with  $R_f$  as shown in Figure 5-30, the circuit exhibits a time constant of  $C_s \cdot R_f$ . This limits the bandwidth. Depending on the application. This may cause a problem. As illustrated in the figure, passing  $R_f$  through a hole in a shield plate can reduce  $C_s$ , resulting in an improvement of the response speed.



THBV3\_0530EA

Figure 5-30: Canceling the stray capacitance by Rf

If the signal output cable for a photomultiplier tube is long and its equivalent capacitance is  $C_C$  as shown in Figure 5-31, the  $C_C$  and  $R_f$  create a rolloff in the frequency response of the feedback loop. This rolloff may be the cause of oscillations. Connecting  $C_f$  in parallel with  $R_f$  is effective in canceling out the rolloff and avoiding this oscillation, but degradation of the response speed is inevitable.



THBV3\_0531EA

Figure 5-31: Canceling the signal cable capacitance

### (3) Charge-sensitive amplifier using an operational amplifier

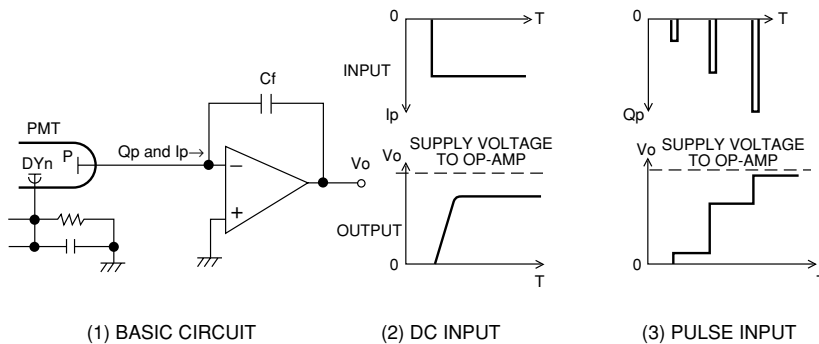
Figure 5-32 (1) shows the basic circuit of a charge-sensitive amplifier using an operational amplifier. The output charge  $Q_p$  of a photomultiplier tube is stored in  $C_f$ , and the output voltage  $V_0$  is expressed by the

$$V_0 = Q_p / C_f \dots\dots\dots \text{(Eq. 5-11)}$$

Here, if the output current of the photomultiplier tube is  $I_p$ ,  $V_0$  becomes

$$V_0 = -\frac{1}{C_f} \int_0^t I_p \cdot dt \dots\dots\dots \text{(Eq. 5-12)}$$

When the output charge is accumulated continuously,  $V_0$  finally increases up to a level near the supply voltage for the preamplifier, as shown in Figure 5-32 (2) and (3).



THBV3\_0532EA

Figure 5-32: Charge-sensitive amplifier circuit and its operation

In Figure 5-32 (1), if a circuit is added by connecting a FET switch in parallel to  $C_f$  so that the charge stored in  $C_f$  can be discharged as needed, this circuit acts as an integrator that stores the output charge during the measurement time, regardless of whether the photomultiplier tube output is DC or pulse. In scintillation counting, the individual output pulses of a photomultiplier tube must be converted into corresponding voltage pulses. Therefore,  $R_f$  is connected in parallel with  $C_f$  as shown in Figure 5-33, so that a circuit having a discharge time constant  $\tau=C_f R_f$  is used.

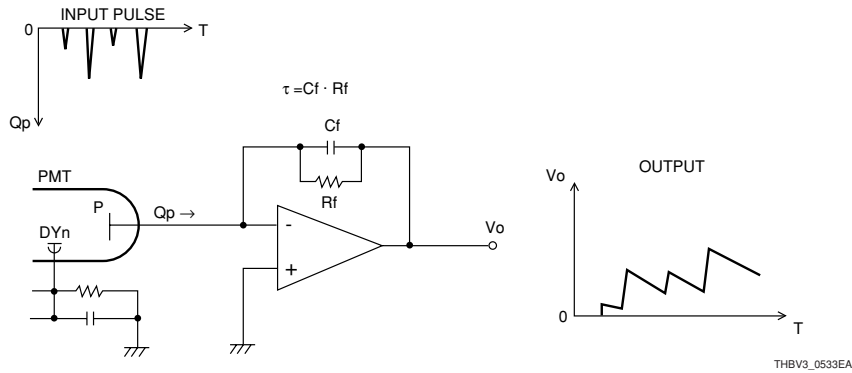


Figure 5-33: Pulse input type charge-sensitive amplifier

If the time constant  $\tau$  is made small, the output  $V_0$  is more dependent on the pulse height of the input current. Conversely, if  $\tau$  is made large,  $V_0$  will be more dependent on the input pulse charge and eventually approaches the value of  $-Q_p/C_f$ . In scintillation counting, from the relation between the circuit time constant  $\tau=RC$  and the fluorescent decay constant of the scintillator  $\tau_s$ , the output-pulse voltage waveform  $V(t)$  is given by<sup>4)</sup>

$$V(t) = \frac{Q \cdot \tau}{\tau - \tau_s} (e^{-t/\tau} - e^{-t/\tau_s}) \dots\dots\dots \text{(Eq. 5-13)}$$

when  $\tau \gg \tau_s$ ,  $V(t)$  becomes

$$V(t) \approx \frac{Q}{C} (e^{-t/\tau} - e^{-t/\tau_s}) \dots\dots\dots \text{(Eq. 5-14)}$$

While, when  $\tau \ll \tau_s$ ,  $V(t)$  is

$$V(t) \approx \frac{Q}{C} \cdot \frac{\tau}{\tau_s} (e^{-t/\tau_s} - e^{-t/\tau}) \dots\dots\dots \text{(Eq. 5-15)}$$

When the circuit time constant  $\tau$  is larger than the scintillator decay constant  $\tau_s$ , the rise of the output waveform depends on  $\tau_s$ , while the fall depends on  $\tau$ , with the maximum pulse height given by  $Q/C$ . In contrast, when the circuit time constant  $\tau$  is smaller than  $\tau_s$ , the rise of the output waveform depends on  $\tau$ , while the fall depends on  $\tau_s$ , with the maximum pulse height given by  $Q/C \cdot \tau/\tau_s$ . In most cases, the condition of  $\tau \gg \tau_s$  is used since higher energy resolution can be expected. This is because the output pulse has a large amplitude so that it is less influenced by such factors as noise, temperature characteristics of the scintillator and variations of the load resistance. In this case, it should be noted that the pulse width becomes longer due to a larger  $\tau$  and, if the repetition rate is high, base-line shift and pile-up tend to occur. If measurement requires a high counting rate, reducing  $\tau$  is effective in creating an output waveform as fast as the scintillator decay time. However, the output pulse height becomes lower and tends to be affected by noise, resulting in a sacrifice of energy resolution. Under either condition, the output voltage  $V(t)$  is proportional to the output charge from the photomultiplier tube anode. Generally, the load capacitance is reduced to obtain higher pulse height as long as the operation permits, and in most cases the resistor value

is changed to alter the time constant. When a NaI(Tl) scintillator is used, the time constant is usually selected to be from several microseconds to several tens of microseconds.

In scintillation counting, noise generated in the charge-sensitive amplifier degrades the energy resolution. This noise mainly originates from the amplifier circuit elements, but care should also be taken with the cable capacitance  $C_S$  indicated in Figure 5-34 because the output charge of the photomultiplier tube is divided and stored in  $C_f$  and  $C_S$ . The  $C_S$  makes the charge of  $C_f$  smaller compared to the amount of charge without  $C_S$ , so the value of  $A \cdot C_f / C_S$  must be large in order to improve the signal-to-noise ratio. In actual operation, however, since  $A \cdot C_f$  cannot be made larger than a certain value due to various limiting conditions, the value of  $C_S$  is usually made as small as possible to improve the signal-to-noise ratio.

In scintillation counting measurements, a common method of reducing the cable capacitance is to place the preamplifier in the vicinity of the photomultiplier tube, remote from the main amplifier.

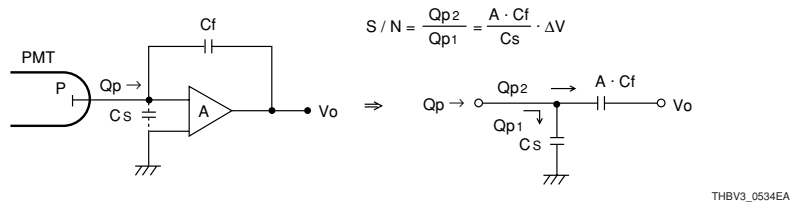


Figure 5-34: Influence of input distribution capacitance

### 5.3.4 Output circuit for a fast response photomultiplier tube

For the detection of light pulses with fast rise and fall times, a coaxial cable with 50-ohm impedance is used to make connection between the photomultiplier tube and the subsequent circuits.

To transmit and receive the signal output waveform with good fidelity, the output end must be terminated in a pure resistance equal to the characteristic impedance of the coaxial cable as shown in Figure 5-35. This allows the impedance seen from the photomultiplier tube to remain constant, independent of the cable length, making it possible to reduce "ringing" which may be observed in the output waveform. However, when using an MCP-PMT for the detection of ultra-fast phenomena, if the cable length is made unnecessarily long, distortion may occur in signal waveforms due to a signal loss in the coaxial cable.

If a proper impedance match is not provided at the output end, the impedance seen from the photomultiplier tube varies with frequency, and further the impedance value is also affected by the coaxial cable length, and as a result, ringing appears in the output. Such a mismatch may be caused not only by the terminated resistance and the coaxial cable but also by the connectors or the termination method of the coaxial cable. Thus, sufficient care must be taken to select a proper connector and also to avoid creating impedance discontinuity when connecting the coaxial cable to the photomultiplier tube or the connector.

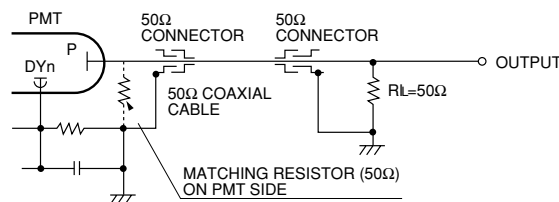
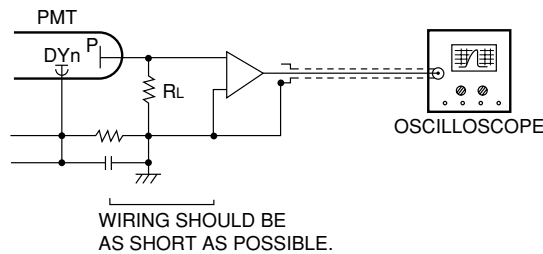


Figure 5-35: Output circuit impedance match

When a mismatch occurs at the coaxial cable ends, all of the output signal energy is not dissipated at the output end, but is partially reflected back to the photomultiplier tube. If a matching resistor is not provided on the photomultiplier tube side, the photomultiplier tube anode is viewed as an open end, so the signal will be reflected from the anode and returned to the output end again. This reflected signal is observed as a pulse which appears after the main pulse with a time delay equal to the round trip through the coaxial cable. This signal repeats its round trip until its total energy is dissipated, as a result, ringing occurs at the output end. To prevent this, providing an impedance match not only at the output end but also at the photomultiplier tube side is effective to some extent, although the output voltage will be reduced to one-half in comparison with that obtained when impedance match is done only at the output end. When using a photomultiplier tube which is not a fast response type or using a coaxial cable with a short length, an impedance matching resistor is not necessarily required on the photomultiplier tube side. Whether or not to connect this resistor to the photomultiplier tube can be determined by doing trial-and-error impedance matching. Among photomultiplier tubes, there are special types having a 50-ohm matched output impedance. These tubes do not require any matching resistor.

Next, let us consider waveform observation of fast pulses using an oscilloscope. A coaxial cable terminated with a matching resistor offers the advantage that the cable length will not greatly affect the pulse shape. Since the matching resistance is usually as low as 50 to 100 ohms, the output voltage becomes very low. Even so the signal output waveform can be directly observed with an oscilloscope using its internal impedance (50 ohms or 1 megohm), but some cases may require a wide-band amplifier with high gain. Such an amplifier usually has large noise and possibly makes it difficult to measure low-level signals. In this case, to achieve the desired output voltage, it is more advantageous to bring the photomultiplier tube as close as possible to the amplifier to reduce the stray capacitance as shown in Figure 5-36, and also to use a large load resistance as long as the frequency response is not degraded.



THBV3\_0536EA

**Figure 5-36: Waveform observation using an oscilloscope**

It is relatively simple to fabricate a fast amplifier with a wide bandwidth using a video IC or pulse type IC. However, in exchange for such design convenience, these ICs tend to reduce performance, such as introducing noise. For optimum operation, it is therefore necessary to know their performance limits and take corrective action.

As the pulse repetition rate increases, a phenomenon called "base-line shift" creates another reason for concern. This base-line shift occurs when the DC signal component has been eliminated from the signal circuit by use of a coupling capacitor. If this occurs, the zero reference level shifts from ground to an apparent zero level equal to the average of the output pulses. Furthermore, when multiple pulses enter within the time resolution of the measuring system including the amplifier, they are integrated so that a large output pulse appears. This is known as "pile-up". Special care should be taken in cases where a pulse height discriminator is used to discern the amplitude of individual pulses.

## 5.4 Housing

A photomultiplier tube housing is primarily used to contain and secure a photomultiplier tube, but it also provides the following functions:

1. To shield extraneous light
2. To eliminate the effect of external electrostatic fields
3. To reduce the effect of external magnetic fields

The following sections explain each of these functions

### 5.4.1 Light shield

Since a photomultiplier tube is a highly sensitive photodetector, the signal light level to be detected is typically very low and therefore care must be exercised in shielding extraneous light. For instance, when a connector is used for signal input/output, there is a possibility of light leakage through the connector itself or through its mounting holes and screw holes. Furthermore, light leakage may occur through seams in the housing.

As a corrective action, when mounting connectors or other components in the housing, use black silicone rubber at any location where light leakage may occur. It is also important to use black soft tape or an O-ring so as to fill in any gaps around the components attached to the housing. In addition, it is necessary to coat the inside of the housing with black mat paint in order to prevent reflection of scattered light.

### 5.4.2 Electrostatic shield

Since photomultiplier tube housings are made of metal such as aluminum, maintaining the housing at ground potential provides an effective shield with respect to external electrostatic fields. The inside of the housing is usually coated with black paint to prevent diffuse reflection of light, so care is required to be certain that the paint does not interfere with the contact of the ground line. If any object at ground potential is brought close to the bulb of a photomultiplier tube, noise increases, so that the housing should have sufficient separation from the photomultiplier tube.

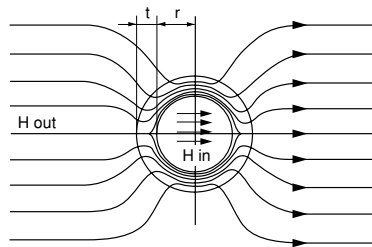
### 5.4.3 Magnetic shield

As will be described in Chapter 13, photomultiplier tubes are very sensitive to a magnetic field. Even terrestrial magnetism will have a detrimental effect on the photomultiplier tube performance<sup>5)</sup>. Therefore, in precision photometry or in applications where the photomultiplier tube must be used in a highly magnetic field, the use of a magnetic shield case is essential. However, unlike the electrostatic shield, there exists no conductors that carry the magnetic flux. Shielding a magnetic field completely is not possible. One common technique for reducing the effect of an external magnetic field is to wrap a metal shield having high permeability around the photomultiplier tube bulb, but such a metal shield cannot completely block the magnetic field. An optimum shielding material and method must also be selected according to both the strength and frequency of the magnetic fields.

In general applications, it is not necessary to fabricate the entire housing from high-permeability materials. Instead, a photomultiplier tube can be wrapped into a cylindrical shield case. Among shielding materials, "Permalloy" is the best and is widely used. The effect of a magnetic shield is described below.

**(1) Shielding factor of magnetic shield case and orientation of magnetic field**

Photomultiplier tubes are very sensitive to an external magnetic field, especially for head-on types, the output varies significantly even with terrestrial magnetism. To eliminate the effect of the terrestrial magnetism or to operate a photomultiplier tube under stable conditions in a magnetic field, a magnetic shield case must be used. (Also refer to Chapter 13.) Utilizing the fact that a magnetic field is shunted through an object with high permeability, it is possible to reduce the influence of an external magnetic field by placing the photomultiplier tube within a magnetic shield case, as illustrated in Figure 5-37.



THBV3\_0537EA

**Figure 5-37: Shielding effect of a magnetic shield case**

Let us consider the shielding effect of a magnetic shield case illustrated in Figure 5-37. As stated, the magnetic shield case is commonly fabricated from metal with high-permeability such as Permalloy. The shielding factor S of such a magnetic shield case is expressed as follows:

$$S = \frac{H_{out}}{H_{in}} = \frac{3t\mu}{4r} \dots\dots\dots (Eq. 5-16)$$

where  $H_{in}$  and  $H_{out}$  are the magnetic field strength inside and outside the shield case respectively,  $t$  is the thickness of the case,  $r$  is the radius of the case and  $\mu$  is the permeability. When two or more magnetic shield cases with different radii are used in combination, the resultant shielding factor  $S'$  will be the product of the shielding factor of each case, as expressed in the following equation:

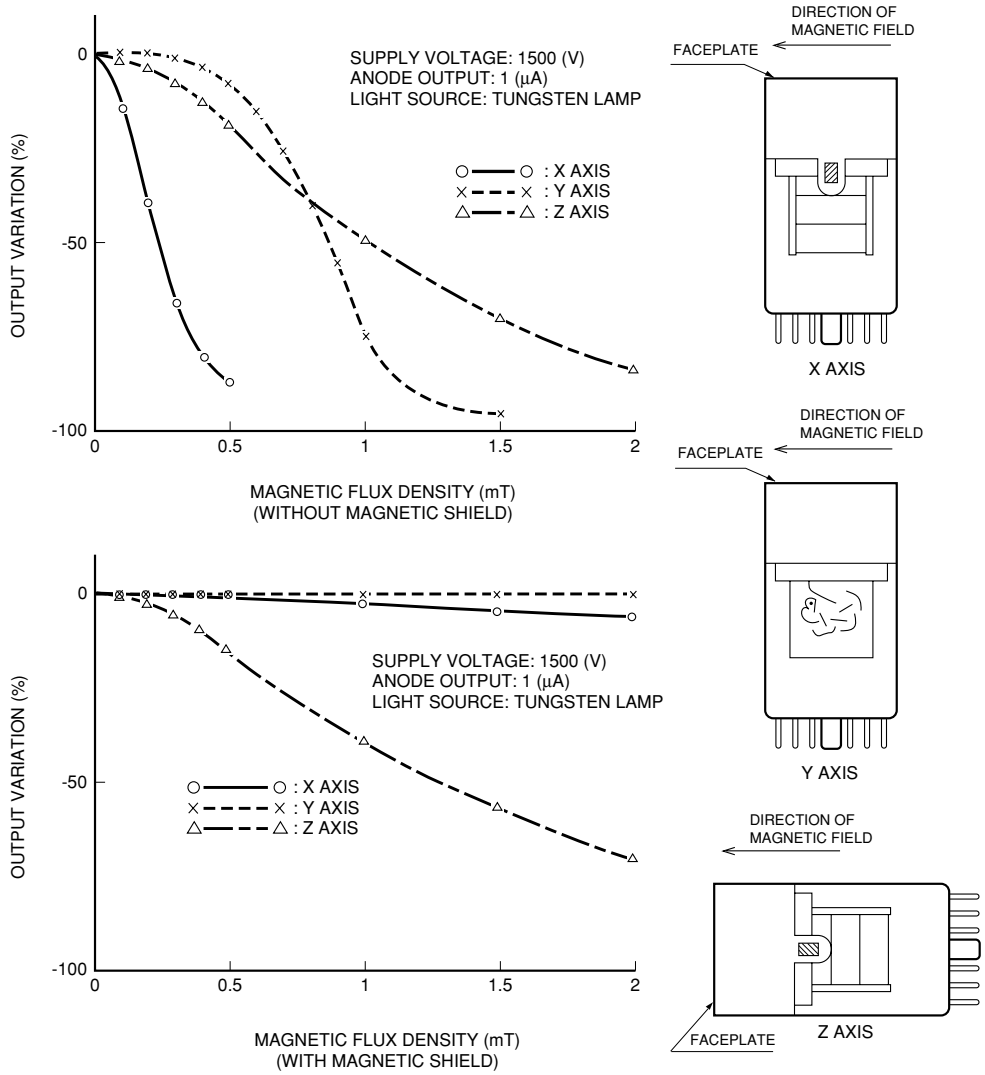
$$S' = S_1 \times S_2 \times S_3 \dots S_n$$

$$= \frac{3t_1\mu_1}{4r_1} \times \frac{3t_2\mu_2}{4r_2} \times \frac{3t_3\mu_3}{4r_3} \times \dots \times \frac{3t_n\mu_n}{4r_n} \dots\dots\dots (Eq. 5-17)$$

When a magnetic shield case is used, the magnetic field strength inside the case  $H_{in}$ , which is actually imposed on the photomultiplier tube, is reduced to a level of  $H_{out}/S$ . For example, if a magnetic shield case with a shielding factor of 10 is employed for a photomultiplier tube operated in an external magnetic field of 3 milliteslas, this means that the photomultiplier tube is operated in a magnetic field of 0.3 milliteslas. In practice, the edge effect of the shield case, as will be described later, creates a loss of the shielding effect. But this approach is basically correct.

Figure 5-38 shows the output variations of a photomultiplier tube with and without a magnetic shield case which is made of "PC" materials with a 0.6 millimeter thickness. It is obvious that the shielding is effective for both X and Y axes. For these axes the shielding factor of the magnetic shield case must be equal. However, the Y axis exhibits better magnetic characteristics than the X axis when not using a magnetic shield case, so that the Y axis provides a slightly better performance when used with the magnetic shield case. In the case of the Z axis which is parallel to the tube axis, the photomultiplier tube used with the magnetic shield case shows larger output variations. It is thought that, as described in the section on the edge effect, this is probably due to the direction of the magnetic field which is bent near the edge of the shield case.



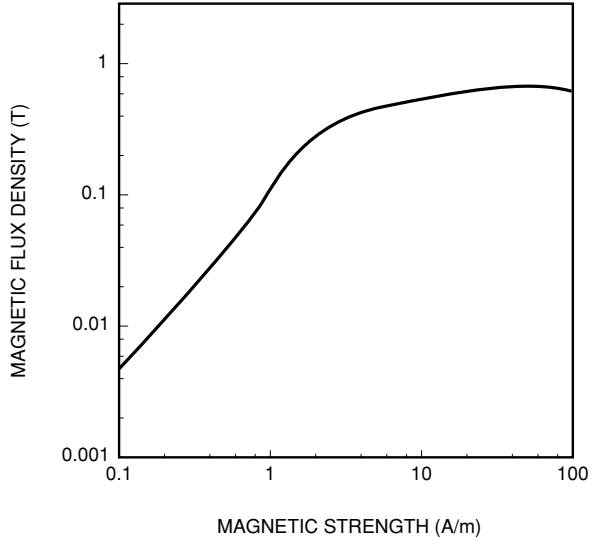


THBV3\_0538EA

Figure 5-38: Magnetic characteristics of a photomultiplier tube

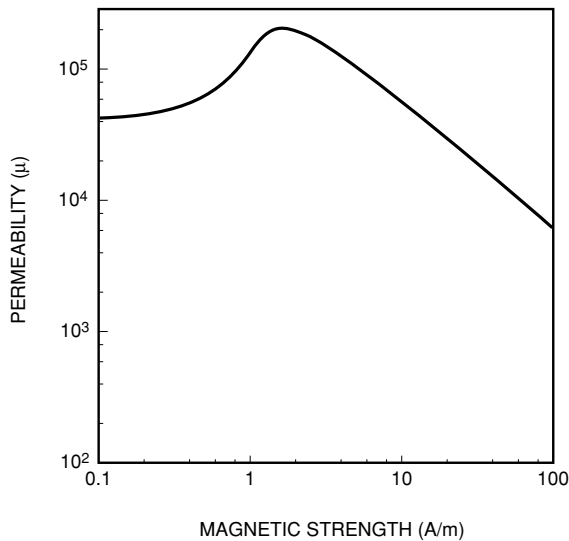
**(2) Saturation characteristics**

When plotting a B-H curve which represents the relationship between the external magnetic field strength (H) and the magnetic flux density (B) traveling through a magnetic material, a saturation characteristic is seen as shown in Figure 5-39.



THBV3\_0539EA

**Figure 5-39: DC magnetization curve (B-H curve)**



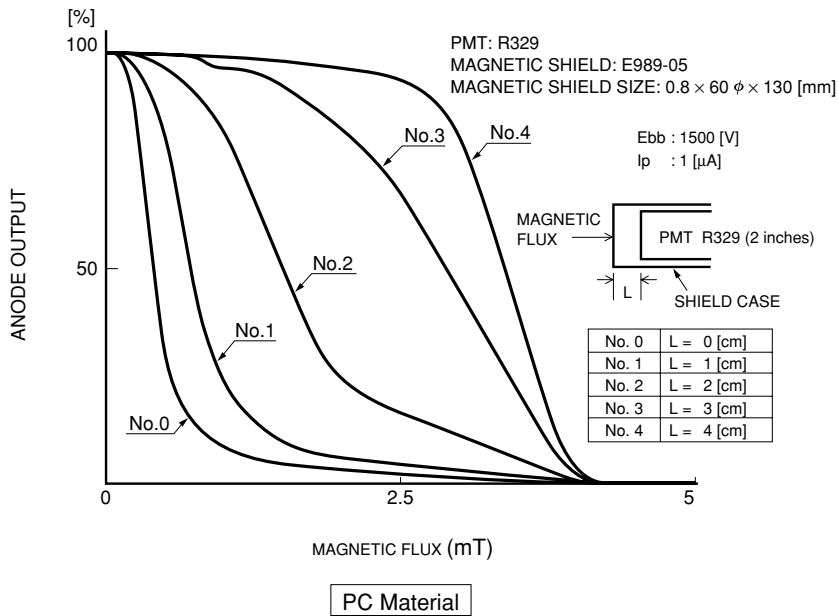
THBV3\_0540EA

**Figure 5-40: Permeability and external magnetic field**

Since the permeability  $\mu$  of a magnetic material is given by the B/H ratio,  $\mu$  varies with H as shown in

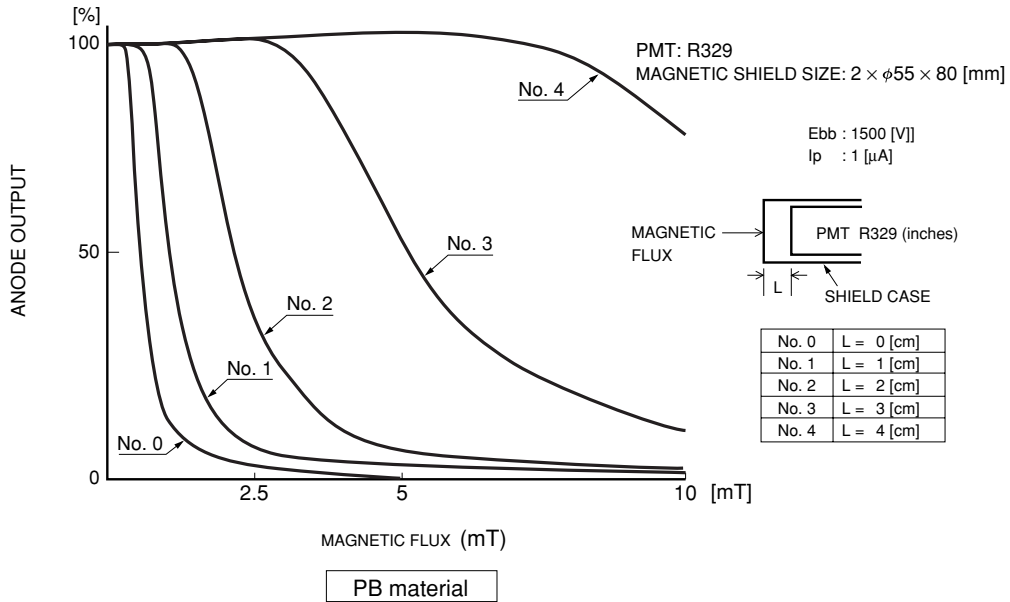
Figure 5-40 with a peak at a certain H level and above it, both  $\mu$  and the shielding factor degrade sharply. Data shown in Figure 5-40 are measured using a magnetic shield case E989 (0.8 millimeter thick) manufactured by Hamamatsu Photonics when a magnetic field is applied in the direction perpendicular to the shield case axis.

Magnetic shield cases are made of a "PC" material which contains large quantities of nickel. This material assures very high permeability, but has a rather low saturation level of magnetic flux density. In a weak magnetic field such as from terrestrial magnetism, the "PC" material provides good shielding factor as high as  $10^3$  and thus proves effective in shielding out terrestrial magnetism. In contrast, "PB" material which contains small quantities of nickel offers high saturation levels of magnetic flux density, though the permeability is lower than that of the "PC" material. Figure 5-41 shows the anode output variations of a photomultiplier tube used with a magnetic shield case made of "PC" or "PB" material. As the magnetic flux density is increased, the anode output of the photomultiplier tube used with the "PC" material shield case drops sharply while that used with the "PB" material shield case drops slowly. Therefore, in a highly magnetic field, a "PC" material shield case should be used in conjunction with a shield material such as soft-iron or thick PB material with a thickness of 3 to 10 millimeters, which exhibits a high saturation level of magnetic flux density.



THBV3\_0541EA

Figure 5-41: Magnetic characteristics of a photomultiplier tube used with magnetic shield case (PC material)

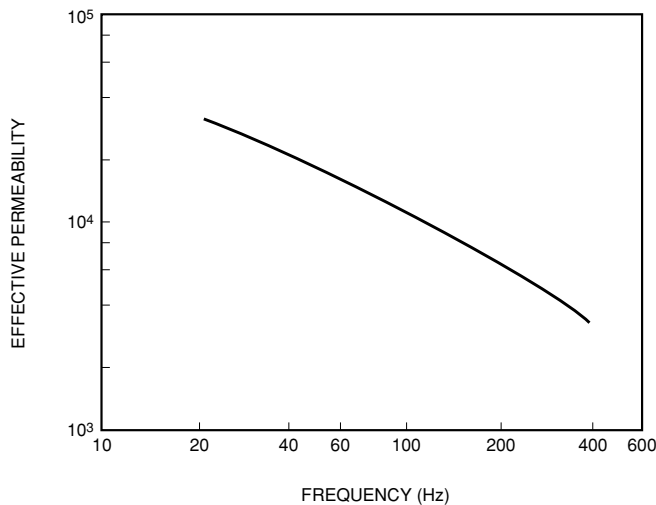


THBV3\_0541EA

Figure 5-41: Magnetic characteristics of a photomultiplier tube used with magnetic shield case (PB material)

### (3) Frequency characteristics

The above description concerning the effect of magnetic shield cases, refers entirely to DC magnetic fields. In AC magnetic fields, the shielding effect of a magnetic shield case decreases with increasing frequency as shown in Figure 5-42. This is particularly noticeable for thick materials, so it will be preferable to use a thin shield case of 0.05 to 0.1 millimeter thickness when a photomultiplier tube is operated in a magnetic field at frequencies from 1 kHz to 10 kHz. The thickness of a magnetic shield case must be carefully determined to find the optimum compromise between the saturated magnetic flux density and frequency characteristics.

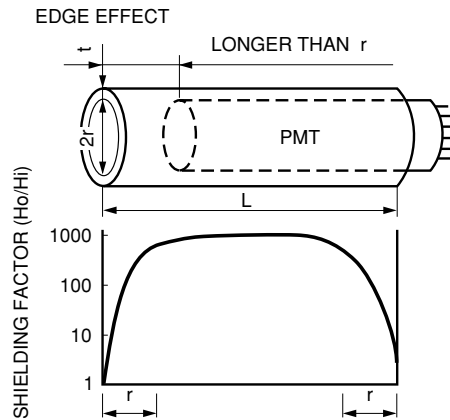


THBV3\_0542EA

Figure 5-42: Frequency characteristics of a magnetic shield case

#### (4) Edge effect

The shielding effect given by  $3t \mu/4r$  applies to the case in which the magnetic shield case is sufficiently long with respect to the overall length of the photomultiplier tube. Actual magnetic shield cases have a finite length which is typically only several millimeters to several centimeters longer than the photomultiplier tube, and their shielding effects deteriorate near both ends as shown in Figure 5-43. Since the photocathode to the first dynode region is most affected by a magnetic field, this region must be carefully shielded. For example, in the case of a head-on photomultiplier tube, the tube should be positioned deep inside the magnetic shield case so that the photocathode surface is hidden from the shield case edge by a length equal to the shield case radius or diameter. (See Figure 5-41.)



THBV3\_0543EA

Figure 5-43: Edge effect of a magnetic shield case

#### (5) Photomultiplier tube magnetic characteristics and shielding effect

Figure 5-44 shows magnetic characteristics of typical photomultiplier tubes (anode output variations versus magnetic flux density characteristics) and the shielding effects of magnetic shield cases (Hamamatsu E989 series). It can be seen from these figures that use of a shield case can greatly reduce the influence of magnetic fields of several milliteslas.

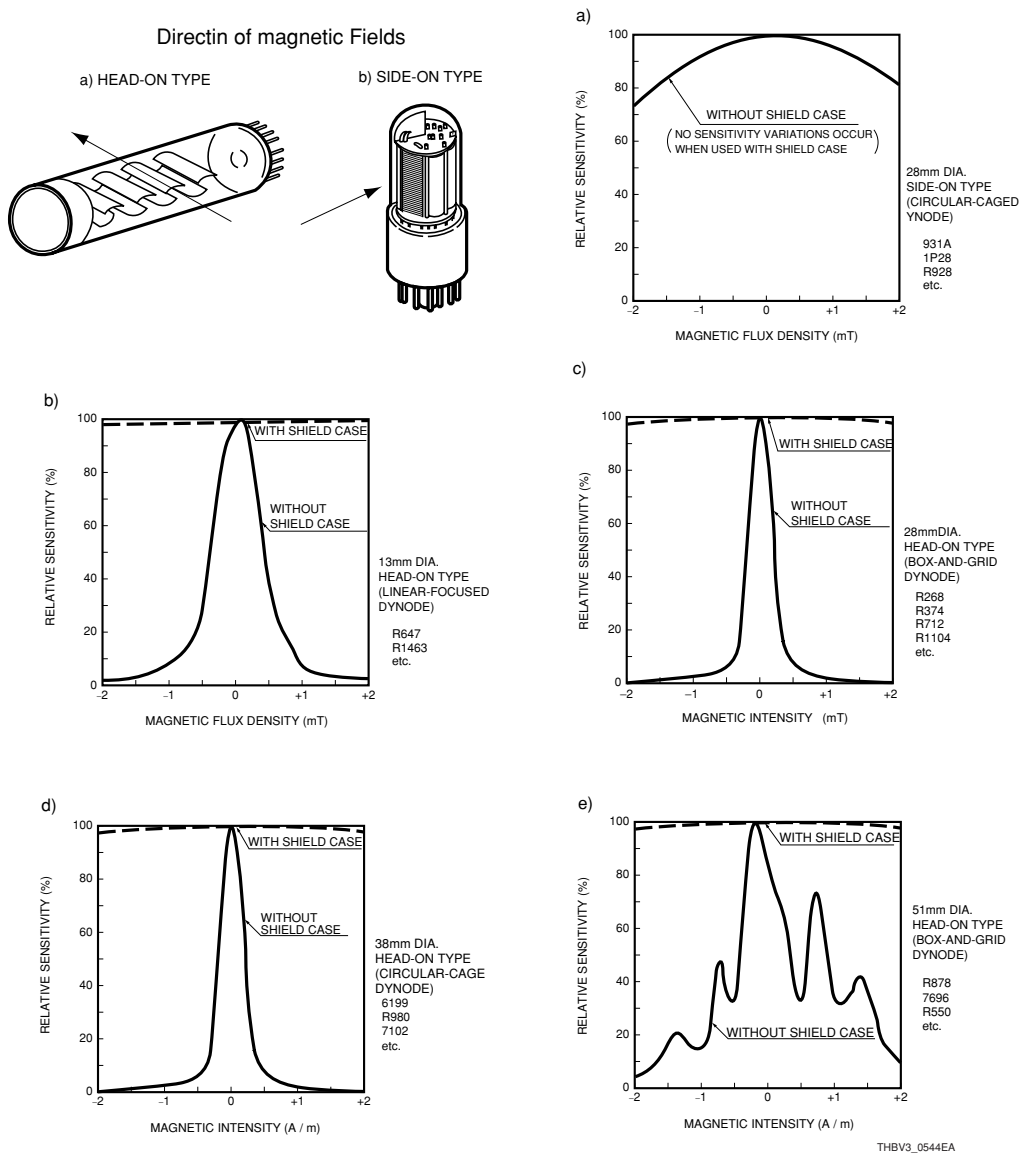


Figure 5-44: Effect of magnetic shield case

## (6) Handling the magnetic shield case

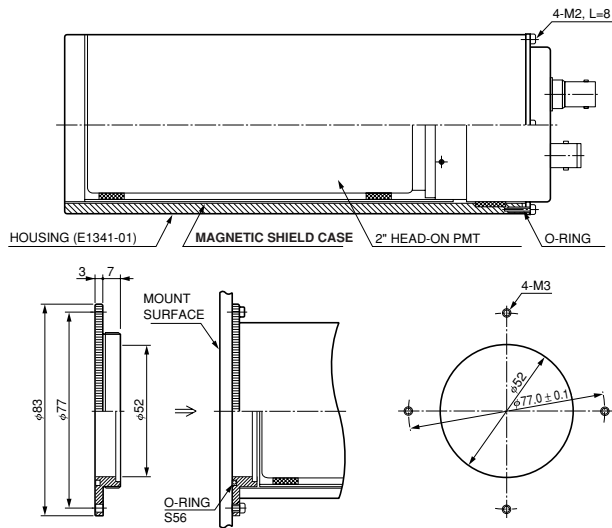
Magnetic shield cases are subject to deterioration in performance due to mechanical shock and deformation therefore sufficient care must be exercised during handling. Once the performance has deteriorated, a special annealing process is required for recovery. In particular, since the permeability characteristics are more susceptible to external shock and stress, avoid any alteration such as drilling and machining the shield case.

If any object at ground potential is brought close to the bulb of a photomultiplier tube, the photomultiplier tube noise increases considerably. Therefore, using a magnetic shield case larger than the photomultiplier tube diameter is recommended. In this case, positioning the photomultiplier tube in the center of the shield case is important, otherwise electrical problem may occur. Foam rubber or similar materials with good buffering and insulating properties can be used to hold the photomultiplier tube in the shield case.

For safety and also for noise suppression reasons it is recommended that the magnetic shield case be grounded via a resistor of 5 to 10 MΩ, although this is not mandatory when a HA-coating photomultiplier tube (See 13.8.2 in Chapter 13) or a photomultiplier tube with the cathode at ground potential and the anode at a positive high voltage is used. In this case, sufficient care must be taken with regards to the insulation of the magnetic shield case.

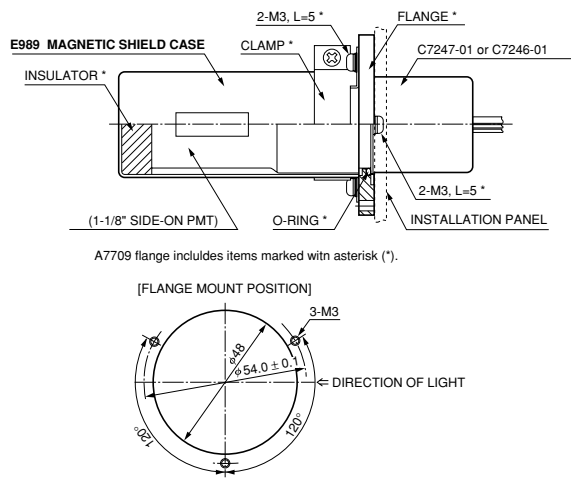
For your reference when installing a magnetic shield case, Figure 5-45 illustrates the structure and dimensions of a housing and flange assembled with a magnetic shield case, which are available from Hamamatsu Photonics.

**Housing: For head-on photomultiplier tube**



THBV3\_0545EAa

**Flange: For side-on photomultiplier tube**



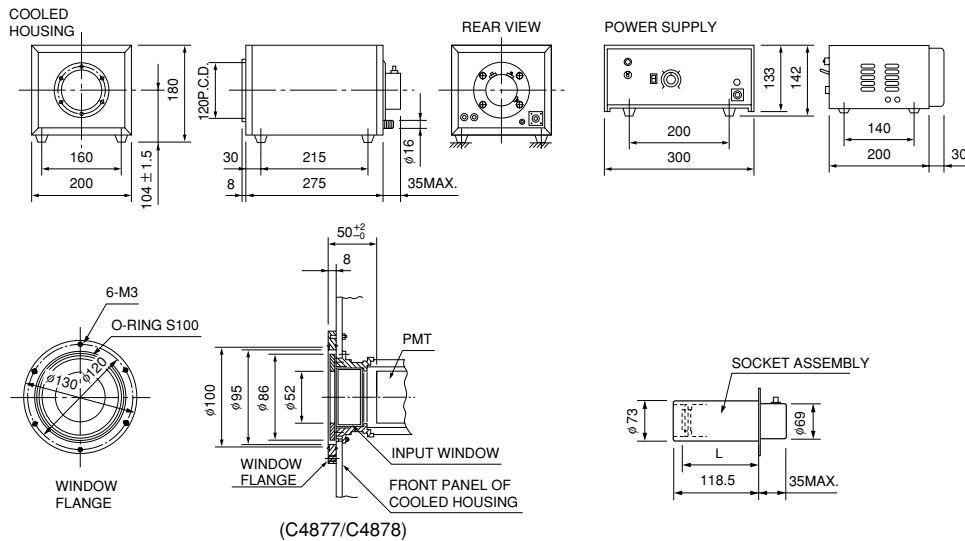
THBV3\_0545EAb

**Figure 5-45: Magnetic shield case assembled in housing and flange**

## 5.5 Cooling

As described in Chapter 4, thermionic emission of electrons is a major cause of dark current. It is especially predominant when the photomultiplier tube is operated in a normal supply voltage range. Because of this, cooling the photomultiplier tube can effectively reduce the dark current and the resulting noise pulses, improving the signal-to-noise ratio and enhancing the lower detection limit. However, the following precautions are required for cooling a photomultiplier tube.

Photomultiplier tube cooling is usually performed in the range from 0°C to -30°C according to the temperature characteristic of the dark current. When a photomultiplier tube is cooled to such a temperature level, moisture condensation may occur at the input window, bulb stem or voltage-divider circuit. This condensation may cause a loss of light at the input window and an increase in the leakage current at the bulb stem or voltage-divider circuit. To prevent this condensation, circulating dry nitrogen gas is recommended, but the equipment configuration or application often limits the use of liquid nitrogen gas. For efficient cooling, Hamamatsu provides thermoelectric coolers having an evacuated double-pane quartz window with a defogger and also air-tight socket assemblies.<sup>6)</sup> An example of thermoelectric coolers is shown in Figure 5-46, along with a suitable socket assembly.



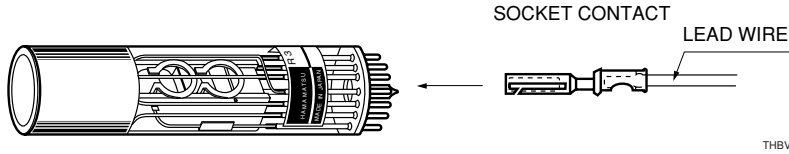
THBV3\_0546EA

**Figure 5-46: Thermoelectric cooler (manufactured by Hamamatsu Photonics)**

The cooler shown in the above figure is identical with the Hamamatsu C4877 and C4878 coolers. The C4877 is designed for 51 mm (2") and 38 mm (1.5") diameter head-on photomultiplier tubes, while the C4878 is for MCP-PMTs. Either model can be cooled down to -30°C by thermoelectric cooling.

If a socket made by other manufacturers is used with a Hamamatsu photomultiplier tube, the bulb stem of the photomultiplier tube may possibly crack during cooling. This is due to the difference in the thermal expansion coefficient between the socket and the bulb stem. Be sure to use the mating socket available from Hamamatsu. Stem cracks may also occur from other causes, for example, a distortion in the stem. When the bulb stem is to be cooled below -50°C, the socket should not be used, instead, the lead pins of the photomultiplier tube should be directly connected to wiring leads. To facilitate this, use of socket contacts, as illustrated in Figure 5-47, will prove helpful.





**Figure 5-47: Connecting the lead pins to the socket contacts**

Thermionic electrons are emitted not only from the photocathode but also from the dynodes. Of these, thermionic emissions that actually affect the dark current are those from the photocathode,  $Dy_1$  and  $Dy_2$ , because the latter-stage dynodes contribute less to the current amplification. Therefore cooling the photocathode,  $Dy_1$ , and  $Dy_2$  proves effective in reducing dark current and besides, this is advantageous in view of possible leakage currents which may occur due to moisture condensation on the bulb stem, base or socket.

The interior of a photomultiplier tube is a vacuum, so heat is conducted through it very slowly. It is therefore recommended that the photomultiplier tube be left for one hour or longer after the ambient temperature has reached a constant level, so that the dark current and noise pulses will become constant. Another point to be observed is that, since heat generated from the voltage-divider resistors may heat the dynodes, the voltage-divider resistor values should not be made any smaller than necessary.

## References in Chapter 5

- 1) Hamamatsu Photonics Catalog: Photomultiplier Tubes and Related Products.
- 2) S. Uda; Musen Kogaku (Wireless Engineering) I, New Edition, Transmission Section, Maruzen.
- 3) Ref. to "Kerns-type PM base" Produced by R.L. McCarthy.
- 4) Hamamatsu Photonics Technical Information: Photomultiplier Tubes for Use in Scintillation Counting.
- 5) H. Igarashi, et al.: Effect of Magnetic Field on Uniformity of Gamma Camera, Nuclear Medicine Vo. 28, No. 2 (1991).  
Ref. to "Improvement of 20-inch diameter photomultiplier tubes" published by A. Suzuki (KEK, Tsukuba) and others.
- 6) Hamamatsu Photonics Catalog: Photomultiplier Tubes and Related Products.

# MEMO

# **CHAPTER 6**

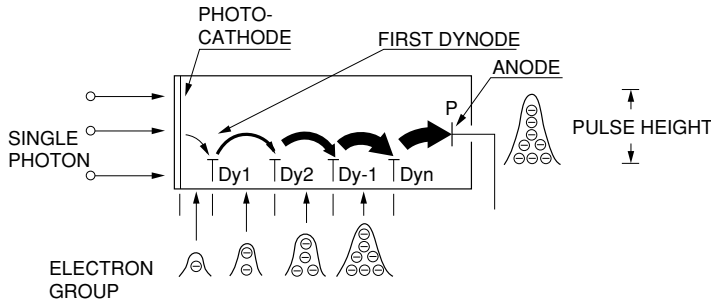
## **PHOTON COUNTING 1) 2) 4) - 12)**

*Photon counting is an effective technique used to detect very-low-level-light such as Raman spectroscopy, fluorescence analysis, and chemical or biological luminescence analysis where the absolute magnitude of the light is extremely low. This section describes the principles of photon counting, its operating methods, detection capabilities, and advantages as well as typical characteristics of photomultiplier tubes designed for photon counting.*

## 6.1 Analog and Digital (Photon Counting) Modes

The methods of processing the output signal of a photomultiplier tube can be broadly divided into analog and digital modes, depending on the incident light intensity and the bandwidth of the output processing circuit.

As Figure 6-1 shows, when light strikes the photocathode of a photomultiplier tube, photoelectrons are emitted. These photoelectrons are multiplied by the cascade process of secondary emission through the dynodes (normally  $10^6$  to  $10^7$  times) and finally reach the anode connected to an output processing circuit.

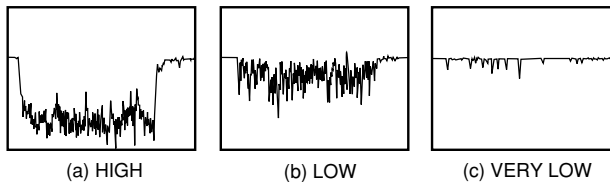


THBV3\_0601

Figure 6-1: Photomultiplier tube operation in photon counting mode

When observing the output signal of a photomultiplier tube with an oscilloscope while varying the incident light level, output pulses like those shown in Figure 6-2 are seen. At higher light levels, the output pulse intervals are narrow so that they overlap each other, producing an analog waveform (similar to (a) and (b) of Figure 6-2). If the light level becomes very low, the ratio of AC component (fluctuation) in the signal increases, and finally the output signal will be discrete pulses (like (c) of Figure 6-2). By discriminating these discrete pulses at a proper binary level, the number of the signal pulses can be counted in a digital mode. This is commonly known as photon counting.

In analog mode measurements, the output signal is the mean value of the signals including the AC components shown in Figure 6-2 (a). In contrast, the photon counting method can detect each pulse shown in Figure 6-2 (c), so the number of counted pulses equals the signal. This photon counting mode uses a pulse height discriminator that separates the signal pulses from the noise pulses, enabling high-precision measurement with a higher signal-to-noise ratio compared to the analog mode and making photon counting exceptionally effective in detecting low level light.



THBV3\_0602

Figure 6-2: Photomultiplier tube output waveforms observed at different light levels

## 6.2 Principle of Photon Counting

When light incident on a photomultiplier tube becomes very low and reaches a state in which no more than two photoelectrons are emitted within the time resolution (pulse width) of the photomultiplier tube, this light level is called the single photoelectron region and photon counting is performed in this region. Quantum efficiency, an important parameter for photon counting, signifies the probability of photoelectron emission when a single photon strikes the photocathode.

In this single photoelectron region, the number of emitted electrons per photon is one or zero and the quantum efficiency can be viewed as the ratio of the number of photoelectrons emitted from the photocathode to the number of incident photons per unit time. The probability that the photoelectrons emitted from the photocathode (primary electrons) will impinge on the first dynode and contribute to gain is referred to as collection efficiency. Some photoelectrons may not contribute to gain because they deviate from the normal trajectories and are not collected by the first dynode. Additionally, in the photon counting mode, the ratio of the number of counted pulses (output pulses) to the number of incident photons is called detection efficiency or photomultiplier tube counting efficiency and is expressed by the following relation:

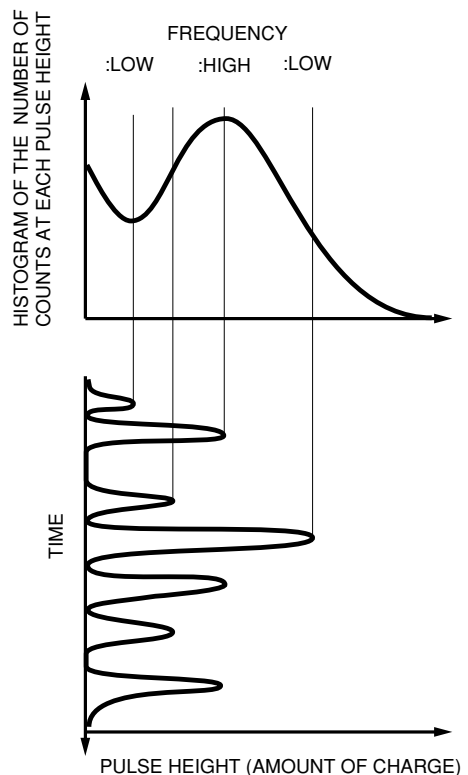
$$\text{Detection efficiency (counting efficiency)} = (N_d/N_p) = \eta \times \alpha \quad \dots \text{(Eq. 6-1)}$$

in the photon counting region

where  $N_d$  is the counted value,  $N_p$  is the number of incident photons,  $\eta$  is the quantum efficiency of the photocathode and  $\alpha$  is the collection efficiency of the dynodes. The detection efficiency greatly depends on the threshold level used for binary processing.

The number of secondary electrons released from the first dynode is not constant. It is around several secondary electrons per primary electron, with a broad probability roughly seen as a Poisson distribution. The average number of electrons per primary electron  $\delta$  corresponds to the secondary-electron multiplication factor of the dynode. Similarly, this process is repeated through the second and subsequent dynodes until the final electron bunch reaches the anode. In this way the output multiplied in accordance with the number of photoelectrons from the photocathode appears at the anode. If the photomultiplier tube has  $n$  stage dynodes, the photoelectrons emitted from the photocathode are multiplied in cascade up to  $\delta^n$  times and derived as an adequate electron bunch from the anode. In this process, each output pulse obtained at the anode exhibits a certain distribution in pulse height because of fluctuations in the secondary multiplication factor at each dynode (statistical fluctuation due to cascade multiplication), non-uniformity of multiplication depending on the dynode position and electrons deviating from their favorable trajectories. Figure 6-3 illustrates a histogram of photomultiplier tube output pulses. The abscissa indicates the pulse height and the anode output pulses are integrated with time. This graph is known as the pulse height distribution.

Figure 6-3 also shows the relation between the pulse height distribution and the actual output pulses obtained with a photomultiplier tube. The pulse height distribu-



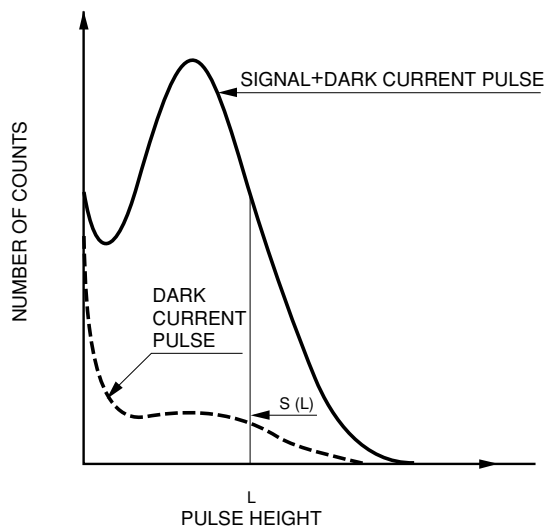
THBV3\_0603EA

**Figure 6-3: Photomultiplier tube output and its pulse height distribution**

tion is usually taken with a multichannel analyzer (MCA) frequently used in scintillation counting applications.

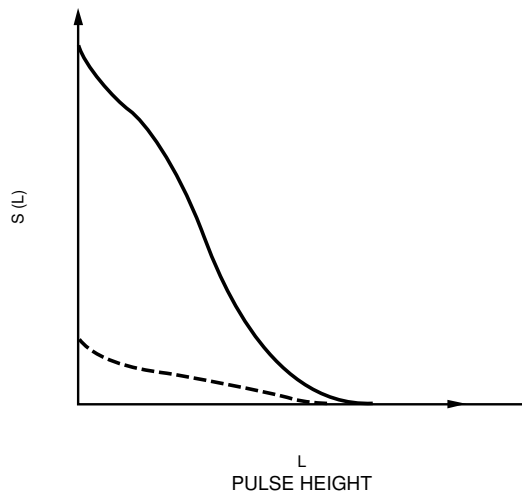
Figure 6-4 (a) shows examples of the pulse height distribution obtained with a photomultiplier tube. There are output pulses present even if no light falls on the photomultiplier tube, and these are called dark current pulses or noise pulses. The broken line indicates the distribution of the dark current pulses, with a tendency to build up somewhat in the lower pulse height region (left side). These dark pulses mainly originate from the thermal electron emission at the photocathode and also at the dynodes. The thermal electrons from the dynodes are multiplied less than those from the photocathode and are therefore distributed in the lower pulse height region.

Figure 6-4 (b) indicates the distribution of the total number of counted pulses  $S(L)$  with amplitudes greater than a threshold level  $L$  shown in (a). (a) and (b) have differential and integral relations to each other. Item (b) is a typical integral curve taken with a photon counting system using a photomultiplier tube.



(a) DIFFERENTIAL SPECTRUM

THBV3\_0604Ea



(b) INTEGRAL SPECTRUM

THBV3\_0604EAb

**Figure 6-4: Differential and integral representations of pulse height distribution**

## 6.3 Operating Method and Characteristics of Photon Counting

This section discusses specific circuit configurations used to perform photon counting and the basic characteristics involved in photon counting.

### (1) Circuit configuration

Figure 6-5 shows a typical circuit configuration for photon counting and a pulse waveform obtained at each circuit.

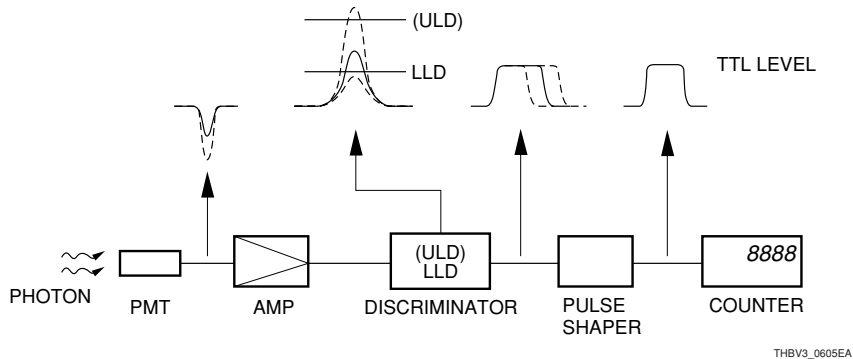


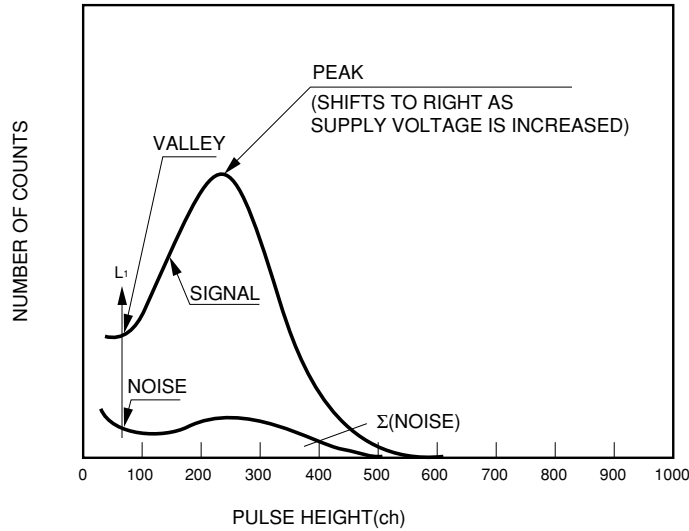
Figure 6-5: Circuit configuration for photon counting

In the above system, current output pulses from a photomultiplier tube are converted to a voltage by a wide-band preamplifier and amplified. These voltage pulse are fed to a discriminator and then to a pulse shaper. Finally the number of pulses is counted by a counter. The discriminator compares the input voltage pulses with the preset reference voltage (threshold level) and eliminates those pulses with amplitudes lower than this value. In general, the LLD (lower level discrimination) level is set at the lower pulse height side. The ULD (upper level discrimination) level may also be often set at the higher pulse height side to eliminate noise pulses with higher amplitudes. The counter is usually equipped with a gate circuit, allowing measurement at different timings and intervals.

### (2) Basic characteristics of photon counting

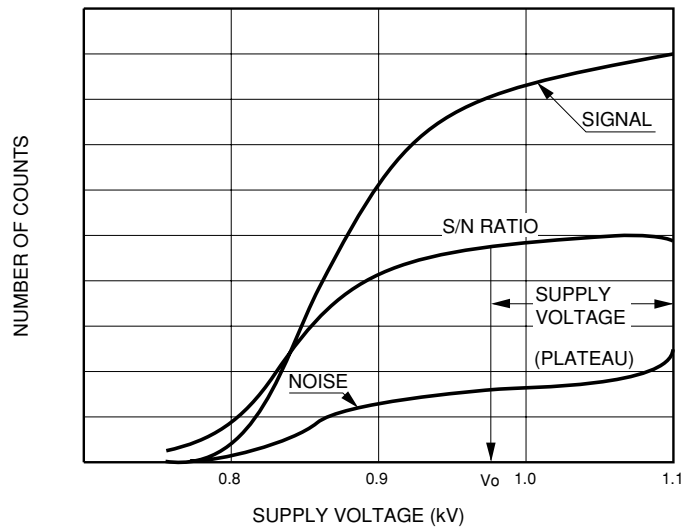
#### a) Pulse height distribution and plateau characteristics

If a multichannel pulse height analyzer is available, a proper threshold level can be set in the pulse height distribution. Typical pulse height distributions of signal pulses and noise pulses are shown in Figure 6-6. Because the dark current pulses are usually distributed in the lower pulse height region, setting the LLD level in the vicinity of the valley ( $L_1$ ) of the distribution can effectively eliminate such noise pulses without sacrificing the detection efficiency. In actual operation, however, using a pulse height analyzer is not so popular. Other methods that find plateau characteristics using the circuit of Figure 6-5 are more commonly employed. By counting the total number of pulses with amplitudes higher than the preset threshold level while varying the supply voltage for the photomultiplier tube, plots similar to those shown in Figure 6-7 can be obtained. These plots are called the plateau characteristics. In the plateau range, the change in the number of counts less depends on the supply voltage. This is because only the number of pulses is digitally counted in photon counting, while in the analog mode the gain change of the photomultiplier tube directly affects the change of the output pulse height.



THBV3\_0606EA

Figure 6-6: Typical example of pulse height distributions



THBV3\_0607EA

Figure 6-7: Plateau characteristics

### b) Setting the photomultiplier tube supply voltage

The signal-to-noise ratio is an important factor from the viewpoint of accurate measurements. Here the signal-to-noise ratio is defined as the ratio of the mean value of the signal count rate to the fluctuation of the counted signal and noise pulses (expressed in standard deviation or root mean square). The signal-to-noise ratio curve shown in Figure 6-7 is plotted by varying the supply voltage, the same procedure which is used to obtain the plateau characteristics. This figure implies that the photomultiplier tube should be operated in the range between the voltage ( $V_0$ ) at which the plateau region begins and the maximum supply voltage.



**c) Count rate linearity**

The photon counting mode offers excellent linearity over a wide range. The lower limit of the count rate linearity is determined by the number of dark current pulses, and the upper limit by the maximum count rate. The maximum count rate further depends on pulse-pair resolution, which is the minimum time interval at which each pulse can be separated. The reciprocal of this pulse pair resolution would be the maximum count rate. However, since most events in the photon counting region usually occur at random, the counted pulses may possibly overlap. Considering this probability of pulse overlapping (count error caused by pulse overlapping), the actual maximum count rate will be about one-tenth of the calculated above. Here, if we let the true count rate be  $N$  ( $s^{-1}$ ), measured count rate be  $M$  ( $s^{-1}$ ) and time resolution be  $t$  ( $s^{-1}$ ), the loss of count rate  $N - M$  can also be expressed using the dead time  $M \cdot t$  caused by pulse overlapping, as follows:

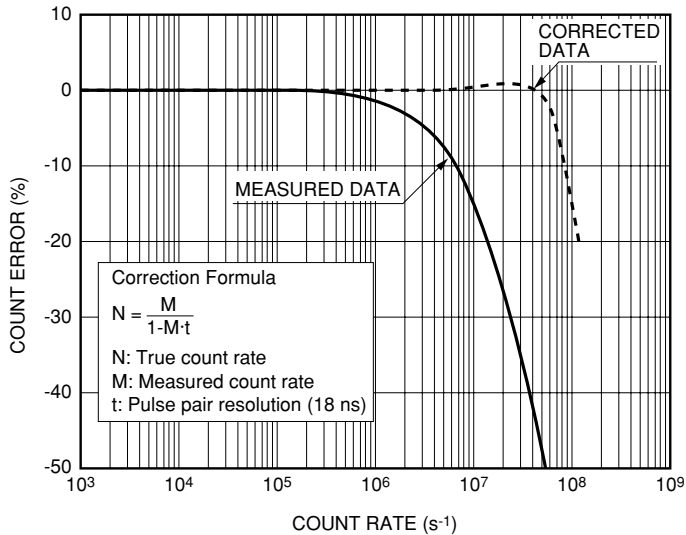
$$N - M = N \cdot M \cdot t$$

The true count rate  $N$  then becomes

$$N = \frac{M}{1 - M \cdot t} \dots\dots\dots \text{(Eq. 6-2)}$$

The count error can be corrected by using this relation.

Figure 6-8 shows examples of count rate linearity data before and after correction, measured using a system with a pulse pair resolution of 18 nanoseconds. The count error is corrected to within 1 % even at a count rate exceeding  $10^7 s^{-1}$ .



**Figure 6-8: Linearity of count rate**

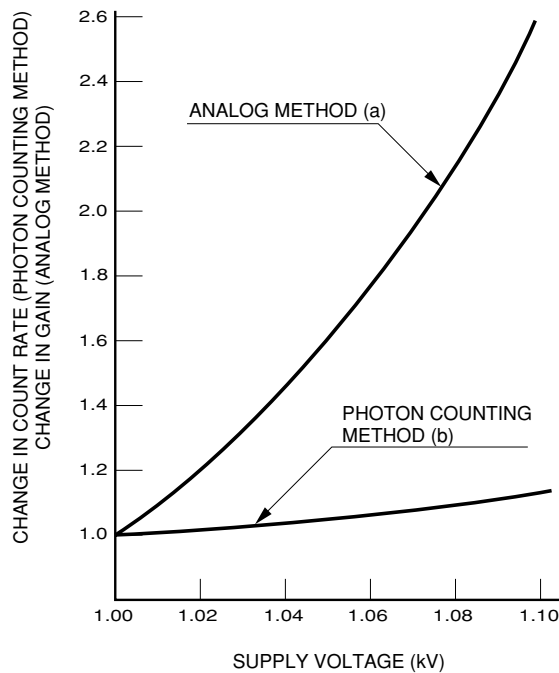
THBV3\_0608EA

#### d) Advantages of photon counting

Photon counting has many advantages in comparison with the analog mode. Among them, stability and signal-to-noise ratio are discussed in this section.

##### (I) Stability

One of the significant advantages photon counting offers is operating stability. The photon counting mode is resistant to variations in supply voltage and photomultiplier tube gain. If the supply voltage is set within the plateau region, a change in the voltage has less effect on the output counts. In the analog mode, however, it affects the output current considerably. Immunity to variations in the supply voltage means that the photon counting mode also assures high stability against gain fluctuation of the photomultiplier tube. Normally the photon counting mode offers several times higher immunity to such variations than the analog mode. (Refer to Figure 6-9.)



THEV3\_0609EA

Figure 6-9: Stability versus changes in supply voltage

##### (II) Signal-to-noise ratio

When signal light strikes the photocathode of a photomultiplier tube, photoelectrons are emitted and directed to the dynode section where secondary electrons are produced. The number of photoelectrons produced per unit time and also the number of secondary electrons produced are determined by statistical probability of events which is represented by a Poisson distribution. The signal-to-noise ratio is also described in 4.3.7 in Chapter 4. The AC component noise which is superimposed on the signal can be categorized by origin as follows

- (1) Shot Noise resulting from signal light
- (2) Shot Noise resulting from background light
- (3) Shot Noise resulting from dark current

In the analog mode, the signal-to-noise ratio<sup>2)-9, 11)</sup> of the photomultiplier tube output including these shot noises becomes

$$\text{SN ratio(current)} = \frac{I_{ph}}{\sqrt{2eNFB\{I_{ph}+2(I_b+I_d)\}}} \dots\dots\dots (\text{Eq. 6-3})$$

where

- I<sub>ph</sub>: signal current produced by incident light (A)
- e: electron charge (c)
- NF: noise figure of the photomultiplier tube
- I<sub>b</sub>: cathode current resulting from background light (A)
- I<sub>d</sub>: cathode current resulting from dark current (A)
- B: Bandwidth of measurement system (Hz)

Here the true signal current I<sub>ph</sub> is obtained by subtracting I<sub>b</sub>+I<sub>d</sub> from the total current. The noise originating from the latter-stage amplifier is considered to be negligible because the typical gain μ of a photomultiplier tube is sufficiently large.

The signal-to-noise ratio in the photon counting mode is given by the following equation.

$$\text{SN ratio} = \frac{N_s\sqrt{T}}{\sqrt{N_s+2(N_b+N_d)}} \dots\dots\dots (\text{Eq. 6-4})$$

where

- N<sub>s</sub>: number of counts/sec resulting from incident light per second
- N<sub>b</sub>: number of counts/sec resulting from background light per second
- N<sub>d</sub>: number of counts/sec resulting from dark current per second
- T: measurement time (s)

Here the number of counts/sec of true signals N<sub>s</sub> is obtained by subtracting N<sub>b</sub>+N<sub>d</sub> from the total number of counts.

From the common equivalent relation between the time and frequency (T=1/2B), if B=1 (Hz) and T=0.5 (s), then the signal-to-noise ratio will be as follows:

in the analog mode

$$\text{SN ratio(current)} = \frac{I_{ph}}{\sqrt{2eNFB\{I_{ph}+2(I_b+I_d)\}}} \dots\dots\dots (\text{Eq. 6-5})$$

in the photon counting mode

$$\text{SN ratio} = \frac{N_s}{\sqrt{2\{N_s+2(N_b+N_d)\}}} \dots\dots\dots (\text{Eq. 6-6})$$

Through the above analysis, it is understood that the photon counting mode provides a better signal-to-noise ratio by a factor of the noise figure NF. Since the dark current includes thermal electrons emitted from the dynodes in addition to those from the photocathode, its pulse height distribution will be shifted toward the lower pulse height side. Therefore, the dark current component can be effectively eliminated by use of a pulse height discriminator while maintaining the signal component, assuring further improvement in the signal-to-noise ratio. In addition, because only AC pulses are counted, the photon counting mode is not influenced by the DC leakage current. Amplifier noises can totally be eliminated by a discriminator.

## References in Chapter 6

- 1) IEC PUBLICATION 306-4, 1971.
- 2) Illes P. Csorba "Image Tubes" Howard W. Sams & Co. (1985).
- 3) F. Robben: Noise in the Measurement of Light with PMs, pp. 776-, Appl. Opt., 10, 4 (1971).
- 4) R. Foord, R. Jones, C. J. Oliver and E. R. Pike: Appl. Opt., 8, 10, (1969).
- 5) R. Foord, R. Jones, C.J. Oliver and E.R. Pike: Appl. Opt. 1975, 8 (1969).
- 6) J.K. Nakamura and S.E. Schmarz: Appl. Opt., 1073, 7, 6 (1968).
- 7) J.K. Nakamura and S. E. Schwarz: Appl. Opt., 7, 6 (1968).
- 8) R.R. Alfano and N. Ockman: Journal of the Optical Society of America, 58, 1 (1968).
- 9) T. Yoshimura, K. Hara and N. Wakabayashi: Appl. Optics, 18, 23 (1979).
- 10) T.S. Durrani and C. A. Greated: Appl. Optics, 14, 3 (1975).
- 11) Hamamatsu Photonics Technical Publication: Photon Counting (2001).
- 12) A. Kamiya, K. Nakamura, M. Niigaki: Journal of the Spectroscopical Society of Japan, 52, 4, 249 (2003).

# **CHAPTER 7**

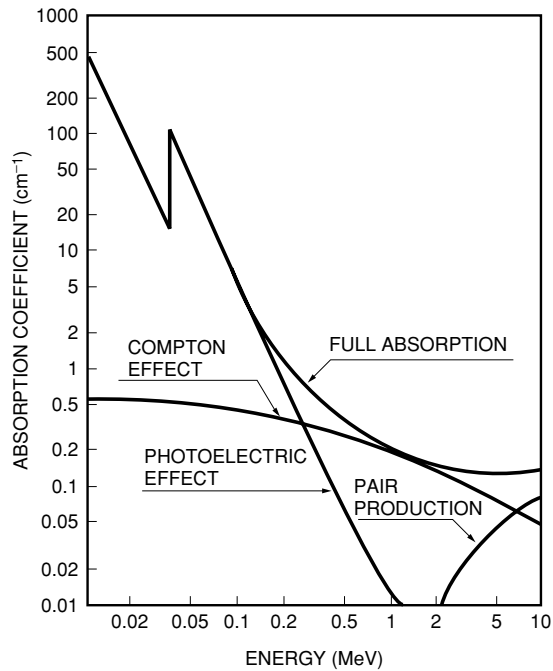
## **SCINTILLATION COUNTING**

*Radiation of various types is widely utilized for non-destructive inspection and testing such as in medical diagnosis, industrial inspection, material analysis and other diverse fields. In such applications, radiation detectors play an important role. There are various methods for detecting radiation.<sup>1) 2) 3) 4)</sup> For example, typical detectors include proportional counters, semiconductor detectors that make use of gas and solid ionization respectively, radiation-sensitive films, cloud chambers, and scintillation counters.*

*In scintillation counting, the combination of a scintillator and photomultiplier tube is one of the most commonly used detectors for practical applications.<sup>5) 6)</sup> Scintillation counting has many advantages over other detection methods, for example, a wide choice of scintillator materials, fast time response, high detection efficiency, and a large detection area. This section gives definitions of photomultiplier tube characteristics required for scintillation counting and explains their measurement methods and typical data.*

## 7.1 Scintillators and Photomultiplier Tubes

When ionizing radiation enters a scintillator, it produces a fluorescent flash with a short decay time. This is known as scintillation. In the case of gamma rays, this scintillation occurs as a result of excitation of the bound electrons by means of free electrons inside the scintillator. These free electrons are generated by the following three mutual interactions: the photoelectric effect, Compton effect, and pair production. The probability of occurrence of these interactions depends on the type of scintillators and the energy level of the gamma rays. Figure 7-1 shows the extent of these interactions when gamma-ray energy is absorbed by a NaI(Tl) scintillator.



THBV3\_0701EA

**Figure 7-1: Gamma-ray absorption characteristics of NaI(Tl) scintillator**

From Figure 7-1, it is clear that the photoelectric effect predominates at low energy levels of gamma rays, but pair production increases at high energy levels. Of these three interactions, the amount of scintillation produced by the photoelectric effect is proportional to gamma-ray energy because all the energy of the gamma ray is given to the orbital electrons. The photomultiplier tube outputs an electrical charge in proportion to the amount of this scintillation, as a result, the output pulse height from the photomultiplier tube is essentially proportional to the incident radiation energy. Accordingly, a scintillation counter consisting of a scintillator and a photomultiplier tube provides accurate radiation energy distribution and its dose rate by measuring the photomultiplier tube output pulse height and count rate. To carry out energy analysis, the current output from the photomultiplier tube is converted into a voltage output by an integrating preamplifier and fed to a PHA (pulse height analyzer) for analyzing the pulse height.<sup>2)</sup> A typical block diagram for scintillation counting is shown in Figure 7-2.

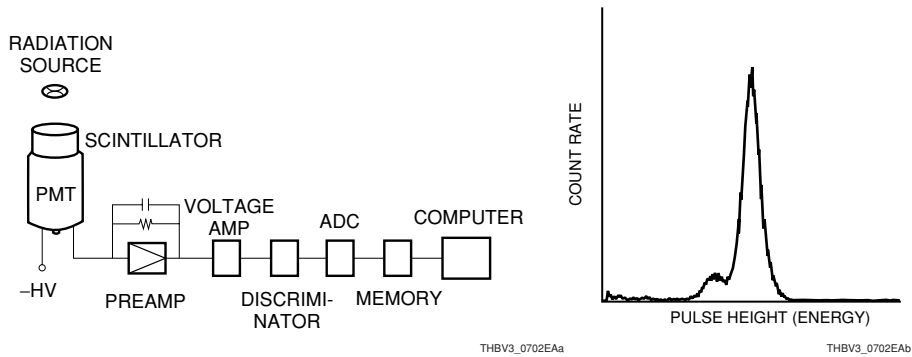


Figure 7-2: Block diagram for scintillation counting and pulse height distribution

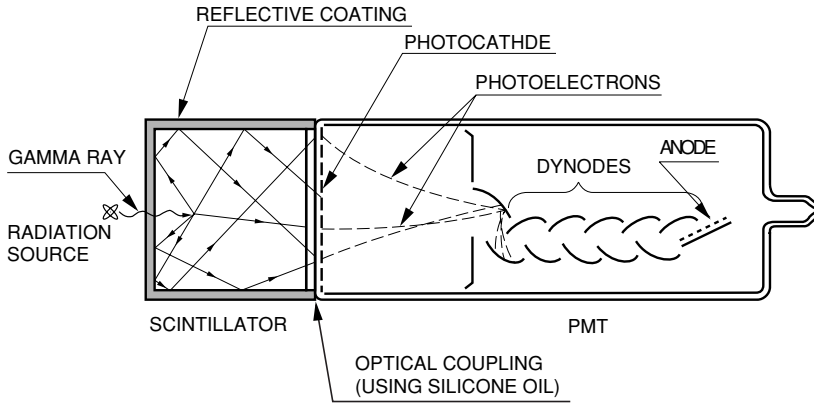
Scintillators are divided into inorganic scintillators and organic scintillators. Most inorganic scintillators are made of a halogen compound such as NaI(Tl), BGO, BaF<sub>2</sub>, CsI(Tl) and ZnS. Of these, the NaI(Tl) scintillator is most commonly used. These inorganic scintillators offer advantages of excellent energy conversion efficiency, high absorption efficiency and a good probability for the photoelectric effect compared to organic scintillators. Unfortunately, however, they are not easy to handle because of deliquescence and vulnerability to shock and impact. Recently, as an alternative for NaI(Tl) scintillators, YAP:Ce with high density and no deliquescence has been developed. Other scintillators such as LSO:Ce and GSO:Ce have also been developed for PET (Positron Emission Tomography) scanners.

Organic scintillators include plastic scintillators, liquid scintillators and anthracene of organic crystal. These scintillators display a short decay time and have no deliquescence. Plastic scintillators are easy to cut and shape, so they are available in various shapes including large sizes and special configurations. They are also easy to handle. In the detection of gamma rays, organic scintillators have a low absorption coefficient and exhibit less probability for the photoelectric effect, making them unsuitable for energy analysis applications. Table 7-1 shows typical characteristics and applications of major scintillators which have been developed up to the present.

Scintillators	Density (g/cm <sup>3</sup> )	Emission Intensity (NaI(Tl) normalized at 100)	Emission Time (ns)	Peak Emission Wavelength (nm)	Applications
NaI(Tl)	3.67	100	230	410	Surveymeter, area monitor, gamma camera
BGO	7.13	15	300	480	PET
CsI(Tl)	4.51	45 to 50	1000	530	Surveymeter, area monitor
Pure CsI	4.51	<10	10	310	High energy physics
BaF <sub>2</sub>	4.88	20	0.9/630	220/325	TOF, PET, high energy physics
GSO:Ce	6.71	20	30	310/430	Area monitor, PET
Plastic	1.03	25	2	400	Area monitor, neutron detection
LSO:Ce	7.35	70	40	420	PET
PWO	8.28	0.7	15	470	High energy physics
YAP:Ce	5.55	40	30	380	Surveymeter, compact gamma camera

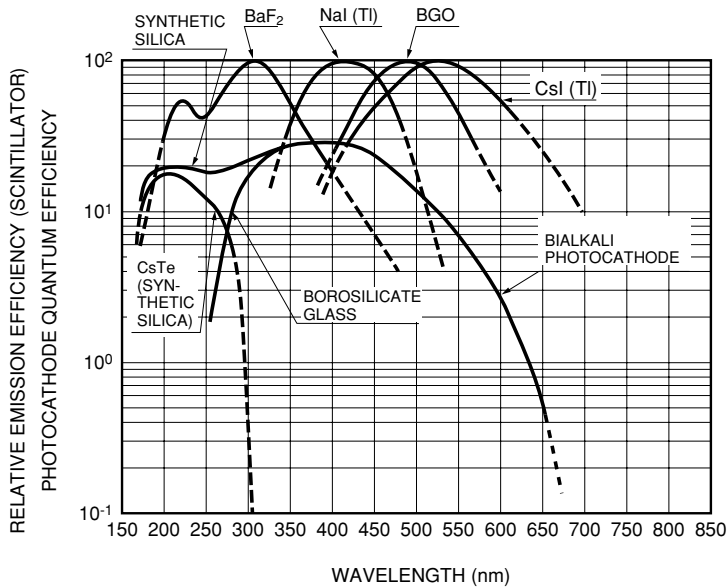
Table 7-1: Typical characteristics and applications of scintillators

A scintillator is attached to a photomultiplier tube with coupling material as shown in Figure 7-3. The coupling material is used in place of an air layer in order to minimize optical loss between the scintillator and the photocathode faceplate. Silicone oil having an index of refraction close to that of the glass faceplate is most widely used as a coupling material. However, selecting the proper material which provides good transmittance over the emission spectrum of the scintillator is necessary. Figure 7-4 indicates typical emission spectra of major scintillators and photocathode spectral responses of photomultiplier tubes.



THBV3\_0703EA

Figure 7-3: Gamma-ray detection using a NaI(Tl) scintillator and a photomultiplier tube



THBV3\_0704EA

Figure 7-4: Photocathode quantum efficiency and emission spectra of major scintillators



## 7.2 Characteristics

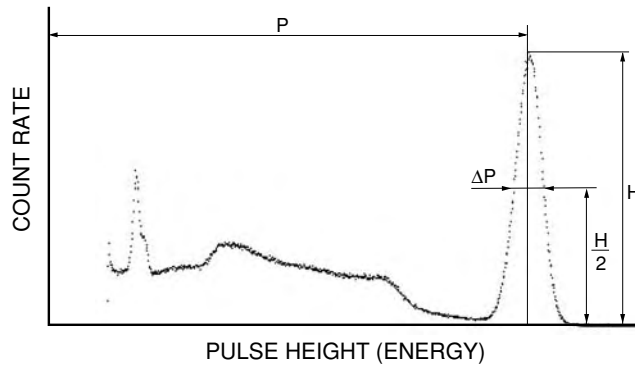
### (1) Energy resolution

There are two measurement methods in scintillation counting. One is the spectrum method that use a pulse height analyzer to measure an energy spectrum. The other is the counting method (described later on) that does not use a pulse height analyzer. In the spectrum method, pulse height discrimination is very important to determine photoelectric peaks produced by various types of radiation. This is evaluated as "energy resolution" or "pulse height resolution (PHR)".

Energy resolution is defined by the following equation using Figure 7-5. It is generally expressed as a percent:

$$R = \frac{\Delta P}{P} \dots\dots\dots \text{(Eq. 7-1)}$$

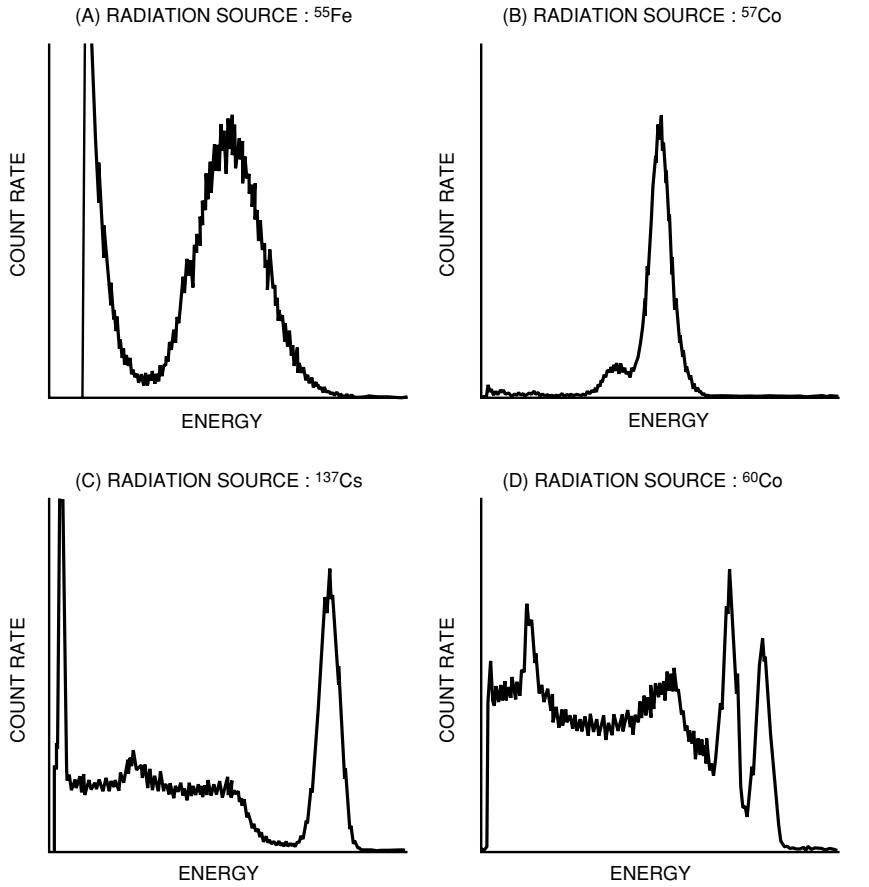
- R : energy resolution  
 P : peak value  
 $\Delta P$  : FWHM (Full width at half maximum)



THBV3\_0705EA

**Figure 7-5: Definition of energy resolution**

Figure 7-6 shows typical pulse height distributions for characteristic X-rays of  $^{55}\text{Fe}$  and various kinds of gamma rays ( $^{57}\text{Co}$ ,  $^{137}\text{Cs}$ ,  $^{60}\text{Co}$ ) detected by a photomultiplier tube coupled to an NaI(Tl) scintillator (measured using the same method as in Figure 7-2).



THBV3\_0706EA

**Figure 7-6: Typical pulse height distributions**

The following factors affect the energy resolution.

- (1) Energy conversion efficiency of the scintillator
- (2) Intrinsic energy resolution of the scintillator
- (3) Light collection efficiency of the photomultiplier tube photocathode
- (4) Quantum efficiency ( $\eta$ ) of the photomultiplier tube photocathode
- (5) Collection efficiency ( $\alpha$ ) at first dynode
- (6) Fluctuations in the multiplier section of photomultiplier tube

Generally, energy resolution is given by

$$R^2(E) = R_s^2(E) + R_p^2(E) \quad \text{..... (Eq. 7-2)}$$

where

$$R_p^2(E) = \frac{5.56}{N\eta\alpha} \left( \frac{\delta}{\delta-1} \right) \quad \text{..... (Eq. 7-3)}$$

in which  $N$  is the average number of photons incident on the photocathode per unit disintegration,  $\eta$  is the quantum efficiency,  $\alpha$  is the collection efficiency and  $\sigma$  is the secondary emission yield at each dynode (assumed to be constant here).

In the above equations,  $R_s(E)$  is the energy resolution of the scintillator and  $R_p(E)$  is that of the photomultiplier tube, both of which depend on the energy ( $E$ ) of the incident gamma ray.  $R_p^2(E)$  is inversely proportional to  $E$ .

When a 2-inch diameter by 2-inch length NaI(Tl) scintillator and a 2-inch diameter photomultiplier tube (Hamamatsu R6231) are used,  $R$ ,  $R_s$  and  $R_p$  will be approximately as follows:

With  $E = 122 \text{ keV}$  ( $^{57}\text{Co}$ ),  $R = 8.5 \%$ ,  $R_s = 6 \%$ ,  $R_p = 6\%$

With  $E = 662 \text{ keV}$  ( $^{137}\text{Cs}$ ),  $R = 6.5 \%$ ,  $R_s = 5.5 \%$ ,  $R_p = 3.4 \%$

To obtain higher energy resolution, the photomultiplier tubes must have high quantum efficiency and collection efficiency. Along with using a scintillator with high conversion efficiency and good inherent energy resolution, good optical coupling between the scintillator and the photomultiplier tube should be provided to reduce optical loss. For this purpose, as mentioned previously it is helpful to couple the scintillator and the photomultiplier tube using silicone oil having an index of refraction close to that of the faceplate of the photomultiplier tube.

When the scintillator is sufficiently thick, the intensity distribution of light entering the photomultiplier tube is always constant over the photocathode regardless of the radiation input position, so the photomultiplier tube uniformity has little effect on the energy resolution. However, if the scintillator is thin, the distribution of light flash from the scintillator varies with the radiation input position. This may affect the energy resolution depending on the photomultiplier tube uniformity. To avoid this problem, a light-guide is sometimes placed between the scintillator and the photomultiplier tube so that the light flash from the scintillator is diffused and allowed to enter uniformly over the photocathode. But this technique is not necessary when using a photomultiplier tube with normal uniformity.

$\gamma$ -ray source	Energy (keV)	NaI(Tl) + PMT	BGO + PMT
$^{55}\text{Fe}$	5.9	40 to 50%	—
$^{241}\text{Am}$	59.5	12 to 15%	70 to 150%
$^{57}\text{Co}$	122	8.5 to 10%	35 to 50%
$^{22}\text{Na}$	511	7.5 to 9.0%	13 to 25%
$^{137}\text{Cs}$	662	6.5 to 8.5%	11 to 20%
$^{60}\text{Co}$	1,170	5 to 6.5%	8.5 to 11%
	1,330	4.5 to 5.5%	8.0 to 9.5%

**Table 7-2: Energy resolution for typical gamma-rays, obtained with NaI(Tl) or BGO scintillator**

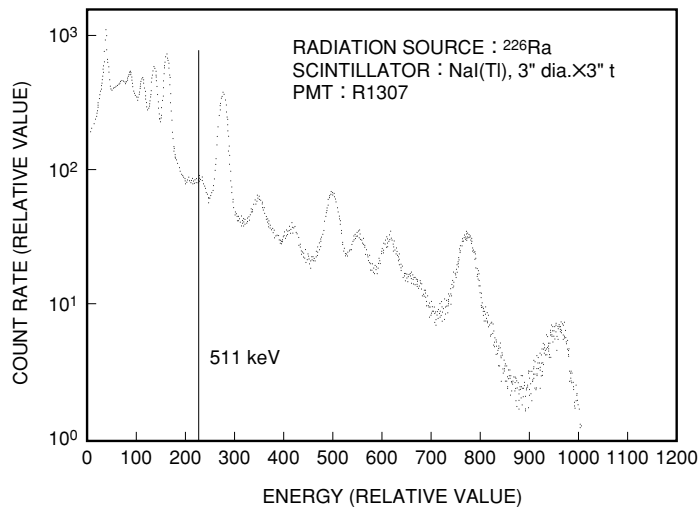
Energy resolution is one of the most important characteristics in radiation measurement such as gamma cameras and spectrometers. Photomultiplier tubes used in these applications are usually tested for energy resolution. Table 7-2 summarizes energy resolution for typical gamma rays measured with a NaI(Tl)/photomultiplier tube or a BGO/photomultiplier tube combination device. As shown in the table, each data has a certain width in energy resolution. This is due to the non-uniformity of the physical size of the scintillator or photomultiplier tube and also the performance variations between individual photomultiplier tubes. If necessary, it is possible to select only those photomultiplier tubes that meet specific specifications.

## (2) Relative pulse height

In scintillation counting, when a photomultiplier tube is operated at a constant supply voltage and the amplification factor of the measuring circuit is fixed, the variation of the pulse height at a photoelectric peak is referred to as the relative pulse height (RPH) and is commonly stated in terms of the channel number. This relative pulse height indicates the variation of the pulse height obtained with a photomultiplier tube in scintillation counting. It usually shows a good correlation with measurement data taken by users (instrument manufacturers) and is therefore used to select the gain range of photomultiplier tubes. When used with a NaI(Tl) scintillator, the relative pulse height provides a close correlation with blue sensitivity because the emission spectrum of the NaI(Tl) resembles the spectral transmittance of the Corning filter CS No.5-58 which is used for the blue sensitivity measurement, so the relative pulse height has a strong correlation with the anode blue sensitivity index. (Refer to 4.1.5 in Chapter 4.)

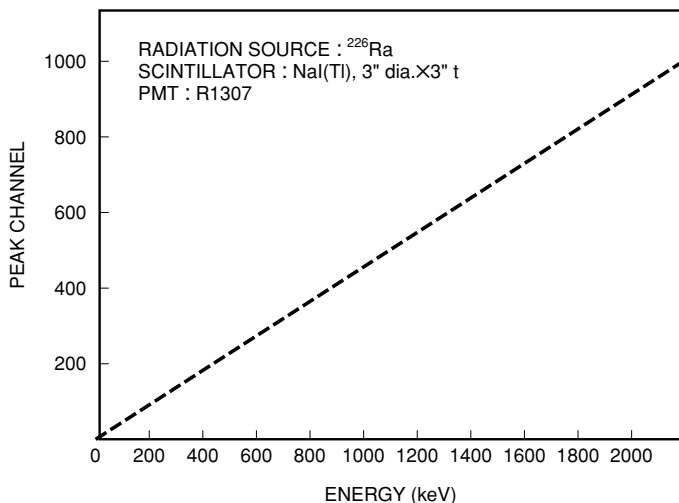
## (3) Linearity

Linearity of the output pulse height of a photomultiplier tube with respect to the amount of scintillation flash is another important parameter to discuss. Since linearity of general-purpose photomultiplier tubes has already been described earlier, this section explains how to measure linearity related to scintillation counting. Figure 7-7 shows a typical pulse height distribution for the  $^{226}\text{Ra}$  taken with a NaI(Tl) and Figure 7-8 indicates the relationship between each peak channel and the gamma-ray energy. Because  $^{226}\text{Ra}$  releases various kinds of radiation ranging in energy from 10.8 keV to 2.2 MeV, it is used for linearity measurements over a wide energy range.



THBV3\_0707EA

Figure 7-7: Pulse height distribution for  $^{226}\text{Ra}$  taken with NaI(Tl)



THBV3\_0708EA

**Figure 7-8: Relation between peak channel and gamma-ray energy**

Amount of emission from a NaI(Tl) scintillator equals about 30 photons per 1 keV of gamma-ray energy. Accordingly, some 20,000 photons ( $662 \text{ keV} \times 30$ ) are generated with  $^{137}\text{Cs}$  and some 40,000 photons ( $1330 \text{ keV} \times 30$ ) are generated with  $^{60}\text{Co}$ . When  $^{60}\text{Co}$  is used for linearity measurements under the conditions that the photomultiplier tube gain is at  $10^6$  and the decay constant ( $\tau$  s) of the NaI(Tl) scintillator is 230 nanoseconds, the photomultiplier tube output current ( $I_p$ ) is given by

$$\begin{aligned}
 I_p &= \frac{N \times \eta \times \alpha \times \mu \times e}{\tau s} \dots\dots\dots (\text{Eq. 7-4}) \\
 &= \frac{4 \times 10^4 \times 0.25 \times 0.9 \times 10^6 \times 1.6 \times 10^{-19}}{230 \times 10^{-9}} \\
 &= 6.3 \times 10^{-3} (\text{A})
 \end{aligned}$$

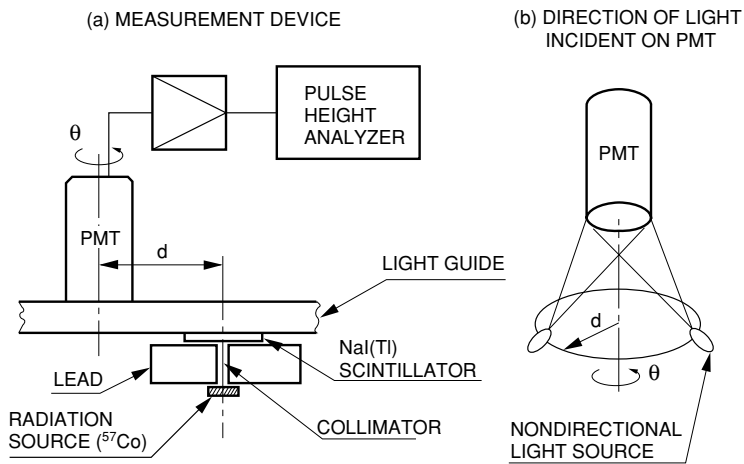
- N : amount of light flash per event produced from scintillator
- $\eta$  : quantum efficiency of photocathode (assumed to be 25 %)
- $\alpha$  : collection efficiency of photomultiplier tube (assumed to be 90 %)
- $\mu$  : gain of photomultiplier tube
- e : electron charge
- $\tau s$  : decay time of NaI(Tl)

Thus in this measurement the photomultiplier tube must have a pulse linearity over 6.3 milliamperes. In particular, care should be taken with respect to the linearity range when measuring radiation at higher energy levels as the photomultiplier tube detects a large amount of light flash.

**(4) Uniformity**

The uniformity of a photomultiplier tube affects the performance of systems utilizing scintillation counting, especially in such equipment as Anger cameras used to detect the incident position of radiation. Uniformity of a photomultiplier tube is commonly defined as the variation in the output current with respect to the photocathode position on which a light spot is scanned.

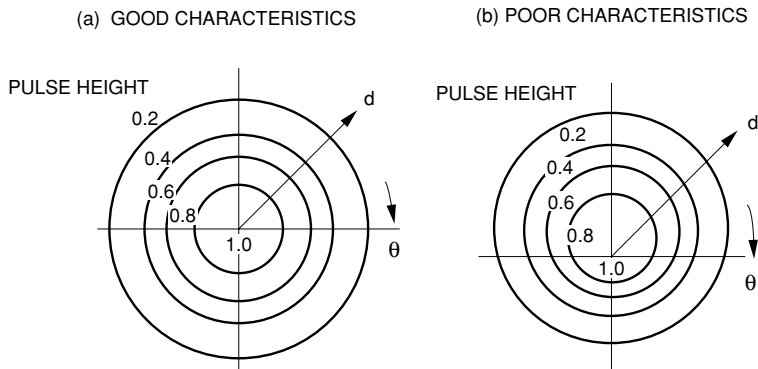
However, another evaluation method like that illustrated in Figure 7-9 provides more useful data which allows users to predict the direct effects of uniformity on the equipment.



THBV3\_0709EA

**Figure 7-9: Measurement method for azimuth uniformity**

In Figure 7-9, the photomultiplier tube is set at a distance ( $d$ ) from a light source. The output variations of the photomultiplier tube are measured while the light source is rotated around the tube (by changing angle  $\theta$ ). The same procedure is repeated at different values of  $d$ . Then plotting the positions ( $d, \theta$ ) of the light source providing equal output gives a graph similar to a contour map (Figure 7-10). Uniformity data evaluated by this method is called the azimuth uniformity.



THBV3\_0710EA

**Figure 7-10: Examples of azimuth uniformity data**

## (5) Stability

There are two types of stability tests used in scintillation counting: long term stability and short term stability. Both stability tests employ a  $^{137}\text{Cs}$  radiation source and a NaI(Tl) scintillator. The variation in the photopeak obtained from a photomultiplier tube is measured with a pulse height analyzer (PHA). These stability tests differ slightly from those applied to the general-purpose photomultiplier tubes which were discussed in the previous section.

### a) Long term stability

The long term stability is also referred to as the photopeak drift. In this stability test, the photomultiplier tube is allowed to warm up for one hour with the photopeak count rate maintained at  $1 \text{ ks}^{-1}$ . After this, the variation rate of the photopeak pulse height (channel number) is measured for a period of 16 hours.

The same measurement setup shown in Figure 7-2 is used and the variation occurring in the peak channel is recorded as the time elapses. This variation ( $D_{\text{LTD}}$ ) is calculated by Eq. 7-5 and typical variation data is shown in Figure 7-11 below.

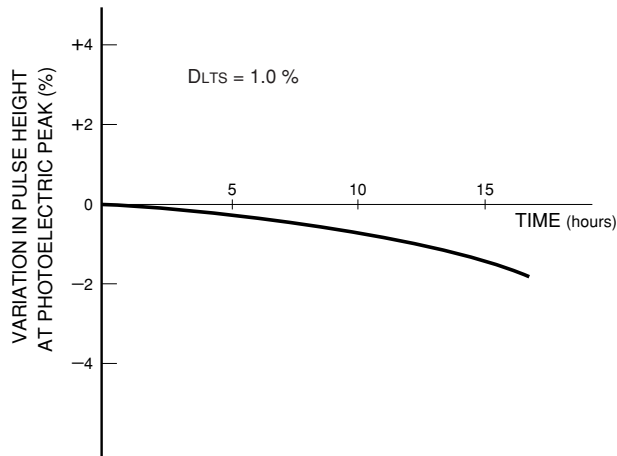
$$D_{\text{LTS}} = \frac{\sum_{i=1}^n |P_i - \bar{P}|}{n} \cdot \frac{100}{\bar{P}} \dots\dots\dots (\text{Eq. 7-5})$$

where

$\bar{P}$  : mean value of photopeak pulse height (channel)

$P_i$ : peak pulse height at the  $i$ -th reading

$n$  : total number of readings for 16 hours



THBV3\_0711EA

Figure 7-11: Typical long-term stability of photomultiplier tube

There are a few photomultiplier tube types that exhibit somewhat of a tendency to increase variation in photopeak pulse height during the period of 16 hours. However, most photomultiplier tubes tend to show decreasing values, with a variation rate within plus or minus several percent. This tendency is analogous to the drift characteristic explained earlier, but this test method is more practical for scintillation applications. Numerically, as shown in Eq. 7-5, the long term stability is defined as the mean deviation of the peak pulse height (or mean gain deviation) with respect to the mean pulse height. It usually has a value of 1 or 2 percent. A major cause of this output variation is that the secondary electron multiplication factor of the dynodes (particularly at the latter stages) changes over time.

### b) Short term stability

The short term stability is also referred to as the count rate stability or count rate dependence. To evaluate this stability, the variation in the photopeak pulse height is measured by changing the photopeak count rate from  $10 \text{ ks}^{-1}$  to  $1 \text{ ks}^{-1}$ . If the photopeak pulse height at a count rate of  $10 \text{ ks}^{-1}$  is given by A and that at  $1 \text{ ks}^{-1}$  by B, the variation ( $D_{\text{STS}}$ ) is given by the following equation. This value is expected to be about  $\pm 1$  percent.

$$D_{\text{STS}} = \left(1 - \frac{B}{A}\right) \times 100 (\%) \dots\dots\dots (\text{Eq. 7-6})$$

It is thought that this output instability is caused mainly by a change of the electron trajectories occurring in the electron multiplier section of a photomultiplier tube. This instability is also caused by a change in the voltage applied to the latter-stage dynodes, which may occur when operated at a high count rate and the output current increases to near the voltage-divider current. (Refer to 5.2.3 in Chapter 5.) In this case, photomultiplier tubes whose gain is less dependent on voltage (the slope of gain-voltage curve is not sharp) are less affected by the dynode voltage change. Short term stability is also closely related to the hysteresis effect in photomultiplier tubes. (Refer to 4.3.5 in Chapter 4.)

## (6) Noise

In scintillation counting, a signal pulse is usually produced by multiple photoelectrons simultaneously emitted from the photocathode, which create a higher pulse height than most dark current pulses do. Using a discriminator effectively eliminates most dark current pulses with lower amplitudes. Accordingly, only noise pulses with higher amplitudes will be a problem in scintillation counting. To remove this type of noise pulse, the coincident counting technique is commonly used.

Noise pulses with higher amplitudes may be caused by radiation released from natural radioactive elements contained in a reinforced concrete building or in the atmosphere. These noise pulses may be a significant problem, particularly in low-level-radiation measurements. Concrete used to construct a building usually contains Rn, Th and  $^{40}\text{Fe}$ , and steel contains U, Th and  $^{60}\text{Co}$ . Radioactive floating dust and Rn or Th gases may be present in the atmosphere, and a scintillator may also contain minute amounts of  $^{40}\text{K}$  and  $^{208}\text{Tl}$ . Furthermore, borosilicate glass used to fabricate the faceplate of photomultiplier tubes contains potassium of which  $^{40}\text{K}$  comprises 0.118 percent. The  $^{40}\text{K}$  releases gamma rays of 1.46 MeV which can also be a cause of high-amplitude noise pulses.

Figure 7-12 shows background noise data measured with a Hamamatsu R877 photomultiplier tube (5-inch diameter, borosilicate glass, bialkali photocathode) coupled to a NaI(Tl) scintillator (5-inch diameter  $\times$  2-inch length). (1) in Figure 7-12 is measured without taking any countermeasures, while (2) is measured by shielding the tube with two lead blocks of 100 and 50 millimeter thickness, each being placed respectively in the lower section and upper section. (3) is data taken with an R877-01 that employs a so-called K-free glass containing a very minute amount of potassium for its faceplate and side bulb envelope.

Since these measurements were made using the setup in which the peak of  $^{137}\text{Cs}$  (662 keV) becomes 300 channels, the energy range measured covers from about several keV to 2.2 MeV. In this energy range,



the background noise, which is as high as  $470 \text{ s}^{-1}$  during normal measurement, can be drastically reduced to  $26 \text{ s}^{-1}$  (about 1/20) by shielding the tube with lead blocks. This means that most background noise originate from environmental radiation. In addition, use of the R877-01 with K-free glass (refer to 4.1.2 Chapter 4) further reduces the total noise counts down to about  $16 \text{ s}^{-1}$ . Particularly, in the energy range from 1.2 to 1.6 MeV where noise count mainly results from the  $^{40}\text{K}$  (1.46 MeV), the noise count of  $3.3 \text{ s}^{-1}$  measured with the R877 (normal borosilicate glass) is reduced to  $0.9 \text{ s}^{-1}$  (below 1/3) with the R877-01 (K-free glass).

Recently in high energy physics experiments, there is a demand for photomultiplier tubes using materials that contain extremely low levels of radioactive impurities. Such experiments are often performed deep underground where natural radioactive impurities are eliminated and therefore impose heavy demands on the photomultiplier tubes to be used there. Glass materials used for these photomultiplier tubes must be investigated to make sure the content of radioactive impurities, not only  $^{40}\text{K}$  but also uranium and thorium series, is sufficiently low.

The external parts of a photomultiplier tube and the scintillator are usually maintained at ground potential. Therefore, a cathode ground scheme with the high voltage applied to the anode is often used in scintillation counting. (Refer to 5.1.2 in Chapter 5.)

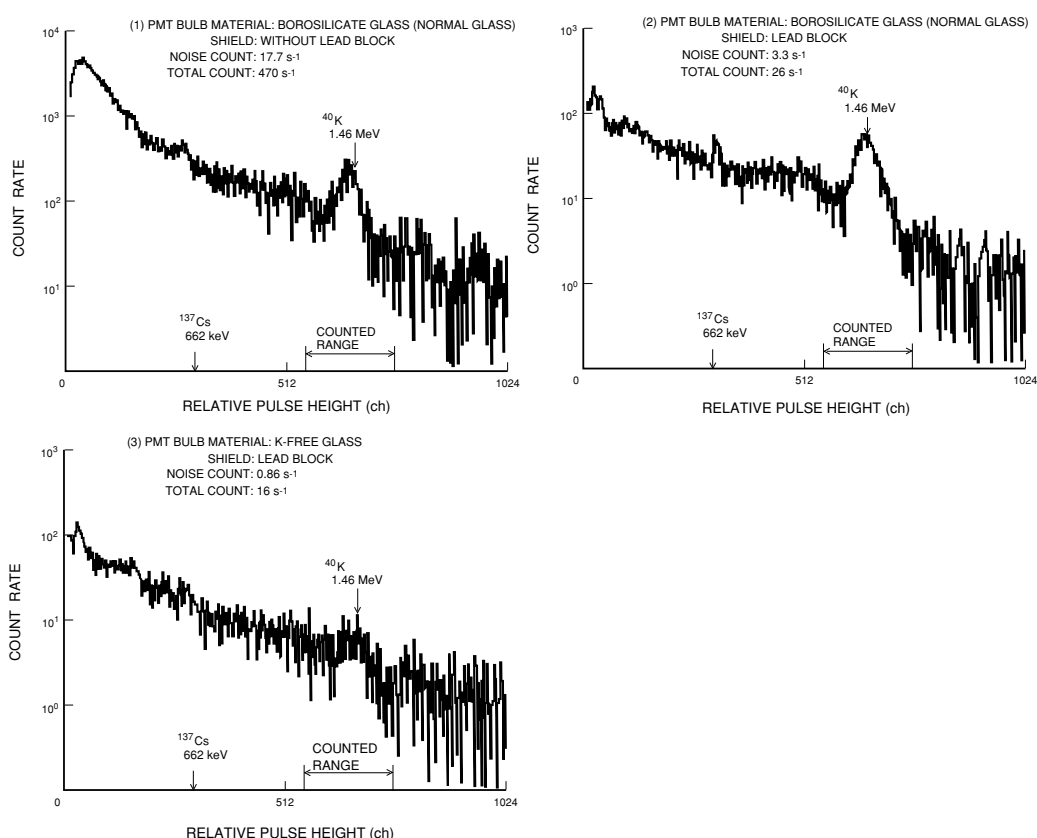
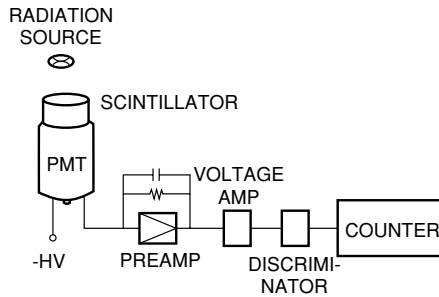


Figure 7-12: Background noise of 5-inch photomultiplier tube + NaI(Tl)

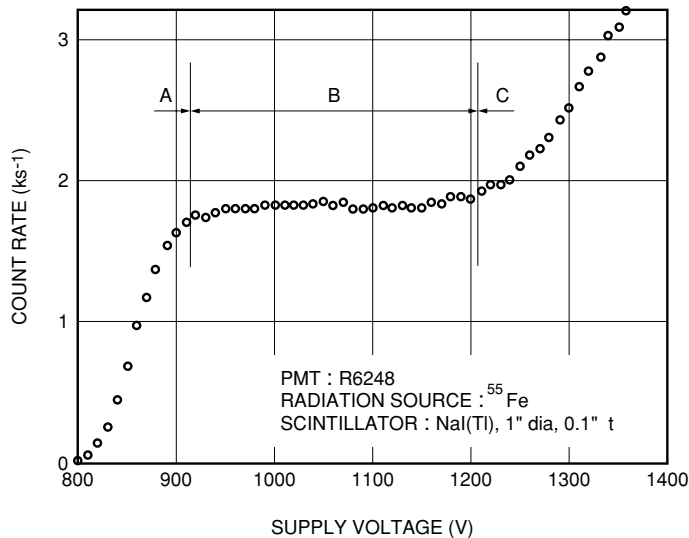
## (7) Plateau characteristic

As stated, there are two measurement methods in scintillation counting. One method called the spectrum method that uses a pulse height analyzer has already been explained. This section will describe the other method called the counting method that does not use a pulse height analyzer. In the counting method, plateau characteristics are very important. Plateau characteristics are measured by setting a discrimination level and counting all pulses with amplitudes greater than that level. This operation is done while changing the supply voltage for the photomultiplier tube. Figure 7-13 (a) shows a block diagram for plateau characteristic measurement. Figures 7-13 (b) and (c) show typical plateau characteristics and pulse height distribution when a NaI(Tl) scintillator and  $^{55}\text{Fe}$  radiation source are used.



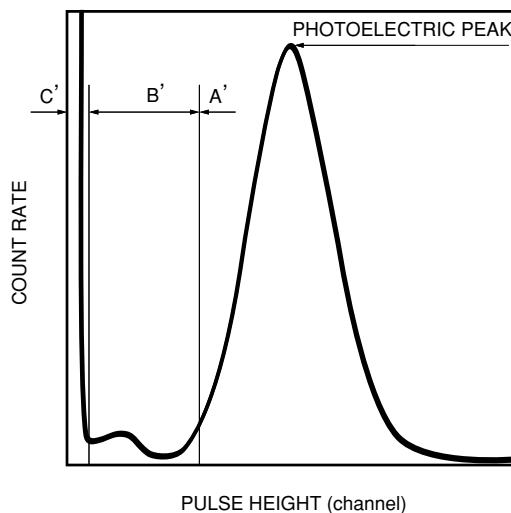
THBV3\_0713EAa

Figure 7-13 (a): Block diagram for plateau characteristic measurement



THBV3\_0713EAb

Figure 7-13 (b): Example of plateau characteristics

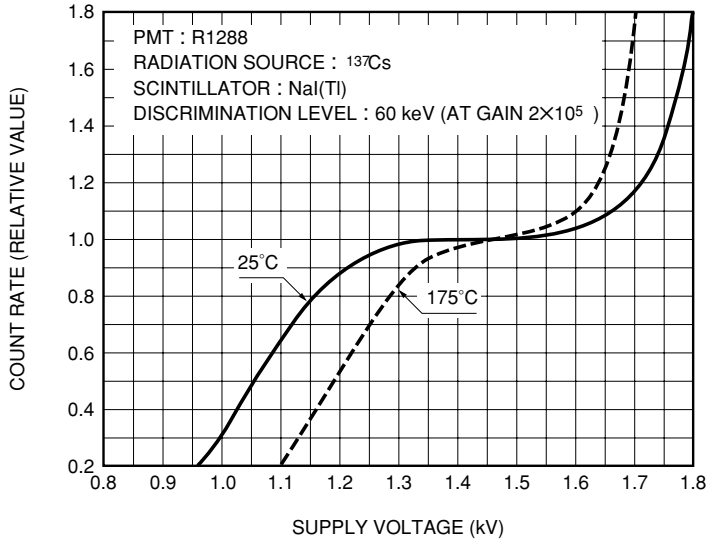


THBV3\_0713EA.c

**Figure 7-13 (c): Pulse height ( $^{55}\text{Fe}$  and NaI(Tl) combination)**

The photomultiplier tube supply voltage is increased while the discrimination level is kept constant, the output pulses are counted in order from the photopeak region to the valley and the dark current regions. Plotting the count rate versus the photomultiplier tube supply voltage gives a curve like that shown in Figure 7-13 (b). This data can be divided into three regions (A, B and C). Region B is referred to as the plateau, and the supply voltage should be set within this region. The count rate will not vary even if the supply voltage is changed within this region, showing a constant photopeak count rate. The wider the plateau region, the less the count rate will be affected by fluctuations in the dark current. This plateau region corresponds to the valley of a pulse height distribution, that is, region B' in Figure 7-13 (c). Photomultiplier tubes with better energy resolution and lower dark current pulses provide a wider region B'.

As an application example, plateau characteristics are widely employed to evaluate photomultiplier tubes designed for use in oil well logging (refer to 14.5 in Chapter 14). In this application, geological strata type and density are measured by detecting and analyzing the number of scattered radiations or natural radiations from strata. Photomultiplier tubes used for oil well logging (sometimes called "high-temperature photomultiplier tubes") are usually tested in combination with a  $^{137}\text{Cs}$  radiation source and a NaI(Tl) scintillator. Typical plateau characteristics obtained by this test are shown in Figure 7-14.



THBV3\_0714EA

**Figure 7-14: Typical plateau characteristics of a high-temperature photomultiplier tube**

In the measurement shown in Figure 7-14, a photomultiplier tube designed for high temperature operation is used. The plateau characteristic taken at 175°C is shown along with that obtained at 25°C. Because the gain of the photomultiplier tube decreases as the temperature increases, the supply voltage at which the signal appears (corresponding to region A in Figure 7-13 (b)) shifts to the higher voltage side. The dark current on the other hand increases with temperature, so its count rate sharply increases (corresponding to region C in Figure 7-13 (b)) at a low supply voltage. Consequently, the plateau width (supply voltage range) measured at a higher temperature (175°C) becomes narrower than that obtained at room temperatures (25°C).

## References in Chapter 7

- 1) Glenn. F. Knoll: "RADIATION DETECTION and MEASUREMENT (Third Edition)" John Wiley & Sons, Inc. (1999).
- 2) Nicholas Tsoulfanidis: "Measurement and Detection of Radiation", Hemispherev Publication Corporation (1983).
- 3) William J. Price: "Nuclear Radiation Detection", McGraw-Hill Book Company Inc. (1964).
- 4) Emil Kowalski: "Nuclear Electronics", Springer-Verlag Berlin (1970).
- 5) H. Kume, T. Watanabe, M. Iida, T. Matsushita and S. Suzuki: IEEE Trans. Nucl. Sci, NS-33[1], 364 (1986).
- 6) R.L. Heath, R. Hofstadter and E. B. Hughes: Nucl. Inst. and Meth, 162, 431 (1979).

# MEMO

# **CHAPTER 8**

## **PHOTOMULTIPLIER TUBE MODULES**

*This chapter describes the structure, usage, and characteristics of photomultiplier tube (PMT) modules. These PMT modules consist of a photomultiplier tube, a voltage-divider circuit and a high-voltage power supply circuit carefully assembled into the same package.*

## 8.1 What Are Photomultiplier Tube Modules?

Photomultiplier tube (PMT) modules are basically comprised of a photomultiplier tube, a high-voltage power supply circuit, and a voltage-divider circuit to distribute a voltage to each dynode. In addition to this basic configuration, various functions such as a signal conversion circuit, photon counting circuit, interface to the PC and cooling device are integrated into a single package. PMT modules eliminate troublesome wiring for high voltages and allow easy handling since they operate from a low external voltage. Figure 8-1 shows the functions of PMT modules.

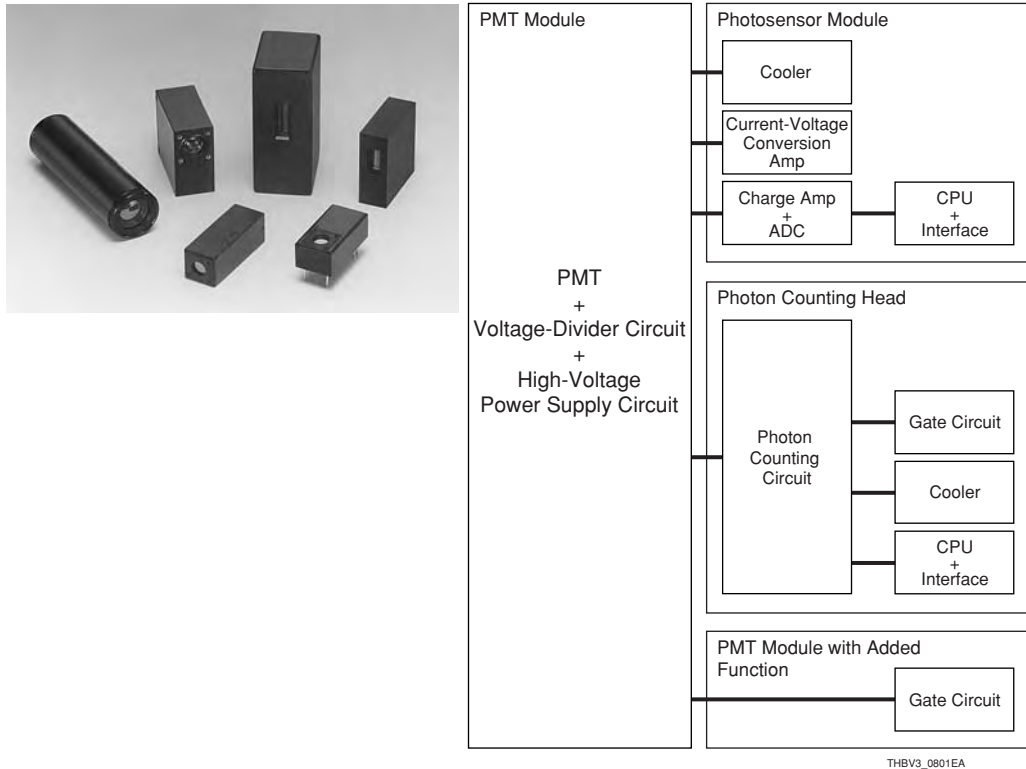


Figure 8-1: PMT module functions

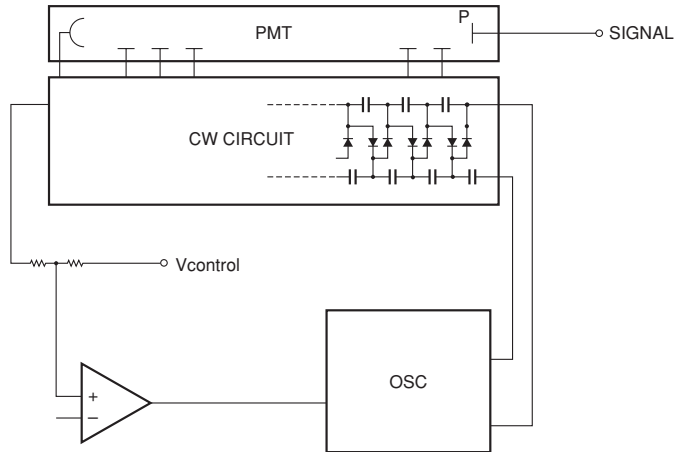
## 8.2 Characteristics of Power Supply Circuits

### (1) Power supply circuits

There are two major types of power supply circuits used in PMT modules. One is a Cockcroft-Walton (CW) circuit and the other is a combination of a Cockcroft-Walton circuit and active divider circuit.

The Cockcroft-Walton circuit is a voltage multiplier circuit using only capacitors and diodes. As shown in Figure 8-2, capacitors are arranged along each side of the alternate connection points of the serially connected diodes. The reference voltage supplied to this circuit are doubled, tripled ... and the boosted voltage is applied to each dynode. This circuit features low power consumption and good linearity for both DC and pulsed currents and is designed to be compact.

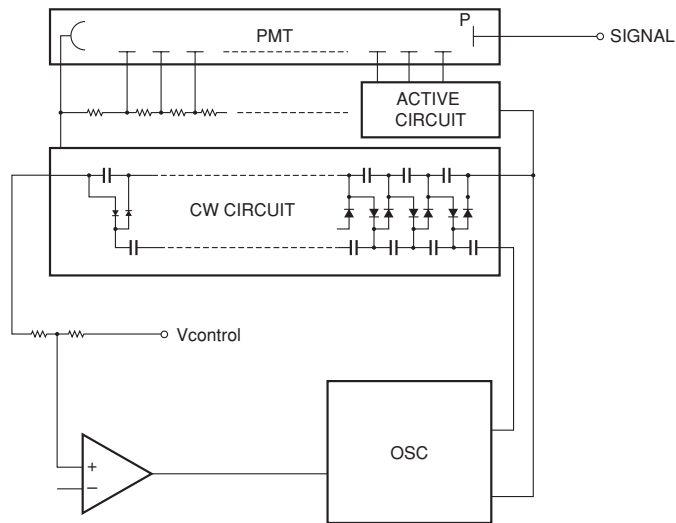




THBV3\_0802EA

**Figure 8-2: Cockcroft-Walton power supply circuit**

Figure 8-3 shows a power supply circuit using a Cockcroft-Walton circuit combined with an active divider circuit. The Cockcroft-Walton circuit generates a voltage that is applied to the entire photomultiplier tube and the active divider circuit applies a voltage to each dynode. In this active divider circuit, several voltage-divider resistors near the last dynode stages are replaced with transistors. This eliminates the effect of the photomultiplier tube signal current on the interdynode voltage, achieving good linearity up to 60 % to 70 % of the divider circuit current. This circuit also features lower ripple and shorter settling time compared to power supply circuits using only a Cockcroft-Walton circuit.



THBV3\_0803EA

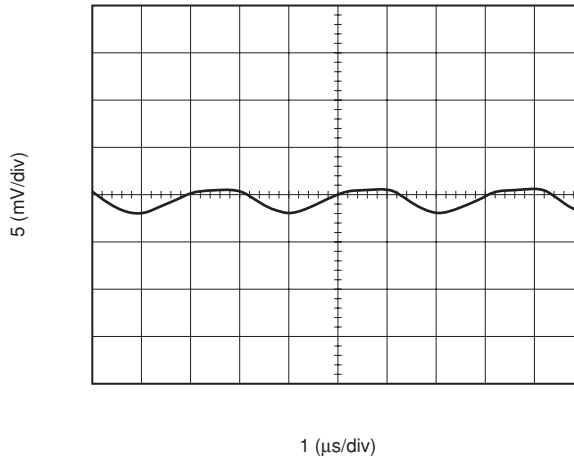
**Figure 8-3: Power supply circuit using Cockcroft-Walton circuit combined with active divider circuit**

## (2) Ripple noise

Since high-voltage power supplies in PMT modules use an oscillating circuit, the unwanted oscillation noise is usually coupled into the signal output by induction. This induction noise is called "ripple". This ripple can be observed on an oscilloscope by connecting the signal cable of a PMT module to the input of the oscilloscope while no light is incident on the PMT module. For example, under the conditions that the load resistance is  $1\text{ M}\Omega$ , load capacitance is  $22\text{ pF}$  and the coaxial cable length is  $45\text{ cm}$ , you will see a signal output along the baseline in a low voltage range. This signal output has an amplitude from a few hundred  $\mu\text{V}$  to about  $3\text{ mV}$  and a frequency bandwidth of about  $300\text{ kHz}$ . Figure 8-4 shows an example of this ripple noise.

Hamamatsu PMT modules are designed to minimize this ripple noise. However, it is not possible to completely eliminate this noise. Use the following methods to further reduce ripple noise.

1. Place a low-pass filter downstream from the PMT module signal output.
2. Raise the control voltage to increase the photomultiplier tube gain and lower the amplifier gain.

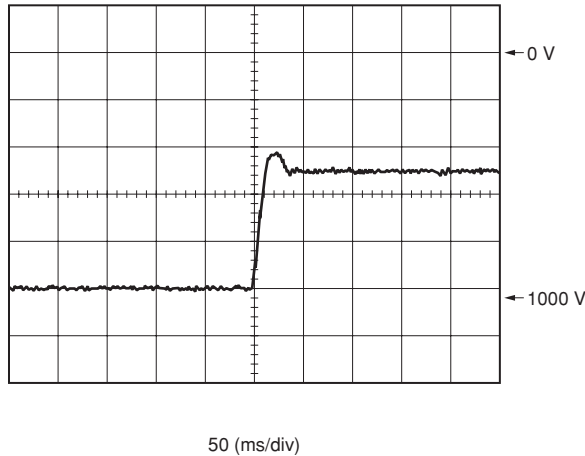


THEBV3\_0804EA

Figure 8-4: Ripple noise

## (3) Settling time

The high voltage applied to the photomultiplier tube changes as the input voltage for the PMT module control voltage is changed. However, this response has a slight delay versus changes in the control voltage. The time required for the high voltage to reach the target voltage is called the "settling time". This settling time is usually defined as the time required to reach the target high voltage when the control voltage is changed from  $+1.0\text{ V}$  to  $+0.5\text{ V}$ . Figure 8-5 shows a change in the high voltage applied to the cathode.



THBV3\_0805EA

Figure 8-5: Changes in cathode voltage when control voltage is changed from +1.0 V to +0.5 V

## 8.3 Current Output Type and Voltage Output Type

### (1) Connection method

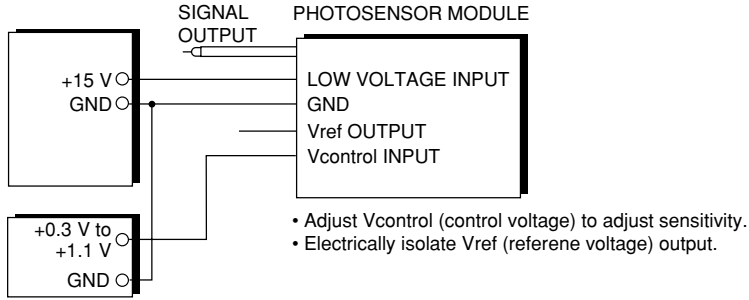
Since PMT modules have an internal high-voltage power supply and voltage divider circuit in their packages, there is no need to apply a high voltage from an external power supply. All that is needed is simple wiring and low voltage input as shown in the connection diagram. When using a typical PMT module, supply approximately 15 V to the low voltage input, ground the GND terminal, and connect the control voltage and reference voltage input according to the gain adjustment method.

When the low voltage input is within the range specified in our catalog, the high voltage applied to the photomultiplier tube from the power supply circuit in the PMT module is kept stable. This holds true even if the output of the low-voltage power supply fluctuates somewhat. However, if high noise pulses are generated from the low-voltage power supply, they may cause erroneous operation or a breakdown in the PMT module.

### (2) Gain adjustment

The photomultiplier tube gain can be adjusted by changing the control voltage. There are two methods for adjusting the control voltage.

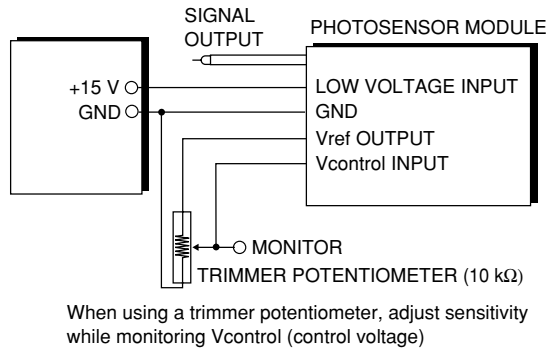
When directly inputting the control voltage as shown in Figure 8-6, the control voltage input range must always be below the maximum rating. The output terminal of the reference voltage must be left unconnected. Be careful not to connect it to ground.



THBV3\_0806EA

**Figure 8-6: Sensitivity adjustment by changing voltage**

Figure 8-7 shows a gain adjustment method using a trimmer potentiometer which is connected between the control voltage and reference voltage outputs. When adjusting the trimmer potentiometer, do so carefully and correctly while monitoring the control voltage with a voltmeter or tester.



THBV3\_0807EA

**Figure 8-7: Sensitivity adjustment using trimmer potentiometer**

### (3) Current output type module

In current output type PMT modules, the anode current of the photomultiplier tube is directly available as the output from the module. This current output from the photomultiplier tube must be converted to a voltage by an external signal processing circuit. An optimal current-to-voltage conversion method must be selected according to the application and measurement purpose.

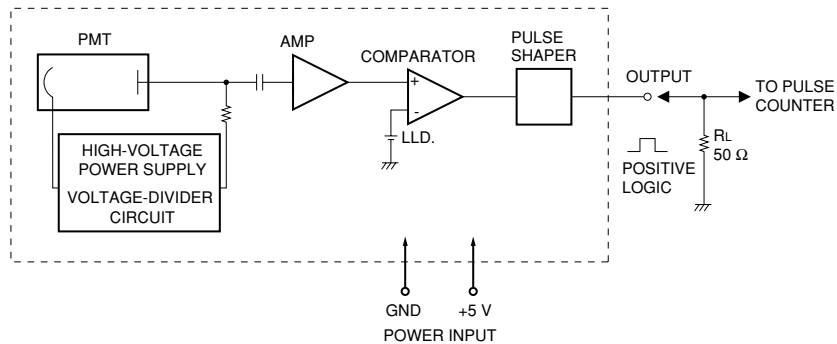
### (4) Voltage output type module

In voltage output type PMT modules, an op-amp is connected near the photomultiplier tube anode to convert the current to a voltage. This is more resistant to external noise than when extracting the current output of a photomultiplier tube by using a signal cable. Using an internal amplifier is especially effective in measurement frequencies ranging from several tens of kilohertz to a few megahertz where external noise effects first become noticeable. However, amplifier power consumption tends to increase in frequency bands higher than 10 MHz. Using an external amplifier connected to a current output type PMT module might be better in this case.

Voltage output type PMT modules incorporate an op-amp for current-to-voltage conversion. The amp's feedback resistor and capacitor also function as a charge amplifier, making it possible to perform pulse measurement such as scintillation counting.

## 8.4 Photon Counting Head

Photon counting heads contain a low level discriminator and pulse shaper along with a photomultiplier tube and a high-voltage power supply. Figure 8-8 shows the block diagram of a typical photon counting head. The current pulses from the photomultiplier tube are amplified by the amplifier, and then only those pulses higher than a certain threshold are discriminated by the comparator and converted to voltage pulses by the pulse shaper for output. In photon counting heads, the high voltage to be applied to the photomultiplier tube is preadjusted based on the plateau voltage measured prior to shipment. Supplying a low voltage from an external power supply is all that is needed for photon counting.



THBV3\_0808EA

Figure 8-8: Block diagram of photon counting head

### (1) Output characteristics

Each type of photon counting head is slightly different so that the internal circuit constants match the time characteristics and pulse waveforms of the photomultiplier tube being used. Because of this, output characteristics such as the pulse voltage and pulse width differ depending on individual photon counting heads, though their output is a positive logic signal.

The output impedance of photon counting heads is designed to be approximately 50 ohms in order to handle high-speed signals. When connecting a photon counting head to a measurement device with a cable, a 50-ohm impedance cable is preferable and the input impedance of the measurement device should be set to 50 ohms. If the input impedance of the external circuit is not around 50 ohms and an impedance mismatch occurs, the pulses reflected from the input end of the external circuit return to the photon counting head and then reflect back from there. This might result in erroneous counts. When the input impedance of the external circuit is 50 ohms, the amplitude of the signal voltage will be one-half that at the input end. So it is necessary to select an external circuit that matches the minimum input voltage specifications.

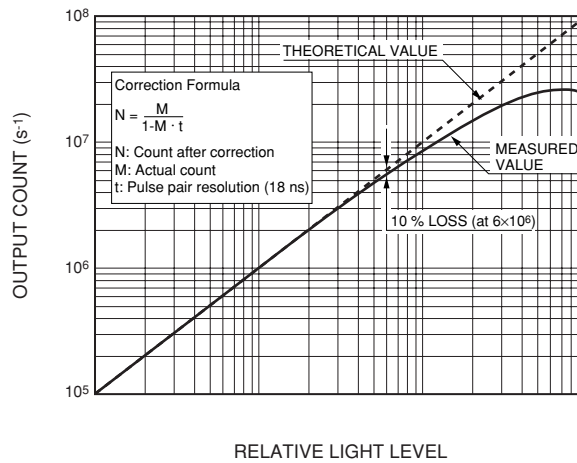
### (2) Counting sensitivity

Counting sensitivity indicates a count value obtained from a photon counting head when an absolute amount of light (pW) at a certain wavelength enters the photon counting head. Counting sensitivity is directly related to quantum efficiency and collection efficiency.

### (3) Count linearity

When individual photons enter at constant intervals within the time resolution of a photon counting head, it is theoretically possible to measure the photons up to the reciprocal of pulse-pair resolution. Photon counting is usually used in low-light-level measurements of chemiluminescence and bioluminescence, so the light input is a random event. In this case, when the light level is increased and exceeds a certain level, the count value becomes saturated and is no longer proportional to the light level. Count linearity is a measure for indicating the loss in the counted value compared to the theoretical value. This is defined as the count value at 10 % loss. The pulse-pair resolution of the internal circuit determines the count linearity characteristics of the photon counting head. At a higher count rate, however, time characteristics of the photomultiplier tube also become an important factor.

Figure 8-9 shows typical count linearity characteristics of a photon counting head with a pulse pair resolution of 18 ns. The count value at 10 % loss is  $6 \times 10^6 \text{ s}^{-1}$ .



THEBV3\_0809EA

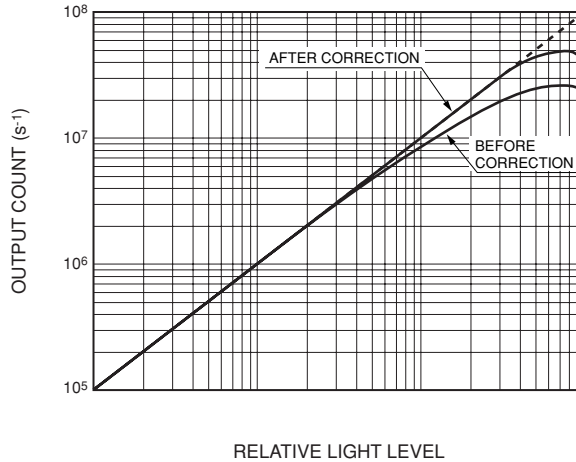
Figure 8-9: Count linearity characteristics

### (4) Improving the count linearity

When the count measured during photon counting exceeds  $10^6 \text{ s}^{-1}$ , the pulses begin to overlap causing counting errors. To increase the count linearity:

1. Increase the pulse-pair resolution of the circuit.
2. Use a prescaler to divide the frequency.
3. Approximate the output by using a correction formula.

Figure 8-10 shows the improvement in count linearity when the output is approximated by a correction formula.

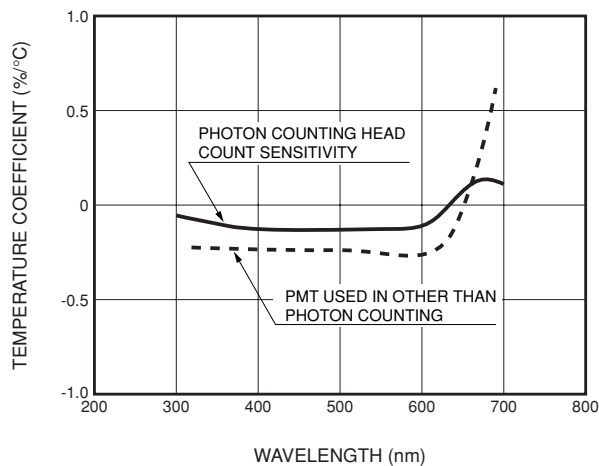


THBV3\_0810EA

Figure 8-10: Count linearity before and after correction

### (5) Temperature characteristics

Since the photon counting method uses a technique that measures pulses higher than a certain threshold value, it is less affected by gain variations in the photomultiplier tube caused by output instability of the power supply and changes in ambient temperature. Changes in the count value versus temperature variations are plotted in Figure 8-11. The rate of these changes is about one-half the anode output temperature coefficient of photomultiplier tubes.

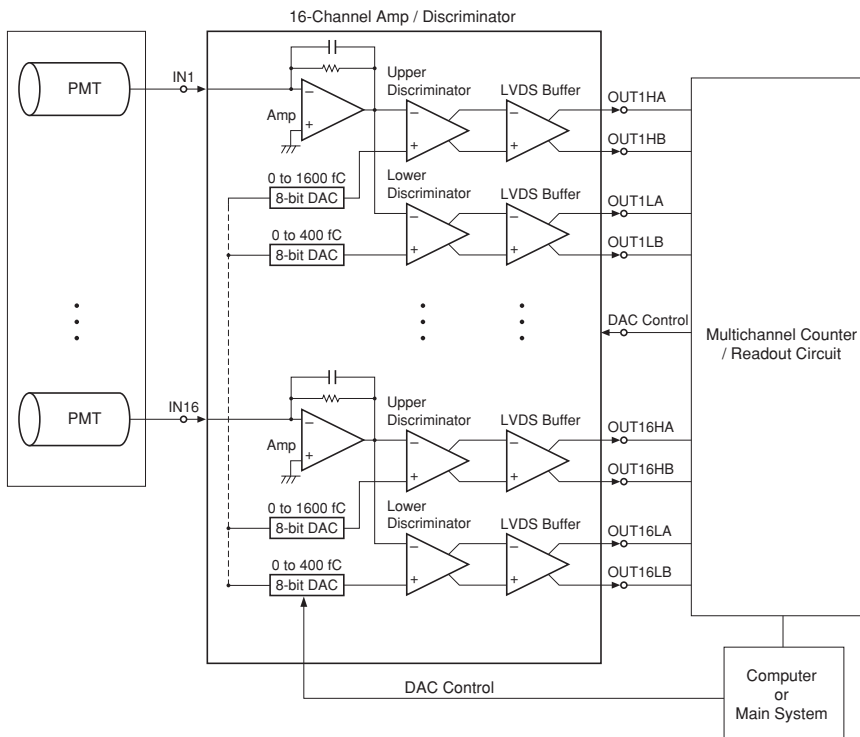


THBV3\_0811EA

Figure 8-11: Temperature coefficient comparison

### (6) Photon counting ASIC (Application Specific Integrated Circuit)

A photon counting circuit is fabricated using many components such as ICs and resistors. The capacitance and inductance of those components and wiring impose limits on the frequency band and power consumption of the circuit. The circuit board of course requires a space for mounting component. The photon counting ASIC is an integrated circuit consisting of 16 amplifiers, 16 discriminators and 16 pulse shaping circuits, which are the basic elements for photon counting circuits. This ASIC simultaneously performs parallel processing of input signals from a maximum of 16 photomultiplier tubes or from a 16-channel multianode photomultiplier tube, and outputs a LVDC voltage pulse according to each input. The block diagram of a photon counting ASIC is shown below in Figure 8-12. Integrating the circuit gives the ASIC a counting efficiency of  $1.0 \times 10^8 \text{ s}^{-1}$  or more per channel, low power consumption and a compact size. This ASIC is also designed to allow LLD and ULD adjustments by 8-bit DAC from external control, so that the gain difference between photomultiplier tubes and the gain fluctuation between the anodes of a multianode photomultiplier tube can be corrected. Furthermore, accurate measurement can be performed not only by single photon counting but also in multi photon events, by matching the photomultiplier tube gain with the input charge range of the ASIC. In this case, one voltage pulse of positive logic is output in response only to a pulse signal that enters within the LLD to ULD input range or a pulse signal higher than the LLD threshold level. This allows measurement for taking timings. However, the output does not contain pulse height information.



THBV3\_0812EA

Figure 8-12: Block diagram of photon counting ASIC



## 8.5 Gate Function

When excitation light such as from a laser or xenon flash lamp enters a photomultiplier tube, the signal processing circuit may become saturated causing adverse effects on the measurement. There is a method to block such excessive light by using a mechanical shutter but this method has problems such a limited mechanical shutter speed and service life. On the other hand, electronic gating, which is controlled by changing the electrical potential on a dynode in the photomultiplier tube, offers much higher speeds and higher extinction ratio. The H7680 is a gated PMT module using a linear focused type photomultiplier tube that features fast time response. The H7680 delivers a high extinction ratio and high-speed gating since it controls the bias voltage applied to multiple dynodes.

There are two modes of gating: a normally-off mode that turns on the gate of the photomultiplier tube when a gate signal is input and a normally-on mode that turns off the gate when a gate signal is input. Select the desired mode according to the application.

### (1) Gate noise

Performing high-speed gate operation requires high-speed gate pulses. When a gate pulse is input, induction noise is induced in the anode signal through the electrostatic capacitance present between the electrodes of the photomultiplier tube as shown in Figure 8-13. This is referred to as "gate noise". This gate noise can be reduced by reducing the gate pulse voltage or by using a noise-canceling technique. However, completely eliminating this noise is difficult. So increasing the photomultiplier tube gain or using a photomultiplier tube with a higher gain is required so that the signal output becomes larger than the gate noise.

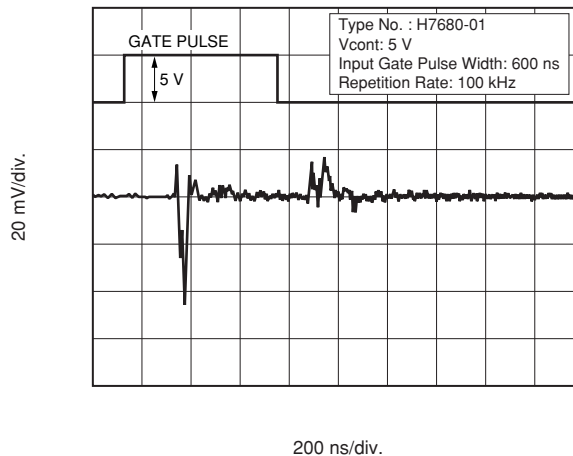


Figure 8-13: Gate noise

## (2) Extinction ratio

Gating allows suppressing the anode current of the photomultiplier tube even if the anode current exceeds the maximum rating or a strong light causing the external circuit to be saturated is input to the photomultiplier tube. The extinction ratio is the ratio of the output when the gate is "on" to the output when the gate is "off" while a constant light level is incident on the photomultiplier tube. For example, if the output at "gate-off" is 1 nA in normally-off mode, and the output at "gate-on" is 10  $\mu$ A, then the extinction ratio is expressed in  $1 \text{ nA} : 10 \text{ } \mu\text{A} = 1 : 10^4$ .

Even if the current is being controlled by gate operation, a small amount of current equal to the percentage of the extinction ratio flows as the anode current. The anode current must be kept below the maximum rating of the photomultiplier tube even during gate operation. If high energy light such as a laser beam enters the photomultiplier tube, the photocathode structure itself might be damaged even if gate operation is performed. So some measures must be taken to prevent strong light from entering the photomultiplier tube.

## 8.6 Built-in CPU and IF Type

This type of PMT module has an internal CPU and interface for connection to an external unit. In this module, the output current of the photomultiplier tube is converted to a voltage signal by a current-to-voltage conversion amplifier. The voltage signal is then converted to digital data, or in photon counting, the output pulses are counted within a certain time. Digital data can be easily transferred to an external processing unit, while the PMT module is controlled by commands from the external unit. Since the signal processing circuit, control CPU and interface for data transfer are housed in a single package, there is no need to design a digital circuit or take noise abatement measures usually required when handling high voltage and high-speed signals.

### (1) Photon counting type

This PMT module has an internal photon counting circuit followed by a 20-bit counter that counts voltage pulses. The 20-bit counter allows a maximum count of 1,048,575 within the gate time that was set. If the gate time is set long while the light level is relatively high, then the counter limits the measurement count to 1,048,575 or less. In this case, shorten the gate time and acquire the data several times. After measurements, software averaging of data acquired several times allows you to obtain the same result as obtained using a long gate time. Figure 8-14 shows the circuit block diagram of a photon counting type module.

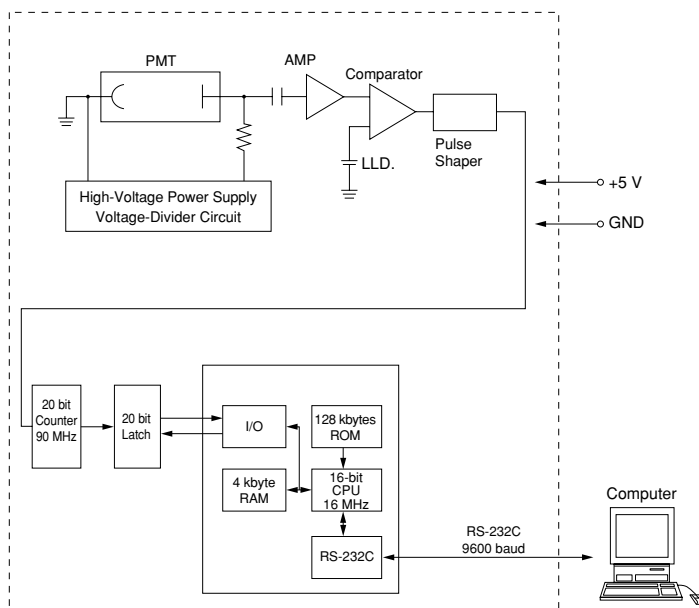
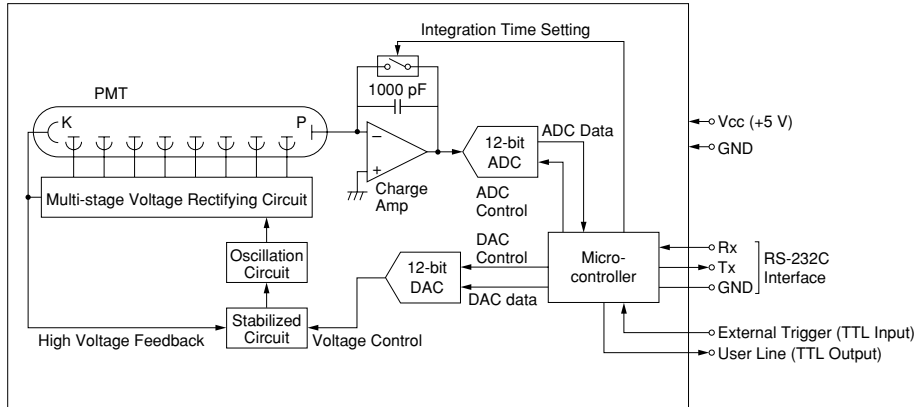


Figure 8-14: Block diagram of photon counting type module

## (2) Charge amplifier and AD converter type

Figure 8-15 shows the block diagram of a PMT module with an internal charge amplifier and AD converter. The anode of the photomultiplier tube is connected to the charge amplifier that accumulates charges obtained from the anode during a sampling time. The accumulated charge quantity is then converted to digital data by the AD converter.



THBV3\_0815EA

Figure 8-15: Block diagram of charge amplifier and AD converter type module

## References in Chapter 8

- 1) Hamamatsu Photonics Product Catalog: "Photomultiplier Tube Modules" (March, 2005)

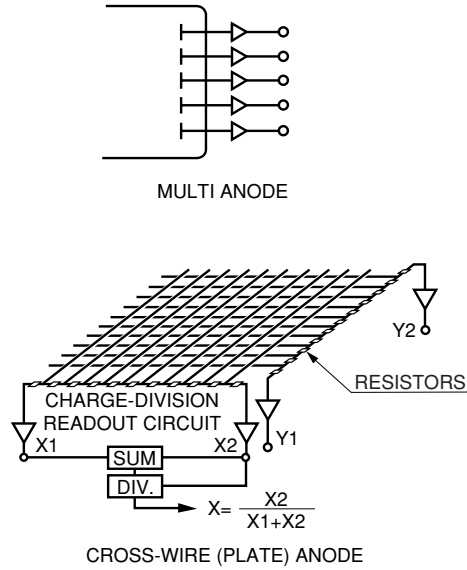
## **CHAPTER 9**

# **POSITION SENSITIVE PHOTOMULTIPLIER TUBES**

*The current multiplication mechanism offered by dynodes makes photomultiplier tubes ideal for low-light-level measurement. As explained earlier, there are various types of dynode structures available for different photometric purposes. Popular conventional dynode structures are the box-and-grid type, linear-focused type, circular-cage type and venetian-blind types. Furthermore, the MCP (microchannel plate) has recently been utilized as a dynode structure.*

*Two unique dynode structures are introduced in this chapter: the "metal channel dynode" and "grid type dynode". These dynode structures provide wide dynamic range, high gain, high position resolution, and are currently used in position-sensitive photomultiplier tubes.*

*Common methods for reading out the output signal from a position-sensitive photomultiplier tube are illustrated in Figure 9-1. In a multianode device, the output signal is read using independent multiple anodes. The cross-plate (wire) anode signal is read out by means of current or charge-dividing center-of-gravity detection.*



THEV3\_0901EA

**Figure 9-1: Anode output readout methods for position sensitive photomultiplier tubes**

*The following sections describe "metal channel dynode structures combined with multianode readout", "metal channel dynode structures combined with a cross-plate anode" and "grid type dynode structures combined with a cross-wire anode" for position sensitive photomultiplier tubes.*

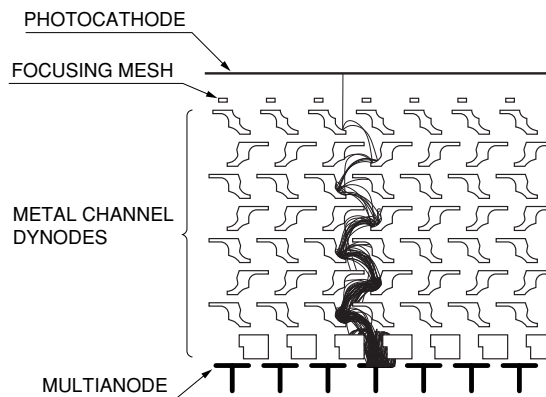
## 9.1 Multianode Photomultiplier Tubes

### 9.1.1 Metal channel dynode type multianode photomultiplier tubes

#### (1) Structure

Figure 9-2 shows the electrode structure for metal channel dynodes and the associated electron trajectories. Compared to the other types of dynodes, metal channel dynode type multianode photomultiplier tubes feature very low crosstalk during secondary electron multiplication. This is because the photoelectrons emitted from the photocathode are directed onto the first dynode by the focusing mesh and then flow to the second dynode, third dynode, . . . last dynode and finally to the anode, while being multiplied with a minimum spatial spread in the secondary electron flow.


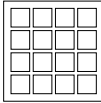
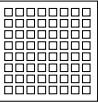
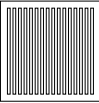
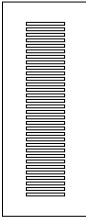
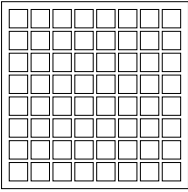
The overall tube length can be kept short because the metal channel dynodes are very thin and assembled in close-proximity to each other.



THBV3\_0902EA

Figure 9-2: Electrode structure and electron trajectories

Multianode photomultiplier tubes using metal channel dynodes can be roughly classified into two groups. One group uses a matrix type multianode and the other group uses a linear type multianode.

Type	Metal Channel Dynode Multianode Photomultiplier Tubes					
	Matrix			Linear		Matrix
	M4	M16	M64	L16	L32	M64
Anode Shape						
Number of Anodes	4	16	64	16	32	64
Pixel Size (mm)	9 × 9	4 × 4	2 × 2	0.8 × 16	0.8 × 7	5.8 × 5.8

THBV3\_0903EA

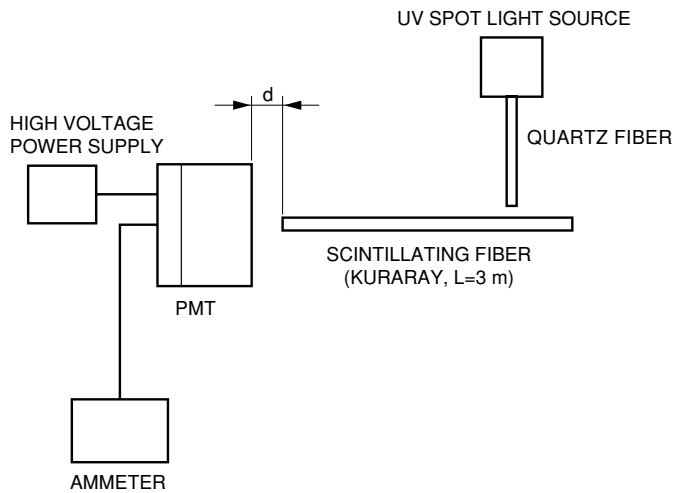
Figure 9-3: Anode patterns for metal channel dynode type multianode photomultiplier tubes

(2) Characteristics

In this section, we first describe basic characteristics of matrix type multianode photomultiplier tubes by discussing "crosstalk", "magnetic immunity" and "uniformity" in 64 channel matrix type multianodes.

"Crosstalk" is a measure to indicate how accurately the light (signal) incident on a certain position of the photocathode is detected while still retaining the position information. In photomultiplier tube operation, crosstalk is mainly caused by the broadening of the electron flow when light is converted into electrons and those electrons are multiplied by the dynode section. The incident light spread within the faceplate is another probable cause of crosstalk.

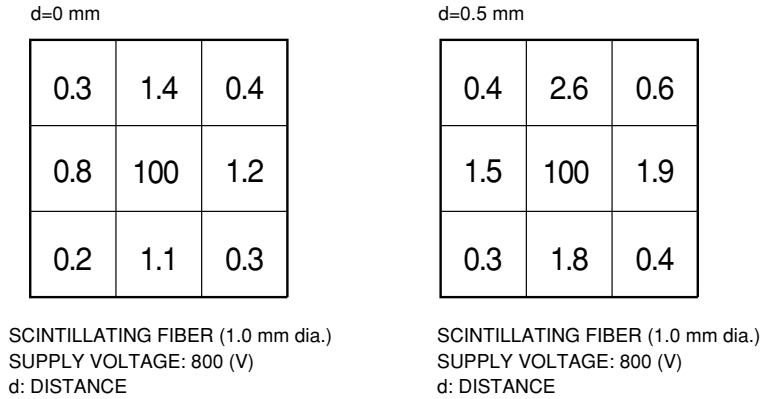
A typical setup for measuring crosstalk is shown in Figure 9-4 and an example of measurement data in Figure 9-5.



THBV3\_0904EA

Figure 9-4: Crosstalk measurement method





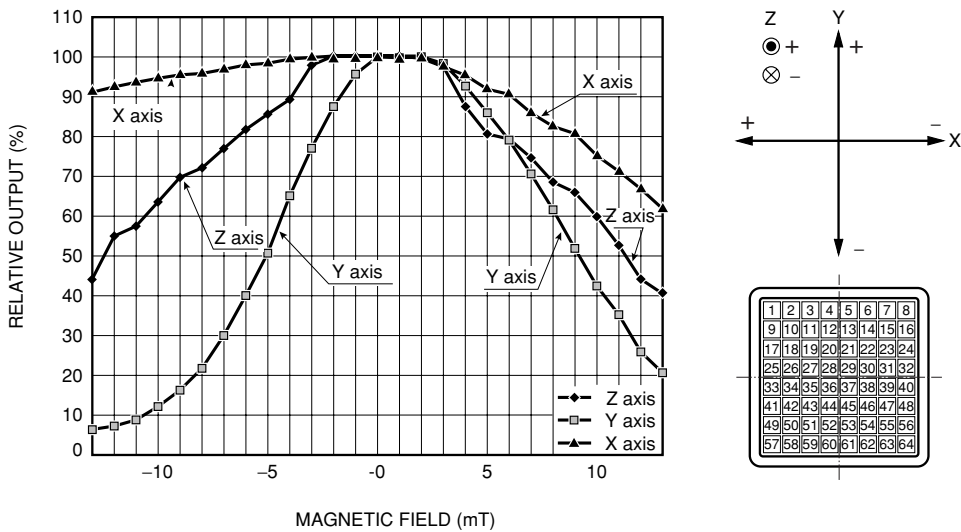
THBV3\_0905EA

**Figure 9-5: Crosstalk measurement example**

Data shown in Figure 9-5 is measured by irradiating a light spot (signal) on the photomultiplier tube faceplate, through a 1 mm diameter optical fiber placed in close contact with the faceplate. The output of each anode is expressed as a relative value, with 100 % being equal to the peak anode output produced from the incident light spot. Results show that crosstalk is 0.2 % to 1.4 % when the 1 mm diameter scintillating fiber is positioned in tight contact with the photomultiplier tube faceplate (d=0 mm). However, the crosstalk becomes 0.3 % to 2.6 % worse when the scintillating fiber is moved 0.5 millimeters away from the faceplate. This is of course due to light spread at the scintillating fiber exit. Bringing the optical fiber into tight contact with the photomultiplier tube faceplate is therefore recommended in order to make accurate measurements using scintillating fibers.

Next, let's discuss magnetic characteristics. Matrix type multianode photomultiplier tubes have excellent immunity to magnetic fields. This is because all parts except the photocathode are housed in a metal package and also because the distance between dynode electrodes is very short. Magnetic characteristics of a 64-channel multianode photomultiplier tube are explained below.

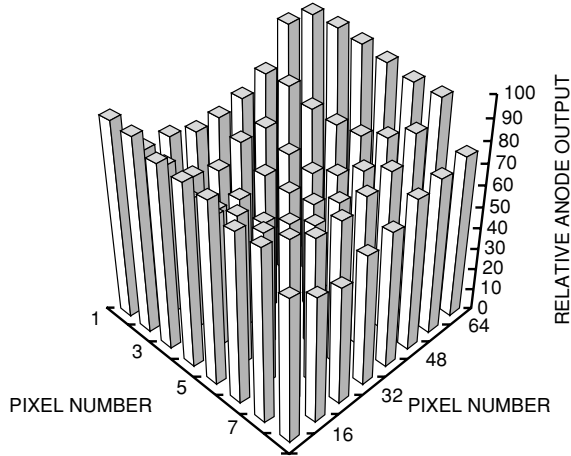
Figure 9-6 shows how the anode output is adversely affected by external magnetic fields applied along the three axes (X, Y, Z). Each data is plotted as a relative output value, with 100 % corresponding to an output with no magnetic field applied. Output is still maintained as high as 60 % versus 13 mT of the magnetic field in the X direction.



THBV3\_0906EA

**Figure 9-6: Effects of external magnetic fields on anode output (anode channel No. 29)**

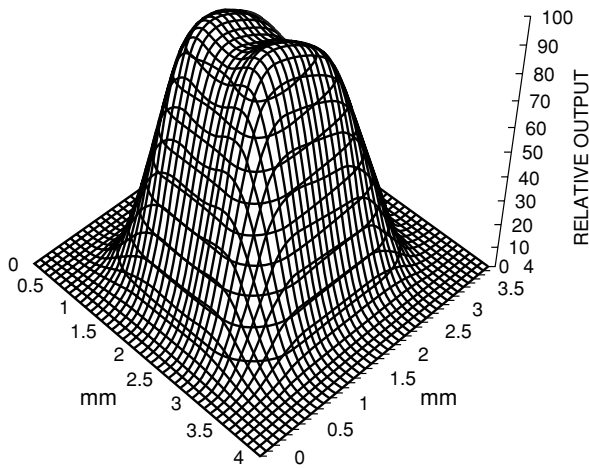
Figure 9-7 shows typical uniformity data obtained from each anode when uniform light is illuminated over the entire photocathode of a 64-channel multianode photomultiplier tube. The non-uniformity observed here probably originates from gain variations in the secondary electron multiplier because the photocathode itself has good uniformity. Currently, non-uniformity between each anode is about "1:3" on average.



THBV3\_0907EA

**Figure 9-7: 64-channel multianode output uniformity**

Uniformity of one pixel (one anode) is shown in Figure 9-8. This data is measured by input of weak DC light of 50  $\mu\text{m}$  diameter to an anode of 2 square millimeters per pixel, while scanning the light every 0.1 millimeters on the photocathode.

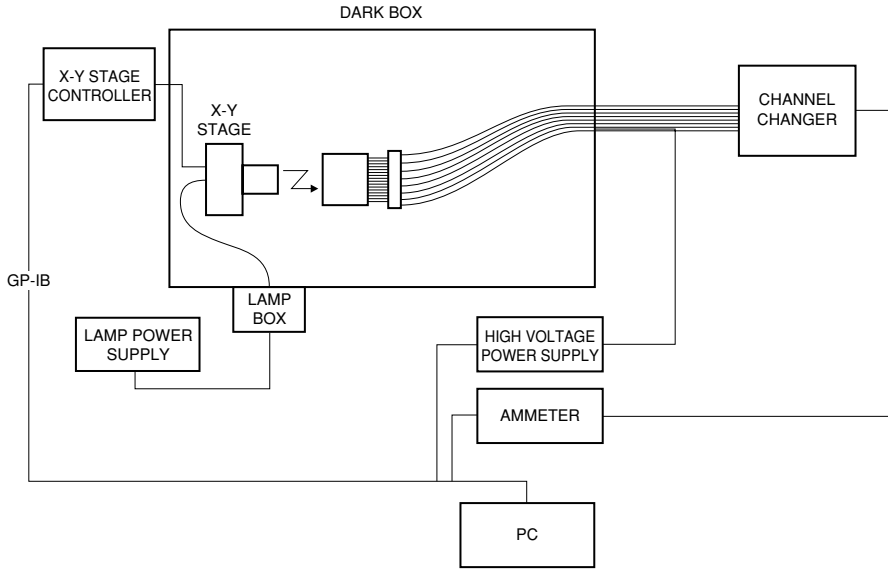


THBV3\_0908EA

**Figure 9-8: Anode output uniformity per pixel**

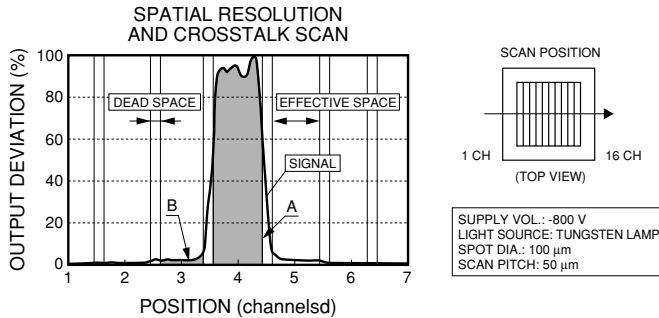
We next describe basic "crosstalk" and "uniformity" characteristics of linear multianode photomultiplier tubes.

A typical setup for measuring crosstalk of a 16-channel linear multianode photomultiplier tube is shown in Figure 9-9 and the typical measurement data in Figure 9-10. In this measurement, a light spot emitted through the 100 μm aperture in the X-Y stage was scanned along the photocathode. Typical crosstalk obtained from the 16-channel linear multianode was approximately 3 %.



THBV3\_0909EA

Figure 9-9: Crosstalk measurement method

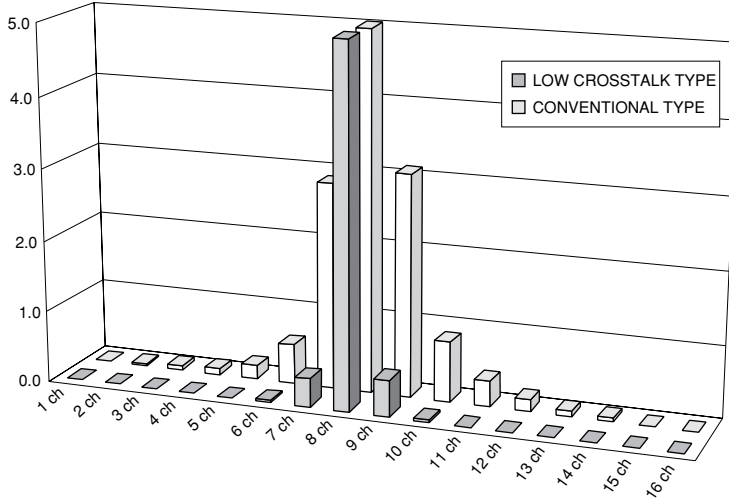


CH	CROSS-TALK RATIO (%)															
	1	2	3	4	5	6	7	8	9	10	11	12	13	14	15	16
1	100	2.9	0.6	0.2	0.1	—	—	—	—	—	—	—	—	—	—	—
2	2.9	100	3.1	0.5	0.2	0.1	—	—	—	—	—	—	—	—	—	—
3	0.8	2.8	100	2.8	0.6	0.2	0.1	—	—	—	—	—	—	—	—	—
4	0.3	0.8	2.7	100	3.2	0.6	0.2	0.1	—	—	—	—	—	—	—	—
5	0.1	0.3	0.8	2.9	100	3.1	0.6	0.2	0.1	—	—	—	—	—	—	—
6	—	0.1	0.3	0.8	2.7	100	3.0	0.6	0.2	0.1	—	—	—	—	—	—
7	—	—	0.1	0.3	0.8	2.7	100	3.0	0.6	0.2	0.1	—	—	—	—	—
8	—	—	—	0.1	0.3	0.8	2.9	100	2.9	0.6	0.2	0.1	—	—	—	—
9	—	—	—	—	0.1	0.3	0.8	2.9	100	2.9	0.6	0.2	0.1	—	—	—
10	—	—	—	—	—	0.1	0.3	0.8	3.1	100	2.7	0.6	0.2	0.1	—	—
11	—	—	—	—	—	—	0.1	0.4	0.8	3.3	100	3.8	0.6	0.2	0.1	—
12	—	—	—	—	—	—	—	0.1	0.4	0.9	3.2	100	2.8	0.6	0.2	0.1
13	—	—	—	—	—	—	—	—	0.1	0.4	0.8	3.1	100	2.8	0.6	0.3
14	—	—	—	—	—	—	—	—	—	0.1	0.4	0.8	3.1	100	2.7	0.6
15	—	—	—	—	—	—	—	—	—	—	0.1	0.4	0.9	3.2	100	2.9
16	—	—	—	—	—	—	—	—	—	—	—	0.1	0.4	0.9	3.1	100

Figure 9-10: Crosstalk of 16-channel linear anode

THBV3\_0910EA

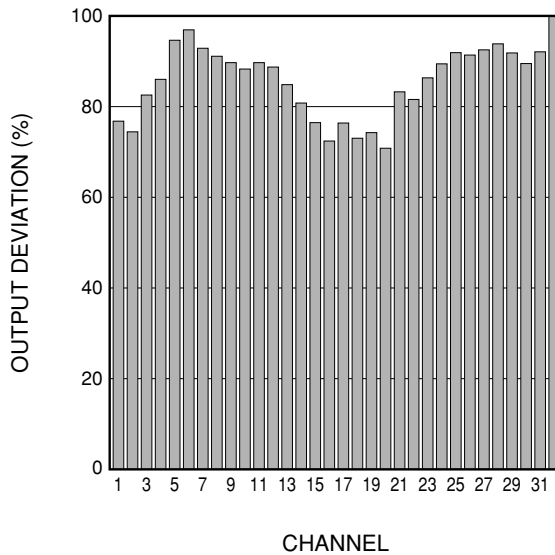
Some 16-channel and 32-channel linear multianode photomultiplier tubes are low crosstalk types. Some use a special faceplate containing black glass partitions or an electrode structure having shielding walls between the anodes of each channel. Typical crosstalk values measured with a low crosstalk type are shown in Figure 9-11.



THBV3\_0911EA

Figure 9-11: Crosstalk values of 16-channel low-crosstalk type

Figure 9-12 shows typical uniformity data of a linear multianode photomultiplier tube. This data was obtained from each anode when uniform light was illuminated over the entire photocathode of a 32-channel linear multianode photomultiplier tube. As with the matrix type, non-uniformity mainly originates from gain variations in the secondary electron multiplier. Currently, non-uniformity between each anode is about "1:1.7" on average.



THBV3\_0912EA

Figure 9-12: 32-channel linear multianode output uniformity

Since 16-channel and 32-channel linear multianode photomultiplier tubes have a one-dimensional array of anodes, they are mainly used as detectors for multichannel spectrophotometry. Due to its shape, the 32-channel type is often used in combination with a grating or prism, and recent applications include laser scanning microscopes.

Linear multianode photomultiplier tubes are also available with a band-pass filter attached to the faceplate. This allows detecting light only in the wavelength range of interest, just like using a grating or prism. There is no loss of light caused by the entrance slit which is used with the grating for separating the light into different wavelengths. Since light must uniformly strike the entire surface of the band-pass filter, Hamamatsu also provides a dedicated mixing fiber combined with a lens for this purpose. Figure 9-13 shows a photomultiplier tube with a band-pass filter and a dedicated mixing fiber combined with a lens.

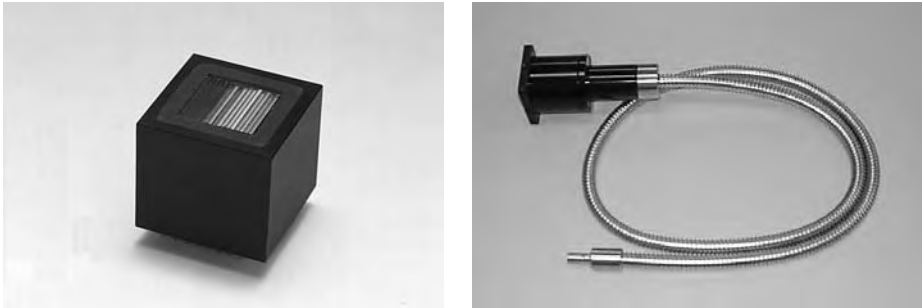
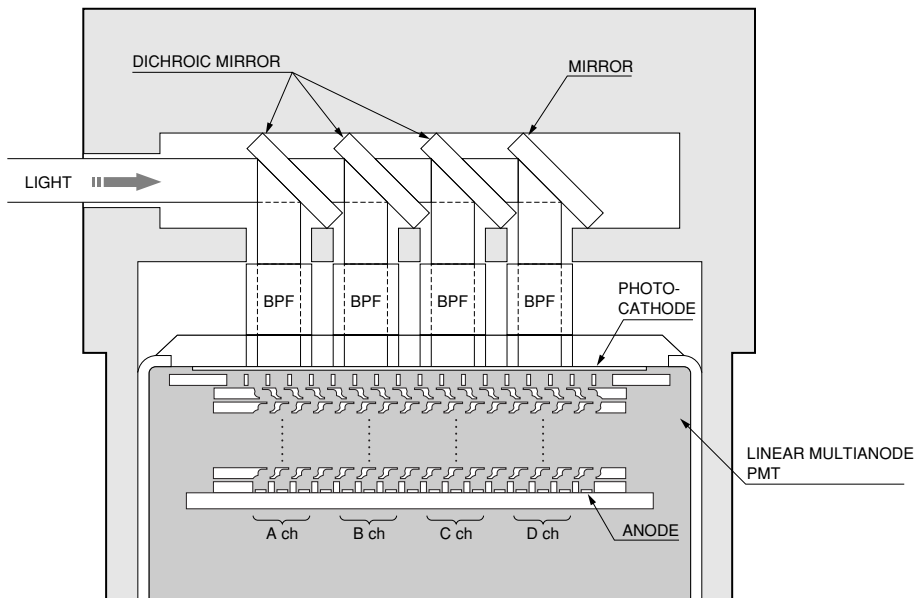


Figure 9-13: Photomultiplier tube with band-pass filter

Mixing fiber + lens

Dichroic mirrors can also be used for dispersing light into a spectrum. One example is illustrated in Figure 9-14 showing a very compact device containing an optical system and a detector.



THBV3\_0914EA

Figure 9-14: Multianode photomultiplier tube assembled with dichroic mirrors

### 9.1.2 Multinode MCP-PMT

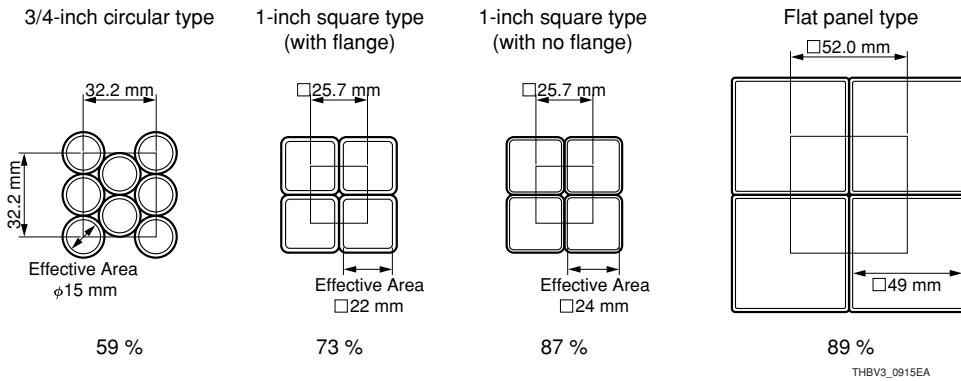
The multinode MCP-PMT is explained in detail in section 10.4 of Chapter 10.

### 9.1.3 Flat panel type multianode photomultiplier tubes

#### (1) Characteristics

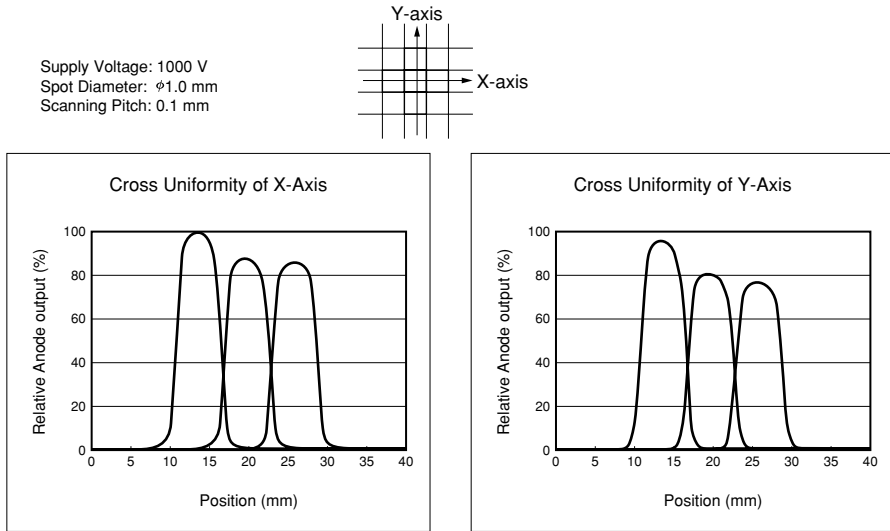
Metal channel dynodes are mainly used in 1-inch square metal package photomultiplier tubes and flat panel type (2 square inches) photomultiplier tubes, which can be selected according to the particular application.

This section introduces a flat panel type photomultiplier tube with an overall height as short as 15 millimeters. As shown in Figure 9-15, this photomultiplier tube features a large effective area and minimal dead area (insensitive area).



**Figure 9-15: Comparison of effective area ratio**

Typical spatial resolution obtained with a flat panel type 64-channel photomultiplier tube is shown in Figure 9-16. This spatial resolution data (output distribution of each anode) was measured by scanning the photocathode surface with a 1-millimeter collimated light beam emitted from a tungsten lamp through a blue filter.



**Figure 9-16: Spatial resolution of center anodes**

Figure 9-17 shows typical crosstalk characteristics measured by irradiating the center of an anode (anode pitch 6 mm) with a light beam of 5 square millimeters. Relative outputs of adjacent anodes are shown in the figure by setting the output of this anode as 100%. As can be seen in the figure, this flat panel type 64-channel multianode photomultiplier tube has a crosstalk of 2 to 3 % at the center anodes.

—	—	—	—	—
—	0.2	1.8	0.2	—
—	1.5	100	2.7	—
—	0.2	2.6	0.3	—
—	—	—	—	—

Supply Voltage: 1000 V  
 Light Source: Tungsten Lamp  
 Spot Size: 5 square millimeters

THBV3\_0917EA

**Figure 9-17: Crosstalk characteristics of center anodes**

To take full advantage of the effective area, the photoelectrons emitted from the edges of the photocathode are focused toward the dynodes. This tends to increase anode crosstalk (3 % to 6 %) particularly in the corner areas. (See Figure 9-18.)

100	5.5	—
3.5	0.5	—
—	—	—

Supply Voltage: 1000 V  
 Light Source: Tungsten Lamp  
 Spot Size: 5 square millimeters

THBV3\_0918EA

Figure 9-18: Crosstalk characteristics of anodes in corner area

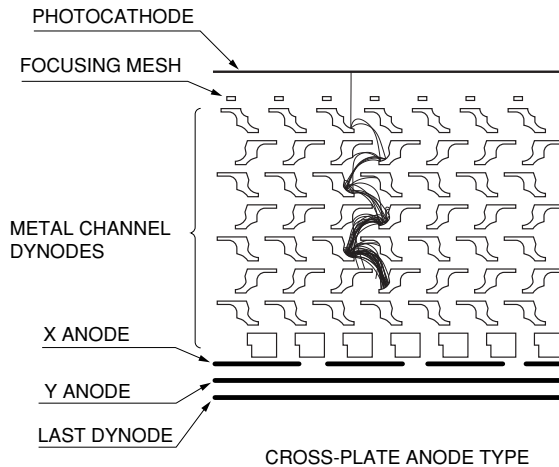
## 9.2 Center-of-Gravity Position Sensitive Photomultiplier Tubes

### 9.2.1 Metal channel dynode type multianode photomultiplier tubes (cross-plate anodes)

#### (1) Structure

Figure 9-19 shows the electrode structure of a metal channel dynode type multianode photomultiplier tube using a cross-plate anode.

In this photomultiplier tube, photoelectrons emitted from the photocathode are multiplied by each dynode and the multiplied secondary electrons are then reflected back from the last dynode and read out from the plate type anodes (cross-plate anodes) arranged in two layers intersecting with each other.



THBV3\_0919EA

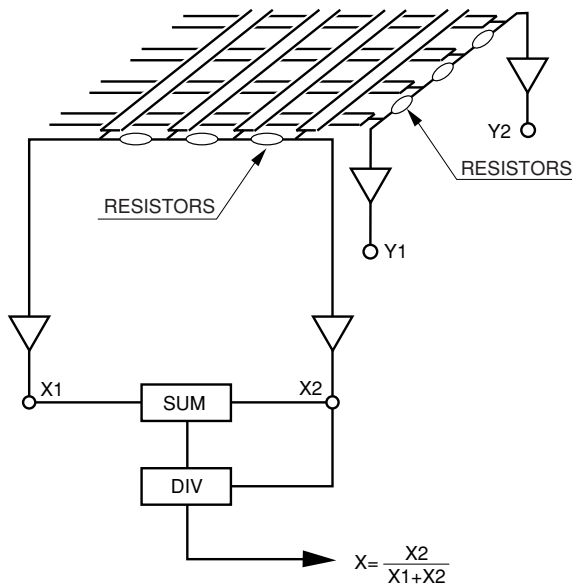
Figure 9-19: Electrode structure



Figure 9-20 illustrates the center-of-gravity detection method for reading out the output signal from a position-sensitive photomultiplier tube using a cross-plate anode. The electron bunch released from the last dynode is collected by anodes linearly arranged in the X and Y directions. Since each anode in the same direction is connected by a resistor string, the collected electrons are divided into four signal components X1, X2, Y1 and Y2 corresponding to the anode position at which the secondary electrons arrive. By inputting these signals to summing (SUM) and divider (DIV) circuits, the center of gravity in the X and Y directions can be obtained from Eq. 9-1.

$$X = \frac{X_2}{(X_1+X_2)}$$

$$Y = \frac{Y_2}{(Y_1+Y_2)} \dots\dots\dots(\text{Eq. 9-1})$$

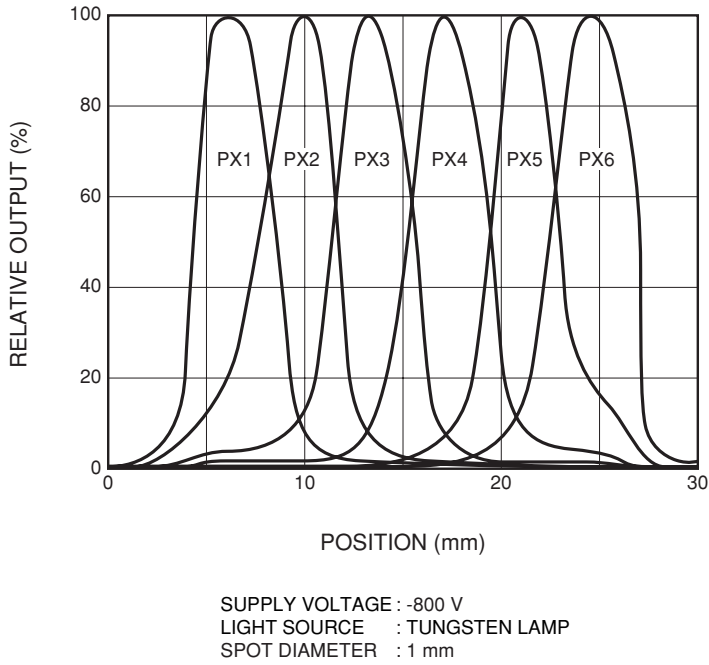


THBV3\_0920EA

Figure 9-20: Center-of-gravity measurement method

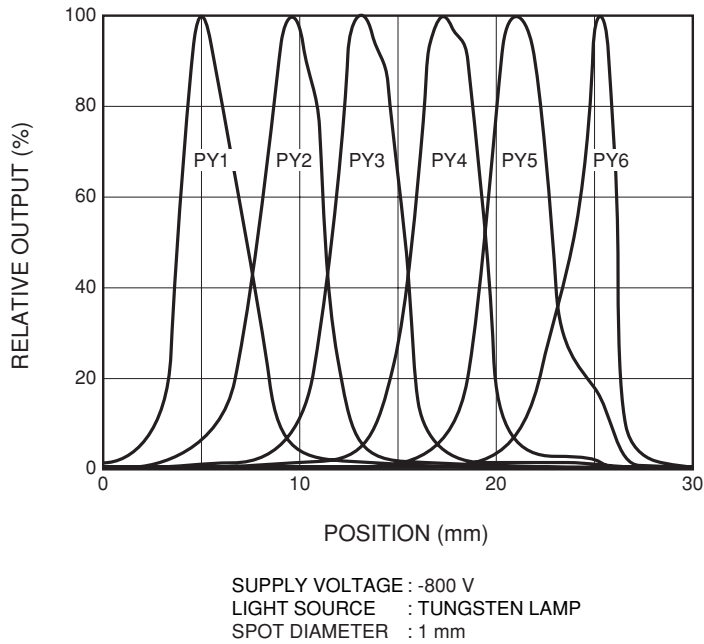
**(2) Characteristics**

This section describes spatial resolution characteristics obtained by center-of-gravity detection using 6(X) + 6(Y) cross-plate anodes respectively arranged in the XY directions. This spatial resolution data (output distribution of each anode) was measured by scanning the photocathode surface with a 1-millimeter collimated light beam emitted from a tungsten lamp. Results are shown in Figures 9-21 and 9-22.



THBV3\_0921EA

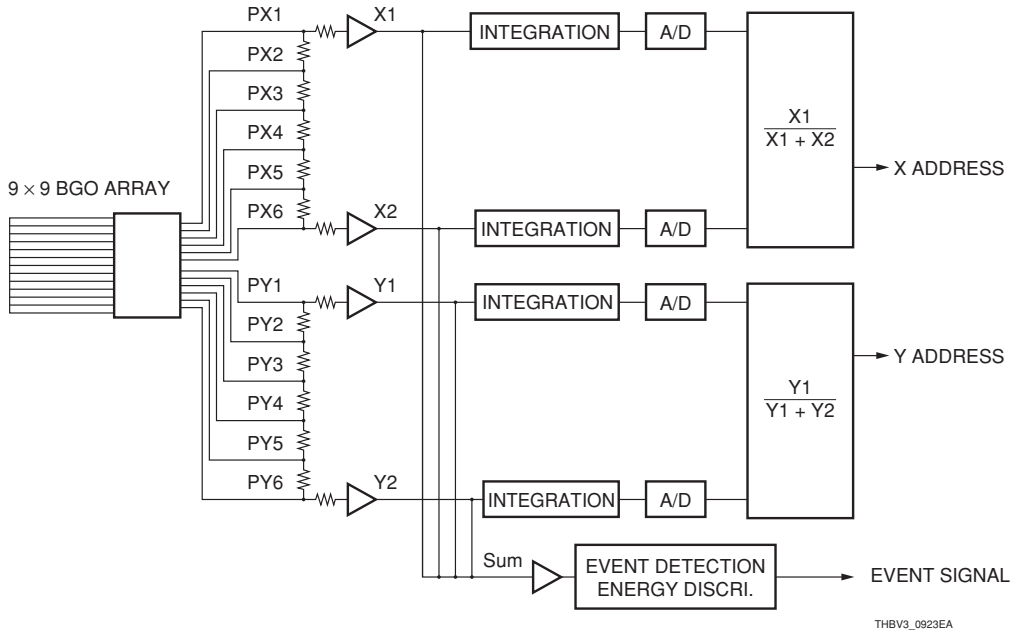
Figure 9-21: Spatial resolution of X anodes



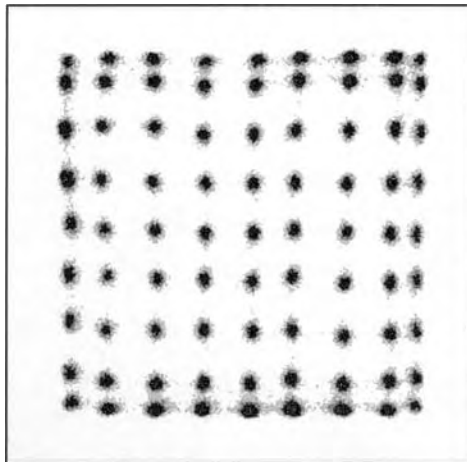
THBV3\_0922EA

Figure 9-22: Spatial resolution of Y anodes

Figure 9-23 introduces a circuit diagram for scintillation imaging of 511 keV gamma-rays. It utilizes a position sensitive photomultiplier tube with 6(X) + 6(Y) cross-plate anodes and a mosaic array of scintillators (BGO of 2.2 mm×2.2 mm×15 mm arranged in a pattern of 9×9=81 pieces). An actual image obtained is shown in Figure 9-24.



**Figure 9-23: Scintillation imaging circuit using gamma-rays irradiated on mosaic pattern scintillators (BGO)**



**Figure 9-24: Scintillation image obtained by gamma-rays irradiated on mosaic pattern scintillators (BGO)**

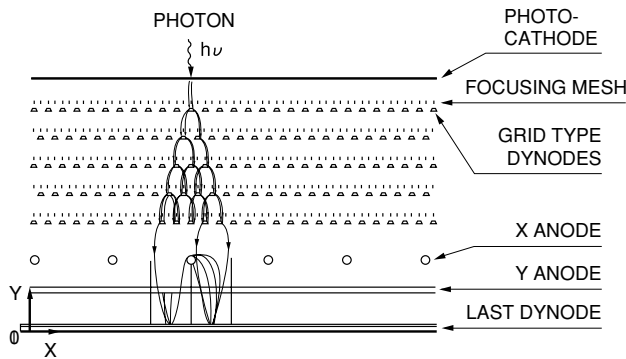
This scintillation imaging shows the mosaic pattern of 81 (9×9) BGO scintillators (2.2 mm×2.2 mm×15 mm). Off-center distortion in the image can be corrected by a lookup table.

## 9.2.2 Grid type dynode photomultiplier tubes (Cross-wire anodes)

### (1) Structure

Figure 9-25 shows the electrode structure for grid type dynodes and the associated electron trajectories. The significant difference compared to ordinary box-and-grid dynodes is that the electron multiplier is fabricated from flat grid-like dynodes. These dynodes have a very fine structure that emits secondary electrons while suppressing the spatial spread of secondary electrons at each dynode.

In this photomultiplier tube, photoelectrons emitted from the photocathode are multiplied by each dynode (up to a total gain of  $10^5$  or more) and then the multiplied secondary electrons are reflected back from the last dynode (reflection type) and read out from the wire type anodes (cross-wire anodes) arranged in two layers intersecting with each other. The first dynode is placed in close proximity to the photocathode to minimize the spatial spread of photoelectrons.



THEBV3\_0925EA

Figure 9-25: Electrode structure and electron trajectories

### (2) Characteristics

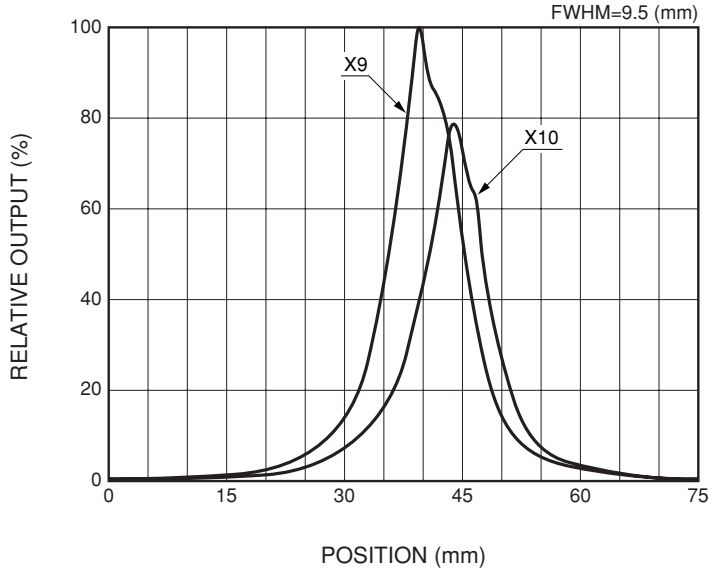
A photomultiplier tube using a 12-stage grid type dynode yields a gain of  $10^5$  or more at 1250 volts. This type of photomultiplier tube is available in a circular envelope of 3 or 5 inches in diameter.

The number of wire anodes in the X and Y directions is  $16(X) + 16(Y)$  for the 3-inch circular type (anode pitch: 3.75 millimeters) and  $28(X) + 28(Y)$  for the 5-inch circular type (anode pitch: 4 millimeters).

Next, let's discuss the center-of-gravity detection method and spatial resolution characteristics. As shown in Figure 9-25, the electron flow spreads spatially between the photocathode and the first dynode and also between each grid dynode. When 50  $\mu\text{m}$  diameter light spot scans the photocathode surface of the 3-inch circular type photomultiplier tube, the X and Y direction spatial resolutions are obtained as shown in Figures 9-27 and 9-28. Since the electron flow spreads in the multiplication process from the photocathode to the anode, the width of spatial resolution measured at each anode broadens to 9.5 millimeters in the X direction and to 8.6 millimeters in the Y direction.

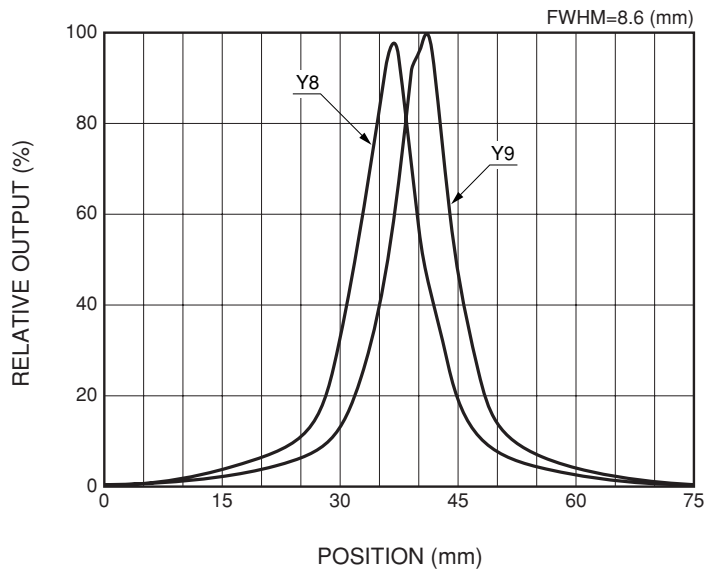


Figure 9-26: Grid type dynode photomultiplier tube



THBV3\_0927EA

Figure 9-27: Spatial resolution in X direction

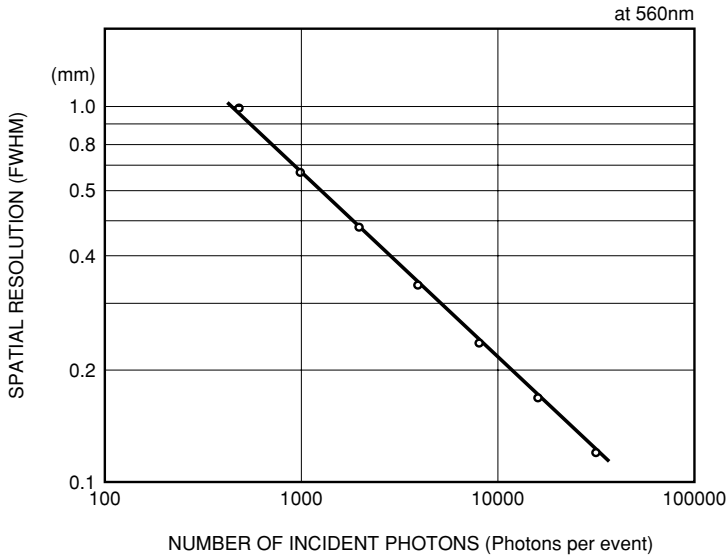


THBV3\_0928EA

Figure 9-28: Spatial resolution in Y direction

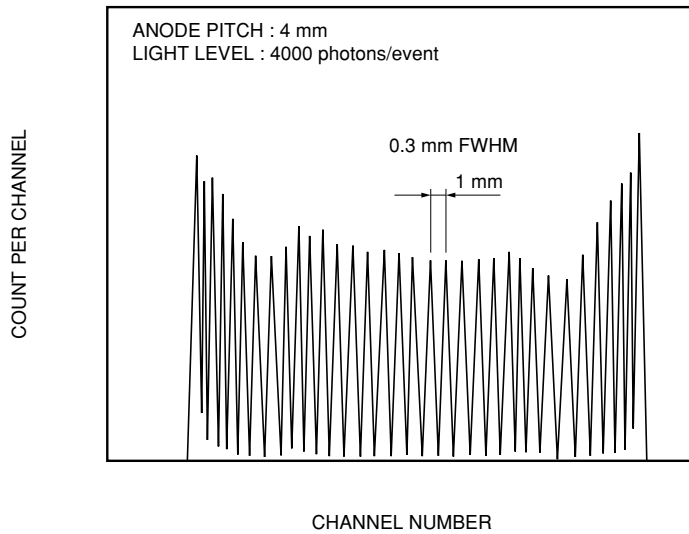
To read out the signal from this photomultiplier tube, the center-of-gravity detection method is used, as described in the previous section 9.2.1, "Metal channel dynode type multianode photomultiplier tubes (cross-plate anodes)".

Figure 9-29 shows plots of spatial resolution measured with light emitted from a pulsed LED while changing the amount of light per pulse. This spatial resolution is determined by the center-of-gravity distribution in the output signal that broadens almost in inverse proportion to the square root of the amount of incident light according to the statistical theory. Figure 9-30 shows the center-of-gravity distribution characteristics measured while moving a light spot on the photocathode in 1 millimeter intervals. It proves that a resolution of 0.3 millimeters (FWHM) is obtained in the center at a light intensity of 4000 photons per pulse. A slight distortion occurs near the off-center region because there are fewer cross-wire anodes involved in the output signal. Figure 9-31 is a spatial linearity graph showing the electrical center-of-gravity position on the vertical axis and the light spot position on the horizontal axis.



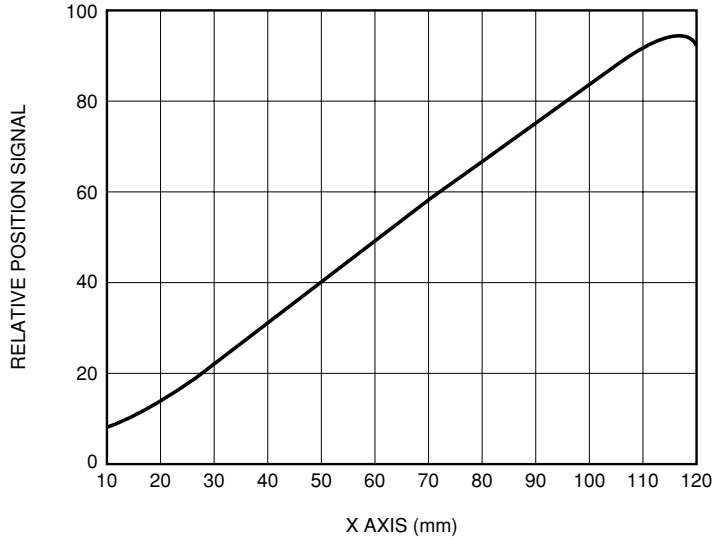
THBV3\_0929EA

Figure 9-29: Spatial resolution vs. incident light level



THBV3\_0930EA

Figure 9-30: Center-of-gravity distribution with light spot movement



THBV3\_0931EA

**Figure 9-31: Spatial linearity of grid type dynode photomultiplier tube**

In the peripheral portion of the photomultiplier tube, not all electrons are focused by the cross-wire anodes, and these electrodes cause distortion as if they are drawn toward the center. But this distortion level is small enough to be corrected by a lookup table or similar techniques.

# MEMO



# **CHAPTER 10**

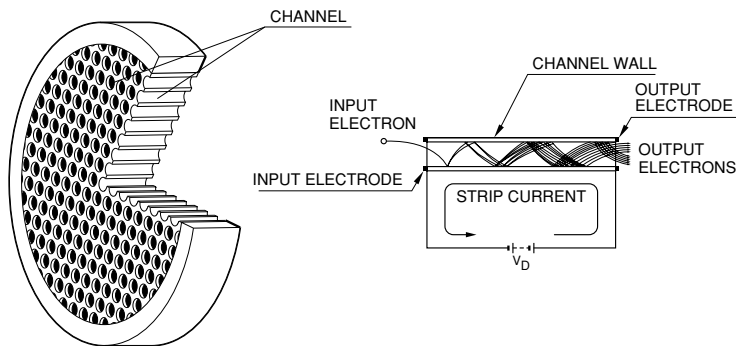
## **MCP-PMT**

*With the advent of the microchannel plate<sup>1)</sup> (abbreviated as MCP hereafter), photomultiplier tubes have evolved into more versatile devices. MCP-PMTs, photomultiplier tubes that incorporate an MCP in place of the conventional discrete dynodes, offer wide-bandwidth measurements down to the picosecond level as well as low-light-level detection at the photon counting level. This chapter describes these ultra-fast and high-sensitivity MCP-PMTs.<sup>2)</sup>*

## 10.1 Structure

### 10.1.1 Structure of MCPs

Figure 10-1 (a) illustrates the schematic structure of an MCP. The MCP consists of a two-dimensional array of a great number of glass capillaries (channels) bundled in parallel and formed into the shape of a thin disk. Each channel has an internal diameter ranging from 6 to 20 microns with the inner wall processed to have the proper electrical resistance and secondary emissive properties. Accordingly, each channel acts as an independent electron multiplier. The cross section of a channel and its principle of multiplication are illustrated in Figure 10-1 (b). When a primary electron impinges on the inner wall of a channel, secondary electrons are emitted. Being accelerated by the electric field created by the voltage  $V_D$  applied across both ends of the MCP, these secondary electrons bombard the channel wall again to produce additional secondary electrons. This process is repeated many times along the channel and as a result, a large number of electrons are released from the output end.



THBV3\_1001EA

(a) Schematic structure of an MCP

(b) Principle of multiplication

Figure 10-1: Schematic structure of an MCP and its principle of multiplication

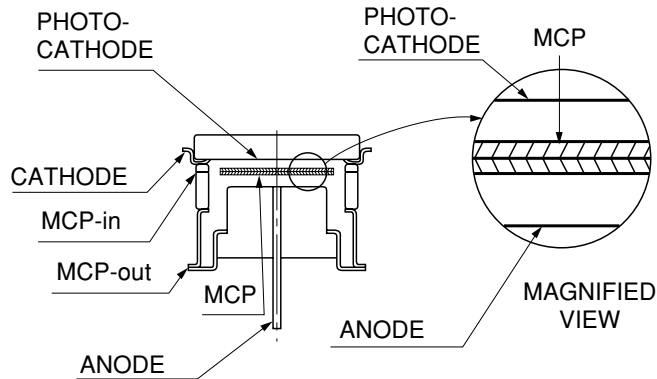
MCPs are quite different in structure and operation from conventional discrete dynodes and therefore offer the following outstanding features:

- 1) High gain despite compact size
- 2) Fast time response
- 3) Two-dimensional detection with high spatial resolution
- 4) Stable operation even in high magnetic fields
- 5) Sensitive to charged particles, ultraviolet radiation, X rays, gamma rays, and neutrons
- 6) Low power consumption

There are various types of detectors that utilize the advantages offered by MCPs, for example image intensifiers for low-light-level imaging, fast time response photomultiplier tubes that incorporate an MCP (MCP-PMTs), position-sensitive multianode photomultiplier tubes, streak tubes for ultra-fast photometry, and photon counting imaging tubes for ultra-low light level imaging.

### 10.1.2 Structure of MCP-PMTs

Figure 10-2 shows the cross section of a typical MCP-PMT. This MCP-PMT consists of an input window, photocathode, MCP, and anode. The photoelectrons emitted from the photocathode enter the channels of the MCP and impinge on the inner wall where they are multiplied by means of secondary emission. This process is repeated along the channels, and finally a large number of electrons are collected by the anode as an output signal. The photocathode to MCP distance is approximately 2 millimeters, forming a close-proximity structure. Two MCPs are stacked to obtain sufficient gain. A thin film called "ion barrier" is usually formed on the photoelectron input side of the MCP in order to prevent ions generated inside the MCP from returning to the photocathode. Figure 10-3 shows an MCP-PMT complete with housing.



THBV3\_1002EA

**Figure 10-2: Cross section of a typical MCP-PMT**



THBV3\_1003EA

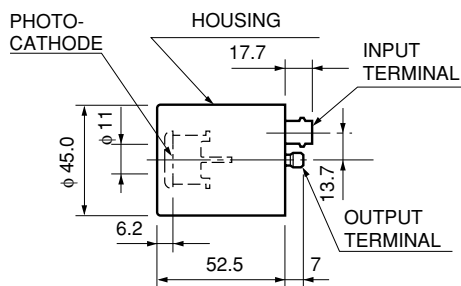
**Figure 10-3: External view of an MCP-PMT**

### 10.1.3 Voltage-divider circuit and housing structure

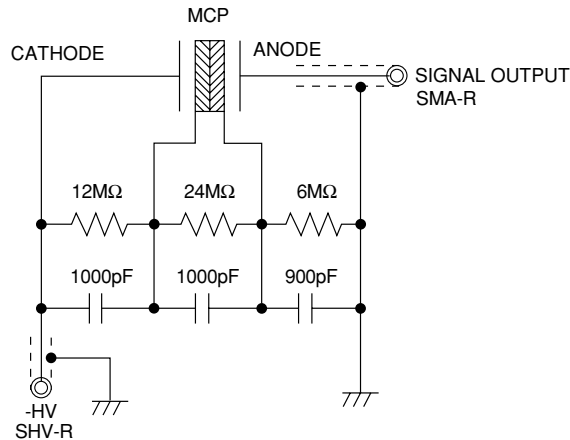
To operate an MCP-PMT, proper voltage must be supplied to each electrode, just as with a photomultiplier tube. A voltage-divider resistor circuit is usually used. Figure 10-4 shows a basic voltage-divider circuit used to operate an MCP-PMT (with a two-stage MCP) and the configuration of the housing that contains the MCP-PMT with the voltage-divider circuit.

As shown in the figure, a negative high voltage is normally applied to the photocathode, and the voltage-divider circuit gives a voltage gradient between the photocathode, MCP-in, MCP-out, and the anode by dividing the high voltage with properly selected resistors. The voltage-divider circuit and housing are designed with careful consideration given to prevent "ringing" which may be caused by high-frequency signals, so that the output waveform distortion is suppressed to a minimum level.

#### Structure



#### Voltage-divider circuit



THBV3\_1004EA

Figure 10-4: Housing configuration and operating circuit for MCP-PMT

## 10.2 Basic Characteristics of MCP-PMTs

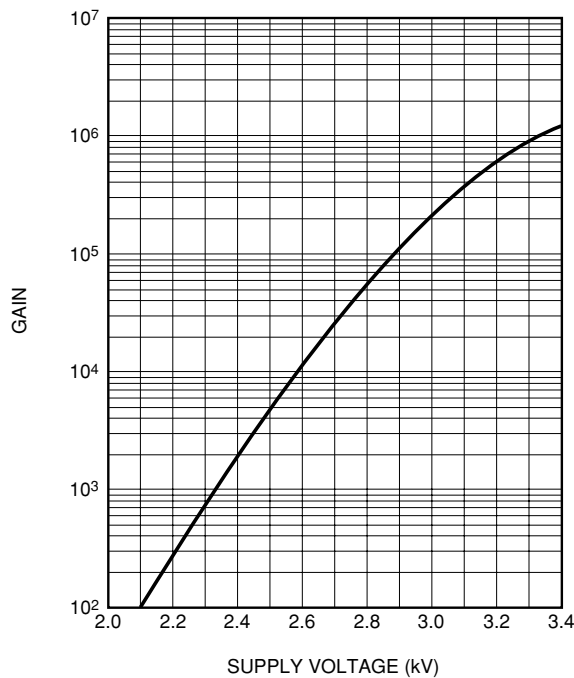
### 10.2.1 Gain characteristics<sup>1)</sup>

The gain of an MCP-PMT depends on the number of MCPs incorporated in the tube. Figure 10-5 shows the typical gain versus supply voltage characteristics of an MCP-PMT.

The gain<sup>1)</sup> ( $\mu$ ) of an MCP is determined by the length-to-diameter ratio  $\alpha$  ( $=L/d$ ) of a channel, and approximated as follows:

$$\mu = \text{EXP}(G \cdot \alpha)$$

where  $G$  is the secondary emission characteristics called the gain factor. This gain factor is an inherent characteristic of the channel wall material and is a function of the electric field intensity inside the channel.



THBV3\_1005EA

**Figure 10-5: Typical gain of an MCP-PMT (using a two-stage MCP of 6  $\mu\text{m}$  channel diameter)**

In general, a higher gain can be obtained as  $\alpha$  is made greater, though the gain rising point moves to the higher supply voltage side. However, if the gain becomes higher than  $10^4$ , noise begins to increase significantly due to ion feedback effects, which causes a serious problem. To avoid this,  $\alpha$  is usually selected to be around 40 so that a single MCP provides a gain of about  $10^4$  at 1 kV supply voltage.

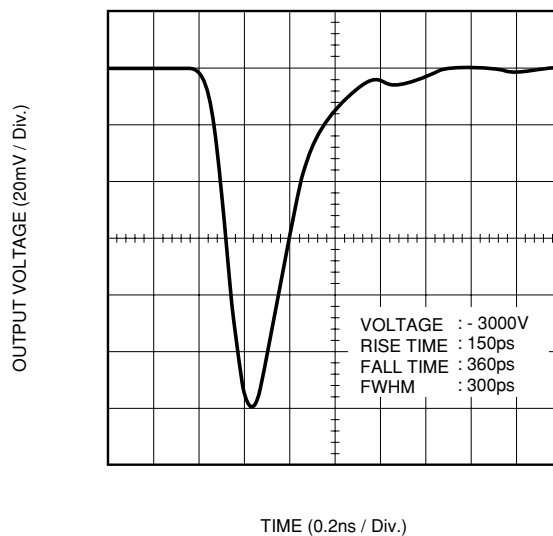
As shown in Figure 10-5 above, a higher gain can be obtained from a two-stage MCP-PMT. This gain level enables photon counting measurements.

## 10.2.2 Time characteristics<sup>2)</sup>

As discussed in the previous chapter on photomultiplier tube time characteristics, the signal pulse can broaden during the multiplication process from the photocathode to the anode. This is due to the emission-angle distribution and initial-velocity distribution of photoelectrons and secondary electrons, as well as the effects of the focusing lens. In an MCP-PMT, a strong electric field is applied in nearly parallel from the photocathode to MCPin and the MCPout to anode, so that the emission-angle distribution and initial-velocity distribution of photoelectrons can be almost ignored. Furthermore, since MCP is used in place of conventional dynodes, the electron transit time in the secondary electron multiplication process is very short, allowing a dramatic improvement in the transit time spread. Due to these features, the MCP-PMT offers time response characteristics that are the best among currently available photomultiplier tubes.

### (1) Rise/fall times

The rise and fall times of an MCP-PMT are evaluated from the output waveform when the MCP-PMT detects a light pulse whose width is sufficiently short compared to the time response of the MCP-PMT. These parameters are especially important when observing the waveform of ultra-short pulsed light. For the measurement method, refer to 4.3.1 in Chapter 4. Figure 10-6 shows an actual waveform obtained with an MCP-PMT.



THBV3\_1008EA

Figure 10-6: Pulse response waveform of MCP-PMT (R3809U-50)

### (2) Transit time

The transit time is the time delay between the input of a light pulse at the photomultiplier tube and the appearance of the output pulse from the photomultiplier tube. For the measurement method, refer to 4.3.1 in Chapter 4.

### (3) TTS (transit time spread)

When one photon enters an MCP-PMT, the photocathode converts it into an electron which travels to the anode while being multiplied. The transit time of an electron bunch differs depending on each input photon. The distribution of this transit time is referred to as the transit time spread or TTS. This TTS is an important parameter, especially in the time-correlated photon counting technique<sup>3)</sup> where the measurement of timing is of prime consideration. For the measurement method, refer to 4.3.1 in Chapter 4.

At Hamamatsu Photonics, TTS is evaluated with the measurement system shown in Figure 10-7. In this system, the IRF (instrument response function) value is measured as the time characteristic for the entire system including the MCP-PMT. This is because the measurement system uses a laser pulse with approximately 35 picosecond pulse width, which acts as a time jitter equal to the TTS of the MCP-PMT. The relation between the TTS and IRF is given by the following equation.

$$(IRF)^2 = (TTS)^2 + Tw^2 + Tj^2$$

TW : laser pulse width

Ti : other time jitter in the measurement system

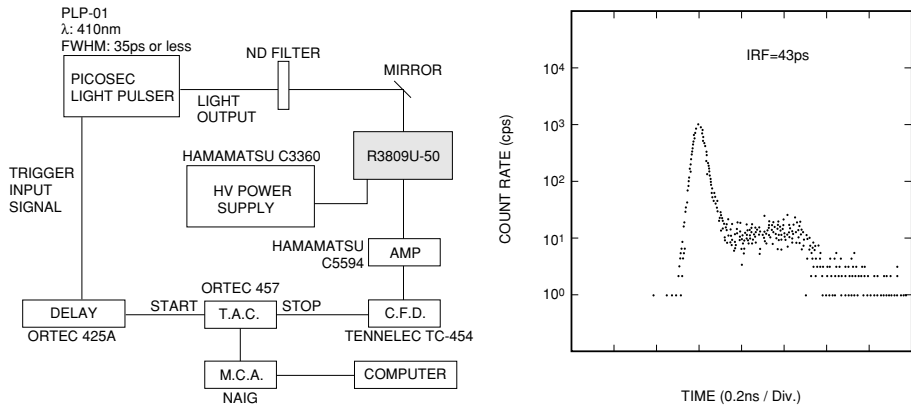


Figure 10-7: IRF measurement using MCP-PMT (R3809U-50)

To evaluate the TTS of an MCP-PMT more accurately, the measurement system shown in Figure 10-8 was used and excellent data of 25.0 picoseconds has been obtained. This system uses a laser pulse with a 5 picosecond pulse width which is shorter than the TTS of the MCP-PMT, therefore enabling accurate measurements.

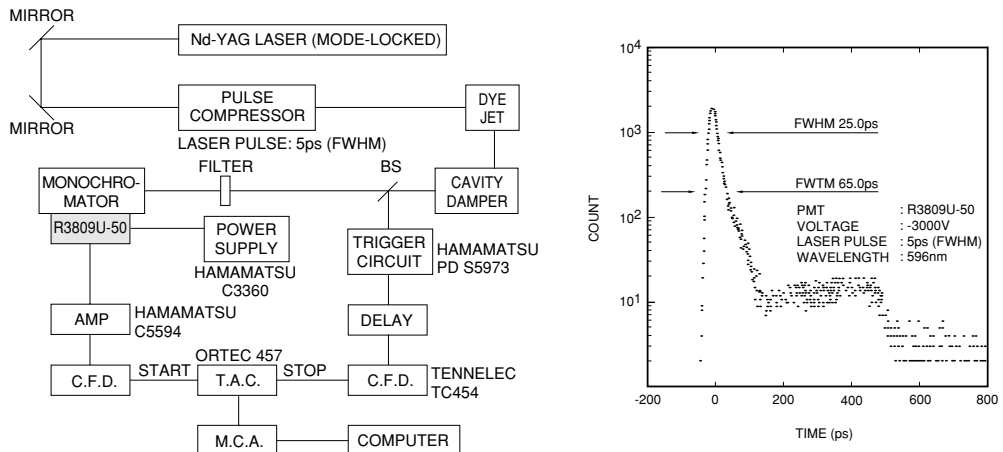


Figure 10-8: Accurate TTS measurement of MCP-PMT (R3809U-50)

#### (4) Cathode transit time difference

In most photomultiplier tubes, the electron transit time differs with the position of photocathode illumination. When the entire photocathode is uniformly illuminated, the difference in transit time with respect to position is referred to as the cathode transit time difference or CTTD. The CTTD usually affects the TTS, but in the case of proximity-focused MCP-PMTs, it has little effect on the TTS. For the measurement method, refer to 4.3.1 in Chapter 4.

#### (5) Time characteristics of various products

Time characteristics of various MCP-PMTs are summarized in Table 10-1 below. The less the number of MCP stages and the smaller the channel diameter, the better the time characteristics. Compared to conventional MCP-PMTs using 12  $\mu\text{m}$  channel MCPs, the R3809U series using 6  $\mu\text{m}$  channel MCPs has improved the rise time by 70 picoseconds and the IRF by 25 picoseconds. The fall time does not show a correlation with the rise time. This is probably due to the difference in electrostatic capacity between the MCP and the anode. The gated MCP-PMT is slightly inferior in time characteristics compared to other types. This is presumably because the electric field between the gate mesh and the cathode is weak so that the photoelectron emission angle and initial velocity distribution tend to affect the time characteristics adversely to some extent.

MCP-PMT Type No.	Rise Time	Fall Time	Transit Time	IRF (FWHM)
R3809U-50 (6 $\mu\text{m}$ , 2-stage MCP)	150ps	360ps	400ps	45ps
R5916U-50 (6 $\mu\text{m}$ , 2-stage MCP)	180ps	700ps	350ps	95ps
R7024U (6 $\mu\text{m}$ , 2-stage MCP)	110ps	120ps	400ps	—

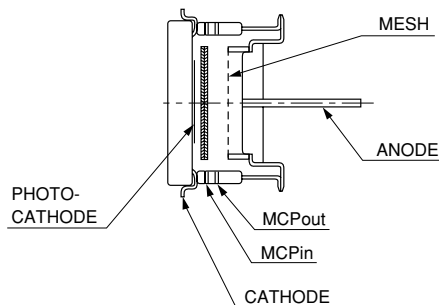
Note: Data in the above table shows typical values including the light source and circuit jitters.

A picosecond laser with a pulse width (FWHM) of less than 35 ps is used for IRF measurement.

The R5916U-50 is a gated MCP-PMT. The R7024U is a triode type MCP-PMT (Figure 10-9).

**Table 10-1: Comparison of MCP-PMT time characteristics**

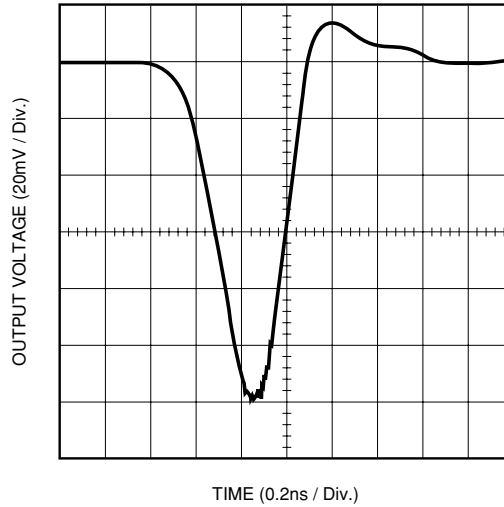
The R7024 MCP-PMT offers significant improvements in rise and fall times. Its structure is shown in Figure 10-9. This tube has been developed specifically for use in ultra-fast photometry. A mesh electrode is provided between the MCPout and the anode as shown in the figure, and the signal output method differs from ordinary MCP-PMTs. The mesh between the MCPout and the anode cancels out the displacement current generated at the time that the secondary electrons emitted from the MCP are accelerated towards the anode. Figure 10-10 shows a typical output waveform from the R7024. Ultrafast time response with 110 picosecond rise time and 120 picosecond fall time is obtained.



THBV3\_1009EA

**Figure 10-9: Structure of the R7024**



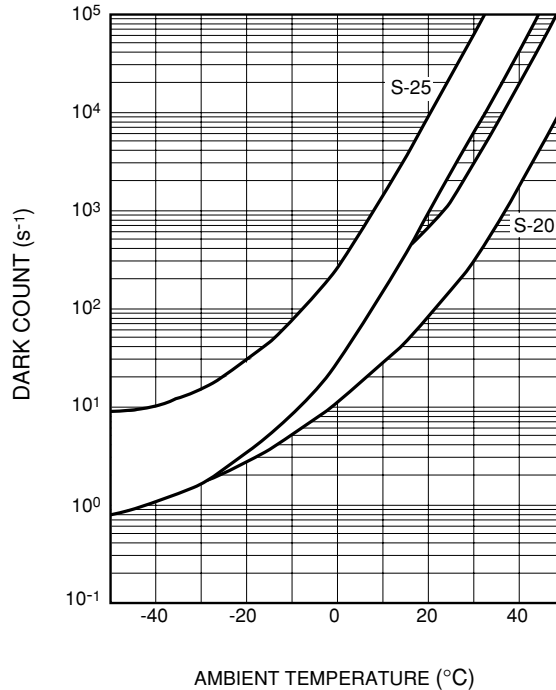


THBV3\_1010EA

Figure 10-10: Time response waveform of the R7024U

### 10.2.3 Temperature characteristics and cooling

As with normal photomultiplier tubes, the dark current and dark count of MCP-PMT greatly depend on the photocathode type and operating temperature. In particular, the dark current and dark count of a multialkali photocathode with enhanced red sensitivity (S-25) are relatively high at room temperatures, so MCP-PMTs using such a photocathode may need to be cooled during operation.



THBV3\_1011EA

**Figure 10-11: Dark count vs. ambient temperature**

Hamamatsu Photonics provides an optional thermoelectric cooler and holder specifically designed for MCP-PMT. Using this cooler and the holder allows easy cooling of an MCP-PMT at a constant temperature of -30°C.

## 10.2.4 Saturation characteristics

In general, the saturation of a photodetector is defined as the phenomenon in which the amount of output signal is no longer proportional to the incident light intensity. In the case of MCP-PMTs, the causes of this saturation are different from those of normal photomultiplier tubes using multiple stages of discrete dynodes. The saturation is caused by the dead time during which the MCP output current is limited and also by space charge effects inside the MCP. Precautions must be taken so that saturation by the dead time will not occur. Saturation characteristics of MCP-PMT are described in detail below.

### (1) Dead time<sup>1)</sup>

When an MCP is irradiated by a pulsed electron current, a positive charge is generated at the MCP output end in accordance with the released electron current. This phenomenon deforms the potential distribution and weakens the electric fields so that the subsequent electron multiplication is suppressed. This charge is neutralized by the strip current flowing through the channel wall. However, a certain amount of time is required for neutralization because the strip current is small due to the high resistance of the MCP. The gain of signals entering within this period is usually low. The time required for neutralization is referred to as the dead time or recovery time. If the output charge per channel is given by  $Q_{out}$  and the strip current per channel by  $I_s$ , then the dead time  $\tau_d$  is given by the following relation:

$$\tau_d = Q_{out} / I_s$$

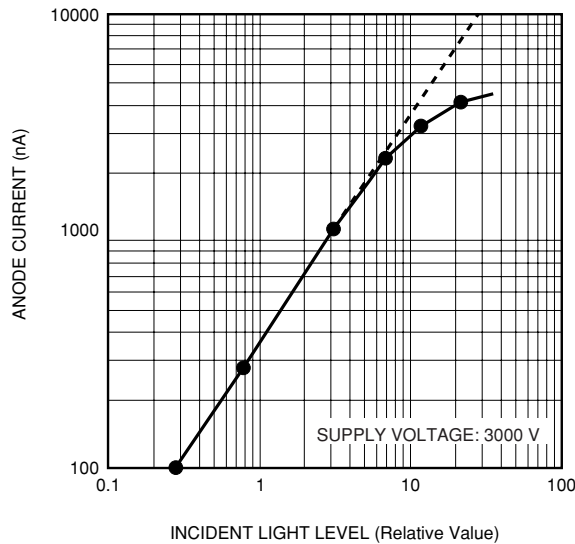
The dead time can be shortened by using a low resistance MCP which allows the strip current  $I_s$  to flow in large quantities. This also improves saturation characteristics.

When an MCP-PMT is operated in such a way that the next electron enters the MCP within this dead time, various types of output saturation occur as described below. If the MCP-PMT is operated at saturated levels, it cannot exhibit adequate performance, and also degrades the photocathode sensitivity and MCP gain.

## (2) Saturation in DC operation

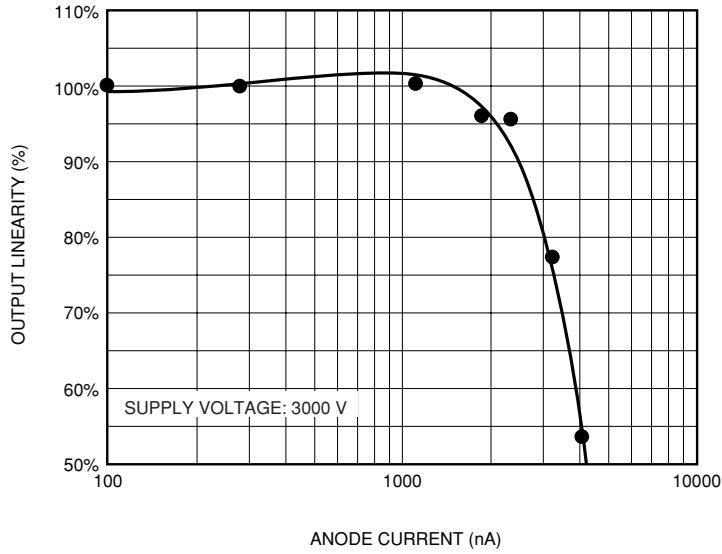
An MCP has a high resistance ranging from tens to hundreds of megohms, which limits the output current from the MCP. Because of this, output current saturation occurs as the input current increases, as shown in Figure 10-12 (a) and (b). This is mainly caused by a decrease in the electric field intensity due to variations in the potential distribution at the output end of the MCP which results from large amounts of secondary electrons from the MCP.

The decrease in the electric field intensity is recovered by the strip current flowing through the channel wall. Saturation in DC operation usually begins to occur when the output current becomes approximately 7 percent or more of the strip current, so use caution.



THBV3\_1012EAa

**Figure 10-12 (a): Saturation characteristics of MCP-PMT (11 mm effective diameter, 6  $\mu\text{m}$  channel diameter) in DC operation (1)**

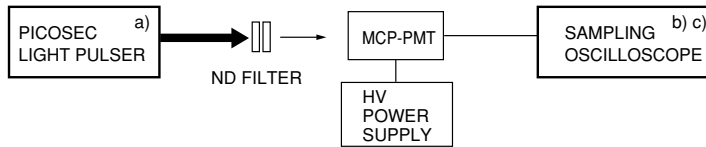


THBV3\_1012EAb

Figure 10-12 (b): Saturation characteristics of MCP-PMT (11 mm effective diameter, 6  $\mu\text{m}$  channel diameter) in DC operation (2)

### (3) Pulse gain saturation characteristics (pulse linearity)

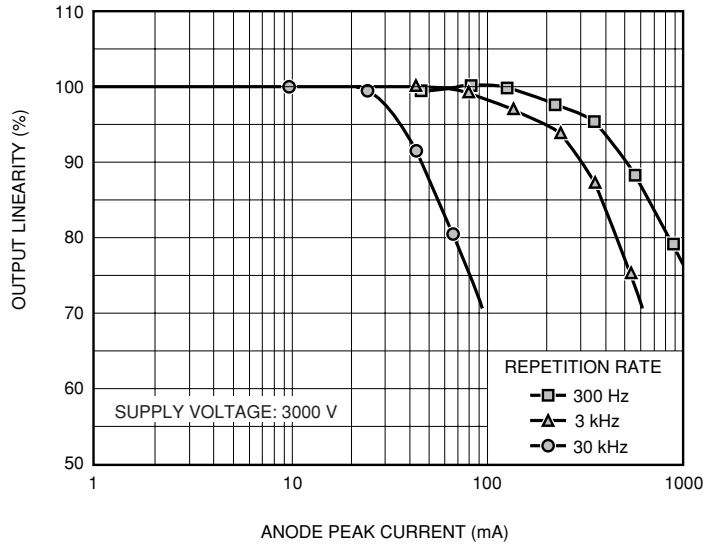
When pulsed light in an extremely short duration enters the MCP-PMT, the output linearity can be maintained to some extent. Figure 10-13 shows the linearity data of an MCP-PMT when it detects pulsed light.



- a) PICOSEC LIGHT PULSER: PLP-01 (HAMAMATSU)  
 WAVELENGTH: 780nm  
 FWHM: 50ps  
 b) SAMPLING OSCILLOSCOPE: 11802 (TEKTRONIX)  
 FREQUENCY BAND: 20GHz  
 c) SAMPLING HEAD: SD-26

THBV3\_1013EAa

Figure 10-13 (a): Block diagram for MCP-PMT pulse linearity measurement



THBV3\_1013Eb

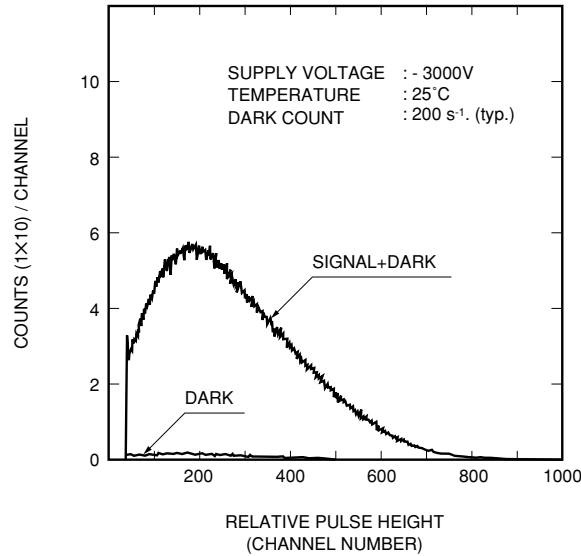
**Figure 10-13 (b): Pulse linearity of an MCP-PMT (11 mm effective diameter, 6 mm channel diameter)**

Figure 10-13 (a) shows a block diagram for measuring pulse linearity. A picosecond light pulser is used as the light source. The intensity of the pulsed light (FWHM 50 ps) is adjusted by ND (neutral density) filters and input to the MCP-PMT. Figure 10-13 (b) shows a typical pulse linearity plot for a proximity-focused MCP-PMT measured at a pulse repetition rate of 300 Hz to 30 kHz. Pulse currents up to a peak of 350 milliamperes can be extracted at a repetition rate of 300 Hz or less. The maximum pulse current at a low repetition rate is determined by the product of the number of electrons released from one channel governed by space charge effects and the number of MCP channels. On the other hand, the maximum pulse current at a high repetition rate is determined by the ratio of the strip current to the total amount of charge which is the product of the charge per pulse and the repetition rate.

When the repetition rate is too high, the MCP gain begins to drop because the next pulse enters within the dead time (see (1) in 10.2.4), causing output saturation.

#### (4) Saturation gain characteristics in photon counting mode

Figure 10-14 shows pulse height distributions of photoelectron signals and dark current pulses taken with an MCP-PMT in the photon counting mode. Unlike single-photon pulse height distributions obtained with normal photomultiplier tubes, a distinct peak is formed in the pulse height distribution obtained with the MCP-PMT. This is due to the saturation occurring in the MCP channel by the space charge effect caused by a single photon.

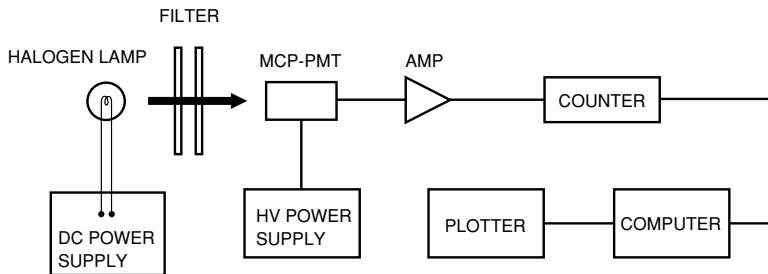


THEV3\_1014EA

Figure 10-14: Typical pulse height distribution in single photon counting

#### (5) Count rate linearity in photon counting

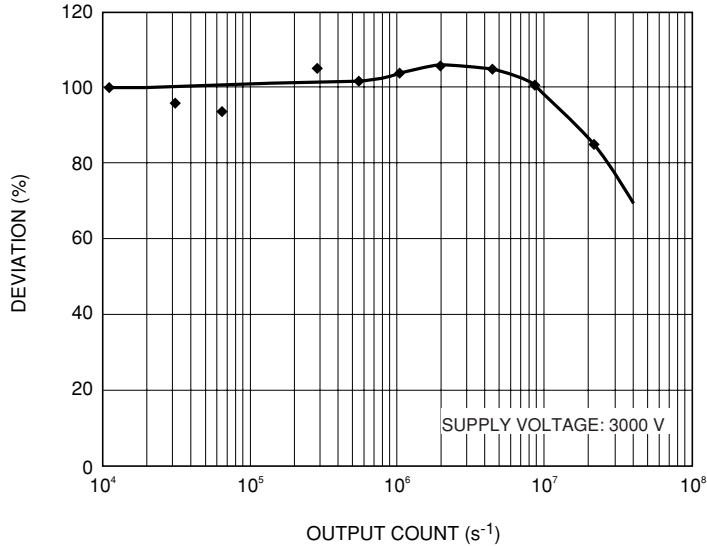
Figure 10-15 illustrates a block diagram for measuring the count-rate pulse linearity in photon counting. Light intensity is reduced by neutral density filters down to the single photoelectron level. The number of single photoelectron pulses is counted by the counter circuit connected to the MCP-PMT, and the count rate is measured and plotted while changing the number of incident photons.



THEV3\_1015EA

Figure 10-15: Block diagram for measuring count-rate linearity in photon counting mode

Figure 10-16 shows count-rate linearity data measured in photon counting mode. A good linearity is maintained up to  $10^7 \text{ s}^{-1}$ .



THBV3\_1016EA

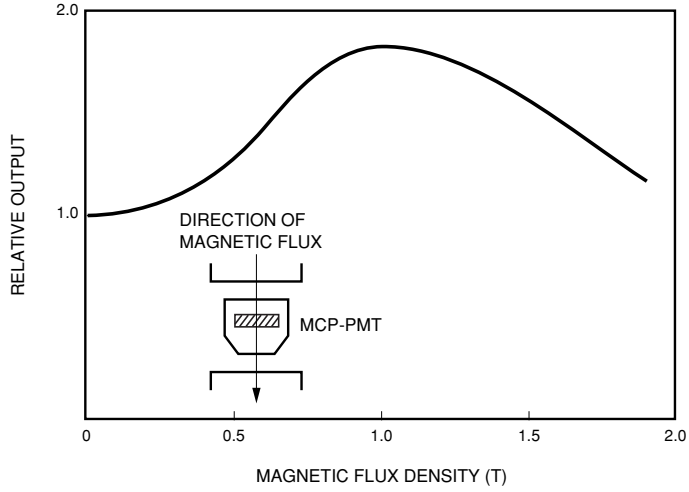
**Figure 10-16: Count-rate linearity of an MCP-PMT (11 mm effective diameter, 6 mm channel diameter) in photon counting mode**

### 10.2.5 Magnetic characteristics<sup>2)</sup>

As stated in the section on photomultiplier tubes designed for use in highly magnetic environments, the following points are essential to improve magnetic characteristics.

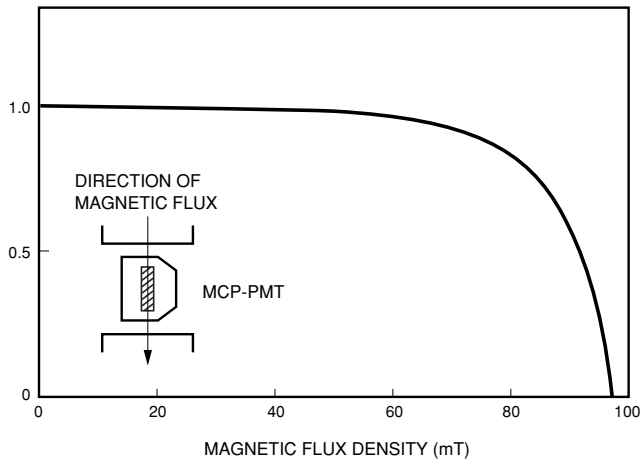
- (1) The distance between the photocathode, dynodes and anode should be shortened to minimize the electron transit distance.
- (2) The electrodes should be designed to apply a parallel electric field from the photocathode to the anode so that the secondary electrons do not converge but travel in parallel to the tube axis.
- (3) A high electric field intensity should be applied.

The MCP-PMT meets all the above requirements and provides superior magnetic characteristics. Figure 10-17 shows typical magnetic characteristics of an MCP-PMT. The extent of the effect of a magnetic field on the output depends on the direction of the magnetic field with respect to the MCP axis. In magnetic fields parallel to the tube axis, the MCP-PMT can operate at up to 2.0 T (20 kilogausses), but in magnetic fields perpendicular to the tube axis, the output drops drastically if fields exceed 70 mT (700 gauss).



THBV3\_1017EAa

(a) When in magnetic fields parallel to tube axis  
 Figure 10-17: Typical magnetic characteristics of an MCP-PMT (1)



THBV3\_1017EAb

(b) When in magnetic fields perpendicular to tube axis  
 Figure 10-17: Typical magnetic characteristics of an MCP-PMT (2)



### 10.3 Gated MCP-PMTs<sup>2)</sup>

In applications in fields such as fluorescence lifetime measurement, laser Raman spectroscopy, and laser radar, photodetectors with a gate function are often required for more precise measurements. The gate function should have the following performance characteristics:

- (1) Highest possible gating speed
- (2) Large switching ratio (gate on/off ratio)
- (3) Low switching noise

Figure 10-18 illustrates the structure of a gated MCP-PMT (R5916U-50). This tube basically consists of a photocathode, gate mesh, MCP and anode. The gating function is performed by controlling the gate mesh which is positioned in close proximity to the photocathode as shown in Figure 10-18. Applying a reverse potential with respect to the photocathode potential to the gate mesh sets the "off" mode, while applying a forward potential sets the gate operation "on" mode.

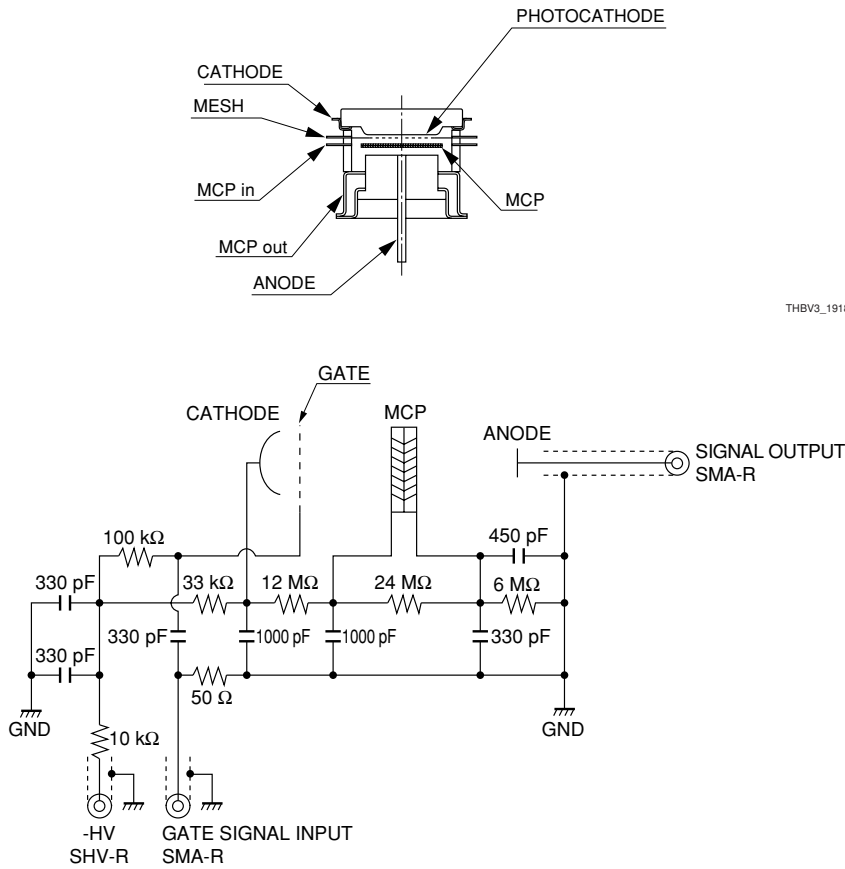
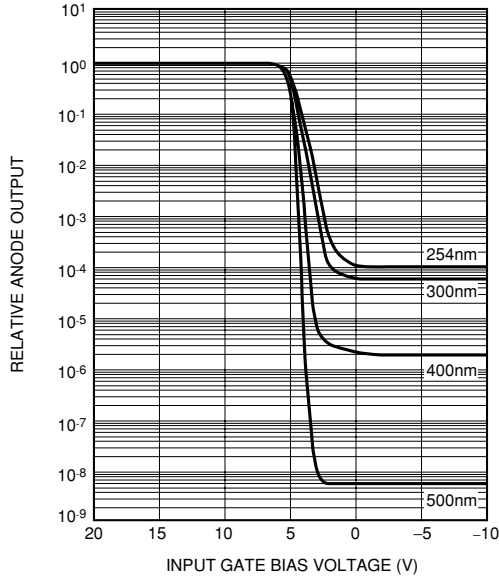


Figure 10-18: Structure of an MCP-PMT with gate mesh and its operating circuit

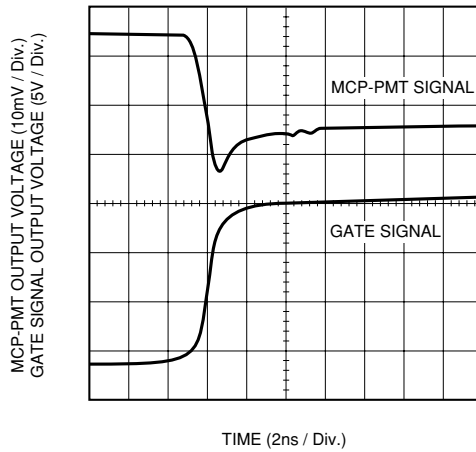
Figure 10-19 shows the basic characteristic of the gate function for a typical switching ratio taken with a gated MCP-PMT operating under static conditions. This data is the relation between the anode output and the voltage applied to the gate mesh (input gate bias voltage) when the photocathode potential is maintained at 0 volts and proves that the switching ratio is better than  $10^8$  (incident light wavelength: 500 nanometers).



THBV3\_1019EA

**Figure 10-19: Switching ratio characteristic under static operating conditions**

Figure 10-20 shows the dynamic gate performance obtained with a gated MCP-PMT when a gate pulse is applied while continuous light is allowed to strike the tube. The MCP-PMT signal starts rising in approximately 1 nanosecond.



THBV3\_1020EA

**Figure 10-20: Dynamic gate characteristic**

As explained above, the gated MCP-PMT offers significant improvement in gate speed and switching ratio in comparison with conventional photomultiplier tubes.

### 10.4 Multianode MCP-PMTs<sup>4)</sup>

The previous sections mainly discussed MCP-PMTs having a single anode. A variety of MCP-PMTs with independent multianodes (R4110U, etc.) have been developed and put to practical use. These multianode MCP-PMTs offer simultaneous, two-dimensional (or one-dimensional) detection as well as fast response speed and low-light-level detection. The structure of a typical multianode MCP-PMT is illustrated in Figure 10-21.

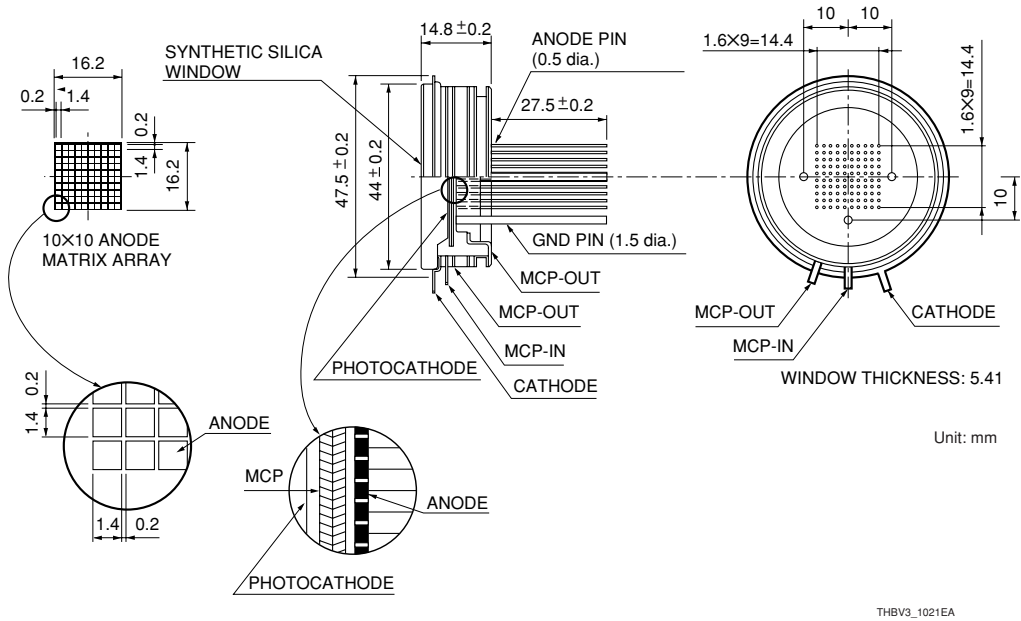
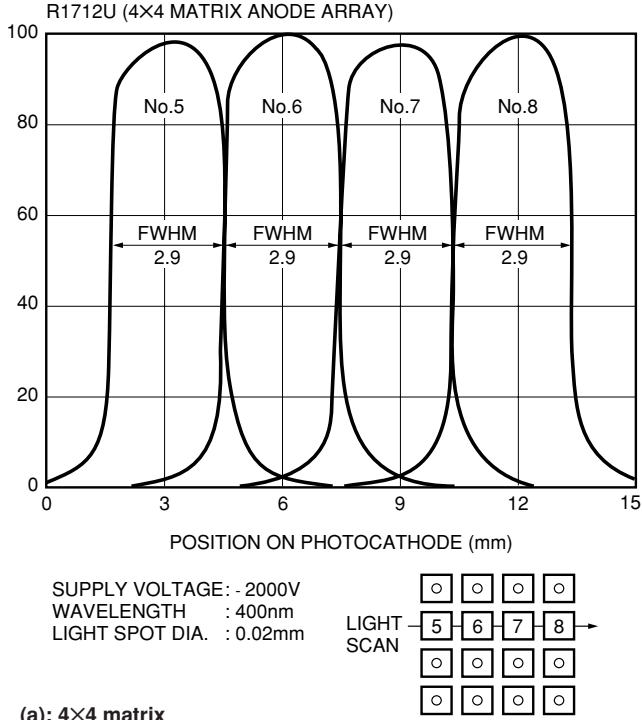
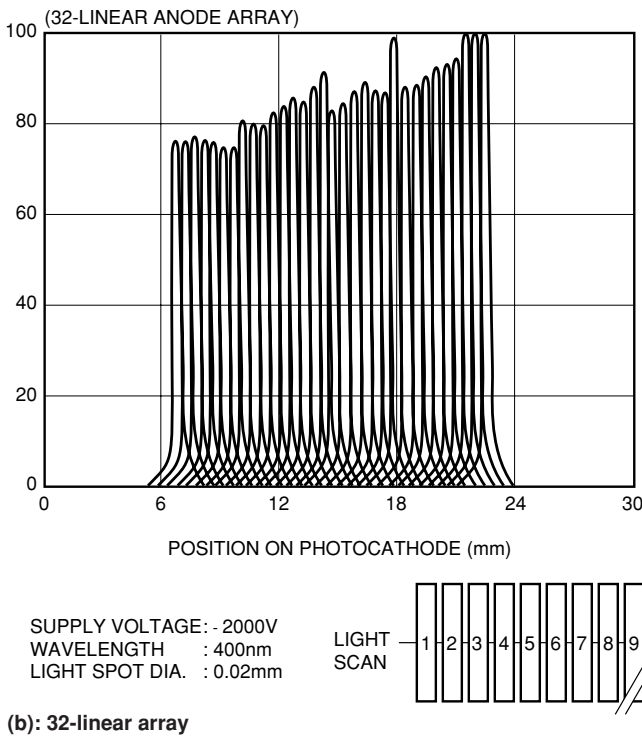


Figure 10-21: Multianode MCP-PMT with 10x10 anode format

Figures 10-22 (a) to (c) show the spatial resolutions of various multianode MCP-PMTs. These consist of the output profile of each anode when a light spot of approximately 20 μm diameter is scanned over the photocathode.

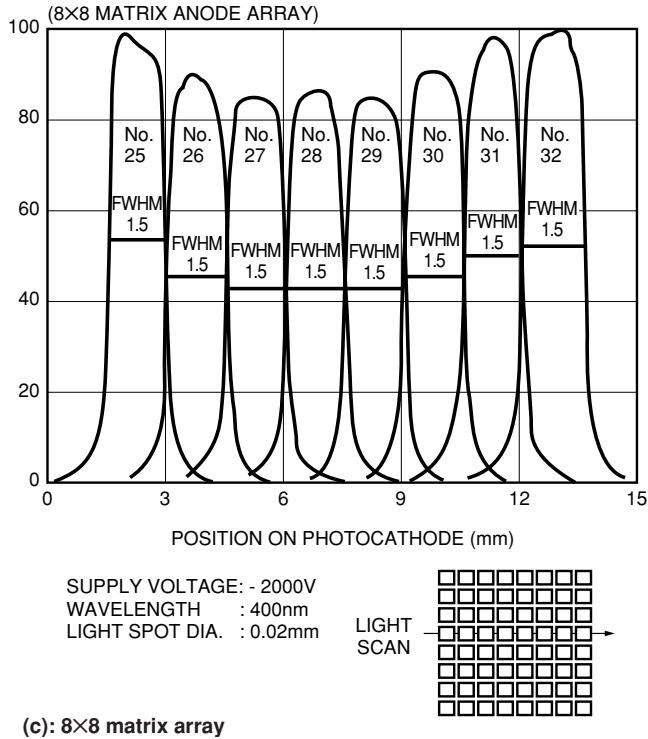


THBV3\_1022EAa



THBV3\_1022EAb

Figure 10-22: Typical spatial resolution (1)



THBV3\_1022EAc

Figure 10-22: Typical spatial resolution (2)

The following applications can take advantage of multianode MCP-PMTs.

- (1) Simultaneous, two-dimensional low-light detection of a luminous body which is spread out over a large space
- (2) Simultaneous, multichannel time-resolved spectroscopy using optical fibers
- (3) Multichannel readout from scintillating fibers

As listed in Table 10-2, the family of multianode MCP-PMTs includes a 4x4 matrix anode type, 8x8 matrix anode type, 10x10 matrix anode type, and a 32 linear anode type. Furthermore, multianode MCP-PMT assembly modules equipped with voltage-divider circuits, connectors and cables are available. The anode configurations listed in Table 10-2 are just typical examples. Other anode configurations and the number of anodes are also available upon request.

Anode Format	
4x4	Matrix anode
8x8	Matrix anode
10x10	Matrix anode
32	Linear anode

Table 10-2: Examples of multianode MCP-PMTs

## References in Chapter 10

- 1) Hamamatsu Photonics Technical Information: MCP assembly, No. TMCP9001E01
- 2) Hamamatsu Photonics Catalog: Ultrafast MCP-PMT R3809U (Feb. 1992).  
Hamamatsu Photonics Catalog: Microchannel Plate - Photomultiplier Tubes (MCP-PMTs), No. T-112-02 (Feb. 1990).  
H. Kume et al.: Ultrafast Microchannel Plate - Photomultiplier Tubes, Applied Optics, Vol. No. 27 (Mar. 15, 1988).
- 3) Hamamatsu Photonics Technical Information: Applications of MCP-PMTs to Time Correlated Single Photon Counting and Related Procedures. No. ET-03 (Feb. 1991).  
Desmond V. O'Connor, David Phillips: Time-Correlated Single Photon Counting, Academic Press (Harcourt Brace Jovanovich, Publishers), The Royal Institution, London, UK.
- 4) Hamamatsu Photonics Catalog: Multianode MCP-PMT Series, No. T-1000 (Feb. 1989).

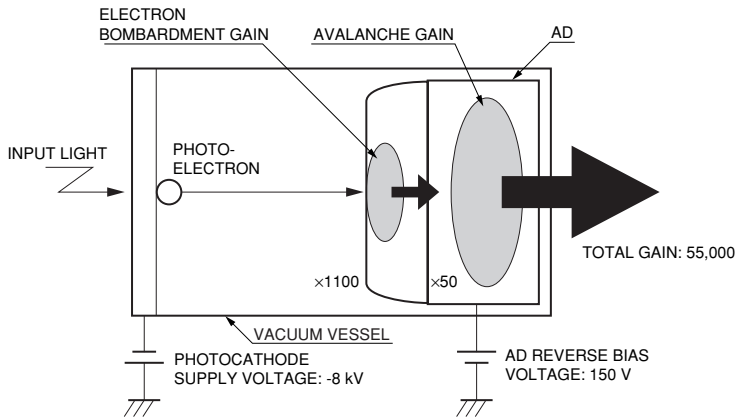
## **CHAPTER 11**

### **HPD (Hybrid Photo-Detector)**

*HPD (Hybrid Photo-Detector) is a completely new photomultiplier tube that incorporates a semiconductor element in an evacuated electron tube. In HPD operation, photoelectrons emitted from the photocathode are accelerated to directly strike the semiconductor where their numbers are increased. Features offered by the HPD are extremely little fluctuation during the multiplication, high electron resolution, and excellent stability.*

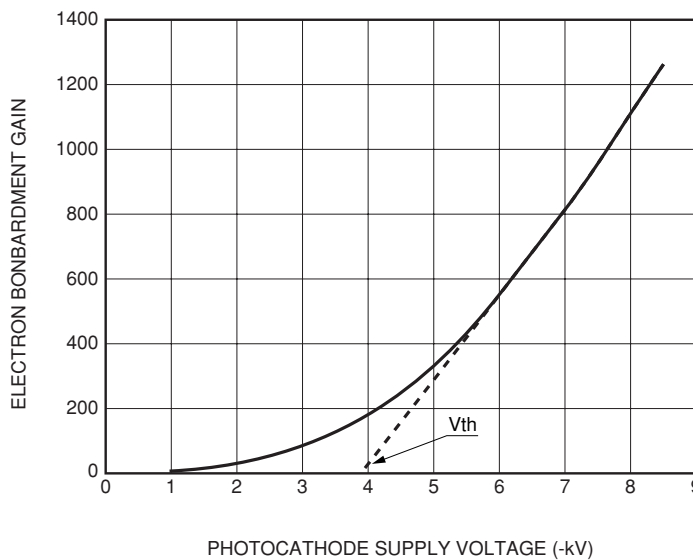
### 11.1 Operating Principle of HPDs

As shown in Figure 11-1, an HPD consists of a photocathode for converting light into photoelectrons and a semiconductor element (avalanche diode or AD) which is the target for "electron bombardment" by photoelectrons. The HPD operates on the following principle: when light enters the photocathode, photoelectrons are emitted according to the amount of light; these photoelectrons are accelerated by a high-intensity electric field of a few kilovolts to several dozen kilovolts applied to the photocathode; they are then bombarded onto the target semiconductor where electron-hole pairs are generated according to the incident energy of the photoelectrons. This is called "electron bombardment gain". A typical relation between this electron bombardment gain and the photocathode supply voltage is plotted in Figure 11-2. In principle, this electron bombardment gain is proportional to the photocathode supply voltage. However, there is actually a loss of energy in the electron bombardment due to the insensitive surface layer of the semiconductor, so their proportional relation does not hold at a low voltage. In Figure 11-2, the voltage at a point on the voltage axis (horizontal axis) where the dotted line intersects is called the threshold voltage [ $V_{th}$ ]. Electron bombardment gain increases in proportion to the electron incident energy in a region higher than a photocathode supply voltage near the threshold voltage.



THBV3\_1101EA

Figure 11-1: Schematic diagram of HPD



THBV3\_1102EA

Figure 11-2: Electron bombardment gain characteristics



The internal silicon avalanche diode (AD) in an HPD generates an electron and hole pair per incident energy of approximately 3.6 eV. The electron bombardment gain  $G_b$  can be expressed by using the electrical potential difference  $V_{pc}$  [V] between the photocathode and the semiconductor element (This is equal to the photocathode supply voltage.) and the threshold voltage [ $V_{th}$ ] determined by the semiconductor element.

$$G_b = \frac{(V_{pc} - V_{th})}{3.6} \dots\dots\dots \text{(Eq. 11-1)}$$

In Figure 11-2,  $V_{th}$  is approximately 4 kilovolts.

The cluster of secondary electrons acquired by electron bombardment is further multiplied by the avalanche gain in the semiconductor (avalanche diode) according to the bias voltage applied to the semiconductor. If the gain of the avalanche diode (AD) is  $G_t$ , then the HPD total gain  $G$  is calculated as follows:

$$G = G_b \times G_t \dots\dots\dots \text{(Eq. 11-2)}$$

In the case of the R7110U series HPD, the electron bombardment gain  $G_b$  is approximately 1,100 when the photocathode supply voltage is -8 kilovolts. Furthermore, the avalanche gain  $G_t$  of approximately 50 times can be attained by applying a proper reverse voltage to the AD. Thus the total gain  $G$  will be approximately 55,000.

## 11.2 Comparison with Photomultiplier Tubes

This section compares HPD with photomultiplier tubes widely used in low-light-level measurement and discusses their different characteristics. The electron bombardment gain of an HPD corresponds to the gain attained by the first dynode of a photomultiplier tube. As stated earlier, the HPD delivers an electron bombardment gain of about 1,100 (at photocathode voltage of -8 kilovolts) which is much higher than conventional photomultiplier tubes, so that the gain fluctuation can be significantly reduced. This means that when used in pulsed light measurement in a region of several photons, the HPD can measure a pulse height distribution with separate peaks that correspond to 1 to 5 photoelectrons. In this point, the HPD is superior to conventional photomultiplier tubes. Moreover, the HPD multiplication mechanism is simple so that it exhibits advantages in applications where quantitative property, reproducibility and stability are essential factors. Table 11-1 compares major HPD and ordinary photomultiplier tube characteristics.

Item	HPD	Description
Pulse height resolution	Extremely good	Since HPD has a high electron bombardment gain that corresponds to the first dynode gain of conventional photomultiplier tubes, a pulse height distribution with separated peaks created by 1 to 5 photoelectrons can be output. Using a low noise amplifier is important to make full use of the HPD characteristics.
Multiplication fluctuation	Extremely small	Fluctuation in the HPD electron multiplication is reduced nearly to the theoretical limit due to high electron bombardment gain.
Drift and life	Good	Short-term instability is called "drift", while long-term variation is called "life". Since HPD has no dynodes, both drift and life characteristics are superior to those of photomultiplier tubes.
Light hysteresis	Good	When incident light is changed in a step function, the output might not be comparable with the same step function. This phenomenon is called "hysteresis". The HPD multiplication process is simple since electrons emitted from the photocathode only enter the AD. Light hysteresis characteristics are good compared to those of photomultiplier tubes.
Afterpulse	Extremely good	In pulse measurement, spurious pulses might appear following the output pulse of a true signal. These spurious pulses are called "afterpulses". Since the HPD structure is simple, there are very few afterpulses compared to those of photomultiplier tubes.
Linearity	Good	The HPD offers good output current linearity over a wide range of input light levels. However, the output deviates from the ideal linearity when extremely strong light is input. The HPD output linearity is limited by two factors: electrical resistance of photocathode and avalanche multiplication linearity.
Gain	Low ( $5 \times 10^4$ )	In applications for detecting low-level light at high speeds, using an ordinary photomultiplier tube with a high gain will prove best. Since the HPD gain is lower than photomultiplier tubes, it should be used with a low noise amplifier.
Gain variation	Extremely small	The HPD features very small variations in the electron bombardment gain.
Uniformity	Good	Uniformity is the variation in sensitivity versus the photocathode position. HPD electron bombardment gain does not depend on the incident position so that the anode output exhibits good uniformity characteristics.
Temperature characteristics	Gain depends greatly on temperature.	Gain depends on temperature characteristics of the internal AD into which electrons are bombarded.
Vibration resistance	Good	HPD is highly resistant to vibration due to its simple structure.
Collection efficiency	Extremely good	Electron trajectories in HPD were designed so that all electrons emitted from the photocathode strike the internal AD for electron bombardment multiplication. (However, there are a few electrons that reflect off the surface of the AD but these have no effect on the signal.)

Table 11-1: Comparison with photomultiplier tubes

## 11.3 Various Characteristics of HPDs

### 11.3.1 Multi-photoelectron resolution

Since the electron bombardment gain that corresponds to the gain of the first dynode of a conventional photomultiplier tube is as high as 1,100 (at photocathode voltage of -8 kilovolts), the HPD offers ideal signal amplification with very little fluctuation in the multiplication. For example, when pulsed light adjusted so the photocathode emits 3 photoelectrons on average is repeatedly input to an HPD, multiple peaks corresponding to 1 to 5 photoelectrons can be detected by measuring the output pulse height. Figure 11-3 shows this example. The reason why these multiple peaks can be detected is that fluctuation in the electron multiplication is extremely small. This is the HPD's most significant feature. Due to this feature, single-electron pulse-height resolution, which is about 30 % (FWHM), is also excellent.

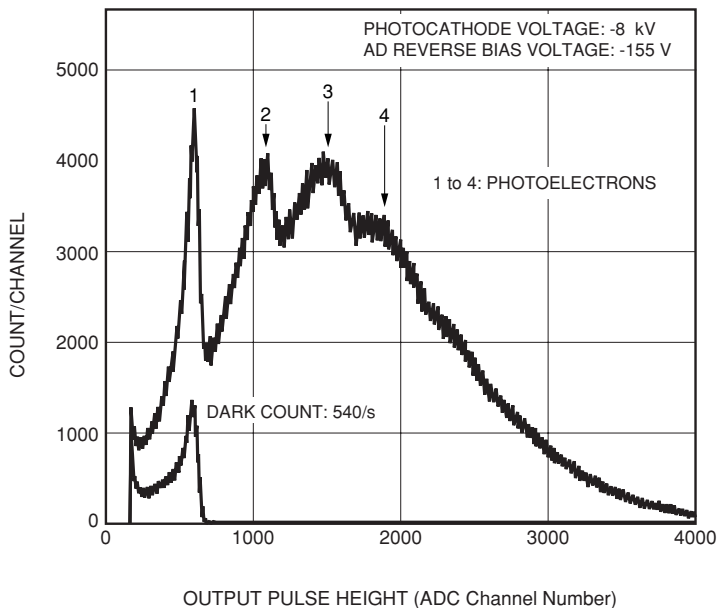
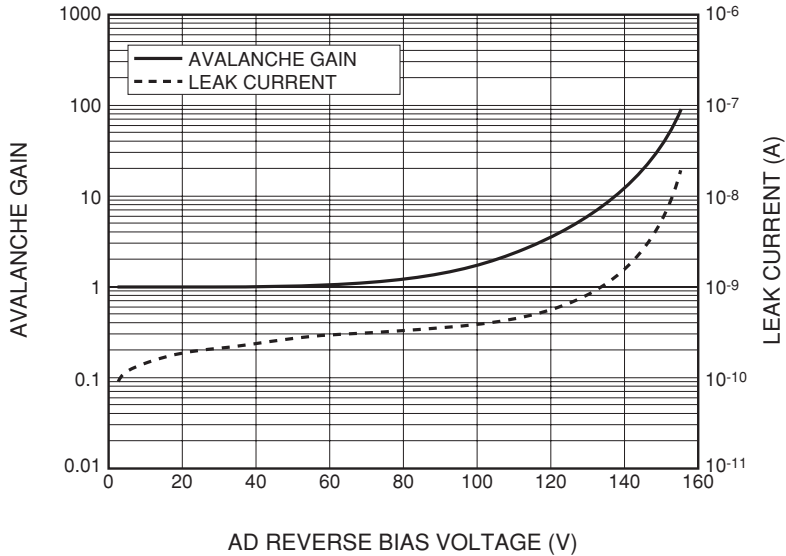


Figure 11-3: Multi-photoelectron counting characteristics

### 11.3.2 Gain characteristics and electron bombardment gain uniformity

As explained in the operating principle section, the HPD gain is expressed by the product of the electron bombardment gain  $G_b$  and the avalanche gain  $G_t$ . (See Eq. 11-2.) As shown in Figure 11-2, when a certain threshold voltage is exceeded, the electron bombardment gain of the R7110U series increases in proportion to the photocathode supply voltage according to Eq. 11-1. The avalanche gain characteristics of the internal AD are plotted in Figure 11-4. The avalanche gain gradually increases from a point where the voltage applied to the AD exceeds about 100 volts and sharply increases when the breakdown voltage (voltage at which the leak current reaches 1 microampere) is approached. It is difficult to maintain stable operation if the reverse bias voltage is set near the breakdown voltage around which the gain increases sharply. Generally, the HPD should be used at an avalanche gain of 50 or less. The avalanche gain differs slightly depending on the production lot of the semiconductor element. In the case of the semiconductor element shown in Figure 11-4, the avalanche gain is 10 at 138 volts, 30 at 149 volts and 60 at 153 volts. Figure 11-4 also shows leak current characteristics versus the reverse bias voltage applied to the AD. These gain characteristics are common to all models of the R7110U series.

The avalanche gain has temperature dependence as discussed later in section 11.3.8, "Temperature characteristics".

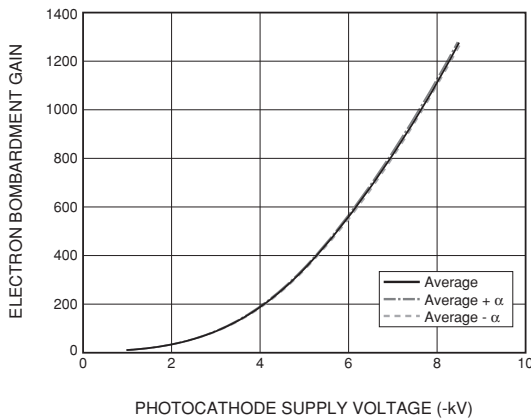


THBV3\_1104EA

Figure 11-4: Avalanche gain and leak current characteristics of internal AD

Individual differences in electron bombardment gain characteristics of the R7110U series are shown in Figure 11-5 and Table 11-2. The HPD electron bombardment gain depends on the electron accelerating voltage and the structure of the AD's electron incident surface. Generally, the AD's electron incident surface is uniform, so individual differences in electron bombardment gain are very small as long as the photocathode supply voltage is the same. This is a large advantage not available from photomultiplier tubes using an array of dynodes.

On the other hand, there are individual differences in avalanche gain even if operated at the same AD reverse bias voltage. Although care should be taken regarding this point, adjusting the reverse bias voltage allows you to easily adjust the avalanche gain to the same level. In this case, unlike photomultiplier tubes, there are almost no adverse effects on time characteristics.



THBV3\_1105EA

Photocathode Supply Voltage (-kV)	Average Electron Bombardment Gain	Standard Deviation ( $\sigma$ )
1	9.3	0.3
2	31.9	0.6
4	181.9	2.4
6	560.0	6.9
8	1118.3	9.9
8.5	1270.7	13.4

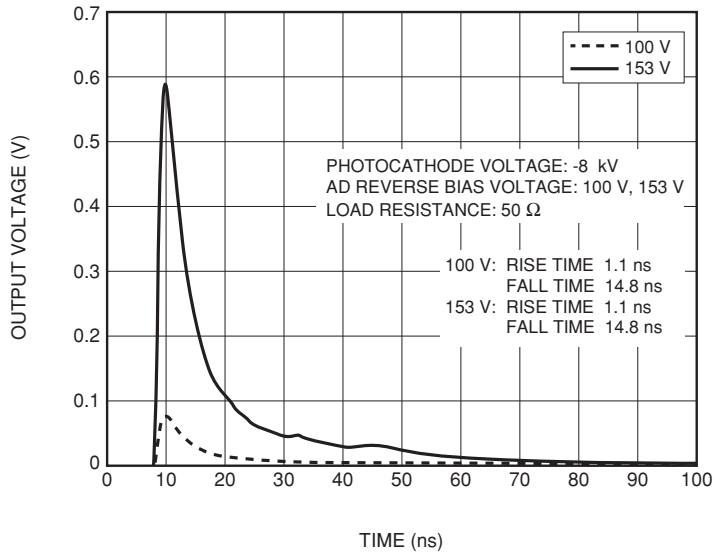
Number of Samples: 19

Figure 11-5: Individual differences in electron bombardment gain

Table 11-2: Numerical data

### 11.3.3 Time response characteristics

Figure 11-6 shows a typical output waveform of the R7110U series. This output waveform was obtained by inputting a light pulse from a PLP (semiconductor pulse laser of approximately 60 picoseconds FWHM and 400 nanometers wavelength). Time response characteristics of the R7110U series are determined by the capacitance (approx. 140 picofarads) of the internal AD which becomes nearly constant when a bias voltage higher than 60 volts is applied to the AD since the AD is fully depleted. The difference in the pulse height between peaks at an AD reverse bias voltage of 100 volts and 153 volts indicates the difference in the avalanche gain between each bias voltage. Transit time spread (TTS) of single photoelectron pulses is approximately 450 picoseconds for the R7110U series. These time characteristics are common to all models of the R7110U series.



THBV3\_1106EA

Figure 11-6: Time response waveform

### 11.3.4 Uniformity

Uniformity is the variation of sensitivity versus the photocathode position. Typical anode uniformity characteristics for the R7110U-07 (effective photocathode area: 8 millimeters in diameter) are shown in Figure 11-7. The HPD anode uniformity is determined by the photocathode sensitivity uniformity and the AD gain uniformity. The figure demonstrates that the HPD has very uniform sensitivity.

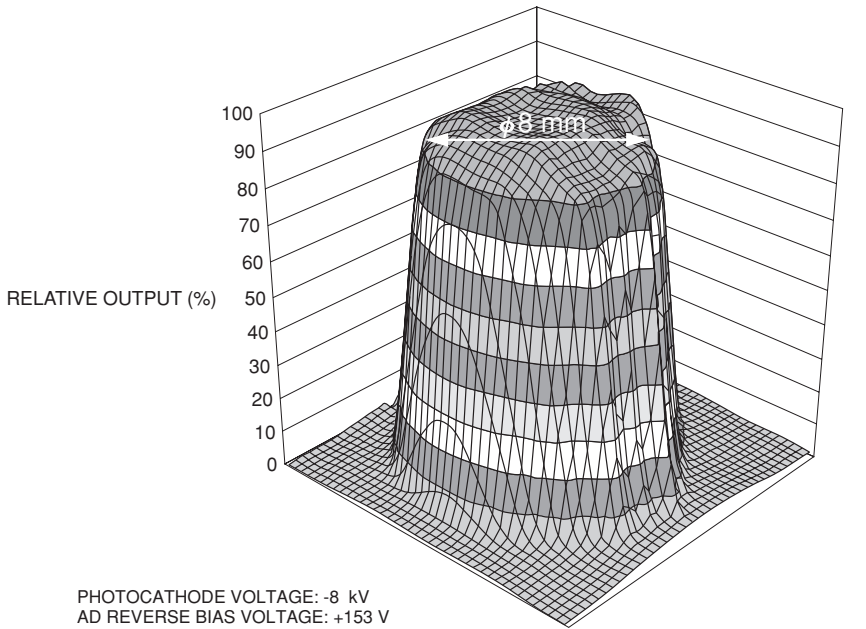
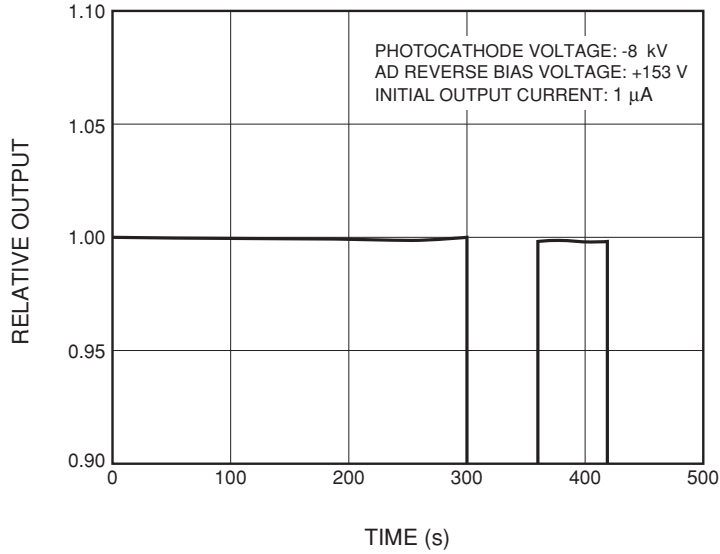


Figure 11-7: Uniformity

### 11.3.5 Light hysteresis characteristics

When incident light is changed in a step function, the output might not be comparable with that same step function. This phenomenon is called "hysteresis". Hysteresis characteristics of an HPD are shown in Figure 11-8. In the case of photomultiplier tubes, light hysteresis tends to occur in the multiplication process repeated by the dynodes. On the other hand, HPD exhibits extremely good hysteresis because the multiplication process is simple since the electrons emitted from the photocathode only enter the AD.

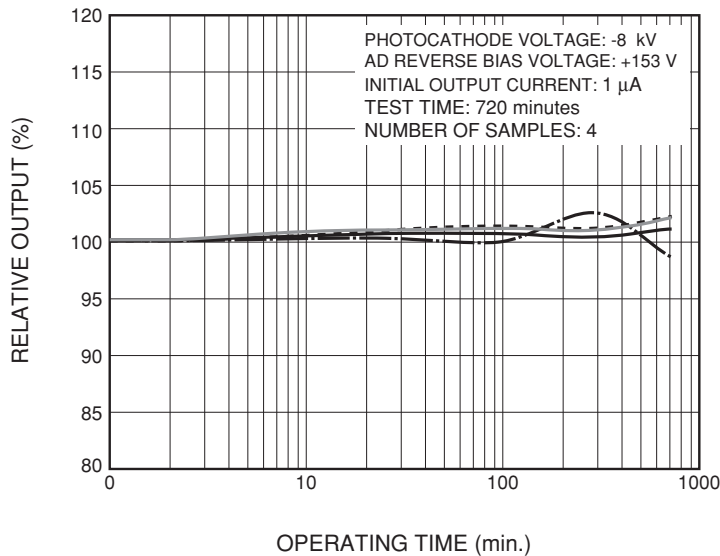


THBV3\_1108EA

Figure 11-8: Light hysteresis characteristics

### 11.3.6 Drift characteristics (short-term stability)

Figure 11-9 shows typical output variations of the R7110U series, measured over a short time period of 12 hours (720 minutes). In photomultiplier tubes, drift is mainly caused by deterioration of the dynodes. Since HPD has no dynodes, good drift characteristics are ensured.



THBV3\_1109EA

Figure 11-9: Drift characteristics

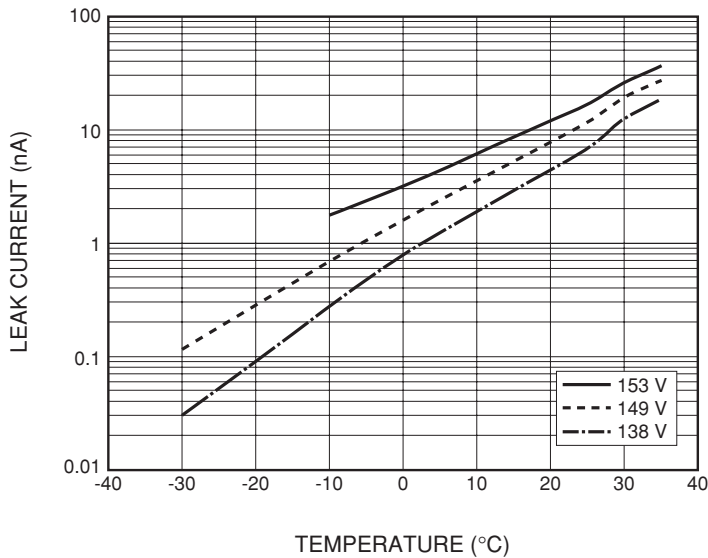
### 11.3.7 Magnetic characteristics

The HPD operation is very simple in that photoelectrons emitted from the photocathode are directly bombarded into the semiconductor (avalanche diode or AD). This makes the electron trajectories simple enough so that the photoelectrons can be focused onto the semiconductor by an electron lens. Because of this, the effective photocathode area is limited to a size equal to the effective diameter of the AD (3 millimeters for the R7110U series). Due to this structure, theoretically the output will not change even in a strong magnetic field as long as its direction is parallel to the HPD tube axial direction.

### 11.3.8 Temperature characteristics

Typical temperature characteristics of AD leak current in the R7110U series are shown in Figure 11-10. Each reverse bias voltage shows a similar tendency in that the AD leak current increases with temperature. The avalanche gain, in contrast, decreases with temperature rise as stated below. (See Figure 11-11.) Nonetheless, the leak current increases with temperature.

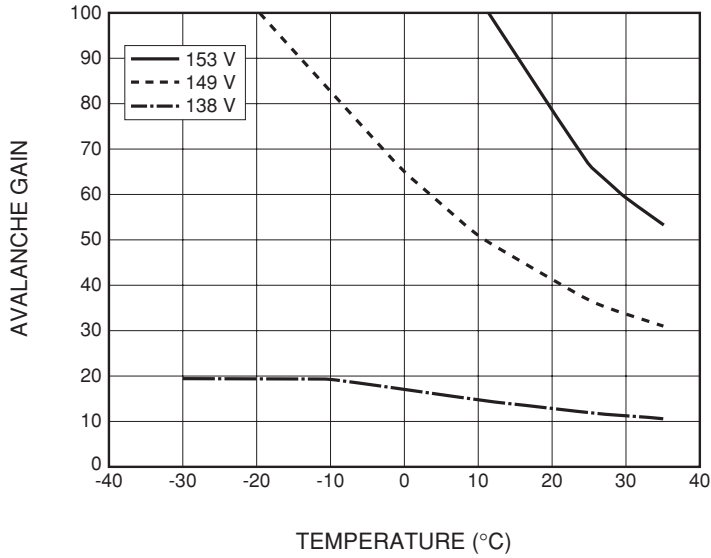
Figure 11-11 shows temperature characteristics of avalanche gain. In a range from  $-10^{\circ}\text{C}$  to  $35^{\circ}\text{C}$ , the avalanche gain temperature coefficient does not change greatly. It is approximately  $-1\%/^{\circ}\text{C}$  at an AD reverse bias voltage of 138 volts. However, it increases to about  $-2.1\%/^{\circ}\text{C}$  at 149 volts and to  $-3.3\%/^{\circ}\text{C}$  at 153 volts. The AD temperature must therefore be controlled to ensure stable HPD operation while obtaining a high avalanche gain. When the HPD is used with the AD reverse bias voltage maintained at a constant value, there is an extreme increase in gain as the temperature lowers. So care must be taken to prevent the AD from being damaged.



THBV3\_1110EA

Figure 11-10: Temperature characteristics of AD leak current



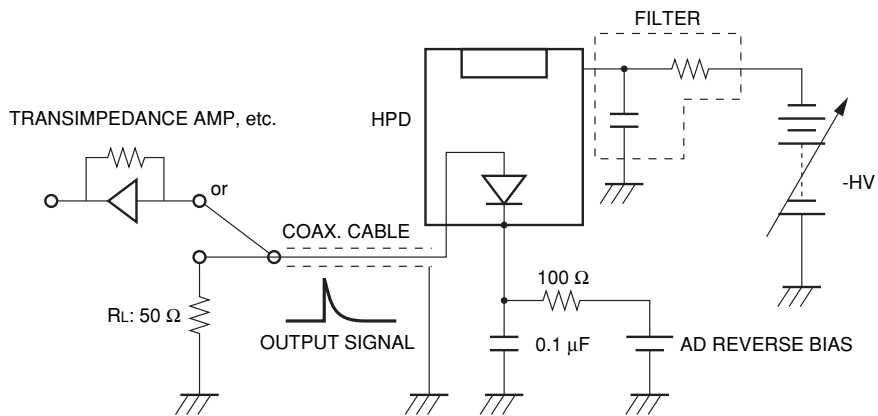


THBV3\_1111EA

Figure 11-11: Temperature characteristics of AD avalanche gain

## 11.4 Connection Examples (R7110U Series)

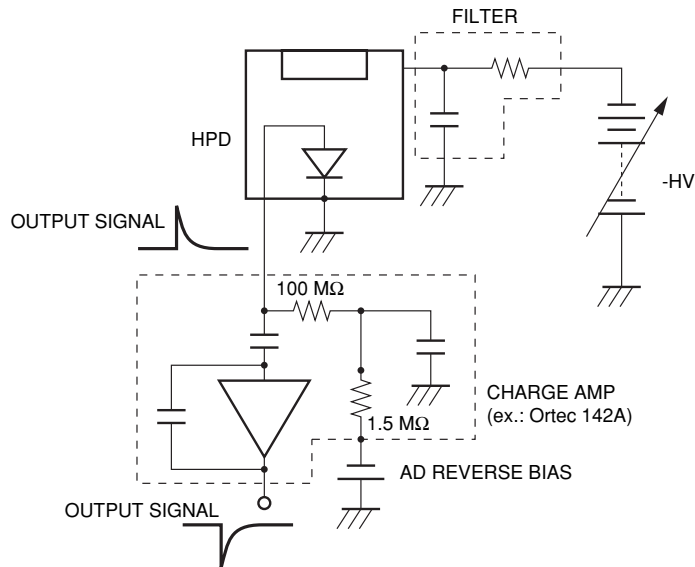
### 11.4.1 When handling DC signal (including connection to transimpedance amp)



THBV3\_1112EA

Figure 11-12: DC mode connection example

### 11.4.2 When handling pulse signal (including connection to charge amp)



THBV3\_1113EA

Figure 11-13: Pulse mode connection example

## References in Chapter 11

- 1) Hamamatsu Photonics: "Hybrid Photo Detector (HPD) R7110U Series" technical manual

# **CHAPTER 12**

## **ELECTRON MULTIPLIER TUBES AND ION DETECTORS**

*Electron multiplier tubes (EMT) are capable of detecting light at relatively short wavelengths such as soft X-rays and vacuum UV (VUV) radiation and charged particles such as electrons and ions. Ion detectors are designed and optimized for ion detection in mass spectrometers.<sup>1)2)3)</sup>*

*This chapter describes the structures and characteristics of electron multiplier tubes and ion detectors.*

## 12.1 Structure

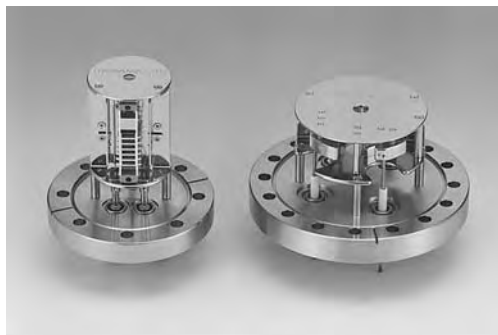
The structure of an electron multiplier tube is basically identical to the dynode assembly and anode used in photomultiplier tubes. The dynode structure is selected according to the required characteristics, size and shape. (See 4.2.1 in Chapter 4.) Figure 12-1 shows typical electron multiplier tubes.



**Figure 12-1: Electron multiplier tubes**

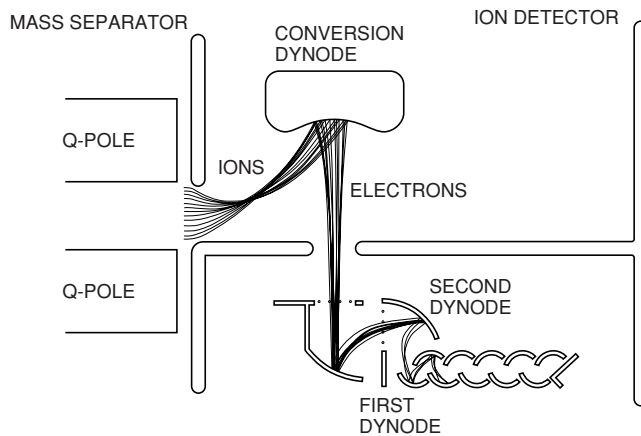
An electron multiplier tube is operated in a vacuum, and the ions, electrons, VUV radiation, or soft X-rays to be detected are guided so as to enter the first dynode. The first dynode excited by such particles or radiation emits secondary electrons or photoelectrons. These generated electrons are multiplied in a cascade by the second and following dynodes and a cluster of secondary electrons finally reaches the anode. Electron multiplier tubes come with built-in voltage-divider resistors that supply an optimum voltage between each dynode. A holder is also mounted for holding the electron multiplier tube.

Ion detectors are used for ion detection in mass spectrometers (see 14.10.1 in Chapter 14). As with electron multiplier tubes, ion detectors consist of a dynode section, an anode, voltage-divider resistors, holder, and a Faraday cup or conversion cup needed for various types of mass spectrometers. The dynode type uses linear-focused type dynodes (see 4.2.1 in Chapter 4). Figure 12-2 shows typical ion detectors assembled with a conversion dynode.



**Figure 12-2: Ion detectors with conversion dynode**

In a mass spectrometer, ions that have passed through the mass separator are accelerated onto the conversion dynode to which a high voltage is applied. Electrons emitted from the conversion dynode by the incident ions then enter the first dynode where secondary electrons are emitted from the secondary emissive surfaces. These secondary electrons are multiplied by the other dynodes and a cluster of electrons finally reaches the anode. Ion detectors are designed so that these electron conversion and multiplication processes are optimized. Figure 12-3 shows the ion detection mechanism in an ion detector with a conversion dynode.



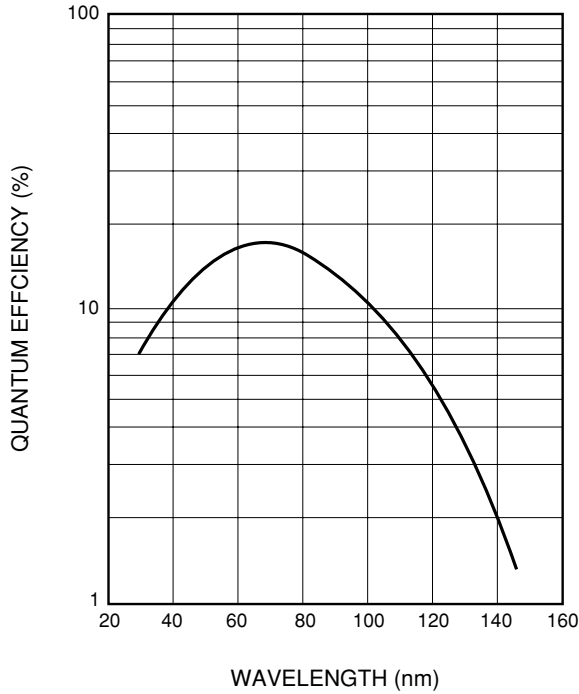
**Figure 12-3: Ion detection by an ion detector with a conversion dynode**

The secondary emissive surface of each dynode is activated by special oxidation processing formed on a copper electrode containing several percent beryllium. This secondary emissive surface efficiently emits secondary electrons from the input of soft rays, vacuum UV radiation, electrons, and ions. Another type of dynode uses a secondary emissive surface made of aluminum oxide which provides stable characteristics with extremely low deterioration even if left in air.

## 12.2 Characteristics

### 12.2.1 Sensitivity to soft X-rays, VUV, electrons and ions

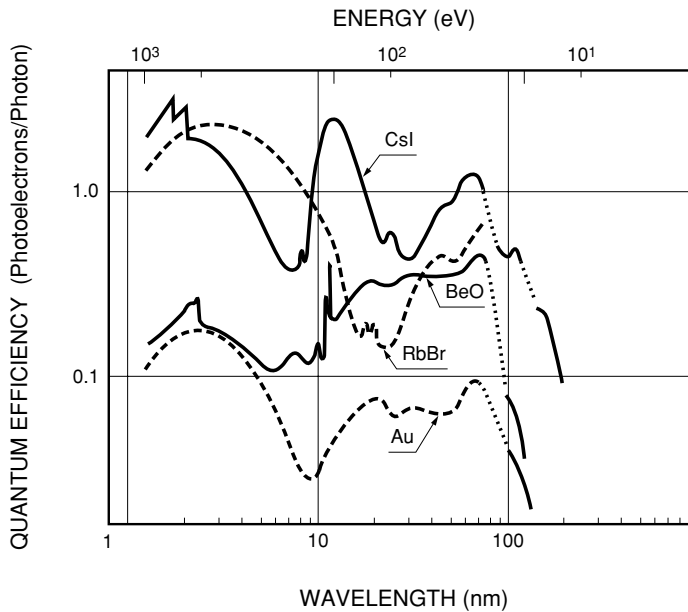
Beryllium oxide (BeO) generally used in the first dynode of electron multiplier tubes is sensitive to soft X-rays to UV radiation at nearly 300 nanometers. Electron multiplier tubes are effective detectors when in a wavelength range shorter than the cutoff wavelength of the MgF<sub>2</sub> window (approximately 115 nanometers). (See 4.1 in Chapter 4.) A typical spectral response for beryllium oxide is shown in Figure 12-4, covering a range from 30 to 140 nanometers.



THBV3\_1204EA

Figure 12-4: Spectral response characteristic of beryllium oxide

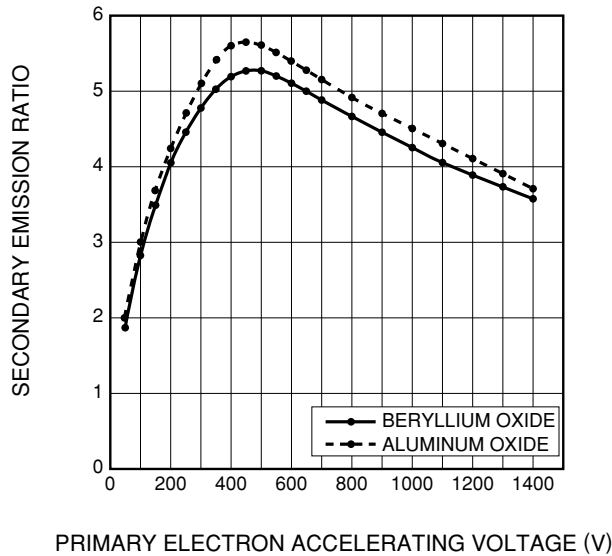
Various spectral response characteristics are available by replacing the first dynode of electron multiplier tubes with another type that are evaporated with alkali halide materials such as CsI, CuI, KCl and MgF<sub>2</sub> optimized for the target wavelength range and operating conditions. However, these materials are subject to deliquescence and require careful handling. Typical spectral response characteristics (reference values) of CsI, BeO, RbBr and Au are shown in Figure 12-5.



THBV3\_1205EA

Figure 12-5: Spectral response characteristics of various substances (reference values)

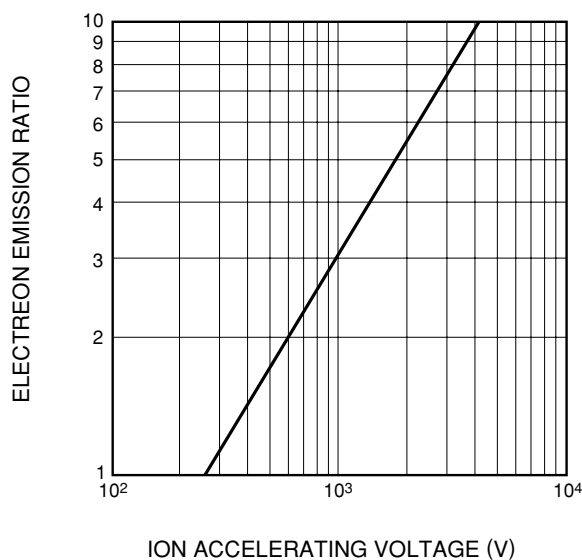
The first dynode of electron multiplier tubes is sensitive to electrons with energy such as Auger electrons, secondary electrons and reflected electrons (see 2.3 in Chapter 2). Figure 12-6 shows typical secondary emission ratio versus primary electron accelerating voltage for beryllium oxide and aluminum oxide. The secondary emission ratio peaks at a primary electron accelerating voltage of about 400 to 500 volts.



THBV3\_1206EA

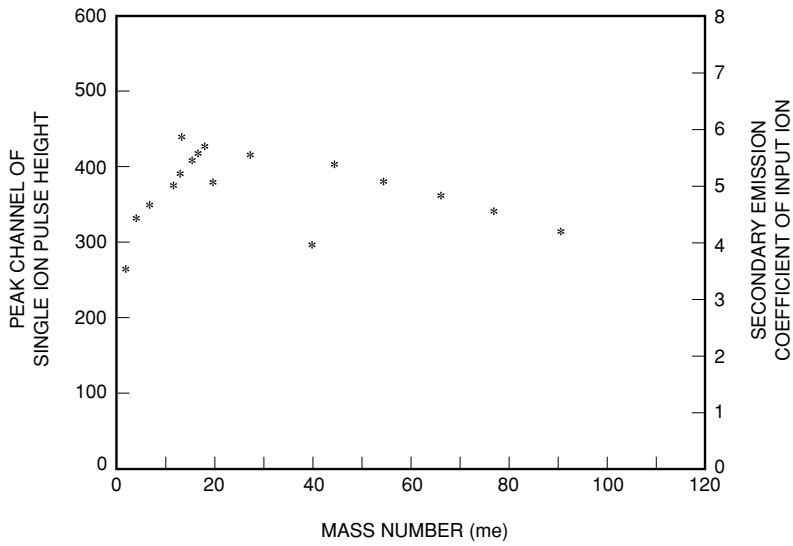
**Figure 12-6: Secondary emission ratio vs. primary electron accelerating voltage**

The first dynode of electron multiplier tubes is also sensitive to ions. Typically, several electrons are emitted in response to one ion, although this ratio depends slightly on the state of the secondary electron emissive surface on the first dynode. The number of emitted electrons is also affected by the molecular weight ( $m/z$ )<sup>5</sup> and ion accelerating voltage. Figure 12-7 shows the relation between the electron emission ratio and the accelerating voltage. In Figure 12-8, typical electron emission ratios at an accelerating voltage of 2,000 volts are plotted for various types of ions.



THBV3\_1207EA

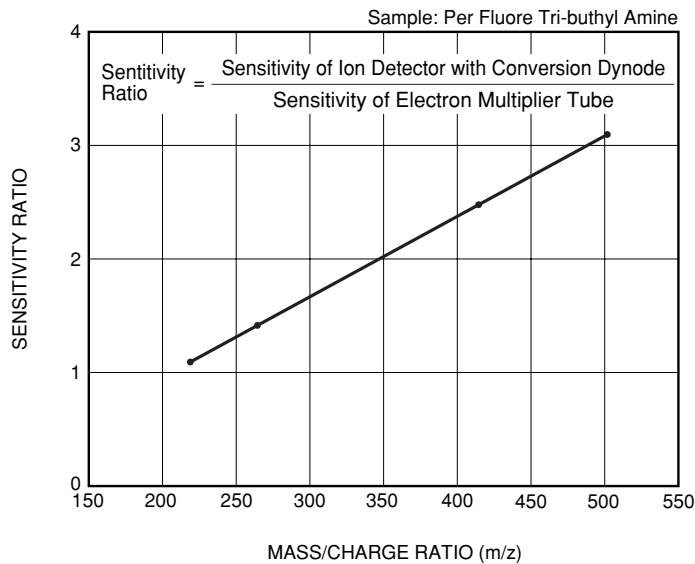
**Figure 12-7: Electron emission ratio vs. accelerating voltage for nitrogen ions**



THBV3\_1208EA

**Figure 12-8: Electron emission ratios for various kinds of ions at 2000 V accelerating voltage**

Most ion detectors have a conversion dynode applied with a high voltage and positioned before the first dynode. This conversion dynode converts ions into electrons like the first dynode used in photomultiplier tubes does. The ion-to-electron conversion efficiency is proportional to the speed at which ions strike the surface of the conversion dynode.<sup>4)</sup> Because of this, the conversion dynode is designed to increase the speed of the incident ions and to enhance the conversion efficiency. Figure 12-9 shows the difference in sensitivity between an electron multiplier and an ion detector with a conversion dynode. The effect of the conversion dynode is more significant in a higher mass/charge ratio region.<sup>5)</sup>



THBV3\_1209EA

**Figure 12-9: Sensitivity improvement in ion detector with conversion dynode**



## 12.2.2 Gain

As in the case of photomultiplier tubes, the current amplification or gain of an electron multiplier tube is expressed as follows.

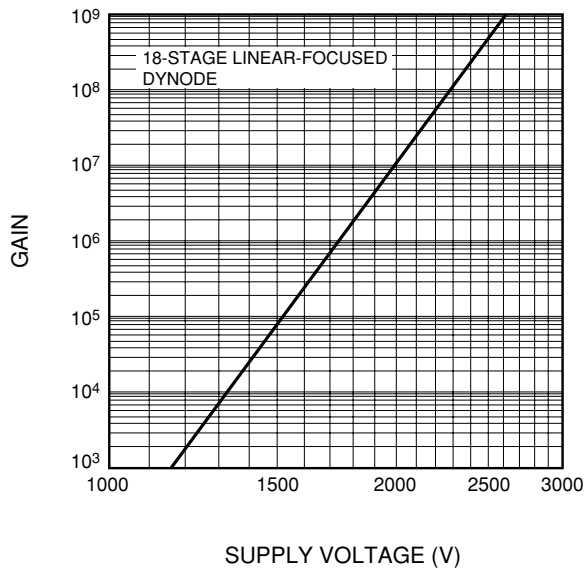
$$\text{Gain } (\mu) = A \cdot E_{bb}^{kn} \dots\dots\dots (\text{Eq. 12-1})$$

E<sub>bb</sub>: supply voltage

k : constant determined by electrode structure and material

n : number of dynode stages

It is clear from this equation that the gain  $\mu$  is proportional to the kn-th power of the supply voltage. Typical gain versus supply voltage is plotted in Figure 12-10.



THBV3\_1210EA

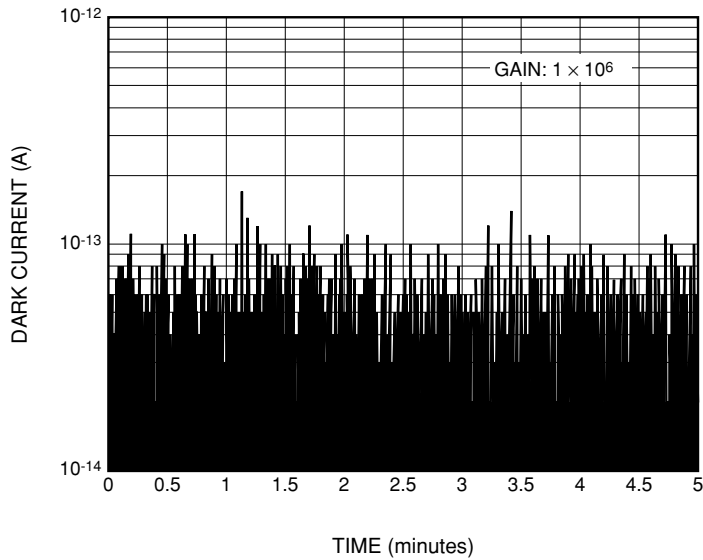
Figure 12-10: Typical gain versus supply voltage characteristics of electron multiplier tube

## 12.2.3 Dark current and noise

The secondary emissive surface of dynodes used for typical electron multiplier tubes and ion detectors is made of beryllium oxide or aluminum oxide. These materials have a high work function and therefore exhibit exceptionally low dark current. Even so, small amounts of dark current may be generated by the following factors:

1. Thermionic emission current from the secondary electron emissive surface
2. Leakage current from electrode support materials
3. Field emission current

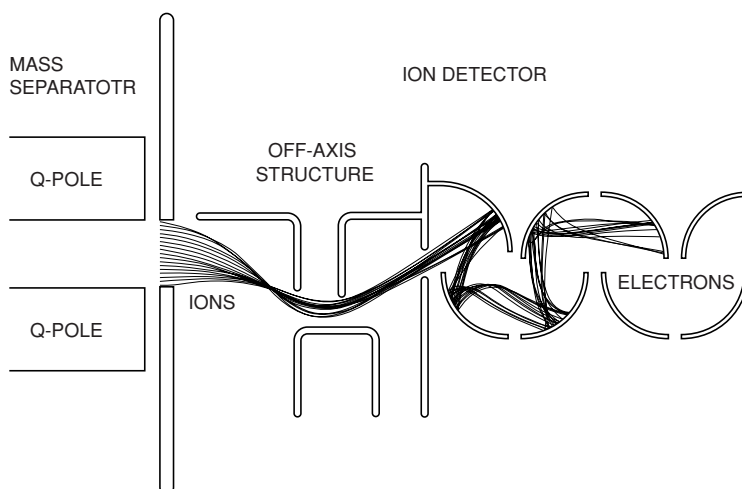
Typical electron multiplier tubes and ion detectors have very low dark current which is less than 1 picoampere when operated at a supply voltage providing a gain of 10<sup>6</sup>. Dark current and noise measurement results are shown in Figure 12-11.



THBV3\_1211EA

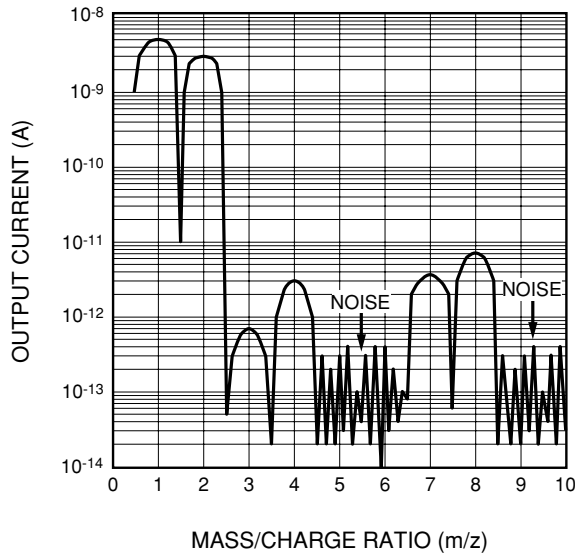
**Figure 12-11: Dark current/noise measurement results**

An ion source used in mass spectrometers ionizes a sample, but simultaneously produces noise components such as UV radiation and X-rays. These noise components also enter the ion detector along with the sample ions and are then multiplied. This noise is generally regarded as internal ion detector noise, although it is not caused by the ion detector itself. To reduce the noise actually originating from the ion source, the first dynode or conversion dynode of the ion detectors is arranged at a position slightly shifted from the ion input opening. Also an electric field lens created by a special electrode is used to allow only sample ions to enter the ion detector. (This is called an "off-axis structure".) Figure 12-12 shows the ion detection mechanism of an off-axis ion detector and Figure 12-13 shows noise measured with the off-axis ion detector installed in a mass spectrometer. The signal at molecular weight ratios ( $m/z$ )<sup>5</sup> where no ions exist appears as noise. This noise level is nearly equal to the intrinsic noise of the ion detector.



THBV3\_1212EA

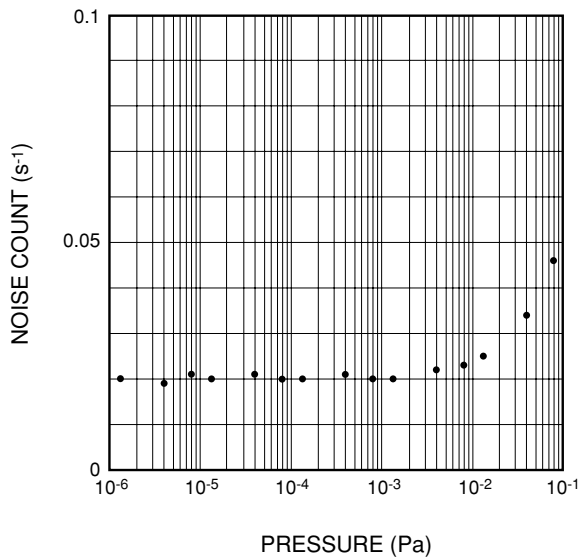
**Figure 12-12: Ion detection in an off-axis ion detector**



THBV3\_1213EA

**Figure 12-13: Ion source noise measured with an off-axis ion detector**

Because electron multiplier tubes and ion detectors are used in a vacuum, the noise level also depends on the pressure. Generally, the lower the pressure level (for example,  $10^{-5}$  Pa), the less the noise will be, and the higher the pressure level, the greater the noise will be. Figure 12-14 shows the relation between the noise count and the pressure level at which an electron multiplier tube and ion detector are operated.

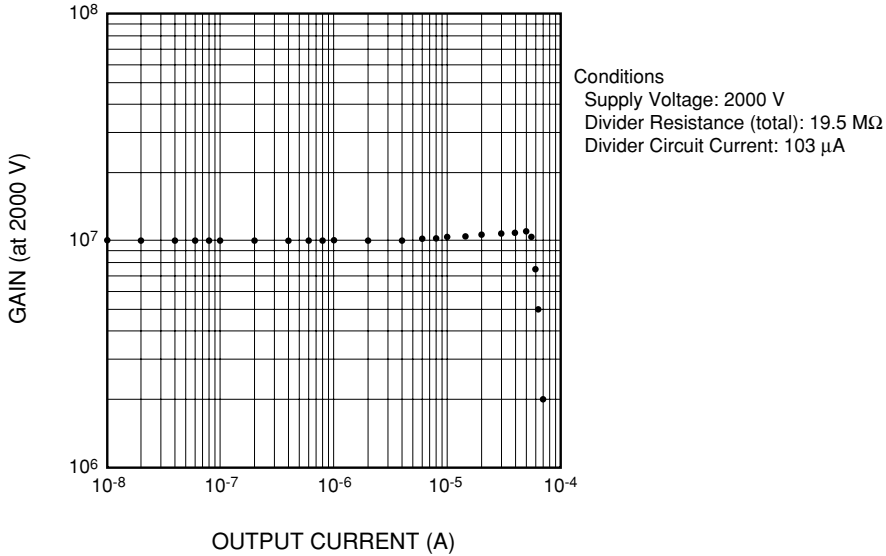


THBV3\_1214EA

**Figure 12-14: Typical noise count vs. pressure level for electron multiplier tubes**

## 12.2.4 Linearity

Most electron multiplier tubes and ion detectors usually incorporate voltage-divider resistors between each successive dynode. This resistor is about  $1\text{ M}\Omega$  per stage, so the total resistance comes to  $20\text{ M}\Omega$ . As in the case of photomultiplier tubes, the value of a linear output current is limited by the current flowing through these voltage-divider resistors. (See 5.1 in Chapter 5.) Figure 12-15 shows the linearity plotted when an electron multiplier tube or ion detector is operated in DC mode.



THBV3\_1215EA

**Figure 12-15: Typical electron multiplier tube linearity in DC operation**

As the output current increases, the gain abruptly drops after increasing slightly. This is a typical pattern for linearity dependent on the voltage-divider current. The linearity can be improved by reducing the total value of the voltage-divider resistors. To suppress the undesired increase in the gain which tends to occur when the output current becomes large, the resistor value between the last stage and ground should be made smaller.

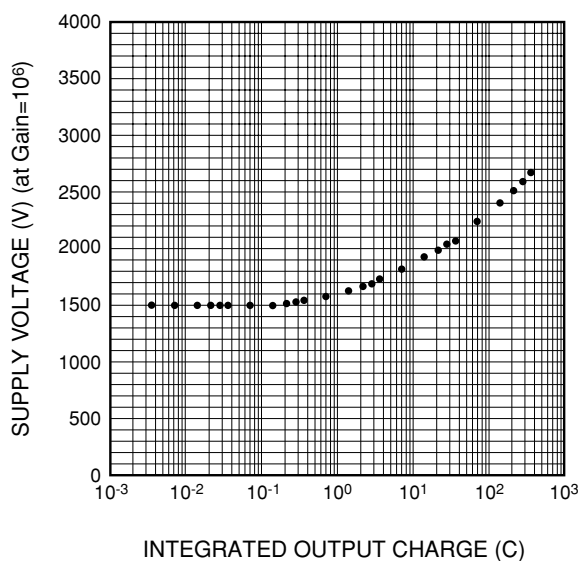
The linearity in pulse counting mode is generally determined by the time response and voltage-divider circuit current of the electron multiplier tube or ion detector. (See 6.2 in Chapter 6.) To maintain high pulse count linearity, tube types using linear-focused dynodes and smaller voltage-divider resistors should be used.

### 12.2.5 Life characteristics

The life of electron multiplier tubes and ion detectors is usually affected by the gain, output current and operating pressure level. Two factors that cause gain deterioration are:

1. Sensitivity deterioration in the first dynode or conversion dynode by incident ions
2. Contamination on the secondary emissive surface

Figure 12-16 shows typical life characteristics for electron multiplier tubes and ion detectors. This is the supply voltage change required to maintain a preset gain ( $10^6$ ) measured with the amount of input ions and output current kept constant.



THBV2\_1216EA

Figure 12-16: Typical life characteristics for electron multiplier tubes and ion detectors

## References in Chapter 12

- 1) S. Araki: Mass Spectroscopy, 3rd Edition, Modern Chemistry Series 2, Tokyo Kagaku Dozin Co., Ltd.
- 2) M. Tsuchiya, M. Ohashi, T. Ueno: New Development of Mass Spectrometry, Modern Chemistry, Extra Number 15, Tokyo Kagaku Dozin Co., Ltd.
- 3) T. Ueno, K. Hirayama, K. Harada: Biological Mass Spectrometry, Modern Chemical, Extra Number 31, Tokyo Kagaku Dozin Co., Ltd.
- 4) T. Akashi, M. Takayama, Y. Hashimoto, et al.: "What is mass spectrometry?", International Academic Printing Co., Ltd.
- 5) K. Okuno, M. Takayama, et al.: Mass Spectrometry Terminology, International Academic Printing Co., Ltd.

# MEMO

## **CHAPTER 13 ENVIRONMENTAL RESISTANCE AND RELIABILITY**

*Photomultiplier tube characteristics, for example, sensitivity and dark current, are susceptible to environmental conditions such as ambient temperature, humidity and magnetic fields. To obtain the fullest capabilities from a photomultiplier tube, it is necessary to know how environmental conditions affect the photomultiplier tube and to take corrective action. This chapter discusses these points and also describes operating stability over time and reliability.*

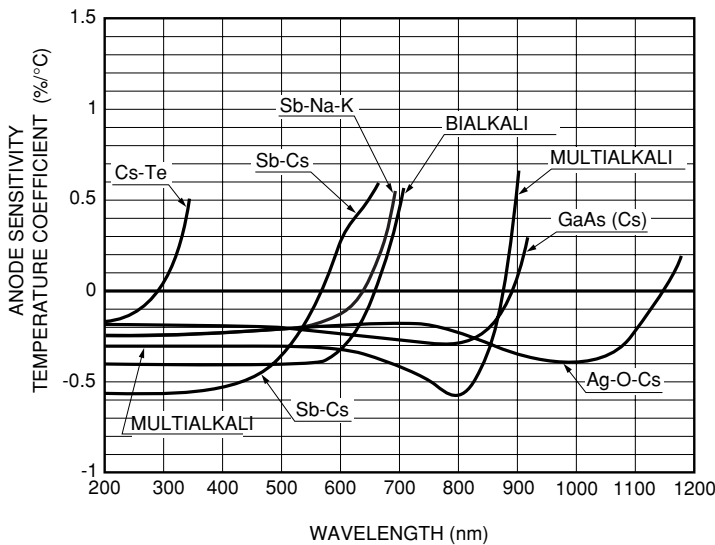
## 13.1 Effects of Ambient Temperature

### 13.1.1 Temperature characteristics

The photomultiplier tube is more susceptible to ambient temperature than ordinary electronic components (such as resistors and capacitors). Therefore in precision measurement, the photomultiplier tube must be operated with temperature control or comparative photometric techniques so that the effects of ambient temperature are minimized. When performing temperature control, note that the interior of a photomultiplier tube is a vacuum and that heat conducts through it very slowly. The photomultiplier tube should be left for one hour or longer until the photomultiplier tube reaches the same level as the ambient temperature and its characteristics become stable.

#### (1) Sensitivity

Temperature characteristics of anode sensitivity can be divided into those for cathode sensitivity (photocathode) and gain (dynode). Temperature characteristics for cathode sensitivity are dependent on the wavelength. In general, the temperature coefficient of cathode sensitivity varies significantly from a negative value to a positive value near the long wavelength limit. In contrast, temperature characteristics of gain have virtually no dependence on wavelength or on supply voltage. Figure 13-1 shows temperature coefficients of major photomultiplier tubes as a function of wavelength.



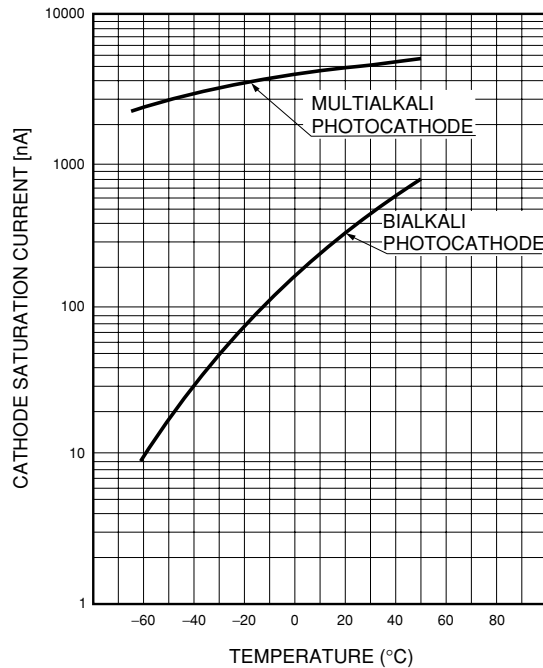
THBV3\_1301EA

Figure 13-1: Temperature coefficients of photomultiplier tube photocathodes

When a photomultiplier tube with a transmission mode photocathode is used at very low temperatures, the subsequent increase in the photocathode surface resistance may cause a cathode current saturation effect, resulting in a loss of output linearity with respect to the incident light level. This effect appears drastically with certain types of bialkali photocathodes, so care is required when using such photomultiplier tubes.



Figure 13-2 shows typical cathode saturation current versus temperature for transmission type bialkali and multialkali photocathodes.

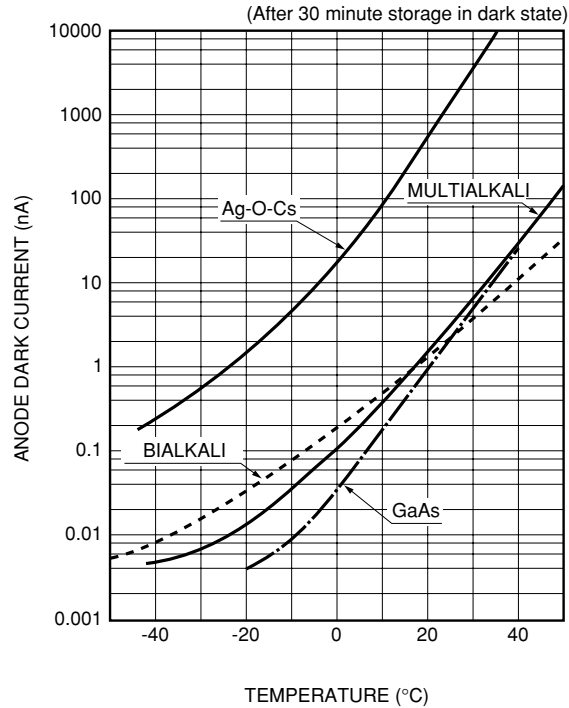


THBV3\_1302EA

Figure 13-2: Cathode saturation current vs. temperature for transmission type photocathodes

## (2) Dark current

A photocathode consists of materials having small energy gap and electron affinity so that photoelectrons can be released efficiently. This means that dark current is very sensitive to the ambient temperature. In low-light-level detection, this effect of the ambient temperature on the dark current is an important factor to consider. For example, cooling a photomultiplier tube is most effective in reducing the dark current and improving the signal-to-noise ratio, especially for photomultiplier tubes with high sensitivity in the red to near infrared region. Conversely, using a photomultiplier tube at a high temperature reduces the signal-to-noise ratio. If a photomultiplier tube must be operated at a high temperature, use of a special photocathode (Sb-Na-K) is recommended. Figure 13-3 shows dark current versus temperature characteristics of the major photocathode types. For details on dark current, refer to 4.3.6 in Chapter 4.



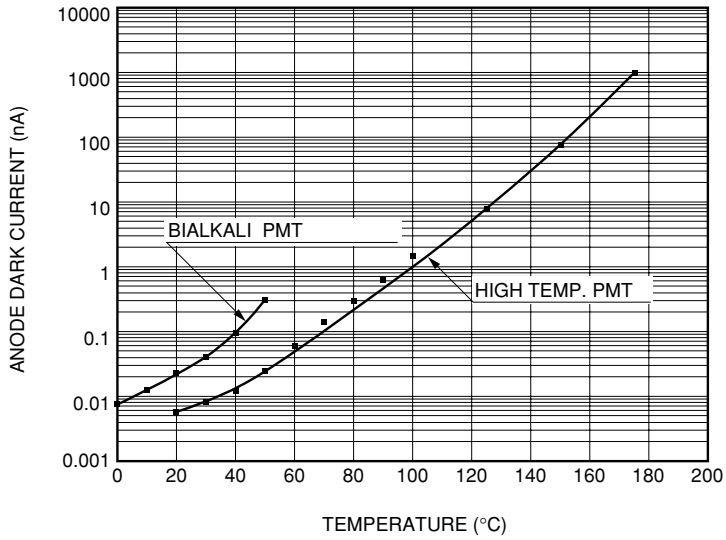
THBV3\_1303EA

Figure 13-3: Anode dark current vs. temperature

### 13.1.2 High temperature photomultiplier tubes

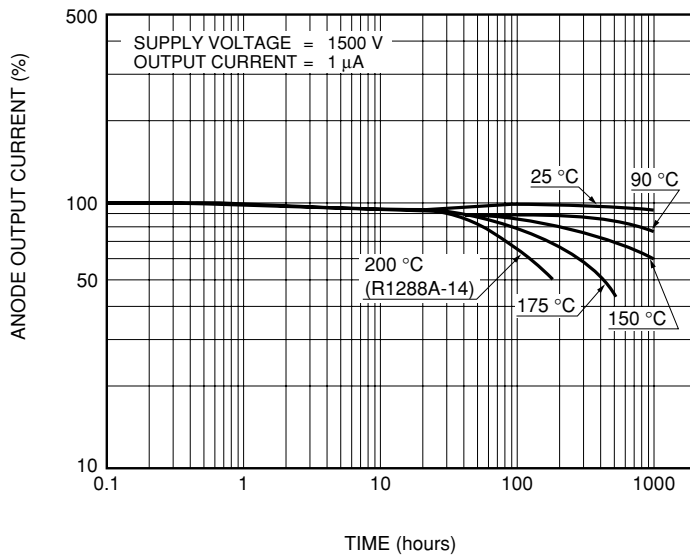
Although the guaranteed operating temperature range for general photomultiplier tubes is up to 50°C, high temperature photomultiplier tubes can operate at high temperatures up to 175°C. These tubes use a specially processed bialkali photocathode that exhibits very low dark current even at high temperatures. The multiplier section employs copper-beryllium (CuBe) dynodes designed and optimized for use at high temperatures.

Typical characteristics for high temperature photomultiplier tubes are shown below. Anode dark current versus temperature characteristics are plotted in Figure 13-4, anode output current change over time at different temperatures in Figure 13-5, gain and energy resolution (pulse height resolution or PHR) versus temperature in Figure 13-6, and plateau characteristics at different temperatures in Figure 13-7.



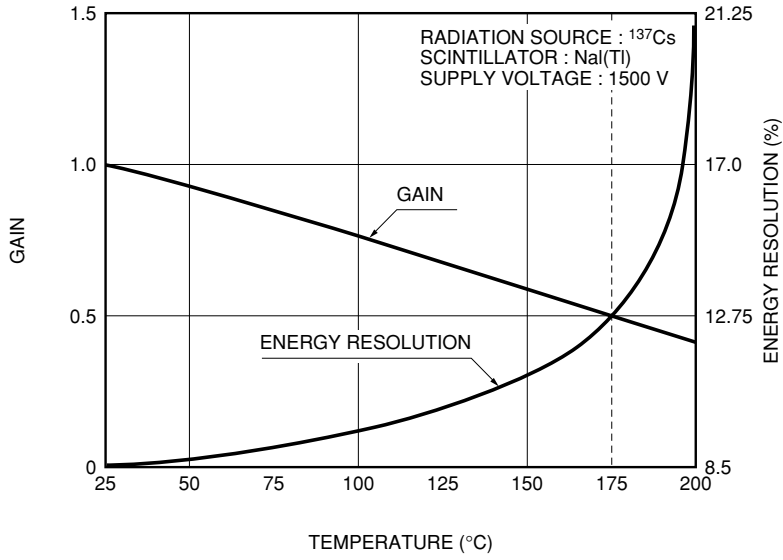
THBV3\_1304EA

Figure 13-4: Anode dark current vs. temperature



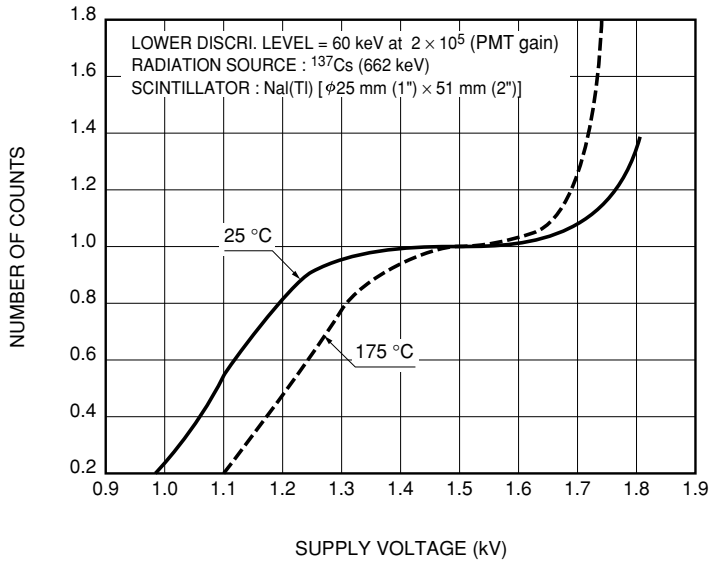
THBV3\_1305EA

Figure 13-5: Anode current change over time at different temperatures



THBV3\_1306EA

Figure 13-6: Gain and energy resolution vs. temperature



THBV3\_1307EA

Figure 13-7: Plateau characteristics at different temperatures

### 13.1.3 Storage temperature and cooling precautions

Photomultiplier tube sensitivity varies somewhat during storage, even at room temperatures. This is probably due to the movement of alkali elements activating the photocathode and dynode surfaces. If a photomultiplier tube is left at a high temperature, this sensitivity variation will be accelerated. It is therefore recommended that the photomultiplier tube be stored at or below room temperatures.

As explained in section 13.1.1 (dark current), photomultiplier tubes using a photocathode with high red-to-white sensitivity such as multialkali, GaAs(Cs), InGaAs and Ag-O-Cs are often cooled during operation to reduce the dark current. In this case, the following precautions should be observed, otherwise the difference in thermal expansion coefficient between the photomultiplier tube glass bulb, base and adhesive (epoxy resin) may cause bulb rupture.

1. Avoid using a photomultiplier tube with a plastic base when cooling to  $-30^{\circ}\text{C}$  or below.
2. Assemble a voltage-divider circuit on a PC board and connect it to the socket using thin, soft wires, so that excessive force is not applied to the lead pins.
3. Avoid subjecting a photomultiplier tube to drastic temperature changes.

## 13.2 Effects of Humidity

### 13.2.1 Operating humidity

Since the photomultiplier tube is operated at high voltages and handles very low current in the order of micro to picoamperes, leakage current between the lead pins may create a significant problem. This leakage current sometimes increases by several orders of magnitude due to a rise in the ambient humidity. It is advisable that the photomultiplier tube be operated at a humidity below 60 percent.

### 13.2.2 Storage humidity

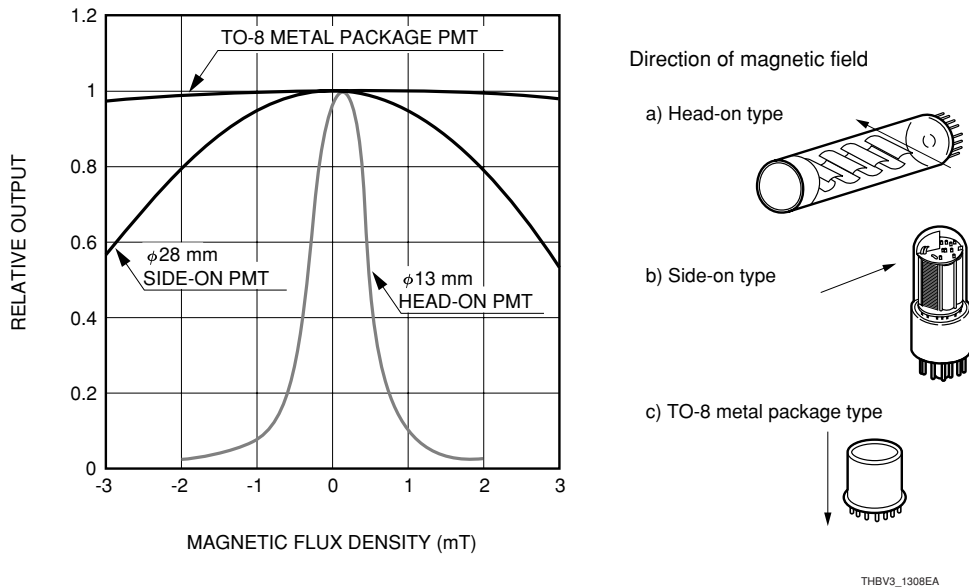
If a photomultiplier tube is left at a high humidity for a long period of time, the following problems may occur: an increase in the leakage current on the bulb stem surface, contact failure due to rust formed on the lead pin surface and, for UV glass, a loss of transmittance. The photomultiplier tube must therefore be stored in locations of low humidity. Since dirt on the photomultiplier tube surface may be a cause of increased leakage current and rust formation on the leads, avoid touching the bulb stem, lead pins and especially around the anode pin of a plastic base with bare hands. These portions must be kept clean but, if they become contaminated, use anhydrous alcohol for cleaning.

## 13.3 Effects of External Magnetic Fields

### 13.3.1 Magnetic characteristics

In photomultiplier tube operation, because low-energy electrons travel along a long path in a vacuum, their trajectories are affected by even a slight magnetic field such as terrestrial magnetism, causing an anode sensitivity variation. A prime reason for this sensitivity variation is that the electron trajectories influenced by the magnetic fields cannot precisely focus the photoelectrons onto the first dynode. This means that photomultiplier tubes having a long distance between the photocathode and the first dynode or a small first-dynode opening in comparison with the photocathode area are more vulnerable to effects of a magnetic field.

For most head-on photomultiplier tubes, the anode sensitivity will be reduced by as much as 50 percent by a magnetic flux density of below 0.1 to several milliteslas. The sensitivity is most vulnerable to a magnetic flux in the direction parallel to the photocathode surface (X axis). Side-on photomultiplier tubes exhibit less sensitivity variations since the distance from the photocathode to the first dynode is short. The magnetic flux density at which the anode sensitivity reduces 50 percent is approximately 3.5 milliteslas for 1-1/8 inch (28 mm) side-on types. Metal-package type photomultiplier tubes (R7400 series) offer excellent immunity to magnetic fields because they have a short distance from the photocathode to the first dynode. Figure 13-8 shows the effects of magnetic fields on typical photomultiplier tubes. Also note that the higher the supply voltage to a photomultiplier tube, the less the effects of magnetic fields.

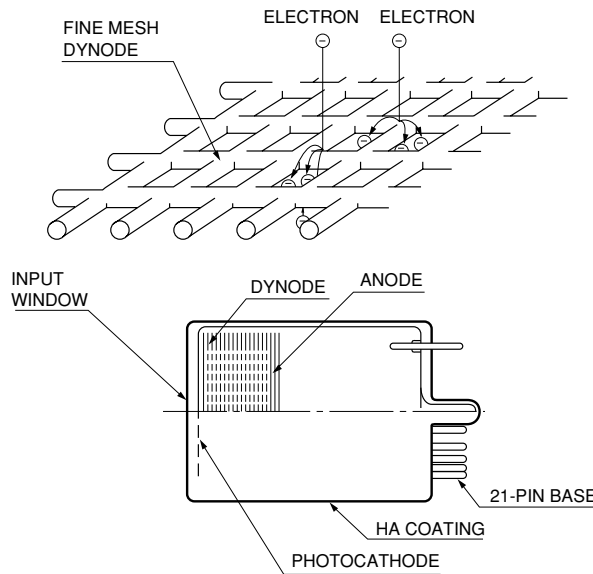


**Figure 13-8: Magnetic characteristics of typical photomultiplier tubes**

As can be seen from Figure 13-8, photomultiplier tubes are susceptible to magnetic fields. It is advisable that the photomultiplier tube be used in locations where no magnetic source is present. In particular, avoid using the photomultiplier tube near such devices as transformers and magnets. If the photomultiplier tube must be operated in a magnetic field, be sure to use a magnetic shield case. Refer to section 5.4 of Chapter 5 for more details and specific usage of magnetic shield cases.

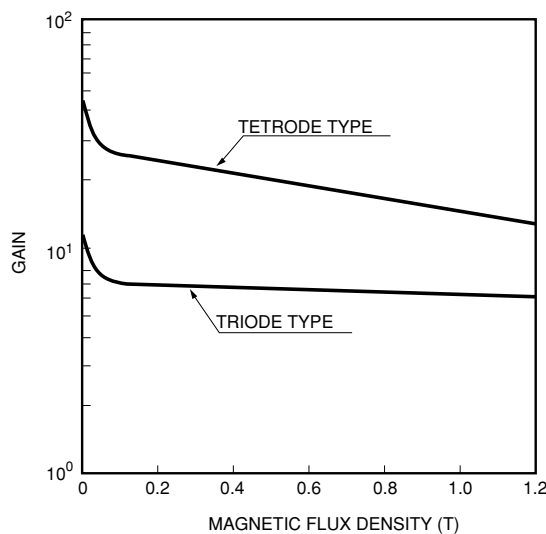
### 13.3.2 Photomultiplier tubes for use in highly magnetic fields

As stated previously, normal photomultiplier tubes exhibit a large variation in a magnetic field, for example, sensitivity reduces at least one order of magnitude in a magnetic field of 10 milliteslas. In high-energy physics applications, however, photomultiplier tubes capable of operating in a magnetic field of more than one tesla are demanded. To meet these demands, special photomultiplier tubes with fine-mesh dynodes have been developed and put into use. These photomultiplier tubes include a "triode" type using a single stage dynode, a "tetrode" type using a two-stage dynode and a high-gain type using multiple dynode stages (19 stages).<sup>1)</sup> The structure of this photomultiplier tube is illustrated in Figure 13-9. Figure 13-10 shows current gain versus magnetic field perpendicular to the photocathode (tube axis) for a tetrode and triode types, and relative output of a 19-stage photomultiplier tube versus magnetic field at different angles.



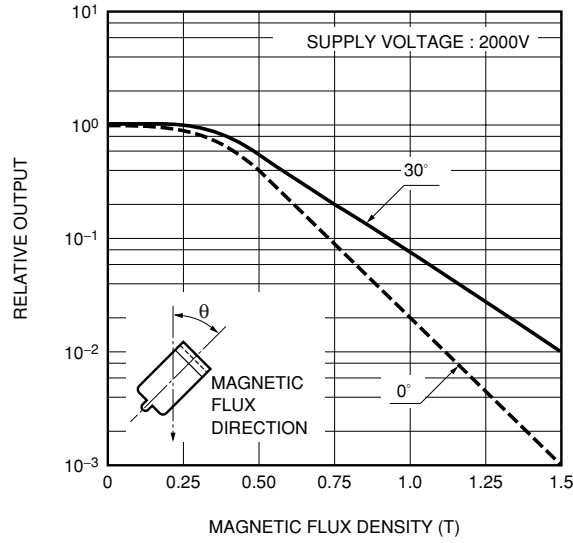
THBV3\_1309EA

Figure 13-9: Structure of a photomultiplier tube designed for use in highly magnetic fields



THBV3\_1310EAa

Figure 13-10: Magnetic characteristics of photomultiplier tubes for highly magnetic fields (1)



THBV3\_1310EAb

Figure 13-10: Magnetic characteristics of photomultiplier tubes for highly magnetic fields (2)

### 13.3.3 Magnetization

The dynode substrate is commonly made from nickel with magnetic properties, and the photomultiplier tube leads and electrodes are also made from similar metals which can be magnetized. There will be no problem as long as the photomultiplier tube is operated in a weak magnetic field such as from terrestrial magnetism. If the magnetic field strength increases and exceeds the initial permeability of the dynode substrate and electrode materials, they will remain magnetized even after the magnetic field has been removed (residual magnetism). The gain after the magnetic field has once been applied will differ from that before the magnetic field is applied. If magnetized, they can be demagnetized by applying an AC magnetic field to the photomultiplier tube and gradually attenuating it.

### 13.3.4 Photomultiplier tubes made of nonmagnetic materials

In applications where a photomultiplier tube must be used in a highly magnetic field or magnetization of the tube is unwanted, photomultiplier tubes made of nonmagnetic materials are sometimes required. Hamamatsu Photonics offers photomultiplier tubes assembled with nonmagnetic materials for the dynode substrate. However, the stem pins and hermetically-sealed portions still must be made from magnetic materials.



## 13.4 Vibration and Shock

Resistance to vibration and shock can be categorized into two conditions: one is under non-operating conditions, for example, during transportation or storage and the other is under conditions when the tube is actually installed and operated in equipment. Except for special tubes designed for such applications as rocket-borne space research and geological surveys, photomultiplier tubes should not be exposed to vibration and shock during operation.

### 13.4.1 Resistance to vibration and shock during non-operation

Photomultiplier tubes are designed to withstand tens of  $m/s^2$  of vibration and several thousand  $m/s^2$  of shock. However, if excessive vibration and shock are applied to a photomultiplier tube, its characteristics may vary and the bulb envelope may break.

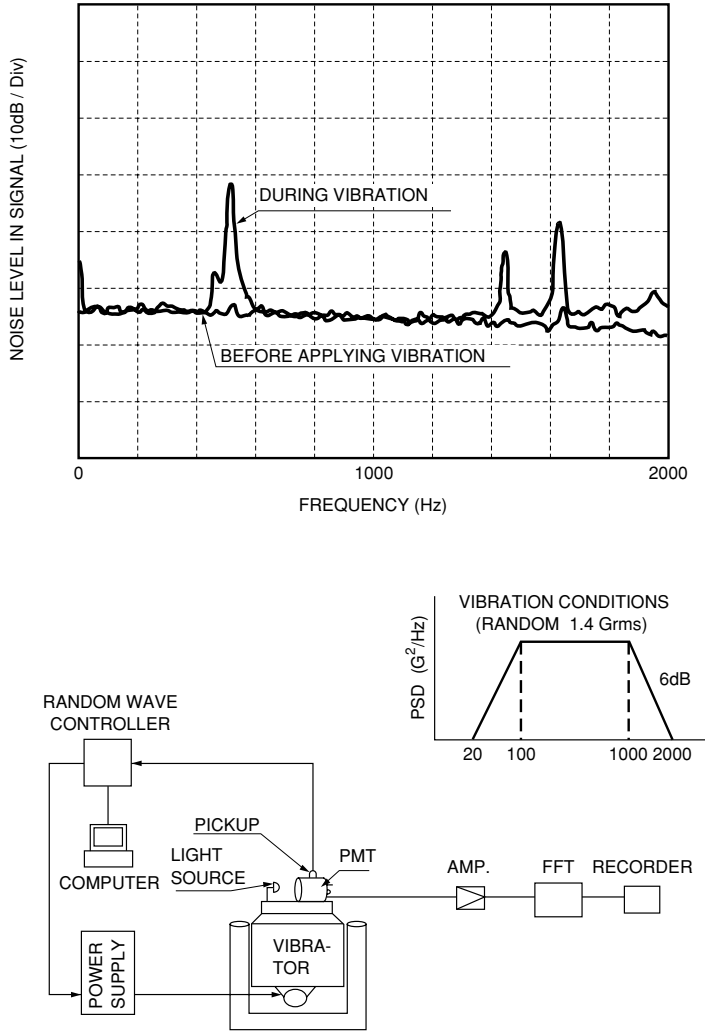
In general, photomultiplier tubes with a smaller size, lighter weight and shorter overall length exhibit better resistance to vibration and shock. Even so, sufficient care must be exercised when handling. The following table shows the maximum vibration and shock values which photomultiplier tubes can withstand.

PMT Type	Maximum Vibration ( $m/s^2$ )	Maximum Shock ( $m/s^2$ )
1/2 inch side-on	150 (10 to 2000 Hz)	2000 (6 ms)
1-1/8 inch side-on	100 (10 to 500 Hz)	1000 (11ms)
Metal package TO-8 type	100 (10 to 500 Hz)	1000 (11 ms)
1/2 inch head-on	100 (10 to 500 Hz)	1000 (11 ms)
1-1/8 inch head-on	50 (10 to 500 Hz)	1000 (11 ms)
2 inch head-on	50 (10 to 500 Hz)	750 (11 ms)
3 inch head-on	50 (10 to 500 Hz)	750 (11 ms)

The photomultiplier tube envelope is made of glass, so it is vulnerable to direct mechanical shock. Envelopes with silica windows are especially vulnerable to shock on the bulb side because of a graded glass seal. Sufficient care must be taken in handling this type of tube. Furthermore, photomultiplier tubes designed for liquid scintillation counting use a very thin faceplate that is 0.5 millimeters thick. Some of them may be broken even by a slight shock. Since the photomultiplier tube is a vacuum tube, if the envelope is broken, implosion may cause it to fly apart in fragments. Precautions are required, especially in handling a large diameter tube of more than 8 inches (204 millimeters).

### 13.4.2 Resistance to vibration and shock during operation (resonance)

The photomultiplier tube is not normally designed to receive vibration and shocks during operation, except for specially-designed ruggedized tubes. If a photomultiplier tube suffers vibration or shocks during operation, problems such as variations of the signal level and an increase in the microphonic noise may occur. Attention should be given to the mounting method and arrangement of the tube. Moreover, the photomultiplier tube may have a resonance at a certain frequency, but this resonant frequency differs from tube to tube. If vibration is increased at this resonance, the above problems will be more noticeable, leading to the breakage of the envelope. Figure 13-11 shows the variations in the frequency spectrum of photomultiplier tube output subjected to vibration, along with the measurement block diagram.



THBV3\_1311EA

**Figure 13-11: Resonance noise in the output signal of a photomultiplier tube subjected to vibration**

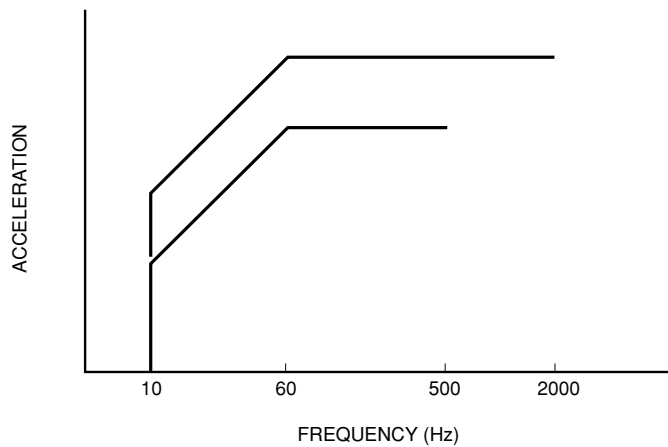
In this experiment, the photomultiplier tube is subjected to random vibration (1.4 Grms) from 20 Hz to 2000 Hz and its output signal is frequency-analyzed using a FFT (fast fourier transform). It is obvious from Figure 13-11 that the noise sharply increases at frequencies near 0.5 kHz, 1.45 kHz and 1.6 kHz.

When measurement is made at extremely low light levels, even a slight vibration caused by the table on which the equipment is placed may be a source of noise. Precautions should be taken to ensure the equipment is installed securely and also the cable length to the preamplifier should be checked.

### 13.4.3 Testing methods and conditions

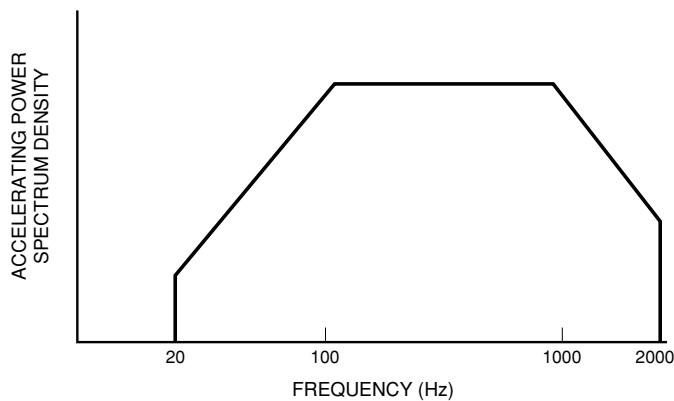
There are two vibration test methods<sup>2)</sup>: sinusoidal-wave and random-wave application tests. In the first method, the sinusoidal wave used for vibration tests is determined by the frequency range, displacement (amplitude), acceleration, vibration duration and sweep time. The frequency sweep method commonly employed is a logarithmic sweep method. In the second method, the random wave is determined by the acceleration, power spectrum density ( $G^2/Hz$ ), and the vibration duration, and is expressed in terms of the RMS value. This method allows tests to be performed under conditions close to the actual environment. In Figures 13-12 (A) and (B), vibration waveform examples created by sinusoidal wave and random wave are shown.

(A): Sinusoidal wave vibration pattern example



THBV3\_1312EAa

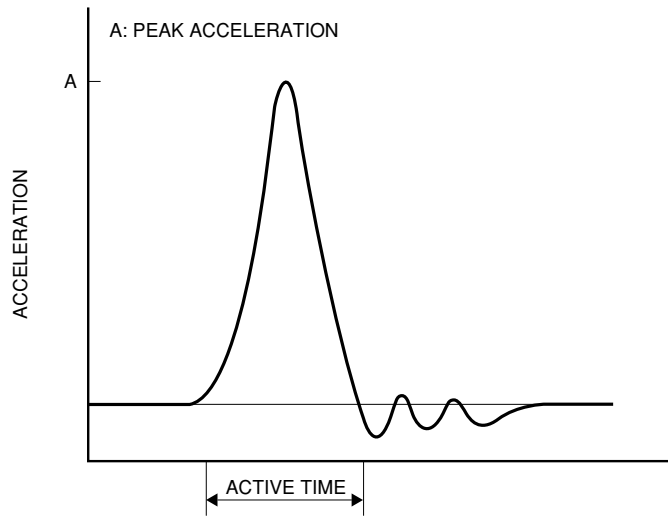
(B) Random vibration pattern example



THBV3\_1312EAa

Figure 13-12: Vibration and shock pattern curves (1)

## (C) Shock-application pattern (half-wave sinusoidal pulse)



THBV3\_1312EAc

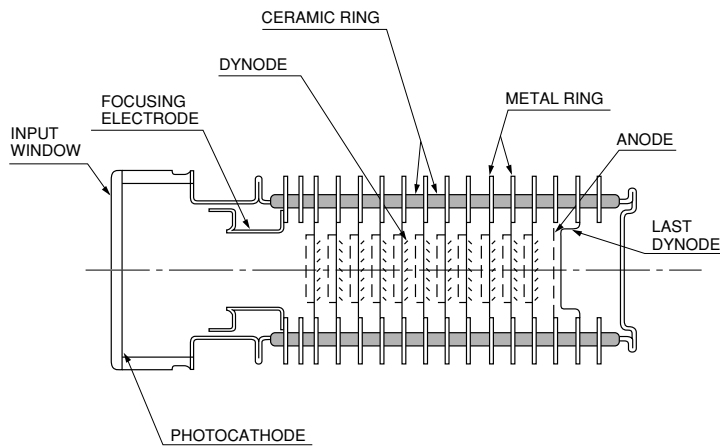
**Figure 13-12: Vibration and shock pattern curves (2)**

Various methods are used in shock tests such as half-wave sinusoidal pulses, sawtooth wave pulses, and trapezoidal wave pulses. Hamamatsu Photonics performs shock tests using half-wave sinusoidal pulses. The test conditions are determined by the peak acceleration, shock duration, and the number of shocks applied. A typical shock-application pattern is shown in Figure 13-12 (C).

Official standards for vibration and shock test methods include IEC 60068, JIS-C0040 (vibration), JIS-C0041 (shock), MIL STD-810E and MIL STD-202F.<sup>3)</sup> Hamamatsu Photonics performs the vibration and shock tests in conformance to these official standards. The above data for vibration and shock tests were measured under these official conditions. For instance, the shock tests were carried out along three orthogonal axes for a shock duration period of 11 milliseconds, three times each in the plus and minus directions, so that shocks were applied a total of 18 times. Accordingly, even if the test proves that a photomultiplier tube withstands a shock of  $1000 \text{ m/s}^2$ , this does not mean that it will survive such shocks dozens or hundreds of times.

### 13.4.4 Ruggedized photomultiplier tubes<sup>4)</sup>

In geological surveys such as oil well logging or in space research in which photomultiplier tubes are launched in a rocket, extremely high resistance to vibration and shock is required.<sup>5)</sup> To meet these applications, ruggedized photomultiplier tubes have been developed, which can operate reliably during periods of  $200 \text{ m/s}^2$  to  $500 \text{ m/s}^2$  vibration and  $1000 \text{ m/s}^2$  to  $10000 \text{ m/s}^2$  shock. A variety of ruggedized types are available ranging in diameter from 1/2 to 2 inches (13 to 51 millimeters) and are also available with different dynode structures. Most ruggedized photomultiplier tubes are based on conventional glass-envelope photomultiplier tubes, but feature improvements to their electrode supports, lead pins and dynode structure so that they will withstand severe shock and vibration. These ruggedized photomultiplier tubes have a diameter of 2 inches (51 millimeters) or less, and can withstand vibrations up to  $200 \text{ m/s}^2$ . If even higher performance is required, specially-designed ruggedized photomultiplier tubes having a stacked ceramic bulb are used. Figure 13-13 shows the cross section of this type of ruggedized photomultiplier tube.



THBV2\_1313EA

**Figure 13-13: Cross section of a ruggedized photomultiplier tube using a stacked ceramic bulb.**

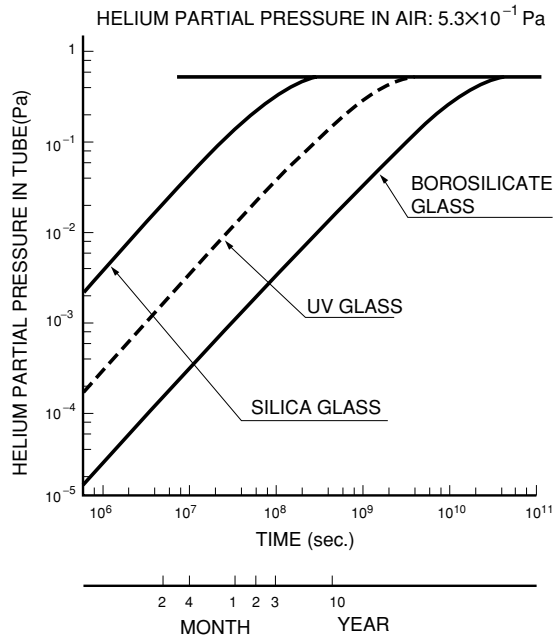
As illustrated in Figure 13-9, each dynode electrode of this ruggedized photomultiplier tube is securely welded to a ceramic ring. This structure resists electrical discontinuity, contact failure and envelope rupture even under severe vibration and shock. This is because the dynodes resist deformation and peeling. No lead wires, ceramic spacers or cathode contacts are required, and few fragile glass parts need to be used. The voltage-divider resistors can be soldered on the outside of the metal rings which are fused to the ceramic rings, assuring high ruggedness even after the voltage-divider circuit has been assembled on the tube. The typical maximum vibration and shock for a 1-3/8 inch (34 mm) stacked-ceramic photomultiplier tube using a high-temperature bialkali photocathode and a 12-stage dynode multiplier is as follows:

Resistance to vibration	$500 \text{ m/s}^2$ (50 to 2000 Hz)
Resistance to shock	$10000 \text{ m/s}^2$ (0.5 ms)

## 13.5 Effects of Helium Gas

It is well known that helium gas permeates through glass.<sup>6)</sup> The extent of helium permeation through glass depends on the glass materials, their composition and ambient temperature. Photomultiplier tubes designed for UV light detection usually employ silica glass for the input window. Helium gas permeates through silica glass more than through other window materials. So if such a photomultiplier tube is stored or operated in environments where helium gas is present, a gas increase occurs inside the tube, leading to an increase in dark current and promoting a degradation of the breakdown voltage level. This eventually results in breakdown and end of the tube service life. For example, if a photomultiplier tube with a silica bulb is placed in helium gas at one atmosphere, a drastic increase of afterpulse due to helium gas will be seen in about 30 minutes. This will cause permanent damage to the tube and must be avoided. To reduce the effects of helium gas, it is best to use alternatives to helium such as argon gas and nitrogen gas.

Helium gas exists on the earth at a partial pressure of about 0.5 Pa. As stated above, the permeability of helium through silica glass is extremely high, as much as  $10^{-19}$  cm<sup>2</sup>/s (at a pressure difference of  $1.013 \times 10^5$  Pa) at room temperatures. Because of this, the helium pressure inside the photomultiplier tube gradually increases and finally reaches a level close to the helium partial-pressure in the atmosphere. The time needed to reach that level depends on the surface area and thickness of the silica glass. For instance, if a 1-1/8 inch (28 mm) diameter side-on photomultiplier tube with a silica bulb is left in the atmosphere, the helium partial-pressure inside the tube will increase to  $9 \times 10^{-2}$  Pa after one year. (Refer to Figure 13-14.)



THBV3\_1314EA

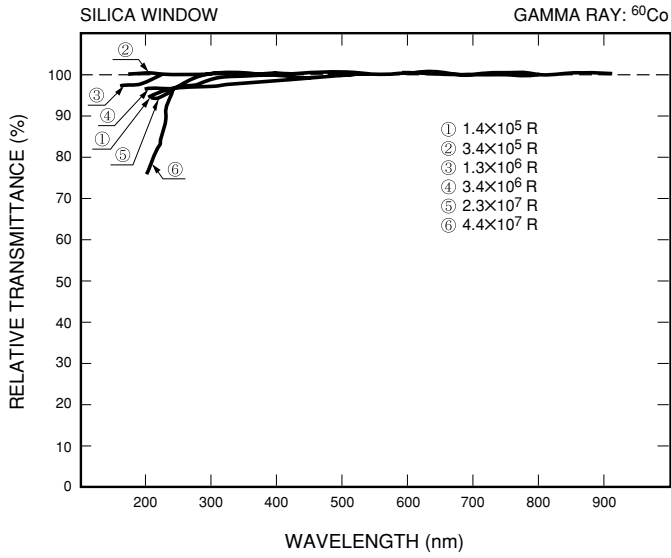
Figure 13-14: Bulb materials and variations in helium partial-pressure inside a tube

## 13.6 Effects of Radiation

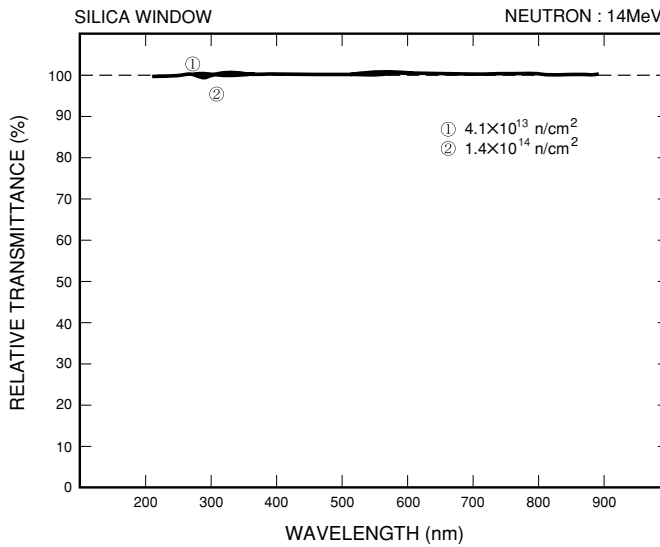
Photomultiplier tube applications are constantly expanding, as stated previously, to such fields as high energy physics, nuclear medicine, X-ray instrumentation, and space research. In these environments, photomultiplier tubes are usually exposed to radiation (X-rays, alpha rays, beta rays, gamma rays, neutrons, etc.) which somewhat affect the performance characteristics of photomultiplier tubes.<sup>7)</sup> For example, radiation causes deterioration of the glass envelope, metals, insulators, and materials used to construct the photomultiplier tube.

### 13.6.1 Deterioration of window transmittance

Even when a photomultiplier tube is exposed to radiation, the cathode sensitivity and secondary emission ratio exhibit very little variation. Sensitivity variation chiefly results from a loss of transmittance through the window due to coloring of the glass, which is an essential part of the photodetector.<sup>8)</sup> Figures 13-15 to 13-17 show variations in the window transmittance when photomultiplier tubes are irradiated by gamma rays from a  $^{60}\text{Co}$  radiation source and also by neutrons (14 MeV). (The windows are 2 mm thick. )



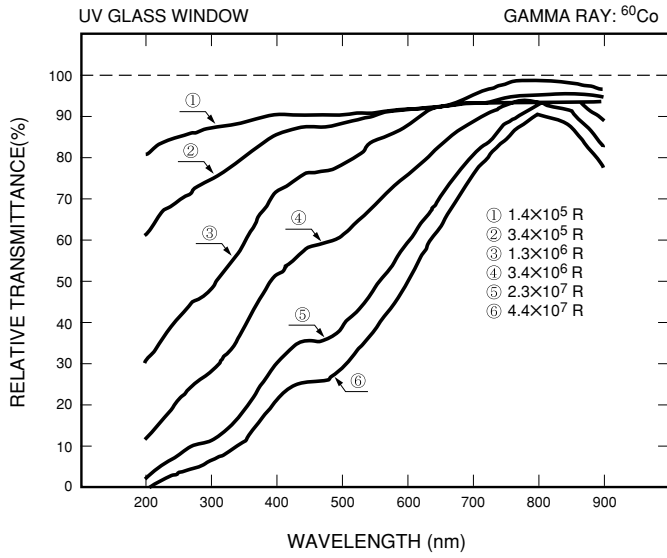
THBV3\_1315EAa



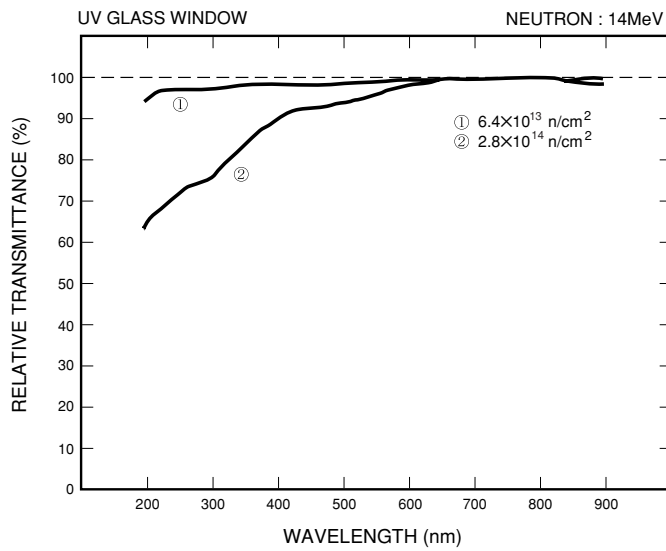
THBV3\_1315EAb

Figure 13-15: Transmittance change of silica window irradiated by gamma rays/neutrons



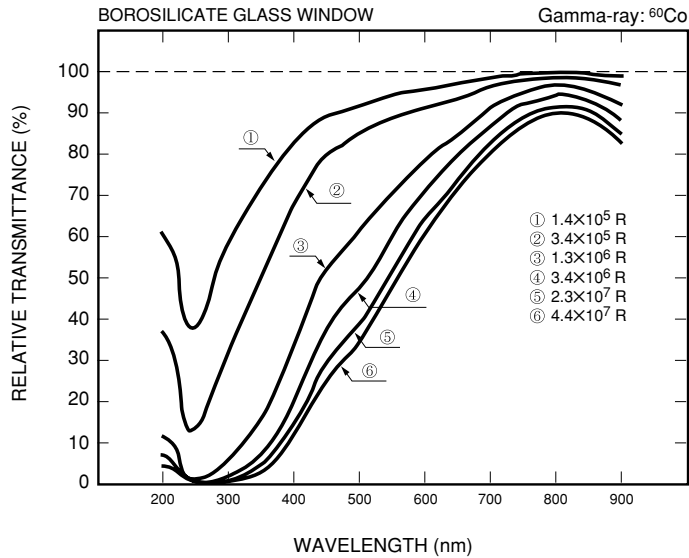


THBV3\_1316EAa

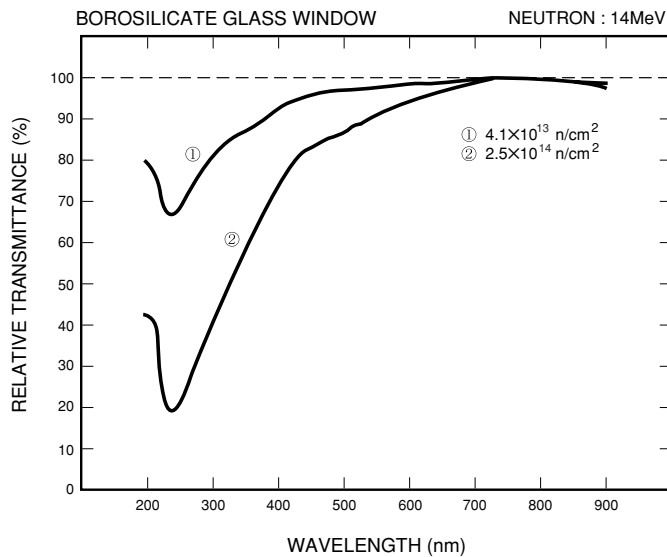


THBV3\_1316EAb

Figure 13-16: Transmittance change of UV glass window irradiated by gamma rays/neutrons



THBV3\_1317EAa



THBV3\_1317EAb

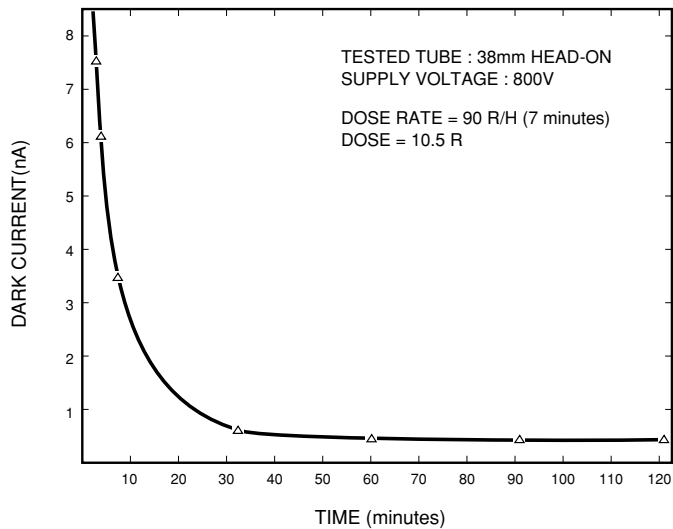
**Figure 13-17: Transmittance change of borosilicate glass window irradiated by gamma rays/neutrons**

As can be seen from these figures showing the data on a synthetic silica, UV glass and borosilicate glass respectively, a loss of transmittance occurs more noticeably in the UV region. The synthetic silica glass is least affected by radiation and virtually no variation is seen after irradiation of gamma rays of  $4.4 \times 10^7$  roentgens and neutrons of  $1.4 \times 10^{14}$  n/cm<sup>2</sup>. There are two types of silica glass: synthetic silica and fused silica. The synthetic silica exhibits a higher resistance to radiation than the fused silica. A loss of transmittance begins to occur from near  $5 \times 10^4$  roentgens for the UV glass, and near  $1 \times 10^4$  roentgens for the borosilicate glass. However, this tendency is not constant even for the same type of glass, because the composition differs depending on the fabrication method. In general, the radiation-resistance characteristic is best with silica, followed by UV glass and borosilicate glass. If the transmittance has dropped due to exposure to radiation, it will recover to some extent after storage. This recovery is more effective when the tube is stored at higher temperatures.

### 13.6.2 Glass scintillation

The photomultiplier tube is slightly sensitive to radiation and produces a resultant noise. This is primarily due to unwanted scintillation of the glass window caused by beta and alpha rays, or scintillation of the glass window and electron emission from the photocathode and dynodes caused by gamma rays and neutrons.<sup>9)</sup>

Of these, the scintillation of the glass window likely has the largest contribution to noise, but the amount of scintillation differs depending on the type of glass. Glass scintillation further causes a continual fluorescence or phosphorescence to occur even after radiation has been removed, resulting in yet another source of noise. Figure 13-18 shows a variation in the dark current when a tube is irradiated by gamma rays, indicating that it takes 40 to 60 minutes to reach a steady level. In the case of neutron irradiation, it has been confirmed that the dynode materials are made radioactive through nuclear reaction (n, p) (n, n, p).



THBV3\_1318EA

Figure 13-18: Dark current variation after exposure to gamma ray

## 13.7 Effects of Atmosphere

The photomultiplier tube may be used in environments not only at one atmosphere ( $1 \times 10^5$  Pa) but also at very low pressures or in depressurized areas such as in aircraft or an artificial satellite.

When there is a pressure drop from the atmospheric pressure down to a near vacuum in outer space, there is a possibility of a discharge occurring between the leads in the photomultiplier tube base. This phenomenon is known as Paschen's Law. The law states that the minimum sparking potential between two electrodes in a gas is a function of the product of the distance between the electrodes and the gas pressure, if the electric field is uniform and the ambient temperature is constant.

The distance between the leads on the outside base and on the socket is set to an interval so that no discharge occurs in environments at one atmosphere or in vacuum. However, these structures tend to discharge most frequently at pressures from 100 Pa to 1000 Pa\*. If the photomultiplier tube is to be operated in this pressure range, sufficient precautions must be taken in the design and wiring of the parts to which a high voltage is applied. (\* 133 Pa = 1 torr.)

Take the following precautions when using photomultiplier tubes in a vacuum.

- (1) After making sure that a sufficient vacuum level is obtained, apply high voltage to the tube (gradually from low to high voltage).
- (2) When the photomultiplier tube has a plastic base, it will take a long time until the inside of the base is evacuated to a specified vacuum. Drilling a small hole in the base is needed.
- (3) A change from 1 to 0.1 Pa may increase the dark current and cause fluctuations in the signal output. Precaution must be taken to maintain the optimal installation conditions.

In high-energy physics applications such as proton decay experiments and neutrino observation, photomultiplier tubes are sometimes operated while underwater or in the sea. In this case, a pressure higher than the atmospheric pressure is applied to the photomultiplier tube. The breaking pressure depends on the configuration, size and bulb material of the photomultiplier tube. In most cases, smaller tubes can withstand higher pressure. However, 8-inch (204 mm) and 20-inch (508 mm) diameter photomultiplier tubes, specifically developed for high energy physics experiments, have a hemispherical shape capable of withstanding a high pressure. For example, 8-inch (204 mm) diameter tubes can withstand up to  $7 \times 10^5$  Pa and 20-inch (508 mm) diameter tubes up to  $6 \times 10^5$  Pa.

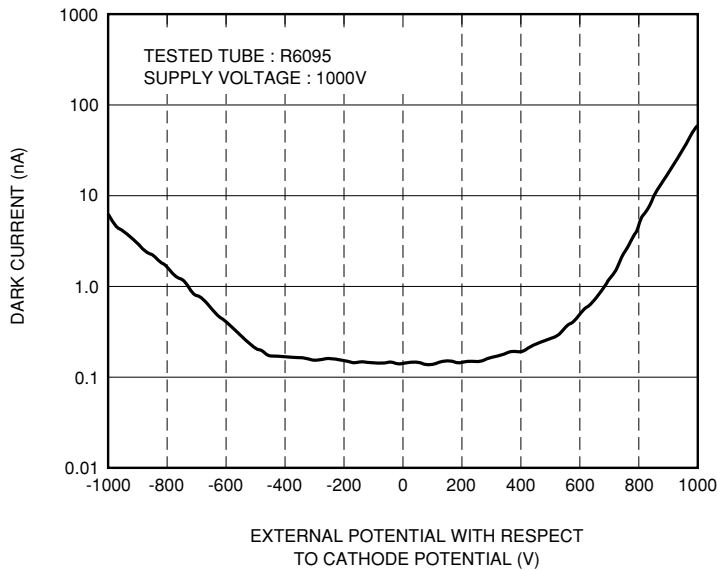
As for the bulb materials, photomultiplier tubes using a silica bulb provide lower pressure-resistance due to the graded seal. There are various shapes of input windows used for head-on photomultiplier tubes, including a plano-plano type (both the faceplate and photocathode are flat), a plano-concave type (the faceplate is flat but the photocathode is concave) and a convex-concave type (the faceplate is convex but the photocathode is concave). Compared to the plano-plano type, the plano-concave and convex-concave types offer higher pressure-resistance.

## 13.8 Effects of External Electric Potential

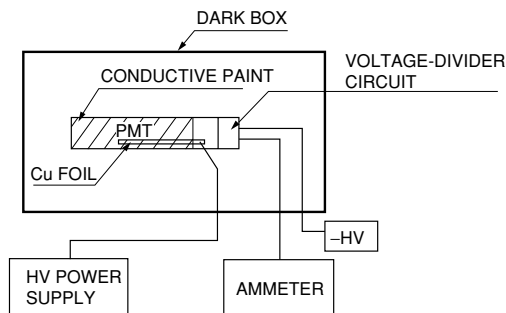
Glass scintillation occurs by exposure to radioactive rays or UV light as explained in section 13.6.2. It also occurs when a strong electric field is applied to the glass. These types of glass scintillations will cause the dark current to increase.

### 13.8.1 Experiment

Figure 13-19 shows the dark current variations of a photomultiplier tube whose side bulb is coated with conductive paint, measured while changing the electric potential of this conductive coating with respect to the cathode potential.



THBV3\_1319EAa

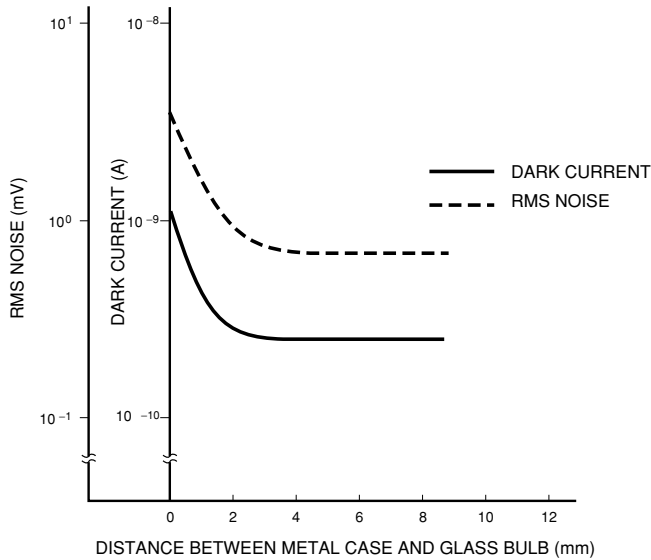
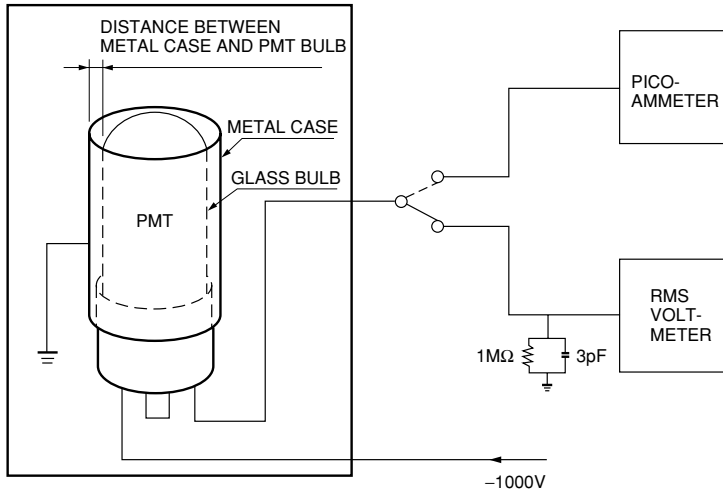


THBV3\_1319EAa

Figure 13-19: Dark current vs. external electric potential

It is clear that the larger the potential difference with respect to the cathode, the higher the dark current. The reason for this effect is that the inner surface of the bulb near the cathode is aluminum-coated and maintained at the cathode potential, and if the outside of the bulb has a large potential difference with respect to the cathode, scintillation will occur in the glass between the two surfaces. This scintillation light will reflect into the photocathode, causing an increase in the dark current.

The housing for photomultiplier tubes is usually made of metal and is grounded. This means that a grounded conductive material is around the photomultiplier tube and may cause the dark current to increase. This problem can be solved by allowing an adequate distance between the photomultiplier tube and the inside of the housing. Figure 13-20 shows the dark current variations while the distance between the photomultiplier tube and the grounded case is changed, proving that there is no increase in the dark current when the separation is 4 millimeters or more.

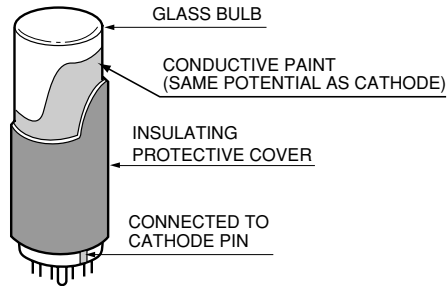


THBV3\_1320EA

Figure 13-20: Dark current vs. distance to grounded case

## 13.8.2 Taking corrective action

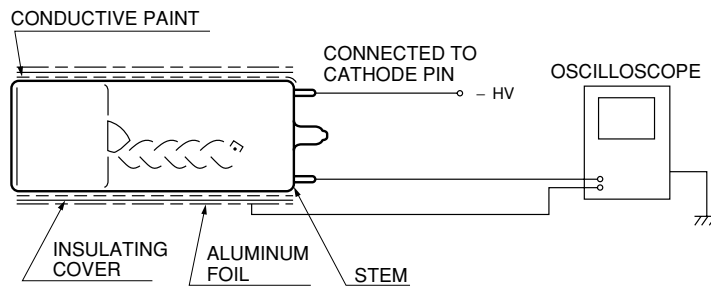
The above effects of external electric potential can be eliminated by use of the cathode grounding scheme with the anode at a positive high voltage, but photomultiplier tubes are frequently operated in the anode grounding scheme with the cathode at a negative high voltage. In this case, a technique of applying a conductive paint around the outside of the bulb and connecting it to the cathode potential can be used, as illustrated in Figure 13-21.



THBV3\_1321EA

**Figure 13-21: HA coating**

This technique is called "HA coating" by Hamamatsu Photonics and, since a negative high voltage is applied to the outside of the bulb, the whole bulb is covered with an insulating cover (heat-shrinkable tube) for safety. The noise problem caused by the surrounding electric potential can be minimized by use of an HA coating. Even so, in cases where a metal foil at ground potential is wrapped around the tube as shown in Figure 13-22, minute amounts of noise may still occur. This noise is probably caused by a small discharge which may sometimes occur due to dielectric breakdown in the insulating cover, which then produces a glass scintillation reaching the photocathode. Therefore, when using the photomultiplier tube with a negative high voltage, do not allow the metal case or housing to make contact with the tube even if it is an HA coating type.



THBV3\_1322EA

**Figure 13-22: Observing the effect of external electric potential on HA coating**

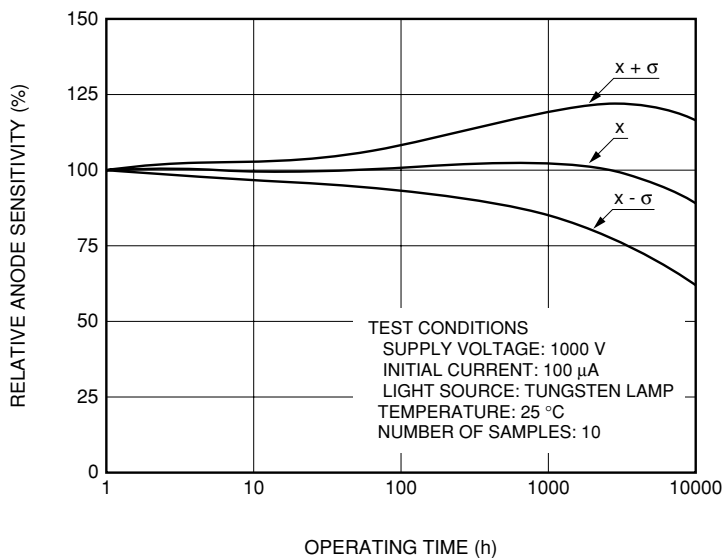
As mentioned above, the HA coating can be effectively used to eliminate the effects of external potential on the side of the bulb. However, if a grounded conductive object is located on the photocathode faceplate, there are no effective countermeasures and what is worse, glass scintillation occurring in the faceplate has a larger influence on the noise. Any grounded object, even insulating materials, should not make contact with the faceplate. If such an object must make contact with the faceplate, use teflon or similar materials with high insulating properties. Another point to be observed is that a grounded object located on the faceplate can cause not only a noise increase but also deterioration of the photocathode sensitivity. Once deteriorated, the sensitivity will never recover to the original level. Take precautions for the mounting method of the photomultiplier tube, so that no object makes contact with the photocathode faceplate and peripheral portions.

Taking account of the above, operating the photomultiplier tube in the cathode grounding scheme with the anode at a positive high voltage is recommended if possible.

## 13.9 Reliability

### 13.9.1 Stability over time (life characteristic)

Stability over time of a photomultiplier tube exhibits a somewhat specific pattern according to the type of photocathode and the dynode materials, but greatly depends on the operating conditions (especially on the output current) and the fabrication process. Also, stability over time widely varies from tube to tube even within the same tube family. In normal operation, the cathode current flowing through the photocathode is on the order of picoamperes, and the photocathode fatigue can virtually be ignored. Accordingly, the operating stability of the dynodes is an important factor that largely affects the stability over time of the photomultiplier tube. Figure 13-23 shows typical data for time stability when photomultiplier tubes are operated under harsh conditions at an anode current of 100  $\mu\text{A}$ .



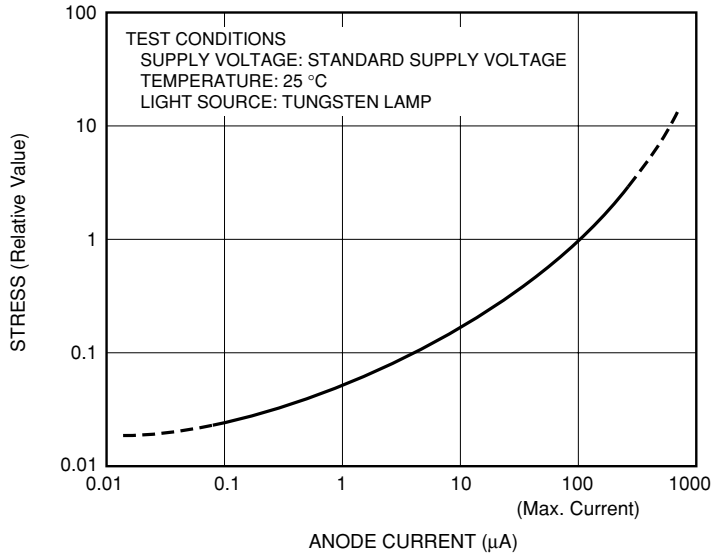
THBV3\_1323EA

Figure 13-23: Stability over time



### 13.9.2 Current stress and stability

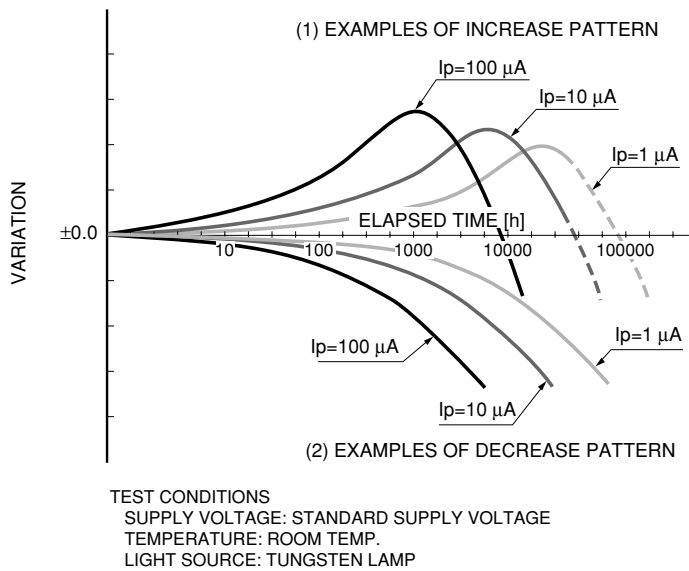
As mentioned in the preceding section, time stability of a photomultiplier tube varies with the operating conditions. In general, the larger the current stress, the earlier and more significant the variation that occurs. Typical stress on photomultiplier tube anode current is shown in Figure 13-24.



THBV3\_1324EA

Figure 13-24: Current stress on photomultiplier tubes (at different anode currents)

Figure 13-25 shows typical time stability of photomultiplier tubes when their operating anode currents  $I_p$  are set to 1, 10 and 100 microamperes, indicating both increasing and decreasing patterns.

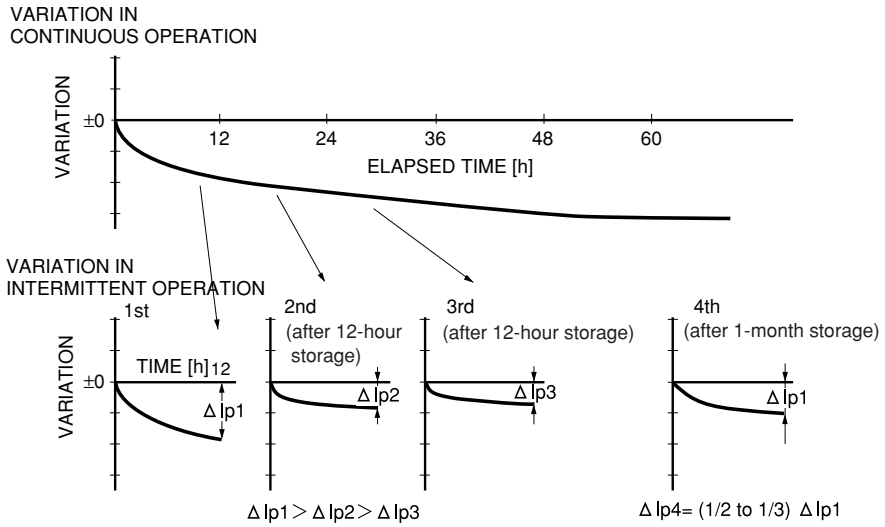


THBV3\_1325EA

Figure 13-25: Typical time stability of photomultiplier tubes (at different anode currents)

Stability over time can be improved to some extent by aging the tube. Figure 13-26 shows the initial output variations when a photomultiplier tube is intermittently operated. It is obvious from the figure that a large variation during the initial operation can be reduced to nearly half, during the second or later operations.

When the photomultiplier tube is left unused for long periods of time, stability will return to its original values. In applications where high stability is prerequisite, we recommend the tube be aged before use.



THBV3\_1326EA

Figure 13-26: Effects of intermittent operation (aging effect)

### 13.9.3 Reliability

Photomultiplier tube applications are constantly expanding to such fields as scintillation counting, high energy physics, nuclear medicine, X-ray applied instrumentation, and aerospace fields. In these application fields, a large number of photomultiplier tubes (sometimes hundreds or occasionally even thousands of tubes) are used in one instrument. In these applications, predicting and verifying the photomultiplier tube reliability are very important.

#### (1) Failure mode

Failure mode for photomultiplier tubes is roughly classified into gradual failure and breakdown failure. The main failure mode is gradual failure, which includes cathode sensitivity degradation, a loss of gain, an increase in dark current and a decrease in dielectric resistance. Breakdown failure includes cracks in the faceplate, bulb envelope and stem portion, and also air leakage through microscopic cracks. Breakdown failure fatally damages the photomultiplier tube, making it permanently unusable.

Since Hamamatsu photomultiplier tubes undergo stringent screening both in the manufacturing and inspection process, most possible failures and their causes are eliminated before shipping. As a result of in-house reliability tests, we have found most of the failure mode causes lie in a loss (or variation) of gain. This means that the photomultiplier tube can still be properly used by adjusting the operating voltage.

#### (2) Failure rate

Failure rate<sup>(1) (2)</sup> is defined as the probability of failure per unit time. Failure rate is generally estimated by using the following two kinds of data:

1. In-house reliability test data
2. Field data

Actual results obtained from field data prove that the photomultiplier tube failure rate is at a level of  $2 \times 10^{-7}$  to  $2 \times 10^{-6}$  failures/hour with operating conditions at room temperatures, a rated supply voltage and an anode output current of 100 nanoamperes. In particular, it is predicted that those tubes which have undergone screening provide a failure rate as small as  $5 \times 10^{-7}$  failures/hour.

#### (3) Mean life

There is a measure of reliability which is commonly referred to as MTBF<sup>(1) (2)</sup> (mean time between failure) or MTTF (mean time to failure). Stated simply, this is the average hours of time until any failure occurs or, in other words, mean life.

Since the definitions and fundamental calculations of these terms are described in detail in various papers, this section only briefly explains these terms.

The relation between the failure rate ( $\lambda$ ) and the mean life ( $\theta$ ) can be expressed on the assumption that it has failure distribution in accordance with exponential distribution, as follows:<sup>(1) (2)</sup>

$$\theta = 1 / \lambda$$

Therefore, the reciprocal of the failure rate is the mean life.

As an example, when a photomultiplier tube is operated in room environments with the anode output current of about 100 nanoamperes, a mean life of  $5 \times 10^5$  to  $5 \times 10^6$  hours can be predicted based on the failure rate explained above. For those tube which have passed screening, the mean life would be more than  $2 \times 10^6$  hours.

**(4) Reliability**

Based on the fundamental calculation for stability data, reliability R is defined as follows.<sup>11) 12)</sup>

$$R(t) = e^{-t\lambda}$$

t: operating time in hours

$\lambda$ : failure rate

Therefore, using a typical failure rate  $\lambda$  of photomultiplier tubes of  $2 \times 10^{-6}$  to  $2 \times 10^{-7}$  failures/hours, reliability R becomes as follows:

Elapsed time in operation	Reliability R(t)	
	at $\lambda = 2 \times 10^{-6}$	at $\lambda = 2 \times 10^{-7}$
One year (8760 hours)	98.3%	99.8%
2 years (17520 hours)	96.6%	99.7%
3 years (26280 hours)	94.9%	99.5%
4 years (35040 hours)	93.2%	99.3%
5 years (43800 hours)	91.6%	99.1%

The above results can be used as a reference in determining reliability levels of photomultiplier tubes, and prove that the photomultiplier tube provides considerably high reliability levels when operated under favorable conditions.

### 13.9.4 Reliability tests and criteria used by Hamamatsu Photonics

Hamamatsu Photonics performs in-house reliability tests by setting the following test conditions and failure criteria to obtain the failure rate.

#### Reliability test conditions

- 1) Environmental stress conditions  
Room temperature (25°C) and high temperature (55°C) (5°C above the maximum rating)
- 2) Test procedures  
Storage and operating life
- 3) Operating conditions (photomultiplier tubes)  
Supply voltage: catalog-listed standard operating voltage, 1000 to 1250 V  
Anode output current: catalog-listed maximum rating, 10 to 100  $\mu$ A

#### Failure criteria

- 1) Anode sensitivity judged as the end of life:  $\pm 50\%$  variation
- 2) Anode sensitivity during non-operation (storage):  $\pm 25\%$  variation
- 3) Cathode sensitivity:  $\pm 25\%$  variation
- 4) Anode dark current (DC): more than 500 times increase, faulty dielectric-resistance
- 5) Breakdown failure: discharge, crack, anode leakage current, etc.

Notice that the above criteria are specified by Hamamatsu Photonics for evaluation and do not necessarily indicate that a tube outside these standards is unusable.

Hamamatsu Photonics has continually performed reliability tests under the above conditions over extended periods of time and has collected large amounts of data. Our evaluation results show that the failure rate of photomultiplier tubes ranges from  $1 \times 10^{-3}$  to  $1 \times 10^{-4}$  failures/hour and the mean time is from 1000 up to 10000 hours. Based on these results, the ratio of the failure rate at room temperatures and an anode output current of 100 nanoamperes, to the failure rate under operating conditions at a maximum rating temperature and current (50°C, 10 to 100 microamperes) will be approximately 400 times. This means that our in-house test conditions have an acceleration factor approximately 400 times that of the field data.

## References in Chapter 13

- 1) Hamamatsu Photonics Technical Data Sheet: T-101.
- 2) Special Committee for Measurement and Research into Vibration and Shock, Society of Electricity: Electric/Electronic Equipment and Vibration/Shock, Corona Publication Co., Ltd.
- 3) IEC Publication 68-2: Basic Environmental Testing Procedures.
- 4) Hamamatsu Photonics Catalog: Ruggedized High-Temperature Photomultiplier Tubes TPMH0001EA.
- 5) Bicon Corp.: Ruggedized High-Temperature Detector Technology.
- 6) J.R. Incandela, S.P. Ahlen, J. Beatty, A. Ciocio, M. Felcini, D. Levin, D. Ficenc, E. Hazen, A. Marin, J.L. Stone, L.R. Sulac, W. Worstell: Nucl. Instrum. & Methods, Phys. Res. A269, 237-245 (1988).
- 7) L.W. Howell, H.F. Kennel: Optical Engineering, 25, 4, 545 (1986).  
M.M. Brinbaum, R.L. Bunker, J. Roderick, K. Stephenson: AIAA Guidance and Control Conference (1984).
- 8) S. Sakubana, T. Kyono, K. Takahashi: Glass Handbook, 825, Asakura Shoten.
- 9) W. Viehamann, A.G. Eubanks, G.F. Pieper, J.H. Bredekamp: Applied Optics, 14,9, 2104 (1975).
- 10) H. Shiomi: Introduction to Failure Physics, Union of Japanese Scientists and Engineers.
- 11) Shinkabe: Introduction to Reliability Engineering, Japanese Standards Association.
- 12) K. Kitagawa: Principles of Reliability and Its Technology, Corona Publication Co., Ltd.

# **CHAPTER 14**

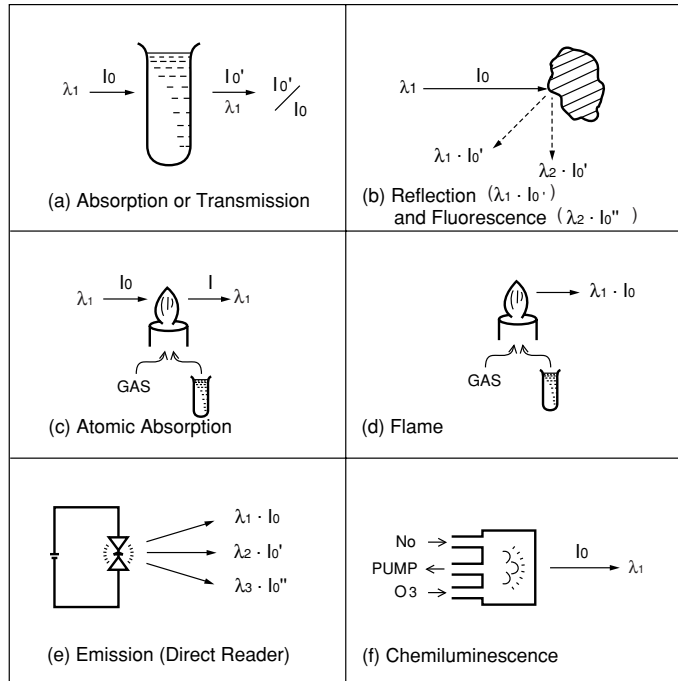
## **APPLICATIONS**

*Photomultiplier tubes (PMTs) are extensively used as photodetectors in fields such as chemical analysis, medical diagnosis, scientific research and industrial measurement. This chapter introduces major applications of photomultiplier tubes and describes the principle and detection methods for each application.*

## 14.1 Spectrophotometry

### 14.1.1 Overview

Spectrophotometry is a study of the transmission and reflection properties of material samples as a function of wavelength, but the term commonly means chemical analysis of various substances utilizing photometry. Photometric instruments used in this field are broadly divided into two methods. One utilizes light absorption, reflection or polarization at specific wavelengths and the other uses external energy to excite a sample and measures the subsequent light emission. Photomultiplier tubes have been most widely used in this field for years. Major principles used in spectrophotometry are classified as illustrated in Figure 14-1 below.



THBV3\_1401EA

**Figure 14-1: Major principles of spectrophotometry**

Specific photometric instruments currently used are:

- 1) Visible to UV spectrophotometers (absorption, reflection)
- 2) Infrared spectrophotometers (absorption, reflection)
- 3) Far UV spectrophotometers (absorption, reflection)
- 4) Emission spectrophotometers
- 5) Fluorescence spectrophotometers
- 6) Atomic absorption spectrophotometers
- 7) Azimuthal, circular dichroism meters
- 8) Raman spectrophotometers
- 9) Densitometers, colorimeters and color analyzers  
etc.



## 14.1.2 Specific applications

The following paragraphs explain specific major applications of spectrophotometers, divided into two methods utilizing absorption or emission.

### (1) UV, visible and infrared spectrophotometers

When light passes through a substance, the light energy causes changes in the electronic state of the substance (electron transition) or induces characteristic vibration of the molecules, resulting in a loss of partial energy. This is referred to as absorption, and quantitative analysis can be performed by measuring the extent of absorption.

The principle and simplified block diagram<sup>1)</sup> of a spectrophotometer are shown in Figure 14-2.

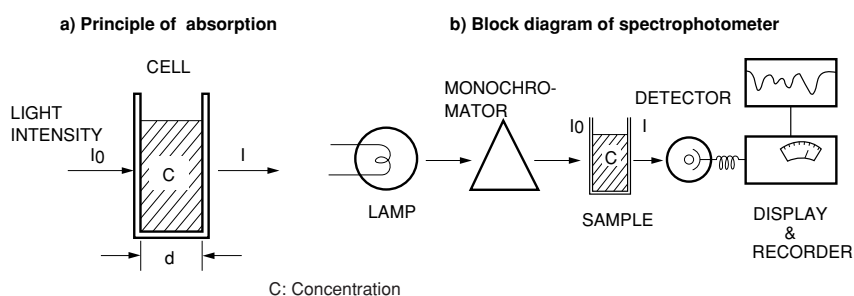


Figure 14-2: Principle and block diagram of a spectrophotometer

There are various optical systems in use today for spectrophotometers. Figure 14-3 illustrates the optical system of a spectrophotometer using light sources that cover from the ultraviolet to visible and near infrared range.

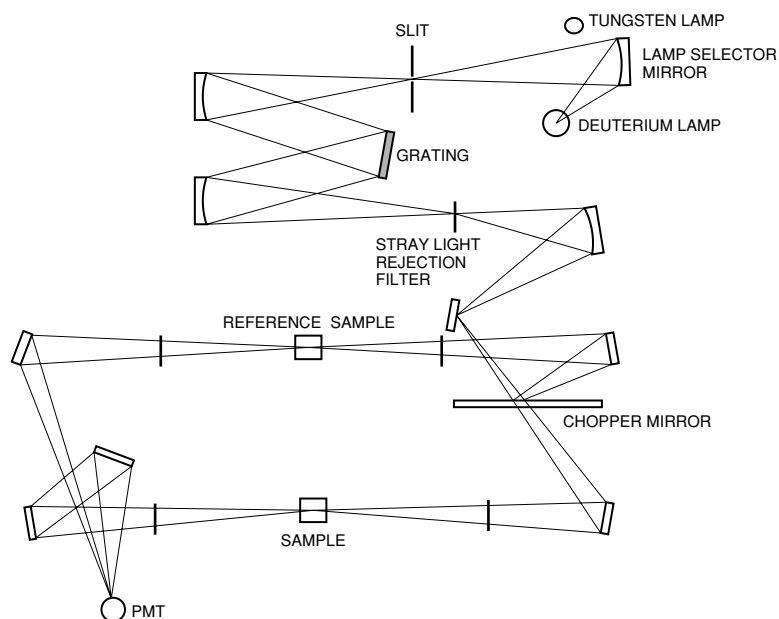
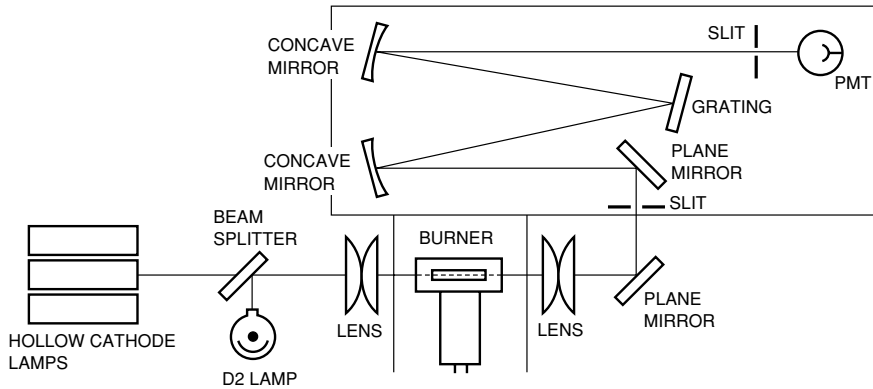


Figure 14-3: Optical system of a UV, visible to near IR spectrophotometer

## (2) Atomic absorption spectrophotometers

The atomic absorption spectrophotometer employs special light sources (hollow cathode lamps) constructed for the particular target elements to be analyzed. A sample is dissolved in solvent and burned to atomize it, and light from a specific hollow cathode lamp is passed through the flame. The amount of light that is absorbed is proportional to the concentration of the sample material. Therefore, by comparing the extent of absorption between the sample to be analyzed and a standard sample measured in advance, it is possible to find the concentration of a specific element in the sample. A typical optical system<sup>2)</sup> used for atomic absorption spectrophotometers is shown in Figure 14-4.

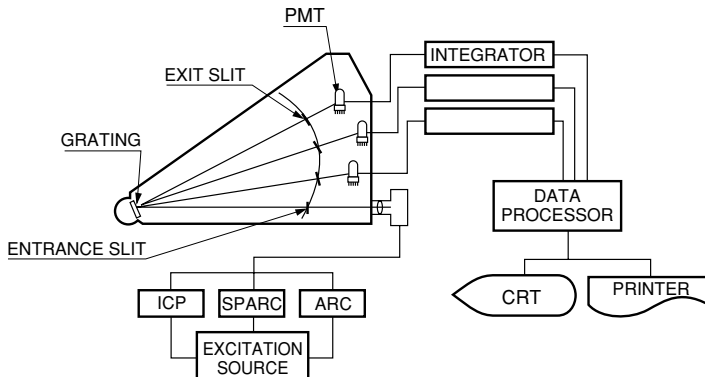


THBV3\_1404EA

Figure 14-4: Optical system used in atomic absorption spectrophotometers

## (3) Atomic emission spectrophotometers

When external energy is applied to a sample, light is emitted from the sample. Dispersing this emission using a monochromator, into characteristic spectral lines of elements and measuring their presence and intensity simultaneously, allows rapid qualitative and quantitative analysis of the elements contained in the sample. Figure 14-5 illustrates the schematic diagram<sup>3)</sup> of a photoelectric emission spectrophotometer in which multiple photomultiplier tubes are used.

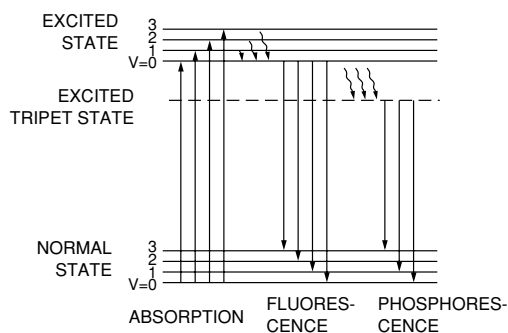


THBV3\_1405EA

Figure 14-5: Block diagram illustrating a photoelectric emission spectrophotometer

#### (4) Fluorospectrophotometers

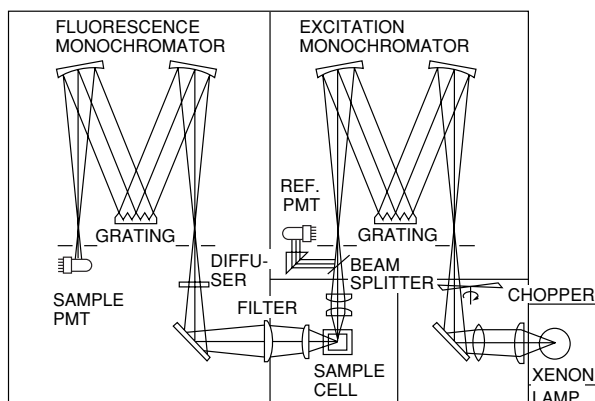
The fluorospectrophotometer is mainly used for chemical analysis in biochemistry, especially in molecular biology. When a substance is illuminated and excited by visible or ultraviolet light, it may emit light with a wavelength longer than the excitation light. This light emission is known as fluorescence and its emission process<sup>4)</sup> is shown in Figure 14-6. Measuring the fluorescent intensity and spectra allows quantitative and qualitative analysis of the elements contained in the substance.



THBV3\_1406EA

Figure 14-6: Fluorescent molecular energy levels

Figure 14-7 shows the structure<sup>5)</sup> of a fluorospectrophotometer using photomultiplier tubes as the detectors. This instrument roughly consists of a light source, excitation monochromator, fluorescence monochromator and fluorescence detector. A xenon lamp is commonly used as the light source because it provides a continuous spectrum output over a wide spectral range. The excitation and fluorescence monochromators use the same diffraction grating or prism as used in general-purpose monochromators.



THBV3\_1407EA

Figure 14-7: Fluorospectrophotometer structure

## 14.2 Medical Equipment

### 14.2.1 PET (Positron Emission Tomography)

In addition to gamma cameras and SPECT described in the next subsection, much attention has recently been focused on positron emission tomography (PET) as an application of nuclear medical diagnosis using photomultiplier tubes. This section explains specific examples of PET. The schematic diagram of a PET scanner is shown in Figure 14-8 and the external view in Figure 14-9.

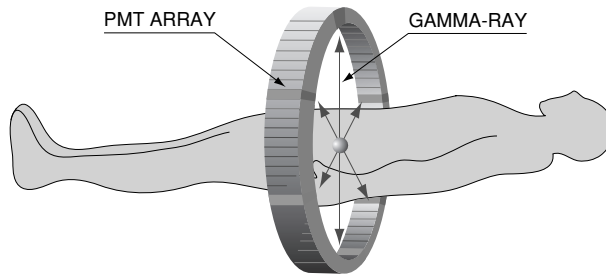


Figure 14-8: Concept view of a PET scanner

**When a positron released from radioactive tracers injected into body annihilates with an electron, two gamma-ray photons of 511 keV are emitted in opposite directions. These gamma-rays are simultaneously detected by the PMT array.**



Figure 14-9: [Reference example] External view of a whole-body PET scanner (Hamamatsu Photonics SHR-92000)

PET provides tomographic images of a living body in the active state and allows early diagnosis of lesions and tumors by injecting pharmaceuticals labeled with positron-emitting radioisotope into the body and measuring their concentrations. Typical positron-emitting radioisotopes used in PET are  $^{11}\text{C}$ ,  $^{13}\text{N}$ ,  $^{15}\text{O}$  and  $^{18}\text{F}$ .

When positrons are emitted within the body, they combine with the electrons in the neighboring tissues, releasing a pair of gamma-rays at 180 degrees opposite each other. Multiple rings of detectors surrounding the subject detect and measure these gamma rays by the coincidence technique. By arranging the acquired transaxial data at each angle, the PET scanner then creates a tomographic image by image reconstruction in the same way as X-ray computed tomography (X-ray CT).

A prime feature of PET is that quantitative measurement of physiological or biochemical information such as metabolism, blood flow and neural transmission within the body can be performed. PET has been chiefly used in research and study on brain functions and other organ mechanisms. Currently, PET is being put to active use in medical diagnosis, proving effective in diagnosing cancer.

A detector used in PET consists of a compact photomultiplier coupled to a scintillator. To efficiently detect gamma-rays of high energy (511keV) released from inside the body, scintillators with high stopping power versus gamma-rays such as BGO and LSO crystals are commonly used.

Another type of measurement technique is now being studied, which utilizes the TOF (time-of-flight) of gamma-rays generated by positron annihilation. This measurement uses high-speed photomultiplier tubes and scintillators with a short emission decay.

Scintillator	Density (g/cm <sup>3</sup> )	Relative Emission Intensity	Emission Time (ns)	Wavelength of Peak Emission (nm)
BaF <sub>2</sub>	4.89	5/26	0.8/620	220/320
BGO	7.13	20	60/300	480
LSO	7.35	72	40	420
GSO	6.71	20	60/600	430
NaI(Tl)	3.67	100	230	410

Numbers separated by a slash (/) indicate there are two emission components.

**Table 14-1: Characteristics of major scintillators**

PET scanners for animals are used in applications such as animal experiments for research that cannot be easily done with humans, as well as for developing new medicines and evaluating the pharmacological effects of general medicines. Small laboratory animals such as mice and rats, and monkeys or baboons are usually used with PET scanners.

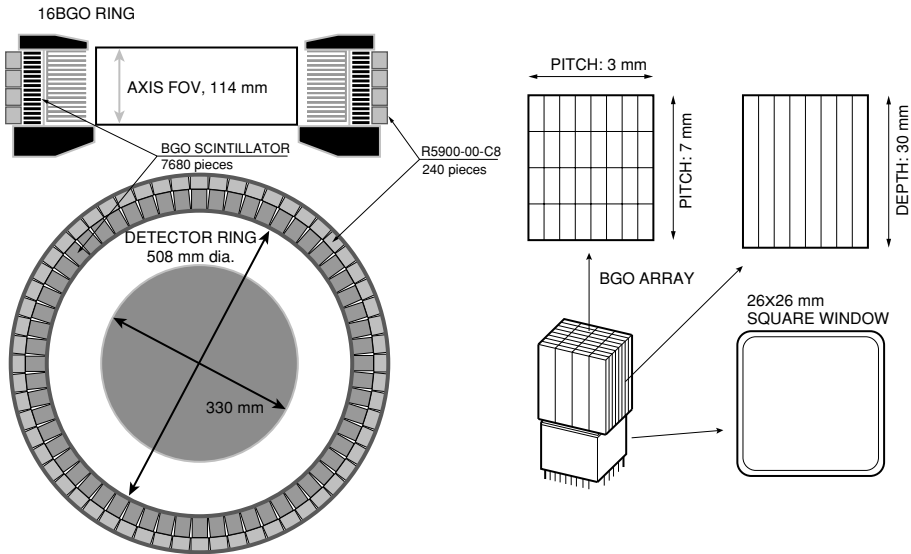
Because those animals' organs are relatively small, PET scanners must provide high resolution. For this purpose, for example, the Hamamatsu Photonics model SHR-7700 PET scanner used a large number of scintillation detectors, each consisting of a position sensitive photomultiplier tube combined with 32 BGO scintillators. A total of 240 photomultiplier tubes and 7,680 BGO scintillators were used in one PET scanner.

The SHR-7700 offered an effective field of view of 330×114 millimeters and a center resolution of 2.6 millimeters.



**Figure 14-10: [Reference example] External view of Hamamatsu Photonics SHR-7700 PET scanner for animals**

The detector ring and scintillation detector used in the SHR-7700 are illustrated in Figure 14-11.



THBV3\_1411EA

Figure 14-11: Cross section of SHR-7700 detector ring and scintillation detector

Figure 14-12 shows images of oxygen metabolic activity in a monkey brain, observed by the SHR-7700.

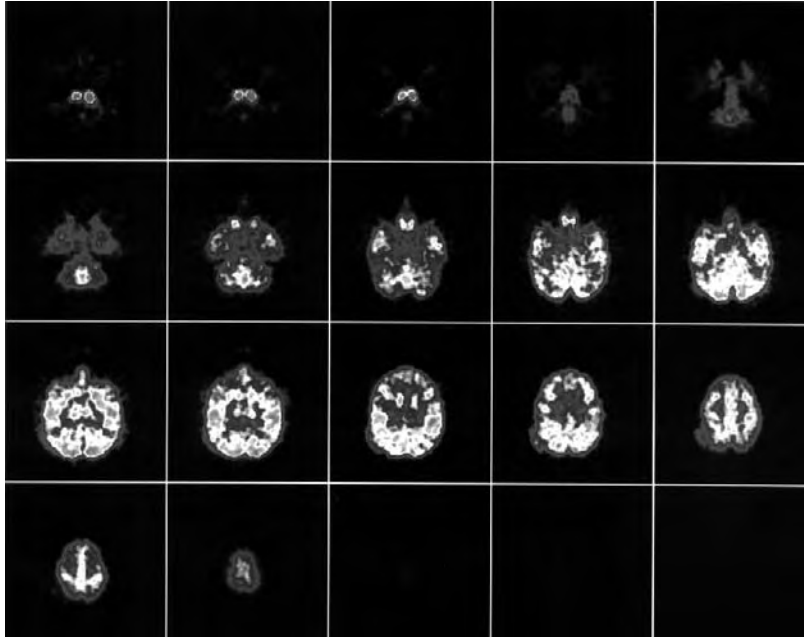
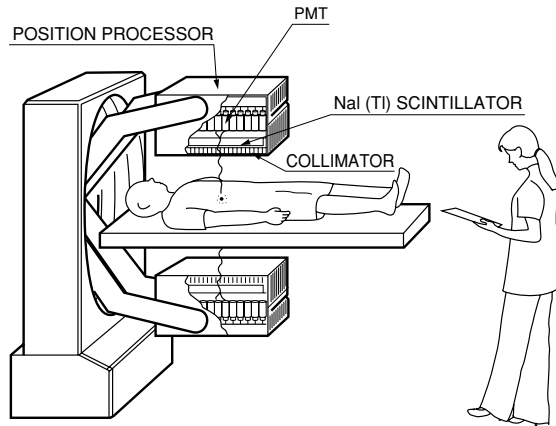


Figure 14-12: Images of oxygen metabolic activity in a monkey brain (positron imaging)

## 14.2.2 Gamma cameras

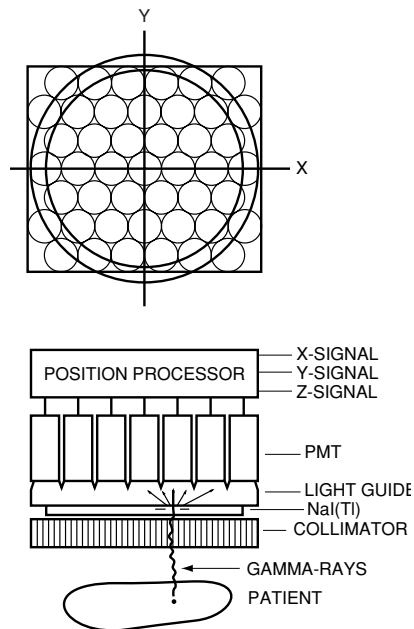
Imaging equipment utilizing a radioactive isotope (RI) first appeared as a scintillation scanner before undergoing successive improvements leading to the currently used gamma camera developed by Anger (U.S.A.). Recently, even more sophisticated equipment called SPECT (single photon emission computed tomography), which utilizes the principle of the gamma camera, has been developed and is now coming into wide use. An external view of a gamma camera is shown in Figure 14-13.



THBV3\_1413EA

**Figure 14-13: External view of a gamma camera**

Figure 14-14 shows sectional views of a detector used in gamma cameras, in which dozens of photomultiplier tubes are installed in a honeycomb arrangement. Each photomultiplier tube is coupled, via a light-guide, to a large-diameter scintillator made from a thallium-activated sodium-iodide (NaI(Tl)) scintillator, serving as a gamma-ray detector.



THBV3\_1414EA

**Figure 14-14: Sectional views of a detector used in gamma cameras**

To make gamma cameras more effective for medical diagnosis, a variety of gamma-ray nuclide drugs have been developed. Improvements in the position processing circuit have also achieved higher resolution, making gamma cameras more popular in medical diagnosis. Major nuclides used for nuclear medical imaging are listed in Table 14-2.

Recently, a SPECT equipped with two or three camera heads is often used to improve sensitivity.

Nuclide	Gamma-ray energy (keV)	Half-life
$^{99m}\text{Tc}$	141(no $\beta$ )	6.01h
$^{133}\text{Xe}$	81( $\beta$ :346)	5.243d
$^{67}\text{Ga}$	93(37%), 185(20%), 300(17%)	78.3h
$^{201}\text{Tl}$	70.8(Hg-X), 16.7(11%), 135(2.8%)	72.91h
$^{131}\text{I}$	364(81%)( $\beta$ :606)	8.04d
$^{123}\text{I}$	159(83%)	13.2h
$^{81m}\text{Kr}$	190(67%)	13s
$^{111}\text{In}$	245(94%), 171(90%)	2.83d

Values in parentheses ( ) indicate stripping efficiency.

**Table 14-2: Major nuclides used for nuclear medical imaging**

### 14.2.3 Planar imaging device

A planar imaging device is designed to capture two-dimensional images using positron-emitting nuclides and a pair of radiation detectors comprised of a position sensitive photomultiplier tube coupled to a scintillator array. The pair of detector units are arranged so that they face each other and an object to be measured is placed between them. Two-dimensional images of a positron-emitting nuclide tracer injected into the subject and their changes over time can be observed.

When a living plant or a small living animal is placed between the two detector units, the activity of substances within its body can be measured as two-dimensional images at nearly real-time. Positron-emitting nuclides such as  $^{11}\text{C}$ ,  $^{13}\text{N}$  and  $^{15}\text{O}$  are major elements that constitute a living body and are also the basic substances used for organic synthesis. This makes it possible to use many kinds of pharmaceutical compounds labeled with positron-emitting nuclides. (Example:  $^{11}\text{CO}_2$ ,  $^{11}\text{C}$ - methionine,  $^{13}\text{NH}_4^+$ ,  $^{13}\text{NO}_3^-$ ,  $^{15}\text{O}$ - water, etc.)

When a positron-emitting nuclide with a short half-life period is used, for example  $^{11}\text{C}$  (20 minutes),  $^{13}\text{N}$  (10 minutes) or  $^{15}\text{O}$  (2 minutes), measurements can be repeated using the same individual. This allows measurement of changes in a day or measurement under two or more different conditions while eliminating errors that may be caused by individual differences.

Since annihilation gamma-rays (511 keV) are used for imaging, self-absorption within the object being measured can be almost ignored, allowing accurate measurement of the distribution of substances in a plant or small animal. Compared to medical PET scanners, the planar imaging device can obtain images with a higher signal-to-noise ratio and spatial resolution because the image generation technique is simple.

Unlike tomographic PET images, when the object being measured is relatively thin, it is easier to visually recognize the image since the image obtained is a (pseudo-) projected image.

The block diagram and external view of a planar imaging device are shown in Figure 14-15.



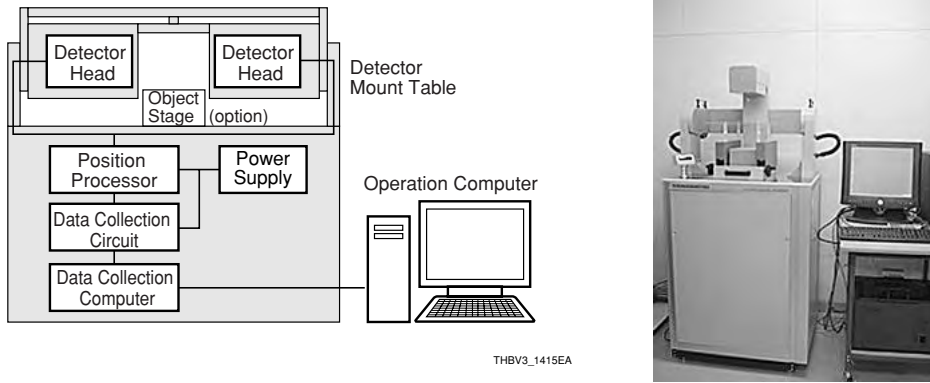


Figure 14-15: Block diagram and external view of a planar imaging device

### 14.2.4 X-ray image diagnostic equipment

X-ray image diagnostic equipment is used in routine examinations at many medical clinics and facilities. Photomultiplier tubes are used in many types of X-ray examination apparatus to monitor the X-ray exposure time or dose. With the recent trend toward filmless X-ray imaging systems, photomultiplier tubes have also been widely used in detectors that read out X-ray images formed on a special phosphor plate instead of X-ray films.

#### (1) X-ray phototimer

The X-ray phototimer automatically controls the X-ray film exposure in X-ray examinations. The X-rays transmitting through a subject are converted into visible light by a phosphor screen. A photomultiplier tube is used to detect this light and provide an electrical signal. When the accumulated electrical signal reaches a preset level, the X-ray irradiation is shut off to obtain an optimum film density.

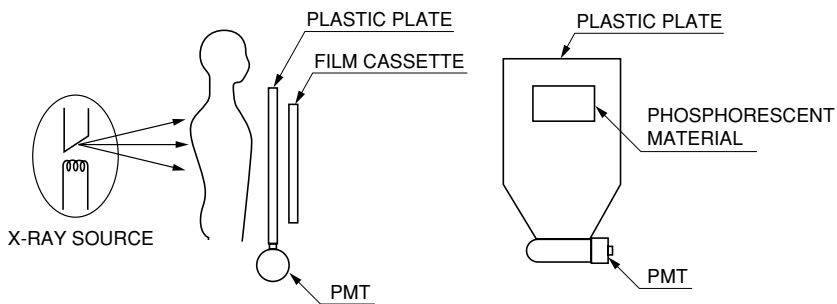


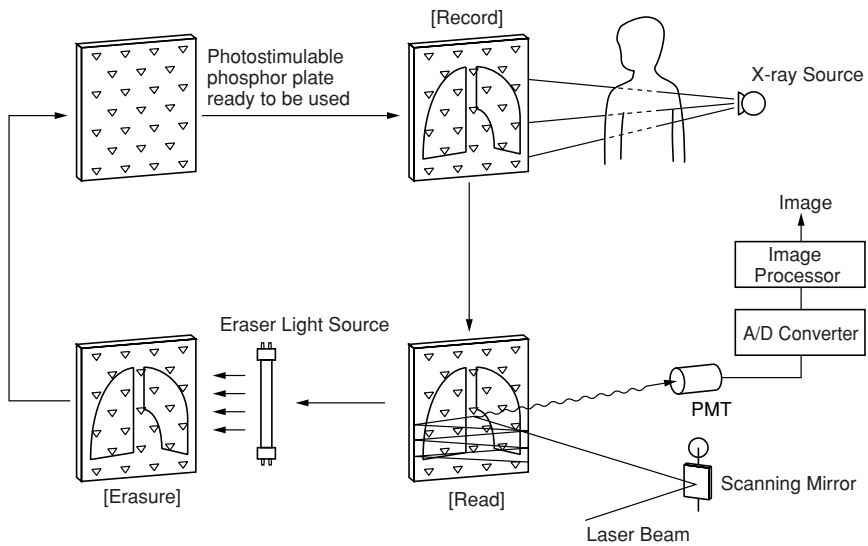
Figure 14-16: X-ray phototimer

THBV3\_1416EA

## (2) Computed radiography (CR)

X-ray image diagnosis systems also includes computed radiography equipment using a special photostimulable phosphor plate. In this equipment, an X-ray image is temporarily accumulated on the phosphor plate and a laser beam then scans (excites) the image formed on the phosphor plate, causing visible light to be emitted according to the amount of accumulated X-rays. A photomultiplier tube is then used to convert this weak visible light into electrical signals which are then digitally processed to reconstruct an image.

Computed radiography has several advantages over conventional techniques using X-ray films. It offers a short imaging time, less imaging errors, and digital image processing and data analysis that permit high-density storage and simple retrieval of image data. These useful features have led to its widespread used in the world.

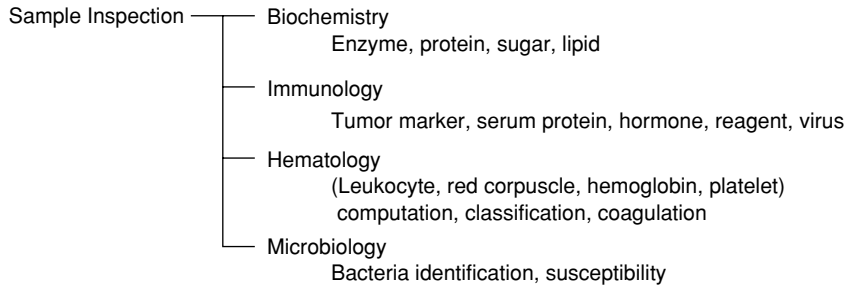


THBV3\_1417EA

**Figure 14-17: X-ray image acquisition using photostimulable phosphor plate**

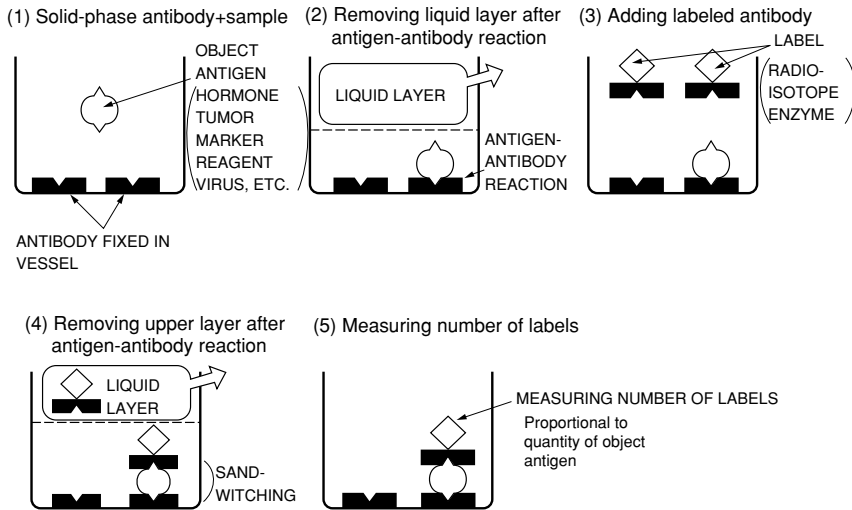
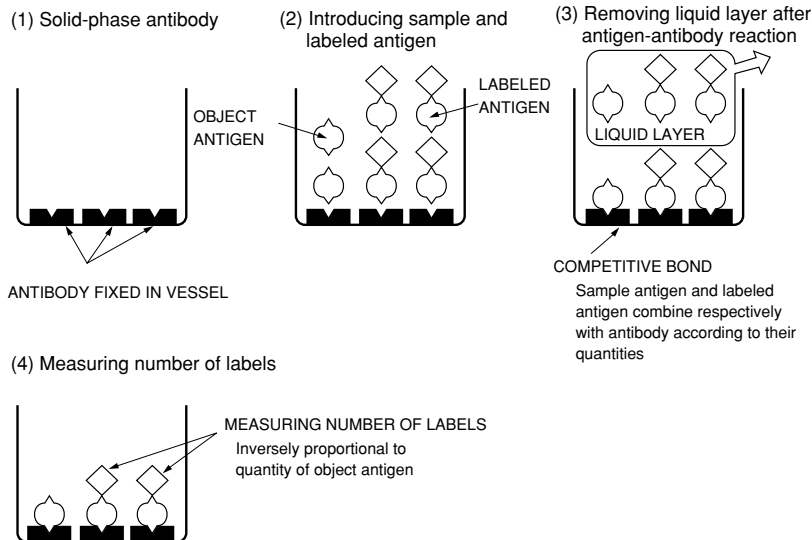
### 14.2.5 In-vitro assay

The analysis and inspection of blood or urine samples collected out of a living body is referred to as in-vitro assay. It is used for physical checkups, diagnosis, and evaluation of drug potency. The in-vitro assay can be classified as shown in Table 14-3. Among these, the concentrations of most tumor markers, hormones, drugs and viruses classified under immunological assay are exceedingly low. Detecting these items requires extremely high-sensitivity inspection equipment that mostly must use photomultiplier tubes.



**Table 14-3: Classification of in-vitro inspection**

Immunoassay, a measurement technique that relies on the specificity of the antigen-antibody reaction is widely used. The principles of immunoassay<sup>6)</sup> are illustrated in Figure 14-18 and the procedures of each method are explained in the subsequent paragraphs.

**(a) Sandwich Method****(b) Competitive Method**

TNBV3\_1418EA

**Figure 14-18: Principles of immunoassay**

Figure 14-18 (a) is a technique known as the sandwich method. Step (1): Samples are introduced into a vessel in which antibodies responding to object antigens (hormones, tumor markers, etc.) are fixed (solid-phase antibody). Step (2): Antigen-antibody reaction occurs and each object antigen combines with a solid-phase antibody. This reaction has an extremely high singularity and hardly ever occurs with a different antigen. After antigen-antibody reaction, the liquid layer is removed leaving the combined antigen and antibody. Step (3): Labeled antibodies are added, which combine with object antigens. Step (4): Antigen-antibody reaction occurs again so that the object antigen is sandwiched between the antibodies. The liquid layer is then removed. Step (5): The quantity of labels is optically measured using a photomultiplier tube.

Figure 14-18 (b) shows another technique called the competitive method. Step (1): Antibodies responding to object antigens are fixed on the bottom of a vessel. Step (2): Samples are added along with the labeled object antigens. Step (3): Competitive reaction occurs in which object antigens and labeled antigens combine with labeled antibodies in proportional to their concentration, reaching a state of equilibrium. After the antigen-antibody reaction, the unnecessary upper layer is removed. Step (4): The quantity of labels is measured using a photomultiplier tube. In the sandwich method, the higher the concentration of object antigens, the larger the signal. Conversely, in the competitive method, the higher the concentration of the object antigens, the lower the signal.

Immunoassay can be further categorized according to the material used for labeling as follows

- (1) Using radioactive isotopes for labeling  
..... RIA (Radioimmunoassay)
- (2) Using enzymes for labeling  
..... EIA (Enzymeimmunoassay)

### (1) RIA (Radioimmunoassay) method

Radioactive isotope (RI) is used for the labeling as was explained above, and radiation (gamma or beta rays) emitting from the RI labels is detected by the combination of a scintillator and a photomultiplier tube, so that the object antigen can be quantitatively measured. Radioactive isotopes most frequently used for labeling are  $^3\text{H}$ ,  $^{14}\text{C}$ ,  $^{57}\text{Co}$ ,  $^{75}\text{Se}$ ,  $^{125}\text{I}$  and  $^{131}\text{I}$ . (See Table 14-4.)<sup>7)</sup> Of these,  $^{125}\text{I}$  offers useful characteristics for labeling and is very widely used. Because radioactive isotopes other than  $^3\text{H}$  and  $^{14}\text{C}$  emit gamma rays, sodium iodide crystals are used as a scintillator to provide a high conversion efficiency.

Radioisotope	Half-life	Energy	Detection Method
$^3\text{H}$	12.26 years	$\beta$	Liquid scintillation
$^{14}\text{C}$	5730 years	$\beta$	Liquid scintillation
$^{57}\text{Co}$	270 days	$\gamma$	Scintillation crystal
$^{75}\text{Se}$	120.4 days	$\gamma$	Scintillation crystal
$^{125}\text{I}$	60 days	$\gamma$	Scintillation crystal
$^{137}\text{I}$	8 days	$\beta, \gamma$	Scintillation crystal

**Table 14-4: Radioactive isotopes used for labeling in radioimmunoassay**

Recently, in in-vitro assays, the quantity of samples and the number of items to be measured are rapidly increasing. To keep pace with this trend, equipment for radioimmunoassay has been automated. A typical piece of automated equipment in use today is the well scintillation counter<sup>8)</sup> that makes use of sodium iodide scintillators having a well-like hole to enhance the conversion efficiency of the radiation into light. Measurements are made by automatically inserting test tubes, which contain a mixture of antigens and antibodies including labels, into each hole in the scintillator. (See Figure 14-19.) Each detector section including a scintillator is covered by lead shield to block extraneous radiation.

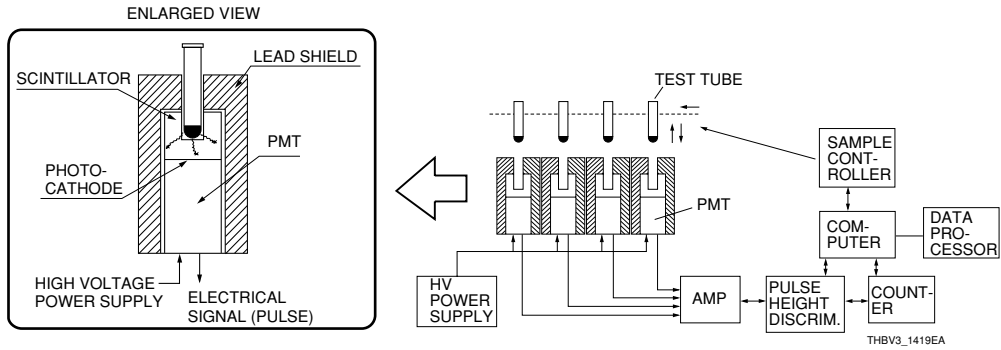


Figure 14-19: Schematic block diagram illustrating a well scintillation counter

## (2) Luminescent / fluorescent immunoassay

Non radioactive immunoassay techniques called "EIA (Enzymeimmunoassay)" that do not rely on radioisotopes are currently under research and development.

One of these is fluorescent immunoassay or fluoroimmunoassay in which a fluorescent substance is used for labeling. The final remaining mixture of antigens and antibodies is irradiated by an excitation light and the resulting fluorescence is measured with regard to the intensity, wavelength shift and polarization. This technique offers slightly higher sensitivity than that of EIA. Figure 14-20 shows the schematic drawing of an immunoreaction measurement system used for fluoroimmunoassay.

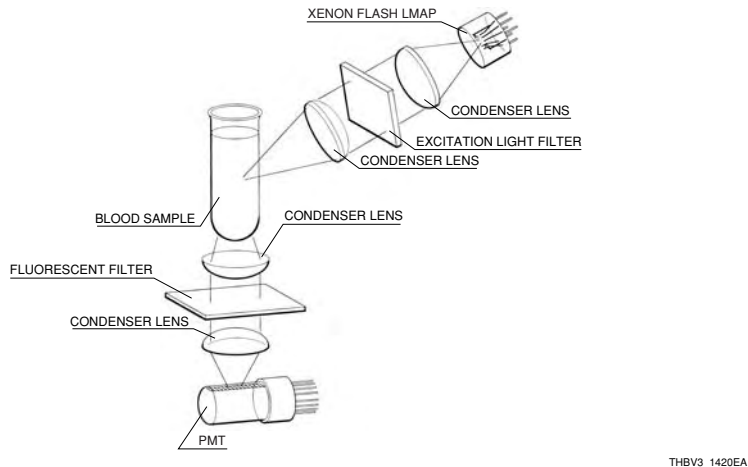


Figure 14-20: Schematic layout of a fluorescent immunoreaction measurement system

To achieve high sensitivity equal to RIA by using non-radioactive immunoassay, intensive research and development of emission-immunoassay has been carried out. This immunoassay uses a chemiluminous substance or bioluminous substance for labeling and allows the final remaining mixture of antigens and antibodies to emit light, which is detected by a photomultiplier tube. There are three types of emission-immunoassay methods, as follows:

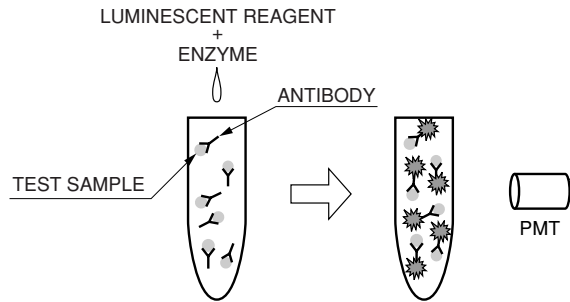
- 1) Use of a chemiluminous substance such as luminol and acridinium for labeling
- 2) Use of chemiluminescence or bioluminescence for activation of the label enzyme used in EIA
- 3) Use of a catalyst for the bioluminescence reaction

Methods 2) and 3) can be thought of as variations of EIA techniques. Luminescent immunoassay has very high sensitivity equivalent to the measurable concentration ranges of RIA.

### (3) Chemiluminescent immunoassay

Chemiluminescent immunoassay has several merits such as high sensitivity, wide dynamic range, and simple measurement without using detection antigens and special facilities which are usually needed by radioimmunoassay.

When enzymes are added to antibodies or antigens labeled with a luminescent reagent, a chemical reaction occurs. Light emission accompanying the reaction is detected by a photomultiplier tube.



THBV3\_1421EA

**Figure 14-21: Principle of chemiluminescent immunoassay**

## 14.3 Biotechnology

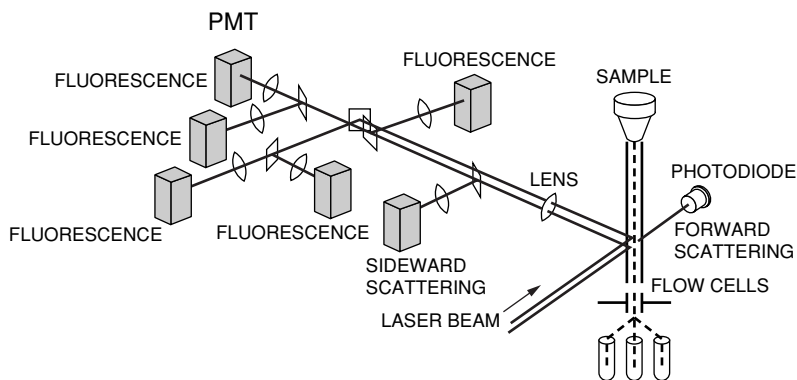
### 14.3.1 Overview

In life science applications, photomultiplier tubes are mainly used for detecting fluorescence and scattered light. Major equipment used for life science includes cell sorters, fluorometers and DNA sequencers.

### 14.3.2 Application examples

#### (1) Flow cytometers

When light is irradiated onto a rapidly flowing solution which contains cells or chromosomes, a scattered light or fluorescence is released from the cells or chromosomes. By analyzing this scattered light or fluorescence, it is possible to elucidate cell properties and structures and separate the cells based on these properties. This field is known as flow cytometry. In this field, a flow cytometer like the one illustrated in Figure 14-22 is most frequently used. The flow cytometer is an instrument that selects and collects only specific cells labeled by a fluorescent substance from a mixture of cells in a solution.



THBV3\_1422EA

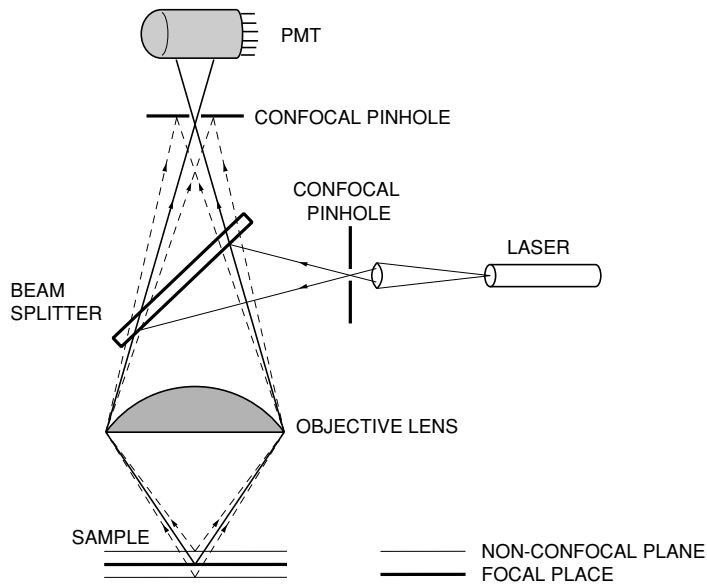
**Figure 14-22: Major components of a flow cytometer**

In a cell sorter, a fluorescent probe is first attached to the cells. The cells pass through a thin tube at a fixed velocity. When each cell passes through a small area onto which an intense laser beam is focused, the fluorescence is emitted from the cell and is detected by a photomultiplier tube. The photomultiplier tube outputs an electrical signal in proportion to the number of fluorescent molecules attached to each cell. At the same time, the laser beam light is scattered forward by the cell, and detecting this scattered light yields information on the cell volume. After processing these two signals, the cell sorter creates an electrical pulse that deflects a drop of liquid, containing the desired cell into one of the collection tubes.



## (2) Confocal laser microscopes

The confocal laser microscope acquires 2 and 3-dimensional fluorescent images of a sample labeled with fluorescent dye by scanning the sample surface with a laser. The laser scans an extremely tiny spot to obtain high-resolution images by means of confocal function. (See Figure 14-23.) A biological sample stained with fluorescent dye and placed beneath the microscope is scanned by an excitation laser beam narrowed to a very small size equal to the light wavelength, and by moving the sample stage up or down, only the fluorescence from sections matching the focus point passes through the pinhole and is detected by a photomultiplier tube. The electrical signals from the photomultiplier tube are then image-processed and reconstructed into high-resolution 2D or 3D images. Confocal laser microscopes are mainly used for observation of biological tissues or sections.



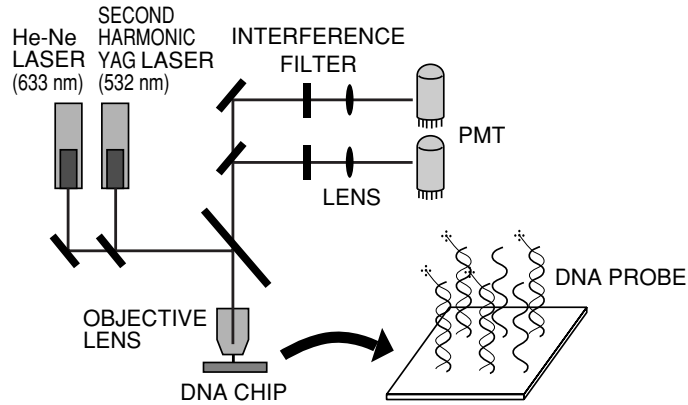
THBV3\_1423EA

Figure 14-23: Confocal laser microscope

## (3) DNA microarray scanners

Biochemical tools called "DNA chips" are used for analyzing vast amounts of genetic information. A DNA chip is a substrate holding large numbers of DNA probes at a high density. Some DNA chips make use of semiconductor photolithographic methods, while on others, DNA is dispensed on a slide glass using a high-precision robot mechanism. DNA probes (arrangement is known) bonded on a slide glass are hybridized with sample DNA segments labeled with fluorescent dye. A laser beam scans the DNA chip and the intensity of fluorescence emitted from the hybridized DNA is measured to acquire genetic information on the sample DNA.

(Hybridization is a process where single DNA strands having the same complementary base link to form a double strand.) (See Figure 14-24.)

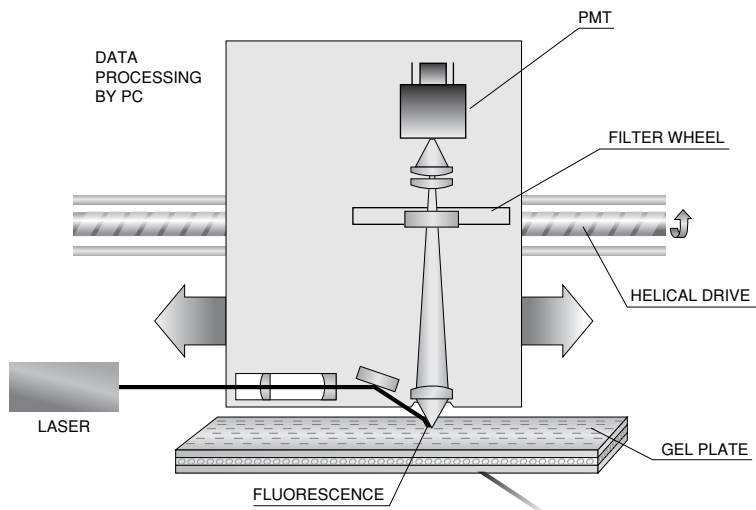


THBV3\_1424EA

Figure 14-24: DNA microarray scanner

#### (4) DNA sequencers

This is an instrument used to decode the base arrangement of DNA extracted from a cell. The principle of a DNA sequencer is shown in Figure 14-25. An extracted DNA segment is injected onto gel electrophoresis plate or into capillary tubes along with a fluorescent label which combines with a specific base of the DNA segment. When an electric potential is applied across the gel, the DNA begins to migrate and separate based on size and charge. When the DNA segment reaches the position of the scanning line, it is excited by a laser, causing only the portion with the labeling pigment to give off fluorescence. This fluorescent light is passed through monochromatic filters and detected by photomultiplier tubes. Computer-processing of the position at which the fluorescence has occurred gives information on where the specific bases are located. The DNA sequencer is used for the genetic study of living organisms, research into the cause and treatment of genetic diseases, tumors and adult diseases, as well as decoding of human genes.



THBV3\_1425EA

Figure 14-25: Principle of a DNA sequencer

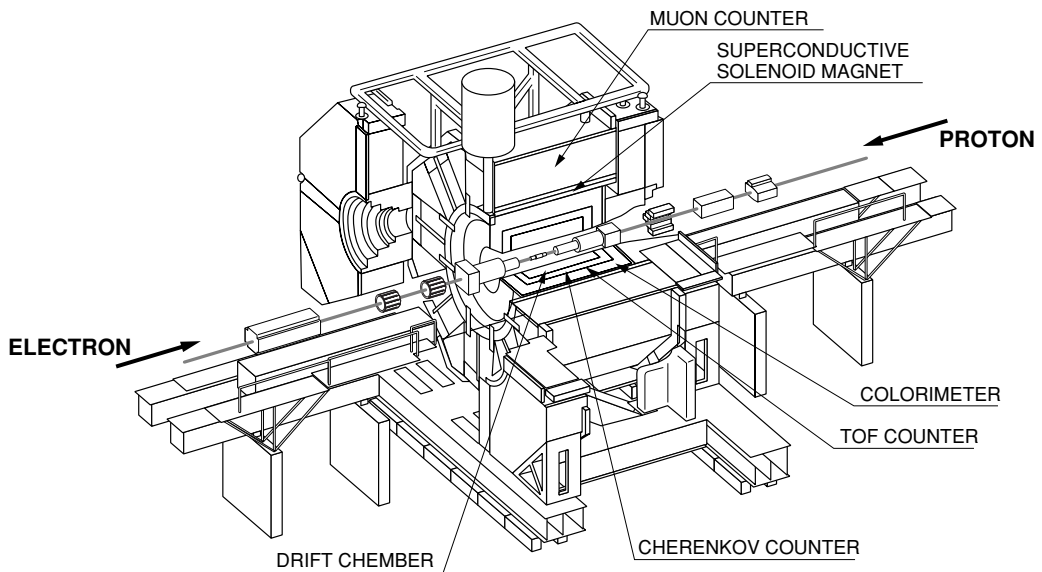
## 14.4 High-Energy Physics Experiments

### 14.4.1 Overview

Photomultiplier tubes are widely used as detectors in high-energy physics experiments. For example, when a charged particle passes through a scintillator, a light flash is given off in accordance with the particle energy. Detecting this light flash makes it possible to measure the energy, speed and direction of the charged particle. This technique is absolutely essential in high-energy physics research which is constantly aiming for the ultimate in scientific technology.

### 14.4.2 Collision experiments

In collision experiments, primary particles such as electrons and protons are accelerated to high energy by an accelerator so that they collide with each other to produce secondary particles. The energy, speed and kinetic momentum of these secondary particles are detected and observed. There are several particle detection methods that use photomultiplier tubes, for example, a hodoscope, TOF counter, calorimeter and Cherenkov counter.

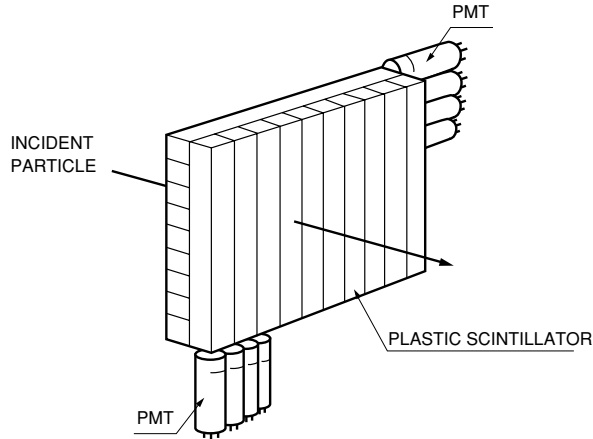


THBV3\_1426EA

Figure 14-26: Example of collision experiment setup

## (1) Hodoscopes

Figure 14-27 shows a simplified diagram<sup>9)</sup> of a hodoscope. Plastic scintillators are arrayed in two orthogonal layers followed by photomultiplier tubes. The position and time at which a charged particle passes through certain scintillators are detected by the corresponding photomultiplier tubes.

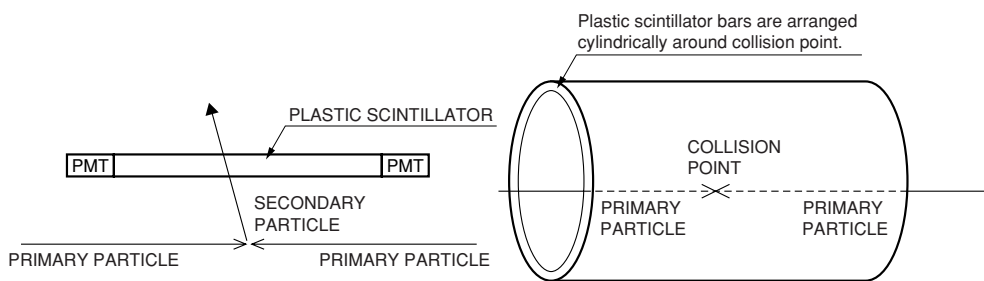


THBV3\_1427EA

Figure 14-27: Simplified diagram of a hodoscope

## (2) TOF counters

TOF counters measure the time of flight (TOF) of particles to identify the type of the particles. A simplified illustration of a TOF counter is shown in Figure 14-28. When primary particles collide with each other, secondary electrons are generated. The time of flight of those particles from the collision point is measured to find the velocity of the particles. A typical detector for TOF counters consists of a long plastic scintillator bar with both ends coupled to a photomultiplier tube. A large number of plastic scintillator bars are arranged cylindrically around the collision point.



THBV3\_1428EA

Figure 14-28: TOF counter setup

Figure 14-28: Entire TOF counter

### (3) Calorimeters

Calorimeters measure the energy of secondary particles such as electrons, photons and hadrons. A simplified illustration of a calorimeter is shown in Figure 14-29. The collision point is surrounded by detectors like a TOF counter. In the case of calorimeters, the energy of particles is released into matter and converted into light or an electric charge. This is usually measured with detectors consisting of an inorganic scintillator or lead glass combined with a photomultiplier tube. Recently, sampling calorimeters are also in use, which employ a multilayer structure of plastic scintillators and heavy metals such as iron and lead instead of using inorganic scintillators.

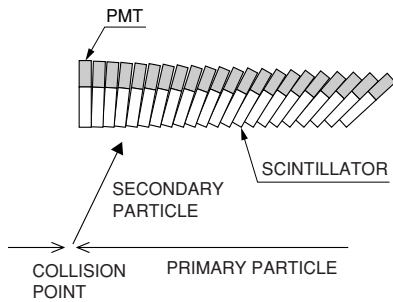


Figure 14-29: Calorimeter setup

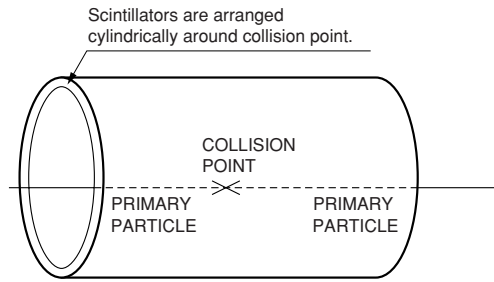


Figure 14-29: Entire calorimeter

THBV3\_1429EA

### (4) Cherenkov counters

Cherenkov radiation is emitted when a charged particle passes through matter called a "radiator" (transparent medium) with a velocity or energy greater than a certain level. This Cherenkov radiation is a kind of shock wave, so it is emitted in a cone around the direction of the charged particle, forming a ring pattern. The energy and type of the particle can be identified on the basis of the size and brightness of this ring.

Figure 14-30 shows a schematic diagram of a Cherenkov counter called "RICH" (Ring Imaging Cherenkov counter). Cherenkov light is emitted when a particle passes through a radiator with energy greater than a certain level. This light reflects on a mirror and is then detected by a photodetector array installed on the opposite side. The energy and type of the particle are identified by measuring the size of the ring.

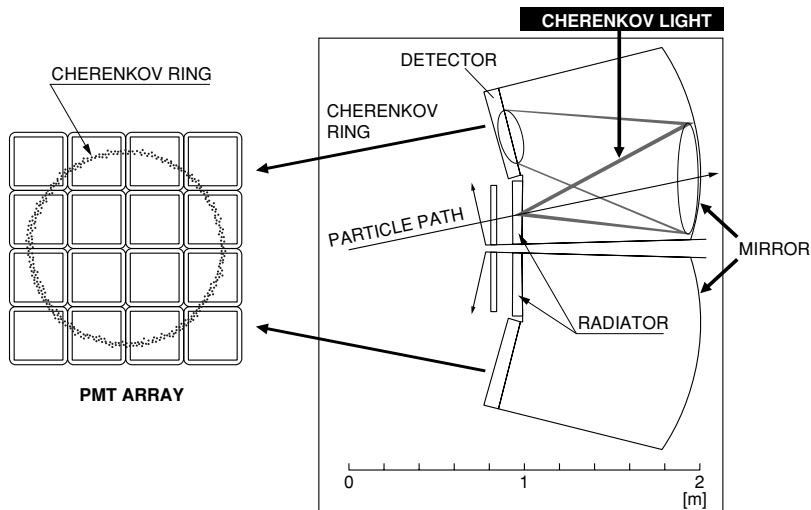


Figure 14-30: Schematic diagram of RICH

THBV3\_1430EA

### 14.4.3 Proton decay, neutrino observation experiments

Proton decay observation is an experiment that attempts to capture the Cherenkov light emitted by high-energy charged particles that are supposedly produced when protons decay. Photomultiplier tubes are used to detect the Cherenkov light.

#### Kamiokande

In 1983, the Kamiokande (KAMIOKA Nucleon Decay Experiment) detector was installed in an underground mine in Hida City, (formerly Kamioka Town) in Gifu Prefecture, Japan, under the guidance of the Institute for Cosmic Ray Research (ICRR) and the High Energy Physics Research Laboratory, Faculty of Science, University of Tokyo. The Kamiokande detector was constructed with a huge tank filled with pure water installed 1 kilometer underground. On the side walls, bottom and roof of this tank, 1,050 photomultiplier tubes, each 20 inches in diameter making them the largest of their class in the world, were installed to wait quietly to catch the instant of photon decay. These photomultiplier tubes were manufactured to exacting specifications, for example, a large diameter glass bulb with a spherical photosensitive surface that allows catching the faint Cherenkov light traveling from a variety of angles and helps withstand the water pressure. High sensitivity, fast time response, and high photoelectron collection efficiency are also important factors.

In January 1987, besides proton decay, the Kamiokande detector was modified to allow observing solar neutrinos generated by nuclear fusion within the Sun. This modified detector catches the Cherenkov light that is rarely emitted when neutrinos flying away from the Sun pass through 3,000 tons of ultra-pure water in the tank. The 20-inch diameter photomultiplier tubes are used to detect this Cherenkov light. While waiting for the instant of proton decay, Kamiokande also detects solar neutrinos at the rate of about once every 9 days.

Since then the Kamiokande neutrino detection facility has yielded big news. At 4:35 AM on February 23rd, 1987, Kamiokande was the first facility in the world to detect neutrinos from the supernova 1987A that appeared in a corner of the Large Magellanic Cloud some 170,000 light years away. This is relatively close to the Earth and the blast from a supernova is said to occur only once every several hundred years. The last actual sighting was observed by the naked eye in 1604. A significant deficit in atmospheric neutrinos was reported from observation results with only about 46 percent of the expected number being detected.

#### Super-Kamiokande

In 1986, new plans for a "Super-Kamiokande" were unveiled by the University of Tokyo. Mainstream thought in the Grand Unified Theory is that proton lifetime may extend to  $10^{34}$  years. To probe predictions in current Grand Unified Theories, plans were drawn up for a neutrino detection facility with 10 to 100 times the performance of Kamiokande. The new facility, called Super-Kamiokande, was constructed in a Kamioka mine 1 kilometer underground and about 200 meters away from Kamiokande. A huge water tank of 39.2 meters in diameter and 41.4 meters in height was constructed and filled with 50,000 tons of ultra-pure water. This is about 16 times the size of the Kamiokande tank. The 11,200 photomultiplier tubes each 20 inches in diameter are a further improvement on the Kamiokande tubes. Observation begun in April 1996 at the Super-Kamiokande.

In 1998, atmospheric neutrino oscillation was discovered indicating that neutrinos have mass. Precision testing of neutrino oscillation was made by means of artificial neutrinos and oscillation of these artificial neutrinos was also verified and observation currently continues.

#### KamLAND

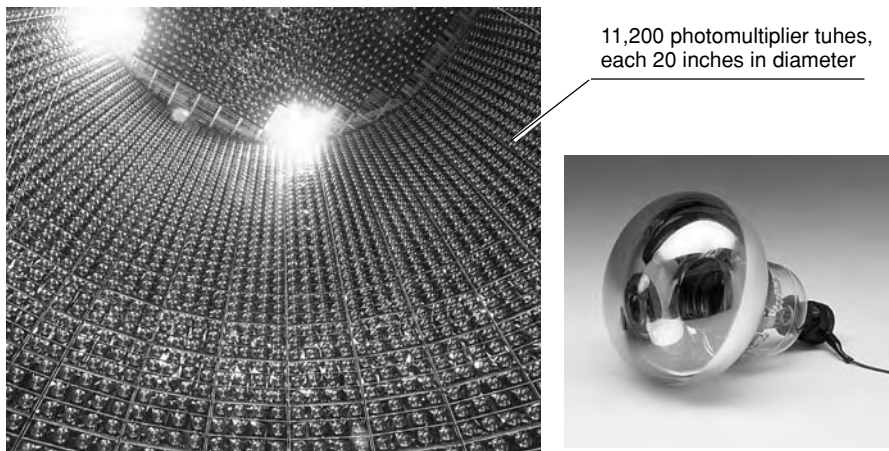
In January 2002, experiments commenced with the "KamLAND" (Kamioka Liquid-scintillator Anti-

Neutrino Detector) operated by the Research Center for Neutrino Science, Tohoku University.

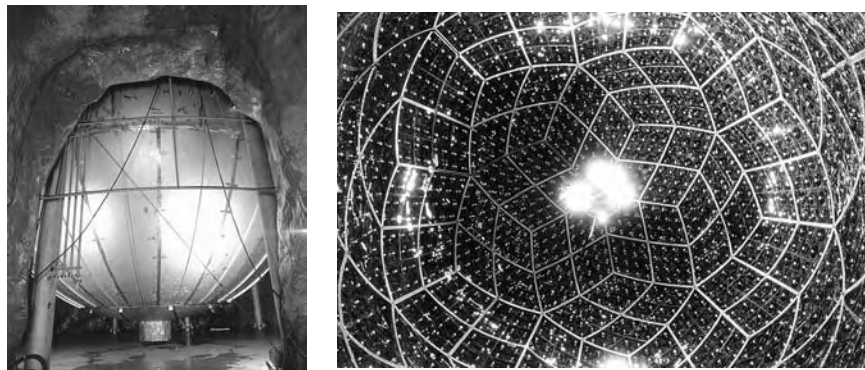
The KamLAND detector was constructed utilizing the former Kamiokande site yet is an even more sophisticated neutrino detector. Instead of pure water, KamLAND makes use of 1,000 tons of liquid scintillator to capture neutrinos. The intensity of the light emitted from the neutrinos reacting with the liquid scintillator is on a much larger scale than the Cherenkov light trapped at Kamiokande, and allows detecting neutrinos at lower energy levels. This liquid scintillator is held in a round balloon of about 13 meters in diameter made from special transparent film. The balloon itself is contained within a spherical tank of stainless steel 18 meters in diameter and having a volume of 3,000 cubic meters.

The inner wall of the tank is lined with approximately 1,900 photomultiplier tubes each 20 inches in diameter (effective area: 17 inches) that are improved versions of the Super-Kamiokande tubes. The outer wall of this spherical tank is further enclosed by a tank filled with pure water and this section is also lined with 20-inch photomultiplier tubes. At KamLAND, the time difference between two light emissions occurring from reaction with the neutrinos, and the time delay from the emission of light until the light reaches the photomultiplier tubes are measured. The location within the balloon where the neutrino reaction occurred can be determined in this way.

In 2002 it was announced that oscillation was present in neutrinos from nuclear power plants, and the mystery of solar neutrinos was determined to be due to this neutrino oscillation. Japan is a leader in the field of neutrino research and these superb devices are certainly one of the main reasons it retains this lead.



**Figure 14-31: Interior of Super-Kamiokande detector tank lined with 20-inch PMT**



Stainless steel spherical tank

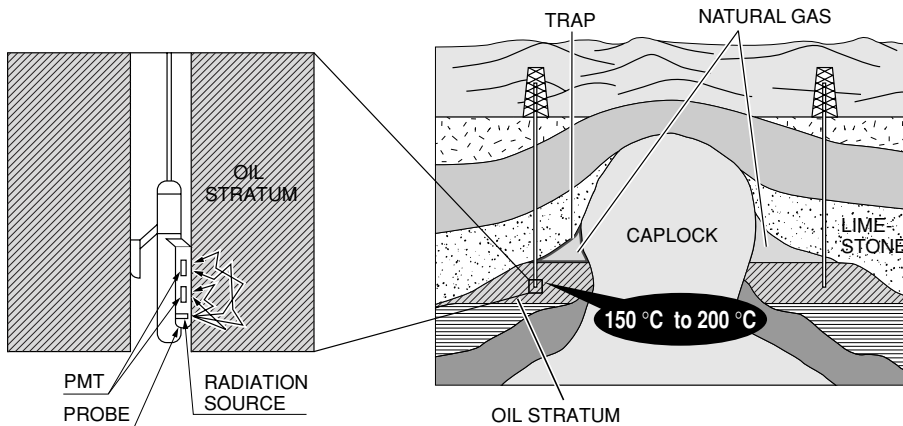
PMT installed on inner wall of spherical tank

**Figure 14-32: KamLAND**

## 14.5 Oil Well Logging

Special photomultiplier tubes have been developed that are capable of operating reliably in harsh environments including high temperature and severe vibration and shock. This section explains oil well exploration (oil well logging) as a sample application of these special tubes.

Oil well logging is used to locate an oil deposit and determine its size. This technique makes use of photomultiplier tubes as detectors for density well logging using radiation, neutron well logging and natural gamma-ray-spectrum well logging. In these well loggings, a probe containing a neutron or gamma ray source is lowered into a well as it is being drilled. The radiation or the neutrons that are scattered by the rock surrounding the well are detected by a scintillator/photomultiplier. The amount of scattered radiation detected is indicative of the density of the rock that surrounds the well. The scattered neutrons indicate the porosity of the rock which is required to ascertain if the oil can be removed. Naturally occurring gamma rays are detected to locate shale which indicates the presence of oil or gas. Figure 14-33 shows the measurement method<sup>(10)</sup> for oil well logging using radiation, and the cross sectional view of the strata layers around an oil well site.



THBV3\_1433EA

**Figure 14-33: Oil well logging using radiation probe and cross sectional view of strata layers**

The depth of a trial hole may be as deep as several thousand meters where the ambient temperature reaches as high as 150 to 200°C. In addition, shock and vibration are also applied to the photomultiplier tubes, imposing an extremely severe environment on the photomultiplier tubes. To meet these requirements, various types of ruggedized, high-temperature photomultiplier tubes have been developed which ensure adequate performance even under these severe environments. These photomultiplier tubes have a special photocathode that exhibits a minimal increase in dark current even at high temperatures and, in the multiplier section, dynode materials capable of withstanding high temperatures are employed. The electrode structures are also designed with careful consideration given to the effects of thermal expansion and vibration.



## 14.6 Environmental Measurement

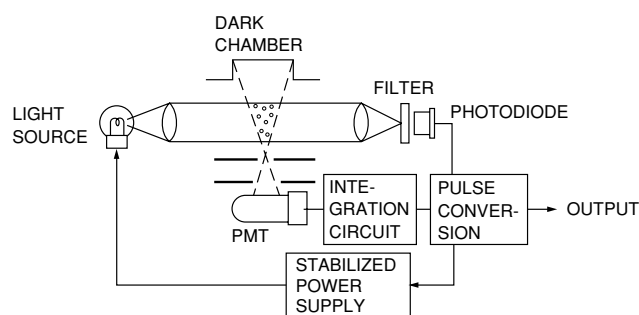
### 14.6.1 Overview

Photomultiplier tubes are also used as detectors in environmental measurement equipment, for example, in dust counters used to detect dust contained in air or liquids, and radiation survey monitors used in nuclear power plants. This section explains some of these applications.

### 14.6.2 Application examples

#### (1) Dust counters

A dust counter measures the concentration of floating dust in the atmosphere or inside a room by making use of principles such as light scattering and absorption of beta rays. Figure 14-34<sup>(11)</sup> shows the principle of a dust counter using light scattering. If dust is present in the light path, light is scattered by the dust. The quantity of this scattered light is proportional to the quantity of dust. The scattered light is detected by a photomultiplier tube and after being integrated, the output signal is converted into a pulse signal, which then corresponds to the particle concentration. This method offers an advantage that the output signal can immediately follow up on changes in the concentration, making it ideal for continuous monitor over time. However, this method has a disadvantage in that even if the mass concentration is constant, the quantity of scattered light varies with such factors as particle shape and the refractive index.



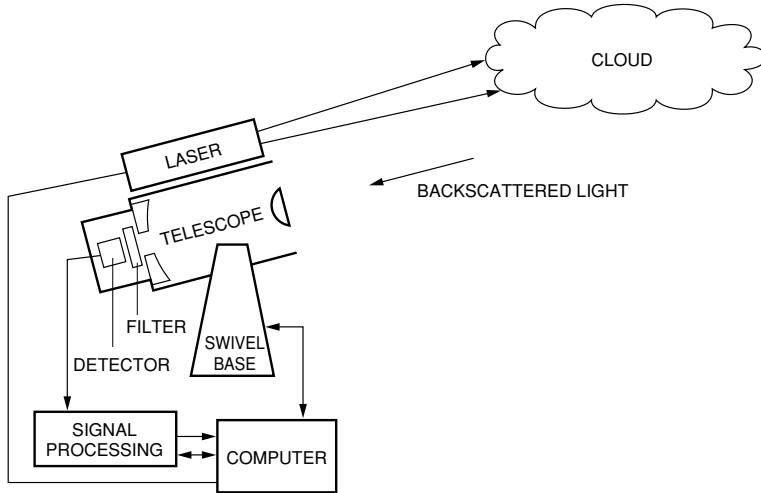
THBV2\_1434EA

**Figure 14-34: Block diagram of a dust counter using light scattering**

Dust counters utilizing scattered light have a drawback in that the amount of scattered light varies depending on the size and refractive index of particles even if the particle concentrations are constant. Another type of dust counters make use of the absorption of beta rays which is proportional to the mass of a substance through which the beta rays are transmitted. A filter paper is used to collect the dust, and the difference in the amount of beta-ray absorption before and after collecting the dust is compared to determine the mass of the suspended particles.

#### (2) Laser radar (LIDAR)<sup>(12)</sup>

Laser radar (LIDAR) transmits pulsed laser light into atmospheric space and receives the light backscattered from scatterers such as suspended matter in the atmosphere (atmospheric molecules, aerosols, clouds, etc.) and flying objects, in order to measure the distance to the scatterers as well as their concentrations, shapes and speeds. The laser transmitter and receiver are installed in the same place and the laser beam is scanned across the target area to obtain a three-dimensional spatial distribution. Optical signals detected by the receiver is converted into electrical signals, which are then converted into digital signals and processed by a computer.



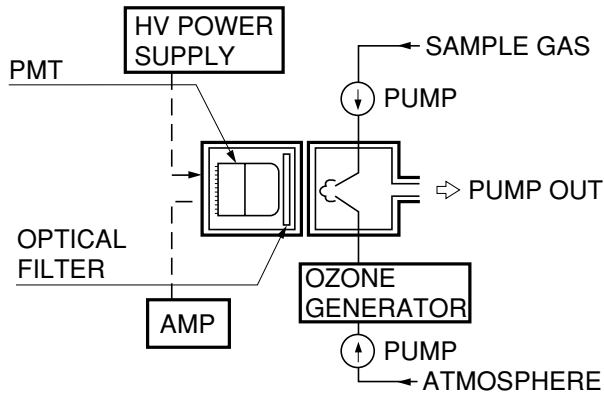
THBV3\_1435EA

Figure 14-35: Schematic diagram of a laser radar for atmospheric observation

### (3) NO<sub>x</sub> analyzers

These instruments are used to measure nitrogen oxide (NO<sub>x</sub>), an air-polluting gas contained in exhaust gases from automobiles and other internal combustion engines. NO<sub>x</sub> is a general term indicating nitrogen monoxide (NO) and nitrogen dioxide (NO<sub>2</sub>) and, in many countries, the concentration of NO<sub>x</sub> is limited by air pollution regulations so that it shall not exceed a certain level.

Figure 14-36 shows the configuration of an NO<sub>x</sub> analyzer making use of chemiluminescence.<sup>13)</sup> When NO gas reacts with ozone (O<sub>3</sub>) to become NO<sub>2</sub> gas, chemiluminescence is released. The intensity of this chemiluminescence is proportional to the concentration of NO gas. Since other gases contained in the exhaust gas do not produce such luminescence, the NO gas concentration can be selectively measured by detecting the intensity of this chemiluminescence.

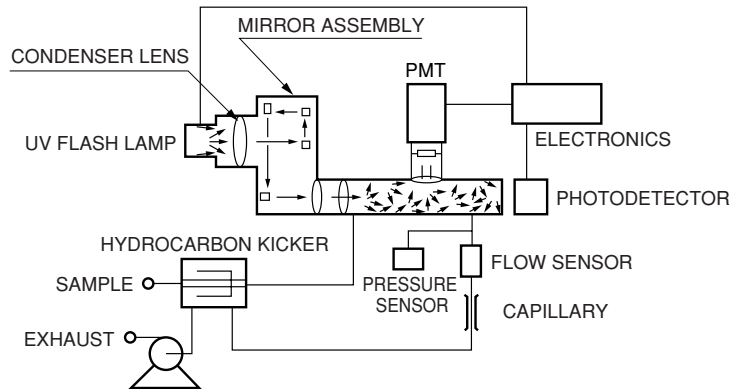


THBV3\_1436EA

Figure 14-36: NO<sub>x</sub> analyzer utilizing chemiluminescence

#### (4) SO<sub>x</sub> analyzers

SO<sub>x</sub> analyzers are used to measure sulfur dioxide concentrations in the atmosphere. Recently, UV fluorescent sulfur dioxide analyzers are in wide use. This method irradiates the sulfur dioxide in the atmosphere with UV light to produce an excited state. The resulting fluorescence is then measured to determine the sulfur dioxide concentrations in the atmosphere. A typical setup of a UV fluorescent sulfur dioxide analyzer is shown in Figure 14-37.



THBV3\_1437EA

**Figure 14-37: Typical setup of a UV fluorescent sulfur dioxide analyzer**

## 14.7 Radiation Monitors

### 14.7.1 Overview

Radiation monitors have long been used at nuclear power plants and nuclear research facilities. In recent years, however, the loss or theft of nuclear materials has become a serious concern so that inspections and detection of nuclear materials has become a high priority at national borders such as harbors and airports. Photomultiplier tubes can be combined with a scintillator matching the radiation emitted from the nuclear material, to create various types of inspection devices and monitors.

### 14.7.2 Application examples

#### (1) Handheld radiation monitor (pager)

Handheld radiation monitors are designed to help customs, border guards and others keep watch for smuggled radioactive materials. A detector consisting of a photomultiplier tube coupled to a scintillator is used to detect radiation. Compact, metal package photomultiplier tubes are usually used for handheld applications. Figure 14-38 shows the internal layout and photo<sup>14)</sup> of a handheld radiation monitor.

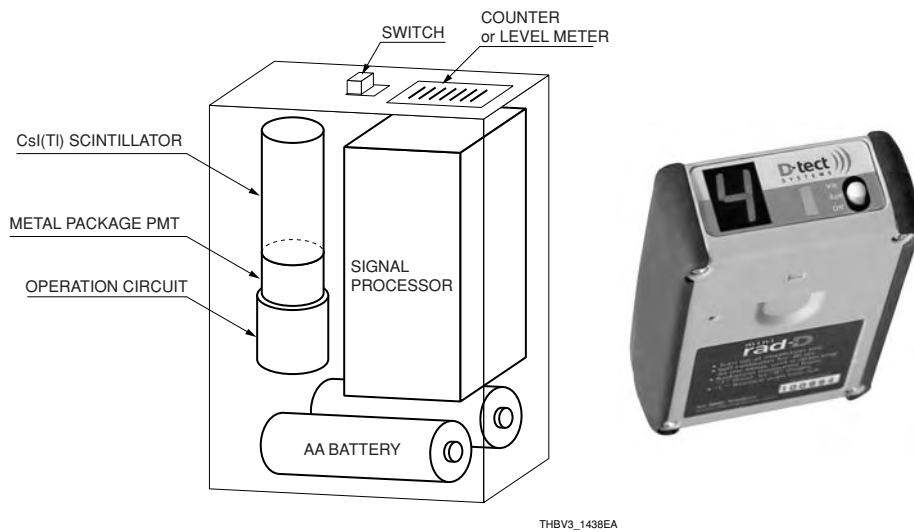
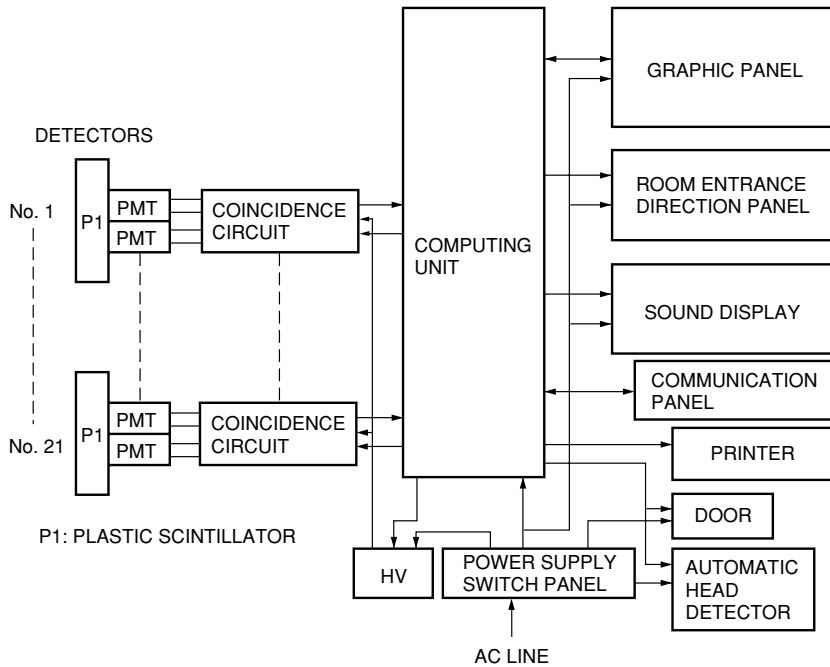


Figure 14-38: Structural view of a handheld radiation monitor

## (2) Door monitors

As the name implies, the door monitor is installed near the exit door in the monitored area of a nuclear power plant in order to check the personnel going out of this area for contamination by radioactive material. A photomultiplier tube is used in conjunction with a scintillator to detect radiation released from the radioactive material. An example<sup>15)</sup> of a door monitor is shown in Figure 14-39. The detector section consists of an array of scintillators coupled to photomultiplier tubes, enabling simultaneous measurement of the location and extent of contamination. Since the number of signals to be detected is usually very low, a coincidence counting circuit is used as in the case of scintillation counting to minimize erroneous signal counting.



THBV3\_1439EA

Figure 14-39: Block diagram of a door monitor

## 14.8 Industrial Measurement

### 14.8.1 Overview

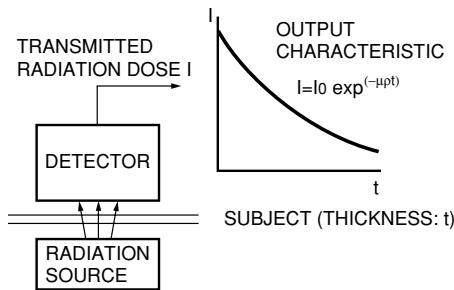
For non-contact measurement on a production line and other industrial measurement applications where rapid measurement with a high degree of accuracy and quality is essential, extensive use is made of various devices having photomultiplier tubes as detectors. These devices include thickness gauges and laser scanners, which are briefly discussed in the following paragraphs.

### 14.8.2 Application examples

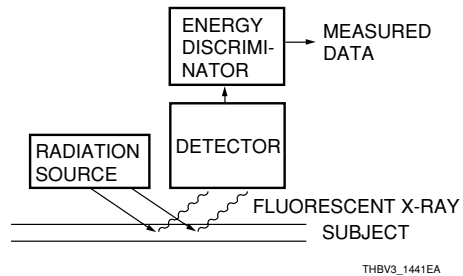
#### (1) Thickness gauges

To measure the thickness of paper, plastics and steel plates on a production line, non-contact measurement techniques that use radiation such as beta rays, X rays or gamma rays are favored.

These techniques can be roughly divided into two methods: one measures the amount of beta or gamma rays transmitted through an object<sup>16)</sup> (Figure 14-40) and the other measures the amount of fluorescent X-rays<sup>17)</sup> (Figure 14-41)



**Figure 14-40: Principle of a transmission-mode thickness gauge**



**Figure 14-41: Principle of a fluorescent X-ray thickness gauge**

When the intensity of radiation incident on a material is  $I_0$ , the transmitted radiation intensity  $I$  can be expressed by the following relation:

$$I = I_0 e^{-\mu\rho t}$$

$t$  : thickness (m)  
 $\rho$  : density ( $\text{g}/\text{m}^3$ )  
 $\mu$  : mass absorption coefficient ( $\text{m}^2/\text{g}$ )

Since the transmitted radiation intensity is proportional to the count rate, the thickness of the material can be obtained by calculating the count rate. In general, beta rays are used to measure rubber, plastics and paper which have a small surface density (thickness $\times$ density), while gamma rays are used to measure material with a large density such as metals. In addition, infrared radiation is also used for measurement of films, plastics and other similar materials.

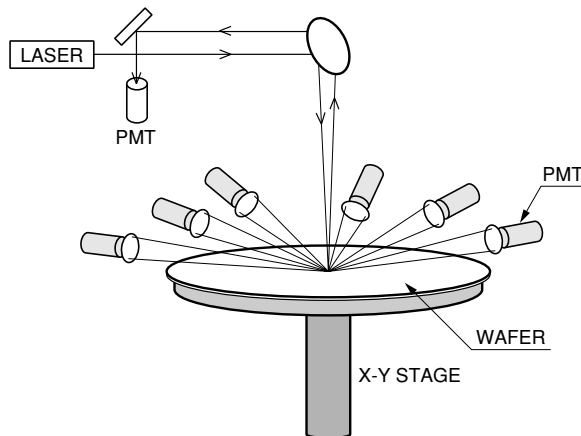
Fluorescent X-rays are used to measure the film thickness of plating and deposition layers. Fluorescent X-rays are secondary X-rays generated when a material is excited by radiation and have characteristic energy of the material. By detecting and discriminating this energy, a quantitative measurement of the object material can be made.

There are a variety of detectors used in these applications, such as proportional counter tubes, photomultiplier tubes and semiconductor radiation detectors. Photomultiplier tubes are used in conjunction with scintillators, mainly for detection of gamma rays and X-rays.

## (2) Laser scanners

Laser scanners are widely used in pattern recognition such as defect inspection and mask alignment of semiconductor wafers.

In semiconductor wafer inspection systems, a laser beam is scanned over the wafer surface or the wafer itself is scanned while a laser beam is focused onto a fixed point. In either case, photomultiplier tubes are commonly used to detect scattered light caused by dirt, stain and defects on the wafer surface. (See Figure 14-42.)



THBV3\_1442EA

Figure 14-42: Optical system layout for a semiconductor wafer inspection system

## 14.9 Aerospace Applications

### 14.9.1 Overview

Photomultiplier tubes are widely used in space research applications such as detection of X-rays from outer space, planetary observation, solar observation, environmental measurement in inner or outer space and aurora observation. In addition, photomultiplier tubes are also used for spectral measurements of various radiation in the atmosphere or outer space and measurement of X-rays from supernovas.

### 14.9.2 Application examples

#### (1) X-ray astronomy

Figure 14-43 illustrates the structure of ASUKA launched and placed in its orbit in February 1993 as the fourth astronomical satellite for X-ray observation in Japan. A gas imaging spectrometer (GIS) is used as the detector, which consists of a gas-scintillation proportional counter coupled to a photomultiplier tube (Hamamatsu R2486X) as illustrated in Figure 14-44.

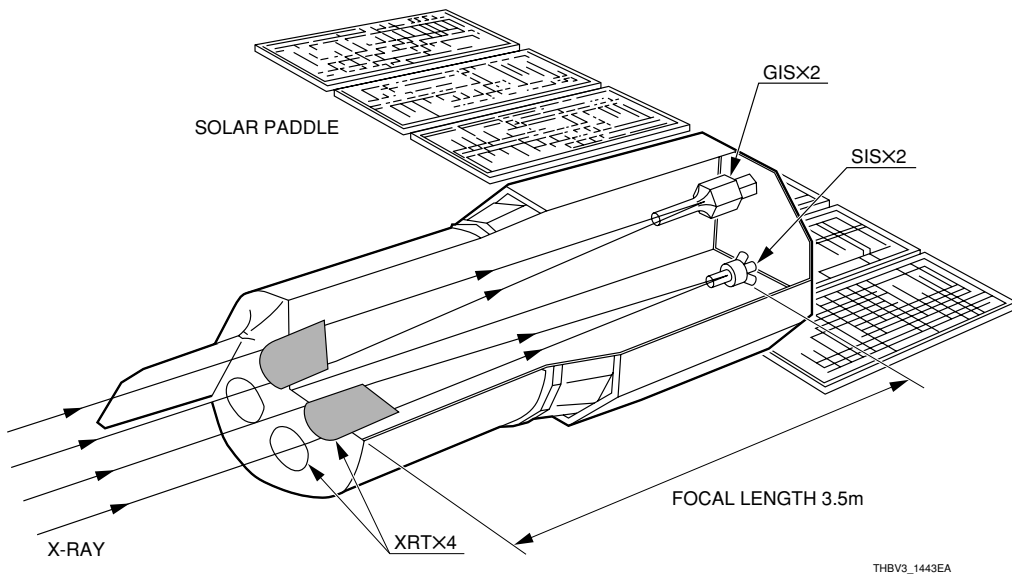
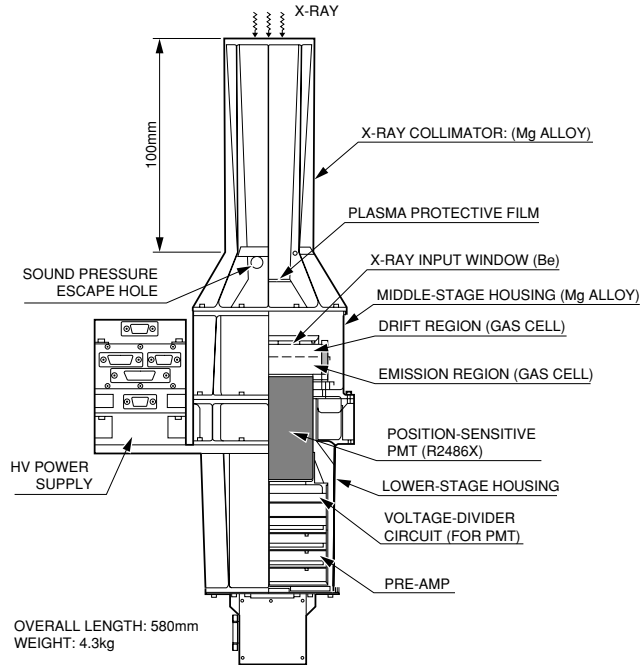


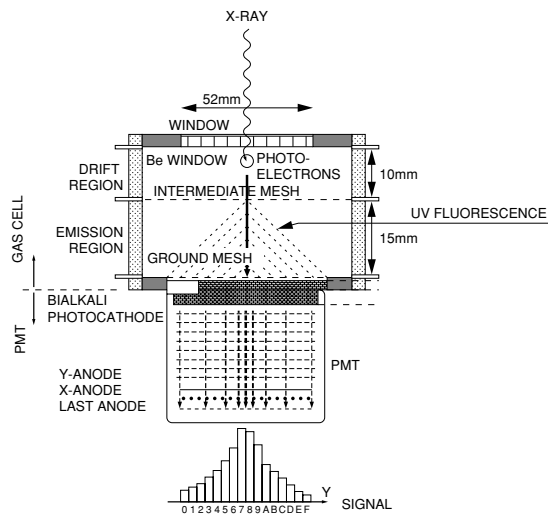
Figure 14-43: Astronomical satellite ASUKA for X-ray observation





THBV3\_1444EA

Figure 14-44: X-ray detector (GIS detector) mounted in ASUKA



THBV3\_1445EA

Figure 14-45: Principle of detection in GIS detector

ASUKA has succeeded in discovering various interesting facts. These include the detection of X-rays travelling from the supernova named "SN1993J", discovery of low-luminosity nucleus in the center of ordinary galaxy, and the world's first detection of inverse Compton X-rays coming from a radio galaxy. Furthermore, the ASUKA successfully revealed that the low energy spectrum of CXB (cosmic X-ray background) extends to 1 keV as single photon fingers. This discovery is expected to elucidate the CXB, which is the primary object of the ASUKA.

## (2) Ozone measurement (solar backscatter radiometer)

There are vast quantities of polluted air in the Earth's atmosphere and this reacts with light from the sun to produce ozone. If this layer spreads and blocks out the sunlight, it could have drastic future effects for humanity and other life on our planet. The photo below shows a photomultiplier tube designed for an ozone detector (right in same photo) to measure ozone concentrations in the Earth's atmosphere. This was assembled in a spectrophotometer inside an artificial satellite launched from the space shuttle. It is capable of converting extremely faint amounts of light into electrical signals for ozone measurement.

Photomultiplier tubes used for outer space applications must provide high reliability, capable of withstanding strong vibrations during liftoff and operating with high stability for long periods. The ozone detector using these photomultiplier tubes was used by NASA/NOAA. It was installed in the satellite-borne SBUV/2 instrument to detect the spectrum of solar backscatter from outer space and measure ozone layer distributions.

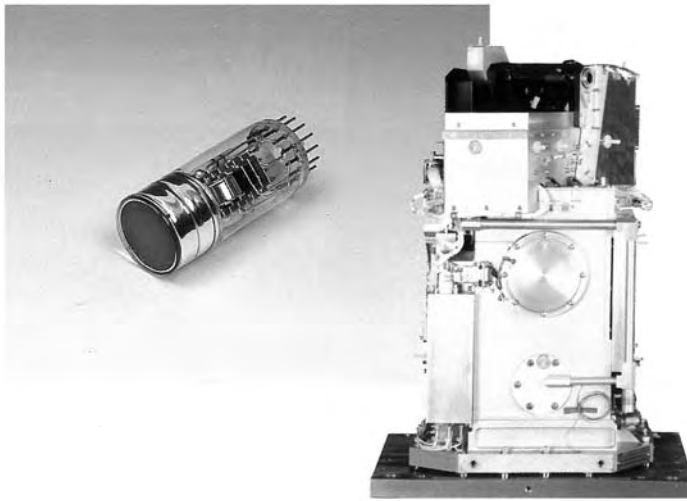


Figure 14-46: Photomultiplier tube (left) and ozone detector (right) mounted in SBUV/2

## 14.10 Mass Spectrometry / Solid Surface Analysis

Mass spectrometry is a technique used to identify and analyze the mass, makeup and minute quantity of a sample through the measurement of the difference in mass and movement of ions by exerting electric or magnetic energy on the sample which is ionized.

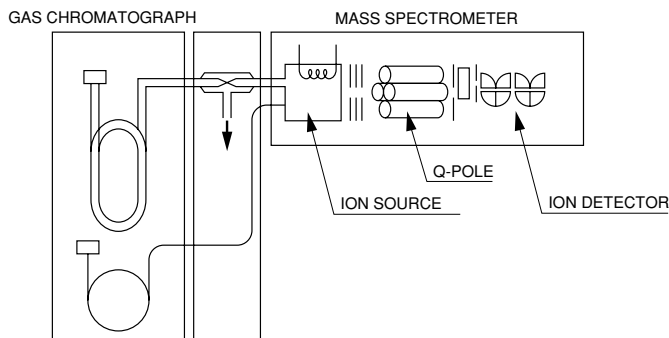
Solid state surface analysis is used to examine the surface state of a sample through the measurement of photoelectrons, secondary electrons, reflected electrons, transmitting electrons, Auger electrons or X-rays generated as a result of interactions of incident electrons with atoms composing the sample, which take place when an electron beam or X-ray irradiates the sample. Ion detectors are used as detectors in these applications.

### 14.10.1 Mass spectrometers<sup>18) 19)</sup>

Mass spectrometers are broadly classified into two groups: one using magnetic force (magnet) and one not using magnetic force. Currently used mass spectrometers fall under one of the following four types.

- Time of flight (TOF) type
- Quadrupole (Q-Pole) or ion trap type
- Magnetic field type
- Ion cyclotron (FTICR) type

Mass spectrometers are often combined with a gas chromatograph or liquid chromatograph to build a gas chromatograph mass spectrometer (GC-MS) or liquid chromatograph mass spectrometer (LC-MS). Mass spectrometers are used to identify, measure and analyze the composition of various samples such as petrochemicals, fragrance materials, medicines, biogenic components and substances causing environmental pollution. Figure 14-47 shows the schematic drawing of a quadrupole type gas chromatograph mass spectrometer.



THBV3\_1447EA

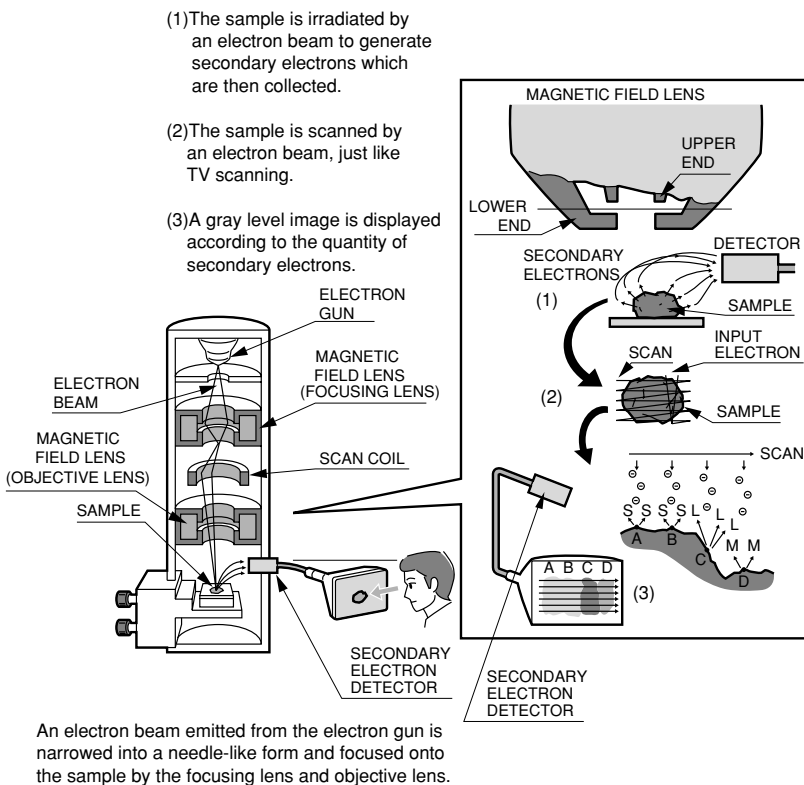
Figure 14-47: Schematic drawing of a gas chromatograph mass spectrometer.

### 14.10.2 Solid surface analyzers<sup>20)</sup>

Solid surface analyzers are broadly divided into two groups: one using electron beams to irradiate a sample and the other using X-rays. Major solid surface analyzers presently used are as follows.

- Scanning electron microscope (SEM)
- Transmission electron microscope (TEM)
- Auger electron spectrometer (AES)
- Electron spectrometer for chemical analysis (ESCA)

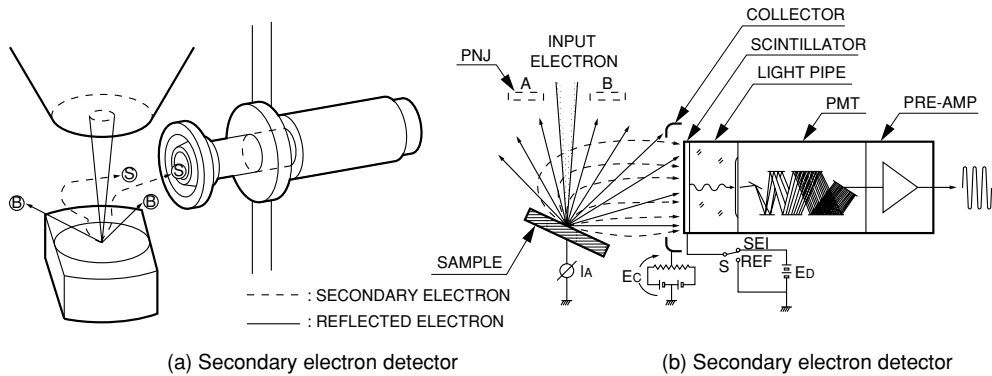
Among these four types of surface analyzers, the scanning electron microscope (SEM) is the most widely used and its structure and principle are illustrated in Figure 14-48.<sup>21)</sup>



THBV3\_1448EA

**Figure 14-48: Structure and principle of a scanning electron microscope**

An electron beam emitted from the electron gun is accelerated at a voltage of 0.5 to 30 kV. This accelerated electron beam is then condensed by the electromagnetic lens action of the focusing lens and objective lens, and finally formed into a very narrow beam of 3 to 100 nm in diameter, irradiating on the surface of a sample. Secondary electrons are then produced from the surface of the sample where the electron beam landed, and are detected with a secondary electron detector. The electron beam can be scanned in the XY directions across the predetermined area on the surface of the sample by scanning the electromagnetic lens. A magnified secondary electron image can be displayed on the CRT in synchronization with the signals of the secondary electron detector. Figure 14-49 shows the structure and operation of the secondary electron detector.



THBV3\_1449EA

**Figure14-49: Structure and operation of a secondary electron detector**

A typical secondary electron detector consists of a collector electrode, scintillator, light pipe, photomultiplier tube and preamplifier. Voltage is applied to the collector electrode and scintillator at a level required to collect secondary electrons efficiently. Most of the secondary electrons produced from the sample enter the scintillator and are converted into light. This converted light then passes through the light pipe and is detected with the photomultiplier tube.

## References in Chapter 14

- 1) Japan Analytical Instruments Manufacturers' Association: Guide to Analytical Instruments, 3rd Edition, 37 (1986).
- 2) H. Daidouji: The Spectroscopical Society of Japan - Measurement Method Series, 20, 129, Japanese Association of Spectroscopy (1985). (Published in Japanese)
- 3) Japan Analytical Instruments Manufacturers' Association: Guide to Analytical Instruments, 3rd Edition, 42 (1986). (Published in Japanese)
- 4) Japan Analytical Instruments Manufacturers' Association: Guide to Analytical Instruments, 3rd Edition, 45 (1986). (Published in Japanese)
- 5) K. Anan, K. Konno, Z. Tamura, M. Matsushashi, J. Matsumoto and M. Watanabe: Fundamental Biochemical Experimental Methods, 4, 32, Maruzen Corp. (1975). (Published in Japanese)
- 6) Y. Endo and K. Miyai: Protein, Nucleic Acid and Enzyme, Separate Volume 31, Enzyme Immunoassay, 13, Kyoritsu Publishing Corp. (1987). (Published in Japanese)
- 7) G. Kawashima: Introduction to Immunoassay, 29, Nanzandou (1987).
- 8) Japan Analytical Instruments Manufacturers' Association: Guide to Analytical Instruments, 3rd Edition, 228 (1986). (Published in Japanese)
- 9) T. Hayashi: Photomultiplier Tubes For Use In High Energy Physics (1992).
- 10) Hamamatsu Photonics: Photomultiplier Tubes and Environmental Conditions (1986)
- 11) Japan Analytical Instruments Manufacturers' Association: Guide to Analytical Instruments, 3rd Edition, 171 (1986). (Published in Japanese)
- 12) Nobuo Takeuti, et al.: Laser Radar, Laser Handbook , Chapter 27, Ohmsha (Published in Japanese)
- 13) Japan Analytical Instruments Manufacturers' Association: Guide to Analytical Instruments, 3rd Edition, 179 (1986). (Published in Japanese)
- 14) D-tect Systems, a division of ATK-mission Research
- 15) Aroka Corp.: Gated Surface Monitor.
- 16) Japan Analytical Instruments Manufacturers' Association: Guide to Analytical Instruments, 3rd Edition, 143 (1986). (Published in Japanese)
- 17) Japan Analytical Instruments Manufacturers' Association: Guide to Analytical Instruments, 3rd Edition, 143 (1986). (Published in Japanese)
- 18) M. Tsuchiya, M. Ohashi, T. Ueno: New Development in Mass Spectrometry, Modern Chemistry Extra Number 15, Tokyo Kagaku Dozin Co., Ltd. (Published in Japanese)
- 19) T. Ueno, K. Hirayama, K. Harada: Biological Mass Spectrometry, Modern Chemistry Extra Number 31, Tokyo Kagaku Dozin Co., Ltd. (Published in Japanese)
- 20) JEOL Ltd.: Introduction to the World of SEM (Published in Japanese)
- 21) The Nikkan Kogyo Shimbun: Structure of Machine/Wonder of Technolgy, No. 3, 42, 1996 (Published in Japanese)

# Index

## A

Aerospace applications 298  
Afterpulsing 77  
Ag-O-Cs 31  
Aging 64  
Al<sub>2</sub>O<sub>3</sub> crystal; window material 36  
Analog mode 126  
Angular response 62  
Anode 18  
Anode grounding and cathode grounding 85  
Anode linearity 54  
Anode luminous sensitivity 40  
Applications 265  
ASUKA 298  
Atmosphere, Effect of 254  
Atomic absorption spectrophotometers 268  
Atomic emission spectrophotometer 268

## B

Base-line shift 104  
Basic operating method 23  
Beryllium oxide (BeO), Dynode material 17  
Bialkali 30  
Biotechnology 282  
Blue sensitivity 41  
Borosilicate glass 36  
Box-and-grid type, Dynode structure 44

## C

Calorimeter 287  
Cathode linearity 54  
Cathode luminous sensitivity 39  
Cathode transit time difference, MCP-PMT 194  
Cell sorter 282  
Center-of-Gravity Position 178  
CFD (constant fraction discriminator) 51  
Charge-sensitive amplifier 109  
Circular-cage type, Dynode structure 44  
Cockcroft-Walton circuit 96  
Collection efficiency 16, 45  
Confocal laser microscope 283  
Connection to the external circuit 102  
Cooling 122  
Cooling precautions 239  
Count rate linearity, Photon counting 131  
Countermeasures for fast response circuits 93  
Coupling capacitor 104  
CPU+IF module 165

CRT (coincident resolving time) 53  
Cs-I, Photocathode material 30  
Cs-Te, Photocathode material 30  
CTTD (cathode transit time difference) 52  
Current output type module 158  
Current-to-voltage conversion 105  
    Using an operational amplifier 107  
    Using load resistance 105

## D

Dark current 67  
    Temperature characteristics 69  
Dead time, MCP-PMT 196  
Digital mode 126  
DNA microarray scanner 283  
DNA sequencer 284  
Door monitor 295  
Drift (time stability) 63  
Dust counter 291  
Dynode 13, 16  
Dynode types 43  
    Box-and-grid type 44  
    Circular-cage type 44  
    Linear-focused type 44  
    MCP (Microchannel plate) 44  
    Mesh type 44  
    Metal channel dynode 44  
    Venetian blind type 44

## E

EADCI (equivalent anode dark current input) 72  
Edge effect, Sheild case 119  
Electron affinity (EA) 15  
Electron multiplier 17  
Electron trajectory 16  
    Box-and-grid type 17  
    Circular-cage type 16  
    Linear-focused type 17  
Electron transit time 49  
Electrostatic shield 113  
Energy resolution, Scintillation counting 139  
ENI (equivalent noise input) 73  
Environmental conditions 233  
Environmental measurement 291  
External electric potential, Effect of 255

## F

Failure mode, Reliability test 261  
Failure rate, Reliability test 261  
Fall time 49  
Field emission 71  
Flat panel type multianode photomultiplier tubes 176

Fluorospectrophotometer 269  
Frequency characteristics, Sheild case 118

## G

GaAs (Cs), Photocathode material 31  
Gain 46  
Gain, MCP-PMT 191  
Gallium arsenide phosphied (GaAsP), Dynode materia 17  
Gallium phosphide (GaP), Dynode material 17  
Gamma camera 273  
Gate function 163  
Gated MCP-PMT 203  
Gating circuit 97  
Glass scintillation 71, 253  
Glass-epoxy PC board 108  
Grid Type Dynode Photomultiplier Tubes 182

## H

HA coating 257  
Helium gas, Effect of 248  
High temperature photomultiplier tube 236  
High-energy physics 285  
High-voltage power supply 23  
Hodoscope 286  
Housing 113  
HPD (Hybrid Photo-Detector) 209  
Humidity  
  Operating humidity 239  
  Storage humidity 239  
Hysteresis 65  
  Light hysteresis 65  
  Voltage hysteresis 66

## I

IEC Pub. 68 246  
III-V compound semiconductor photocathode 14  
Immunoassay 277  
In-vitro Assay 277  
Industrial Measurement 296  
InGaAs (Cs) 31  
InP/InGaAs(Cs) 31  
Integral power supply module 27  
Ion feedback 71  
Irradiance 7

## J

JIS-C0040 (vibration) 246  
JIS-C0041 (shock) 246

## K

K-free glass 36  
K<sup>40</sup> 36  
Kamiokande 288  
KamLAND 288  
Kovar glass 36

## L

Laser radar 291  
Laser scanner 297  
Leakage current (ohmic leakage) 70  
LIDAR 291  
life characteristics 63  
Light hysteresis 65  
Light intensity 5  
Light measurement method 28  
Light shield 113  
Linear-focused type 44  
Linearity 54  
Linearity measurement 56  
Linearity, Scintillation counting 142  
Long term stability, Scintillation counting 145  
Long wavelength limit 38  
Low-pass filter 156  
Luminous sensitivity 38

## M

Magnesium oxide (MgO), Dynode material 17  
Magnetic characteristics 240  
Magnetic characteristics, MCP-PMT 201  
Magnetic shield 114  
Magnetic shielding effect 119  
Magnetization 242  
Mass spectrometer 301  
MCA (multichannel analyzer) 51  
MCP (microchannel plate) 44, 188  
MCP-PMT 187  
  Dead time 196  
  Gain 191  
  Gated MCP-PMT 203  
  Magnetic characteristics 201  
  Multianode MCP-PMT 205  
  Saturation characteristics 196  
  Structure 189  
  Time characteristics 192  
  Voltage -divider circuit 190  
Mean life, Reliability test 261  
Mesh type dynode 44  
Metal channel dynode 44, 169, 178  
MgF<sub>2</sub> crystal 36  
MIL STD-202F 246  
MIL STD-810D 246



Multianode MCP-PMT 205  
 Multianode Photomultiplier Tubes 169

## N

NaI(Tl) scintillator 30  
 NEA (negative electron affinity) 15  
 Neutrino observation 288  
 Noise, Scintillation counting 146  
 NOx analyzer 292

## O

Oil well logging 290  
 Operating method 28  
   AC method 28  
   DC method 28  
   Photon counting method 28  
 Output circuit  
   For fast response photomultiplier tube 111  
 Output control circuit 98  
 Output linearity 86  
   DC operation 86  
   Pulse operation 88  
 Ozone measurement 300

## P

Permalloy 114  
 PET (Positron Emission Tomography) 270  
 Photocathode 14  
   III-V compound semiconductor 14  
 Photocathode band model 14  
 Photocathode materials 30  
   Ag-O-Cs 31  
   Bialkali 30  
   Cs-I 30  
   Cs-Te 30  
   GaAs (Cs) 31  
   High temperature, low noise bialkali 31  
   III-V compound semiconductor 10  
   InGaAs (Cs) 31  
   InP/InGaAs(Cs) 31  
   Multialkali 31  
   Sb-Cs 30  
   Sb-K-Cs 30  
   Sb-Na-K 31  
   Sb-Na-K-Cs 31  
   Sb-Rb-Cs 30  
 Photocathodes, History of 10  
 Photoelectron emission 14  
 Photometric units 4  
 Photomultiplier tubes for highly magnetic field  
 241  
 Photomultiplier tubes, History of 10

Photon counting 126  
   Circuit configuration 129  
   Operating method 129  
   Principle of photon counting 127  
   Signal-to-noise ratio 132  
   Stability 132  
 Photon counting head 159  
 Planar imaging device 274  
 Plateau characteristic, Scintillation counting 148  
 Plateau characteristics, Photon counting 129  
 PMT module 153  
 Polarized-light dependence 78  
 Position-sensitive photomultiplier tubes 168  
 Positron emission tomography (PET) 270  
 Power supply circuit 154  
 Proton decay 288  
 Pulse height distribution, Photon counting 129

## Q

Quantum efficiency 37

## R

Radiance 9  
 Radiant emittance 8  
 Radiant energy 7  
 Radiant flux 6  
 Radiant intensity 8  
 Radiant sensitivity 37  
 Radiation monitor 294  
 Radiation, Effect of 249  
 Radioimmunoassay 279  
 Red-to-white ratio 41  
 Reflection mode photocathodes 34  
 Relative pulse height, Scintillation counting 142  
 Reliability 258, 261, 262  
 Reliability tests and criteria 263  
 Ripple noise 156  
 Rise time 49  
 Rise/fall times, MCP-PMT 192  
 Ruggedized photomultiplier tubes 247

## S

S number 15, 30  
 Sapphire 36  
 Saturation characteristics, MCP-PMT 196  
 Saturation characteristics, Shield case 116  
 Sb-Cs, Photocathode material 30  
 Sb-K-Cs, Photocathode material 30  
 Sb-Na-K, Photocathode material 31  
 Sb-Na-K-Cs, Photocathode material 31  
 Sb-Rb-Cs, Photocathode material 30

- Scintillation counting 136  
  Energy resolution 139  
  Linearity 142  
  Long term stability 145  
  Noise 146  
  Plateau characteristic 148  
  Relative pulse height 142  
  Short term stability 146  
  Stability 145  
  Uniformity 144
- Scintillators  
  BaF<sub>2</sub> 137  
  BGO 137  
  CsI(Tl) 137  
  ZnS 137
- Secondary emission ratio 18  
Secondary emissive materials 17  
Settling time 156  
Shielding factor of magnetic shield case 114  
Short term stability, Scintillation counting 146  
Short wavelength limit 38  
Shot noise 73  
Signal-to-noise ratio 73  
Signal-to-noise ratio, Photon counting 132  
Socket assemblies 24  
Solid surface analysis 301  
Solid surface analyzer 302  
SOx analyzer 293  
Space research 298  
Spatial uniformity 60  
Spectral regions 4  
Spectral response characteristics 32, 33, 37  
Spectral response range 38  
Spectral transmittance 37  
Spectrophotometers 267  
Spectrophotometry 266  
Stability 63  
Stability over time 258  
Stability, Photon counting 132  
Stability, Scintillation counting 145  
Storage temperature 239  
Stress and stability 259  
Super-Kamiokande 288  
Synthetic silica 36
- T**
- TAC (time-to-amplitude converter) 51  
Temperature characteristics 234  
Thermionic emission 68  
Thermoelectric cooler 122  
Thickness gauge 296  
Time characteristics 48  
Time characteristics, MCP-PMT 192  
TOF counter 286
- Transit time, MCP-PMT 192  
Transmission mode photocathodes 35  
TTS (transit time spread) 50  
TTS (transit time spread), MCP-PMT 192
- U**
- Uniformity 59  
  Angular response 62  
  Spatial uniformity 60  
Uniformity, Scintillation counting 144  
UV glass 36
- V**
- Venetian blind type, Dynode structure 44  
Vibration and Shock 243  
Voltage -divider circuit, MCP-PMT 190  
Voltage hysteresis 66  
Voltage output type module 158  
Voltage-divider circuit 24  
  Precautions for mounting components 101  
  Selecting the parts 100  
Voltage-divider circuits  
  Fast-response circuit 94  
  High output linearity circuit 94, 96
- W**
- Warm-up 64  
Well scintillation counter 279  
Window materials 36  
  Borosilicate glass 36  
  MgF<sub>2</sub> 36  
  Sapphire 36  
  Spectral transmittance characteristics 37  
  Synthetic silica 36  
  UV glass 36  
Window transmittance  
  Deterioration 249
- X**
- X-ray astronomy 298  
X-ray image diagnostic equipment 275  
X-ray phototimer 275
- Z**
- Zener diode 84

## "PHOTOMULTIPLIER TUBES" Editorial Committee

Editorial Chief	Toshikazu Hakamata
Editorial Staff	Hidehiro Kume
	Kazuyoshi Okano
	Kimiyuki Tomiyama
	Akifumi Kamiya
	Yuji Yoshizawa
	Hisayuki Matsui
	Ichiro Otsu
	Takeshi Taguchi
	Yoshihiko Kawai
	Haruhisa Yamaguchi
	Kazumi Suzuki
	Seiji Suzuki
	Tetsuya Morita
Editorial Office	Daisuke Uchizono

## PHOTOMULTIPLIER TUBES – Basics and Applications –

---

March 1994 First Edition  
April 1999 Second Edition  
February 2006 Third Edition  
August 2007 Third Edition (Edition 3a with minor revisions)

Authors	Hamamatsu Photonics K.K. Editorial Committee
Editing	Word Technical Writing, Inc.
Publisher	Hamamatsu Photonics K.K. Electron Tube Division

---

© 2007 HAMAMATSU PHOTONICS K.K., Electron Tube Division  
No part of this publication may be reproduced in any form without permission  
of Hamamatsu Photonics K.K. TOTH9001E03a